Taylor dispersion analysis : a powerful size-based characterization technique for monitoring the aggregation of β-amyloid peptides

Mihai Deleanu

THÈSE POUR OBTENIR LE GRADE DE DOCTEUR DE L'UNIVERSITÉ DE MONTPELLIER

En Chimie et Physico-Chimie des Matériaux

École doctorale Sciences Chimiques Balard ED 459

Unité de recherche Institut des Biomolécules Max Mousseron

Taylor dispersion analysis: a powerful size-based characterization technique for monitoring the aggregation of β-amyloid peptides

Présentée par Mihai DELEANU
Le 1 Février 2022

Sous la direction de Joseph CHAMIEH et Hervé COTTET

Devant le jury composé de

Agnès HAGEGE, Chargé de recherche CNRS, Université Lyon I	Rapporteur
Anne VARENNE, Professeur des Universités, Université de Paris Sciences et Lettres	Rapporteur
Eric MARCHIONI, Professeur des Universités, Université de Strasbourg	Président du jury
Sylvain LEHMANN, Professeur des Universités -Praticien Hospitalier, Université de Montpellier	Examinateur
Joseph CHAMIEH, Maître de Conférences, Université de Montpellier	Directeur de thèse
Hervé COTTET, Professeur des Universités, Université de Montpellier	Co-directeur de thèse
Jean-François HERNANDEZ, Directeur de recherche CNRS, Université de Montpellier	Membre invité
Luca CIPELLETTI, Professeur des Universités, Université de Montpellier	Membre invité

UNIVERSITÉ DE MONTPELLIER

Résume en Français

La maladie d'Alzheimer (MA), une maladie neurodégénérative chronique, est l'un des principaux défis de santé publique du XXIe siècle. Il est généralement admis que le développement de la MA est dû, d'une part, à la formation extracellulaire de plaques amyloïdes et, d'autre part, à l'accumulation intracellulaire d'enchevêtrements neurofibrillaires Tau (NFT), causée par l'agrégation de peptides amyloïdes Aβ qui sont générés pendant la phase amyloïdogénique du traitement de la protéine précurseur amyloïde (APP). L'agrégation des peptides Aβ conduit à la formation de plusieurs espèces toxiques qui peuvent se propager aux cellules et aux tissus et, par conséquent, conduire à l'endommagement et à la mort des neurones.

Un large éventail de techniques biophysiques ont été utilisées pour étudier l'agrégation des peptides amyloïdes. Parmi celles-ci, des méthodes de caractérisation structurelle telles que le dichroïsme circulaire (CD), la diffraction des rayons X, la spectroscopie infrarouge (IR), la résonance magnétique nucléaire (RMN) ou la spectrométrie de masse (MS) ont souvent été utilisées pour étudier les changements de conformation, ou pour déterminer les interactions possibles avec entres ces peptides amyloïdes et différentes espèces extrinsèques. Quant à la morphologie des espèces issues de l'agrégation, elle a généralement été évaluée par des méthodes d'imagerie telles que la microscopie électronique (EM) et la microscopie à force atomique (AFM). La cinétique et le mécanisme de l'agrégation ont été principalement évalués par fluorescence de la thioflavine T (ThT), mais d'autres techniques telles que l'électrophorèse capillaire (EC) ont également été utilisées. Quant à la distribution de taille des espèces, plus spécifiquement en termes de rayon hydrodynamique (R_h), les outils les plus courants sont la diffusion dynamique de la lumière (DLS) et la spectroscopie de corrélation de fluorescence (FCS). Piur la distribution de masse molaire, l'électrophorèse sur gel de polyacrylamide (PAGE) et la chromatographie d'exclusion stérique (SEC) couplée à la diffusion de la lumière multiangle (MALS) ont souvent été utilisées. Cependant, une seule méthode ne suffit pas pour démêler l'ensemble des informations concernant le mécanisme d'agrégation, car chaque technique précédemment citée présente des limitations pratiques malgré les données quantitatives et/ou qualitatives utiles qu'elle est en mesure de fournir.

L'analyse de dispersion de Taylor (TDA) est une technique moderne qui permet de déterminer le coefficient de diffusion moléculaire (D) et le rayon hydrodynamique (R_h), sur la base de la

dispersion d'une bande de soluté injectée dans un tube capillaire ouvert sous l'influence d'un écoulement laminaire de Poiseuille. En fonction des conditions d'analyse, la TDA peut dimensionner et quantifier différentes particules et espèces ayant une taille (R_h) de 0,1 nm à < 1 µm.

Jusqu'à présent, la TDA n'a pas encore été employée pour le suivi du processus d'agrégation des peptides Aβ et n'a été utilisée qu'une seule fois pour évaluer un échantillon de Aβ(1-42) sous forme de monomère. Ainsi, l'objectif principal de ce projet de recherche était d'appliquer la TDA pour évaluer le mécanisme d'agrégation de ces peptides amyloïdogènes. La thèse a exploré comment la TDA peut dimensionner, quantifier et spécifier les différents intermédiaires Aβ en temps réel, ainsi que la façon dont les données peuvent être traitées et interprétées. Certains des résultats obtenus par la TDA ont été validés par rapport à des techniques alternatives précédemment utilisées dans les études d'agrégation des peptides Aβ.

Ce manuscrit de thèse est organisé en quatre chapitres : Une étude bibliographique décrivant les connaissances actuelles relatives aux peptides Aβ (chapitre I) ; Une étude sur la spéciation des peptides β-amyloïdes pendant le processus d'agrégation (chapitre II) ; Une étude de co-agrégation de mélanges de peptides Aβ(1-40):Aβ(1-42) (chapitre III) ; et une étude de suivi du processus d'agrégation des peptides Aβ par TDA en utilisant une détection simultanée UV-LEDIF en présence d'un *tag* fluorescent (chapitre IV).

Le chapitre I est basé sur une étude bibliographique approfondie et est divisé en quatre sections couvrant les aspects généraux de l'amyloïdose et de la maladie d'Alzheimer (section 1), les connaissances actuelles concernant le mécanisme d'agrégation des peptides Aβ (section 2), les petites molécules conçues pour inhiber le processus d'agrégation des Aβ (section 3), et une revue de plusieurs techniques biophysiques employées pour évaluer la cinétique, la distribution de taille et la morphologie des espèces Aβ (section 4).

Le chapitre II intitulé "Unraveling the speciation of β-amyloid peptides during the aggregation process by Taylor dispersion analysis" décrit les activités de recherche qui ont déjà été diffusées dans un premier article publié (*Anal. Chem.* 2021). Dans ce chapitre, la TDA a été appliquée pour étudier le processus d'agrégation de deux peptides (Aβ(1-40) et Aβ(1-42)) dans des conditions physiologiques en fournissant une détermination directe de toutes les formes possibles de Aβ amyloïde formées au cours du processus d'agrégation. Ainsi, la TDA a pu fournir une évaluation

complète de la spéciation de l'Aβ pendant le processus d'agrégation in vitro, y compris la consommation du monomère et la formation d'oligomères, de protofibrilles et de fibrilles.

En effet, l'agrégation des peptides Aβ est un processus très complexe qui dépend d'un large éventail de facteurs physico-chimiques (par exemple, l'origine et la nature du peptide, la concentration, la température, etc.). La présence initiale d'agrégats peut influencer ce processus de diverses manières. Par conséquent, les peptides ont été prétraités avec une solution d'hydroxyde d'ammonium NH_4OH pour obtenir des échantillons libre d'agrégats. Le succès de cette étape a été confirmé par le test de fluorescence ThT. Les études cinétiques de fluorescence sur plusieurs lots de peptides, dont l'Aβ(1-40) synthétisé, le cAβ(1-40) commercial et l'Aβ(1-42), ont révélé que seul le cAβ(1-40) commercial était initialement agrégé, malgré l'étape de prétraitement. En revanche, les peptides Aβ(1-40) synthétisé et Aβ(1-42) commercial ont été évalués comme étant exempts d'agrégats.

L'agrégation de l'Aβ(1-40) a montré un comportement de type seuil, ce qui indique que l'étape déterminant le taux d'agrégation est la formation de graines multimériques, c'est-à-dire que l'Aβ(1-40) passe par un mécanisme où les monomères s'ajoutent aux fibrilles déjà présentes pour les allonger et produire des fibrilles de plus grandes tailles, sans passer par des espèces intermédiaires. Le processus d'agrégation de l'Aβ(1-42) présente un chemin différent de celui de l'Aβ(1-40) conduisant à des espèces intermédiaires, et successivement à une étape d'élongation produisant des protofibrilles, puis des fibrilles. On a constaté que la proportion des populations monomères et oligomères de faible masse molaire diminuait rapidement, tandis que les espèces oligomères de masse molaire plus élevée augmentaient pour atteindre un maximum à 1,6 h, après la disparition des espèces monomères. Ensuite, la proportion de protofibrilles a augmenté pour atteindre un maximum à 3,5 h, et enfin, les « spikes » (espèces non diffusantes en suspension) ont augmenté en intensité pour atteindre un maximum à 5,6 h. Deux approches différentes de traitement des données ont été utilisées pour traiter les pics élués et extraire les informations concernant les tailles et les proportions des populations présentes. Premièrement, un ajustement avec un nombre fini de fonctions gaussiennes a été utilisé, et deuxièmement, l'analyse par CRLI normalement utilisée dans la diffusion dynamique de la lumière (DLS) a été appliquée pour obtenir des distributions de taille continues à chaque temps d'incubation.

Les résultats de la TDA ont été confirmés par le dosage par fluorescence de la thioflavine T (ThT). Le test ThT est surtout connu pour détecter les structures fibrillaires amyloïdes, qui se

forment aux dépens des structures solubles provoquant une diminution de leur proportion. Il a été démontré dans ce travail que la courbe de dosage ThT se superpose à l'évolution de la concentration des espèces insolubles déterminée par TDA, démontrant que la TDA capture fidèlement la phase de latence, et le temps pour atteindre le plateau du processus d'agrégation en termes de consommation de monomères et de petits oligomères. De plus, la TDA a permis une estimation quantitative des étapes intermédiaires de l'agrégation, en particulier dans le cas de Aβ(1-42), une caractéristique difficile à obtenir avec d'autres techniques telles que la chromatographie d'exclusion stérique (SEC).

De plus, des simulations moléculaires ont également été réalisées en utilisant les fichiers de banque de données de protéines disponibles dans la littérature, ce qui a permis le calcul des propriétés hydrodynamiques de plusieurs structures monomères et oligomères LMM de l'Aβ(1-42). A partir de ces simulations et en combinaison avec les résultats de la TDA, il a été révélé que le rayon hydrodynamique expérimental de la population de monomères et d'oligomères de faibles masses molaires LMM correspondait principalement à un mélange de monomères et de dimères.

En complément du chapitre II, une étude d'inhibition du processus d'agrégation de Aβ(1-42) a également été réalisée en utilisant un inhibiteur de feuillets β, iAβ5p, connu pour inhiber la formation de fibrilles. Il a été trouvé que iAβ5p avait un effet inhibiteur sur la formation de fibrilles et seulement un léger effet sur le taux d'agrégation a été observé sans changements significatifs sur la formation des espèces lors des premiers stade de l'agrégation. Cependant, ces résultats confirment que la TDA peut être utilisée comme outil de dépistage de médicaments pour trouver des inhibiteurs appropriés capables d'affecter les premiers stades du processus d'agrégation. La puissance du traitement des données décrit dans ce travail réside dans sa capacité à distinguer les petits oligomères potentiellement toxiques dans un mélange polydisperse de plus grands oligomères, de protofibrilles et de fibrilles.

Le chapitre III intitulé "Taylor dispersion analysis and Atomic Force Microscopy provide quantitative insight on the aggregation kinetics of Aβ(1-40)/Aβ(1-42) amyloid peptide mixtures" décrit les activités de recherche qui ont été récemment été accepté comme publication dans *ACS Chemical Neuroscience* en 2022. Dans ce chapitre, la co-agrégation de peptides Aβ à différents rapports Aβ(1-40):Aβ(1-42) (1:0, 3:1, 1:1, 1:3 et 0:1) a été explorée par TDA et par AFM. Le TDA a permis de suivre la cinétique de l'assemblage amyloïde et de quantifier les intermédiaires transitoires. De manière complémentaire, l'AFM a permis de visualiser la formation de fibrilles insolubles.

Ensemble, les deux techniques ont permis d'étudier l'influence des ratios peptidiques sur la cinétique et la formation d'espèces oligomères potentiellement toxiques. Les résultats obtenus ont confirmé que la cinétique d'agrégation dépend fortement de la nature du peptide amyloïde et de son environnement. Dans les conditions étudiées, l'Aβ(1-42) est plus sujet à l'agrégation et s'agrège plus rapidement (quelques minutes) que Aβ(1-40) (diminution de la surface des monomères et des petits oligomères observée à partir de 24h d'incubation). Dans le cas des mélanges, le taux d'agrégation est fortement influencé par le rapport Aβ(1-40):Aβ(1-42). En effet, Aβ(1-40) semble réduire le taux d'agrégation de Aβ(1-42), probablement par un mécanisme d'ensemencement croisé. Lorsque les peptides sont mélangés, des espèces oligomères intermédiaires ont été observées et ont diminué en proportion quand la teneur en Aβ(1-40) augmente. En général, les modèles cinétiques utilisés pour évaluer le mécanisme d'agrégation sont basés sur des données expérimentales qui donnent des informations liées à l'accumulation de masse de fibrilles au cours de l'agrégation, ou en appliquant des simulations numériques. Dans ce travail, un modèle cinétique permettant d'évaluer les constantes cinétiques d'association et de dissociation des différentes espèces a été appliqué, en ajustant l'évolution temporelle de la surface des pics obtenue expérimentalement par TDA pour lesdifférentes populations solubles telles que celle des monomères et les petits oligomères, celle des oligomères de masse molaire plus élevée et celle des protofibrilles. Il a été déterminé que l'augmentation de la quantité d'Aβ(1-42) favorisait l'augmentation des vitesses de réaction, tandis que pour l'expérience indépendante 100% Aβ(1-40), le mécanisme d'agrégation était plus direct, partant des monomères vers la formation de fibrilles insolubles.

La dernière partie (chapitre IV) de la thèse intitulée "Monitoring the aggregation of Aβ peptides by TDA using a simultaneous UV-LEDIF analysis in the presence of a FITC fluorescent dye" décrit l'effet du fluorophore FITC sur l'agrégation et le processus de co-agrégation des peptides Aβ. Les résultats ont démontré que le FITC réduisait considérablement le comportement d'agrégation de Aβ(1-42) lorsque le fluorophore est attaché à cette isoforme, tandis que pour le système contenant Aβ(1-40) tagué par FITC, seul un retard de la cinétique a été observé par rapport au peptide natif. Au cours du processus de co-agrégation des systèmes Aβ natif (nAβ) et tagué (tAβ), l'isoforme 100% native s'est avérée être l'isoforme dominante du processus d'agrégation à cause de l'effet électrostatique et hydrophile conjugué du FITC attaché sur le peptide dérivé, ce qui tend à réduire la propension à l'agrégation du peptide Aβ correspondant. Par ailleurs, l'analyse LEDIF a été affectée par une traînée de pic qui était très probablement causée par l'adsorption du « tag » FITC sur la surface capillaire, ce qui a rendu l'analyse des données plus difficile. En

utilisant un traitement de données adéquat, les résultats obtenus par LEDIF ont été corrélés avec ceux obtenus par UV. Ainsi, le suivi de l'agrégation de mélange de peptides natifs et libellés a permis de montrer que l'agrégation de mélanges Aβ est un mécanisme hétéromoléculaire.

Actuellement, il n'existe aucune technique biophysique rapportée dans la littérature capable de suivre en temps réel l'agrégation Aβ et permettant d'obtenir autant d'informations en une seule analyse. Les travaux présentés dans cette thèse ont démontré, pour la première fois, que la TDA pouvait être utilisée pour le suivi du processus d'agrégation des peptides Aβ. En utilisant un traitement de données adéquat des pics expérimentaux obtenus, des informations quantitatives concernant la taille et la proportion des différentes espèces ont pu être obtenues, ce qui a fourni une image claire des premières étapes du processus d'agrégation des peptides Aβ.

General Introduction

Alzheimer Disease (AD), a chronic neurodegenerative disease, is one of the major public health challenges of the 21st century. The development of AD is thought to be due to extracellular formation of amyloid plaques generated by β-amyloid (Aβ) peptides and to the intracellular accumulation of neurofibrillary Tau tangles (NFTs), caused by the aggregation of Aβ peptides that are generated during the amyloidogenic processing of the amyloid precursor protein (APP). The aggregation of Aβ peptides leads to the formation of several toxic species that are able spread to cells and tissues and consequently lead to the damage and death of neurons.

The aggregation of Aβ peptides is a very dynamic biological process where a wide variety of species are generated through a multistep chain of reactions, often referred to as the amyloid cascade. This cascade occurs via a nucleation-condensation polymerization reaction which is governed by a wide range of physico-chemical factors (e.g. nature of the peptide, concentration, temperature, etc.). Up to the current consensus, the aggregation process presents three main phases: the nucleation, the elongation, and the stationary phase. The main species involved in this process can be divided into four main categories of populations: monomers, oligomers, protofibrils and fibrils. The oligomers are the first intermediates generated during the nucleation phase, and their formation is believed to be favored by a specific conformation of the monomers. Oligomers are highly heterogeneous and unstable in nature. Therefore, they are very difficult to isolate and to characterize. They are considered to be the most toxic species generated during the aggregation process, making them one of the primary therapeutic targets in AD. Therefore, a better understanding of the oligomeric structures and evolution along the aggregation course is still required. Protofibrils represent the last soluble intermediates generated along the nucleation phase and are more stable compared to oligomers. They further react during the elongation phase to form fibrils which represent the final products of the process. Fibrils are insoluble species and represent the most stable species of the process. When “not aggregation-prone” species such as monomers and LMM oligomers are present in the medium, the process reaches a stationary phase that mainly consists of mature fibrils and their further accumulation leads to the formation of amyloid plaques found in the brains of patients suffering from AD.

For unravelling the aggregation mechanism of Aβ peptides, a wide range of biophysical techniques was employed for studying the amyloid cascade of reactions. To name a few, circular dichroism (CD), X-ray diffraction, infrared (IR) spectroscopy, nuclear magnetic resonance (NMR) or advanced MS techniques were often employed to structurally characterize different species. The kinetics and the

mechanism of the aggregation are mainly evaluated by ThT assay, but other techniques such as capillary electrophoresis (CE) can be employed as well. The most common tools for evaluating the size distribution of the species are dynamic light scattering (DLS) and fluorescence correlation spectroscopy (FCS). The morphology of the species is generally assessed by imaging methods such as electron microscopy (EM) and atomic force microscopy (AFM). However, each of these techniques presents several limitations despite the useful quantitative and/or qualitative data that they are able to provide. Only few of these methods can be used to monitor the aggregation in real time with information about the kinetics, size, and the morphology of the species. Therefore, there is still a high demand for the development of novel biophysical techniques which can provide a simple and fast analysis and that can allow the real-time monitoring of all the main species, with a particular focus on the oligomer population.

The main objective of this thesis was to apply Taylor dispersion analysis for the real-time monitoring of the Aβ aggregation process. TDA is a modern technique that does not require calibration allowing the determination of the molecular diffusion coefficient (D), and the hydrodynamic radius (R_h) of the solutes solubilized in the sample. It allows a low sample consumption which is in the range of nL per injection and does not require sample filtration because it is not sensitive to dust. So far TDA has not been employed for a full-scale monitoring of the aggregation process of Aβ peptides and was used once for evaluating a monomeric Aβ(1-42) sample. These facts and advantages, endorse that TDA can be a promising tool for evaluating the soluble Aβ early-stage species.

The thesis is organized in four chapters: A literature survey outlining the current knowledge related to Aβ peptides (Chapter I); A study on the speciation of β-amyloid peptides during the aggregation process (Chapter II); A co-aggregation study of Aβ(1-40):Aβ(1-42) peptide mixtures (Chapter III); and a monitoring study of the aggregation process of Aβ peptides by TDA using a simultaneous UV-LEDIF detection in the presence of a fluorescent dye (Chapter IV).

Chapter I is based on an extensive literature survey and is divided in four sections covering the general aspects of amyloidosis and Alzheimer's disease (Section 1), the current knowledge regarding the aggregation mechanism of Aβ peptides (Section 2), the disease-modifying small molecules designed for inhibiting the aggregation process of Aβ (Section 3), and a review of several biophysical techniques employed for evaluating kinetics, size distribution and morphology of Aβ species (Section 4).

In this work (Chapter II), TDA was first applied to study the aggregation process of two Aβ sequences Aβ(1-40) and Aβ(1-42) under physiological conditions by providing a direct determination of the main Aβ species. TDA allows to get a complete size-speciation (in the range of 0.1-200 nm

hydrodynamic radius) of the soluble species present in the sample. Results were correlated with the ThT assay and DLS. Moreover, molecular simulations that allowed the calculation of the hydrodynamic properties of several monomer and LMM oligomer structures of Aβ(1-42) were also performed by using the available protein data bank files available in the literature. This study was published in a first research article (*Analytical Chemistry* 2021). As a complement of Chapter II, an inhibition study upon the aggregation process of Aβ(1-42) was also performed by using a β-sheet breaker, iAβ5p, known to inhibit the formation of fibrils.

In a second study (Chapter III), performed under collaborative research with different research groups, more complex Aβ systems were explored where TDA and AFM were employed for monitoring the co-aggregation process of Aβ(1-40) and Aβ(1-42) mixtures at different Aβ(1-40):Aβ(1-42) ratios. TDA revealed the size and the real-time evolution of the soluble Aβ populations formed during the aggregation process, while AFM confirmed the results obtained by TDA and allowed the evaluation of fibrils, which cannot be sized by TDA. The kinetics of aggregation obtained at different Aβ(1-40):Aβ(1-42) ratios were compared. Overall, this study showed that by modifying the Aβ ratio changed the onset of the oligomeric species appearance and monomeric species disappearance, further suggesting that different aggregation pathways can occur. These results are part of a second manuscript which was recently accepted as a publication in *ACS Chemical Neuroscience*.

In the last study, a TDA method using a simultaneous UV and LEDIF detections was employed for monitoring the aggregation process of native Aβ peptides (nAβ) in the presence of a certain proportion of FITC tagged peptide (tAβ). This study was performed to investigate the influence of the fluorescent dye on the aggregation process; and to possibly decrease the peptide concentration in the aggregation studies to better fit the physiological conditions.

Acknowledgements

First and foremost, I would like to thank, **Professors Joseph Chamieh** and **Hervé Cottet**. I am grateful to them for accepting me in their group and for assigning me this PhD research project, a new and challenging topic not only for me but also for the entire group. I was very pleased to be accepted in the DSBC group at IBMM, University of Montpellier, as I previously had the opportunity to work within the local academic life and in this wonderful town, and I was looking very much ahead for finding a PhD studentship in this University. Joining their analytical oriented group with my early organic synthesis background was for me a great challenge and, combining this with the biological oriented topic, the overall challenge was even greater. Looking back to the last three years, I am glad that I had this opportunity and I feel now rewarded both in terms of scientific achievements and expertise as well as in terms of personal experiences. I am grateful to **Professors Joseph Chamieh** and **Hervé Cottet** for guiding me all these years with passion and for all the things that they taught me. I will surely use with wisdom and professionalism everything I learned from them and I hope that once I will move further in my professional career, we will further collaborate and take advantage of combining their analytical expertise, particularly TDA, and facilities with my next analytical and synthetic challenges.

I am very grateful to **Dr. Jean-François Hernandez** for guiding me during the peptide synthesis and to **Prof. Luca Cipelletti** for the support with DLS experiments. I have learned so many things from them during this professional path and I wish to continue the collaboration with them once I will move further in my professional career.

My profound gratitude goes to all the Jury members, **Prof. Anne Varenne**, **Dr. Agnès Hagege**, **Prof. Eric Marchioni**, **Prof. Sylvain Lehmann**, **Dr. Jean François Hernandez** and **Prof. Luca Cipelletti** for giving their availability to review and examine my thesis and this work. Our broad and dynamic exchange led to a constructive and didactic discussion. I am very grateful for all the advices and suggestions; it was a unique moment that I will always treasure and cherish. I wish to meet all of them again very soon and to eventually collaborate once I will move forward in my scientific career.

This thesis and the published results would have not been possible without the collaboration and friendly support provided by several great scientists.

Acknowledgements

I am grateful to **Professor Myriam Taverna** and **Dr. Emilie Rossi** for their support with ThT assay and the great collaborative work for the paper published in *Analytical Chemistry* Journal. I am thankful to **Pierre Sanchez** for his kind support and assistance with the LC-MS analyses.

I am grateful to **Professor Carmen Bartic** and **Dr. Olivier Deschaume** for the AFM studies and the wonderful collaborative work on the co-aggregation of Aβ peptides which was accepted in *ACS Chemical Neuroscience*, shortly after my thesis defense.

My warm thoughts and special acknowledgements go to **Laurent Boiteau**, **Philippe Gonzalez**, **Laurent Leclercq**, **Jean-Christophe Rossi**, and **Isabelle Desvignes** for their daily support in the lab and to **Marie-Sophie Monfort** for her kind and very helpful administrative aid.

Special thanks go also to my colleagues **Phu**, **Camille**, **Charly**, **Xiaolin**, **Laura**, **Sebastien** and **Nan**. I will never forget all the funny moments and all the happy and challenging days in the lab! I really hope to meet them again very soon and eventually collaborate in the future.

I am deeply thankful to **Dr. Maria Di Vincenzo** for all her wholehearted support. Her professional expertise together with her wise advices had a huge impact on me during the last years. Without her, many things would not have been possible. She has been a true inspiration for me! I am looking forward to continuing collaborating with her.

Finally, I would like to thank my **parents** for their endless support and unconditional love, which they contagiously spread throughout my entire life. They have been constantly there for me every step of the way. I would like to thank them for always believing in me and for guiding me with wisdom and passion. Without them, I could not be here chasing my dreams!

For me, the PhD was a one-time experience that not only opened the gates for a scientific career, but also prepared me for what comes next in life. Metaphorically, for me the PhD was like a boat trip on the sea. There were so many sunny days when it was so pleasant to stay on the deck, take some sun or go fishing, but there were also moments where I found myself in front of some storms when I thought that the boat was about to sink. However, I was never alone in this enterprise, and in this way, I would like to express my deepest gratitude to everyone who stood by my side and guided me in bringing the ship to its final destination.

Table of Contents

List of Publications

1. **Unraveling the Speciation of β-Amyloid Peptides during the Aggregation Process by Taylor Dispersion Analysis.**
   Deleanu, M.; Hernandez, J.-F.; Cipelletti, L.; Biron, J.-P.; Rossi, E.; Taverna, M.; Cottet, H.*; Chamieh, J.*. Research Article published in *Anal. Chem.*, 2021 (https://doi.org/10.1021/acs.analchem.1c00527)

2. **Taylor Dispersion Analysis and Atomic Force Microscopy Provide a Quantitative Insight into the Aggregation Kinetics of Aβ (1−40)/Aβ (1−42) Amyloid Peptide Mixtures.**
   Deleanu, M.; Deschaume, O.; Cipelletti, L.; Hernandez, J.-F.; Bartic, C.; Cottet, H.*; Chamieh, J.*. Research Article published in *ACS Chem. Neurosci.*, 2022 (https://doi.org/10.1021/acschemneuro.1c00784)

Abbreviations

AA - Amino acid

Aβ - β-amyloid

Aβ40-Aβ42 - Aβ(1-40) and Aβ(1-42) heteromolecular nuclei

Aβ-M+ - β-amyloid metal complexes

AβO - soluble β-amyloid oligomers

ACN - Acetonitrile

Ac_2O - Acetic anhydride

AD - Alzheimer's Disease

ADDLs - Aβ-derived diffusible ligands

AFM - atomic force microscopy

AICD - APP intracellular domain

ANS - 1-anilinonaphthalene-8-sulfonic acid

APP - amyloid precursor protein

ATC - 4-amino-(methyl)-1,3-thiazole-5-carboxylic acid

BGE - background electrolyte

BP - BODIPY® FL-C5

CAC - critical aggregation concentration

CE - Capillary electrophoresis

CD - circular dichroism

CHC - central hydrophobic cluster

CNS - central nervous system

CNT - classical nucleation theory

cAβ - commercial β-amyloid

Abbreviations

CR - congo red

CRLI - Constrained Regularized Linear Inversion

CTR - C-terminal region

CSF - cerebrospinal fluid

D - diffusion coefficient

DAB - 1,4-diaminobutane

DCM - Dichloromethane

DCMP - dicyanomethylene-4H-pyran

DIEA - N,N-diisopropylethylamine

DMF - Dimethylformamide

DLS - dynamic light scattering

DMSO - Dimethyl sulfoxide

DNA - deoxyribonucleic acid

Et_2O - Diethyl ether

EDANS - acetylaminoethyl-5-naphthylamine-1-sulfonic acid

EDTA - Ethylenediaminetetraacetic acid tetrasodium salt dihydrate

EM - electron microscopy

EOF - electroosmotic flow

ESI+ - electrospray ionization mode

FCS - fluorescence correlation spectroscopy

5(6)-FITC - fluorescein 5(6)-isothiocyanate

FTIR - Fourier transform infrared spectroscopy

HSA - human serum albumin

HATU - O-(7-Azabenzotriazol-1-yl)-1,1,3,3-tetramethyluronium hexafluorophosphate

Abbreviations

HCOOH-Formic acid

HFIP - 1,1,1,3,3,3-Hexafluoro-2-propanol

HMM - high molecular mass

iAβ - insoluble β-amyloid aggregates

iAβ5p - Ac-LPFFD-NH2

IDP - intrinsically disordered peptide

3-IPA - 3-indolepropionic acid

IR - infrared spectroscopy

LC - Liquid chromatography

LDH - lactate dehydrogenase

LIF - laser induced fluorescence

LMM - low molecular mass

LOD - limit of detection

MALDI-TOF/MS - Matrix Assisted Laser Desorption/Ionization Time of Flight Mass Spectrometry

MALS - multiangle light scattering

MD - molecular dynamic

MeOH - Methanol

MS - mass spectrometry

MWCO - molecular weight cut-off

NaCl - sodium chloride

NaOH - sodium hydroxide

NaN_3 - sodium azide

NH_4OH - ammonium hydroxide

NFTs - neurofibrillary Tau tangles

Abbreviations

NMR - nuclear magnetic resonance

NTR - N-terminal region

Pbf - 2,2,4,6,7-Pentamethyl-2,3-dihydrobenzofuran-5-sulfonyl

PG - protective group

PICUP - photo-induced cross-linking of unmodified proteins

Pip - Piperidine

PyBOP - Benzotriazol-1-yl-oxytripyrrolidinophosphonium hexafluorophosphate

RB - N-hydroxysuccinimide rhodamine B ester

R_h - Hydrodynamic radius

RITC - rhodamine B isothiocyanate

RP-HPLC - reversed-phase high-performance liquid chromatography

sAβ - soluble β-amyloid aggregates

SEC - Size exclusion chromatography

SDS-PAGE - sodium dodecyl sulfate polyacrylamide gel electrophoresis

5-SFX - hexanoic acid succinimidyl ester

SPPS - solid-phase peptide synthesis

SPM - scanning probe microscopy

TBAB - tetra-n-Butylammonium bromide

TDA -Taylor dispersion analysis

ThT- thioflavin T

TIS -Triisopropylsilane

TMR - tetramethylrhodamine

TRO - trodusquemine

Chapter I

State of the art

I.1. General aspects of amyloidosis and Alzheimer's disease

Amyloidosis refers to a group of rare and serious conditions caused by abnormal functions of proteins. These prion precursor proteins are termed amyloid and have the ability to self-associate with highly ordered cross β-sheet conformations throughout the body. The amyloidogenic pathways are generally driven by those abnormal conformations and can lead to the formation of both soluble species and to the extracellular formation of amyloid deposits, making it difficult for the organs and tissues to work properly[1]. Amyloidosis can be either localized or systemic and it can occur in various organs in the body such as the heart, kidneys, pancreas, and brain. Cerebral amyloidosis conditions are mainly considered to be localized forms as the brain is almost never directly involved in systemic amyloidosis and include several types of diseases such as Alzheimer, Parkinson and Huntington[2,3].

Alzheimer Disease (AD) is a chronic neurodegenerative disease and represents one of the major public health challenges of the 21st century making it the one of the most common types of dementia. It is associated with memory loss and significant changes in patients behavior such as difficulties in discerning time and place, lack of judgment, distress or developing struggles in speaking and writing, and eventually death[4]. It is believed that the early onset of AD begins at least 20 years before symptoms appear[4]. The exact causes leading to AD are still unknown, but it is believed to start in the brain due to a combination of age, genetic, environmental and behavioral factors (https://www.nia.nih.gov/health/what-causes-alzheimers-disease - accessed on October 2021). One of the main hallmarks leading to the development of AD revolves around the amyloid cascade hypothesis, first introduced by Hardy and Higgins in 1992[5], which states that the extracellular formation of amyloid plaques and the intracellular accumulation of neurofibrillary Tau tangles (NFTs), found in the brains of patients suffering from AD, occur as a consequence of the production of several β-amyloid (Aβ) species[4–6]. It is estimated that by 2030, one out of three people over 85 years old will suffer from AD and healthcare costs will increase significantly up to ~$1.1 trillion per year by 2050 unless novel breakthroughs for finding a treatment will emerge. After nearly four decades of extensive funding and research efforts to unravel the mechanisms

underlying AD, none of the currently available strategies for combating this disease were yet successful in providing a significant breakthrough[7,8].

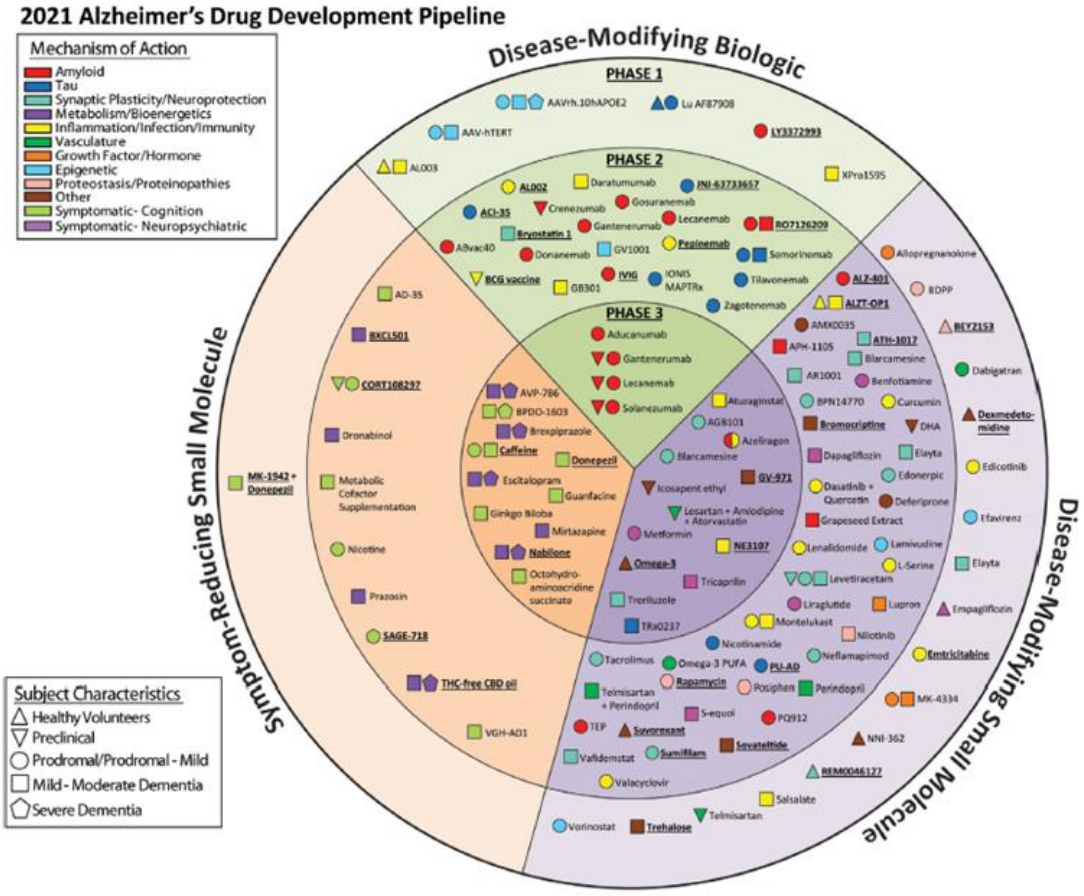

Figure 1. Representative chart of all AD treatments that are in clinical trials since January 5, 2021. The symptom-reducing small molecules are represented with the orange gradient. The disease-modifying biologic treatments are represented with the green gradient. The disease-modifying small molecules are depicted with a purple gradient. The inner, middle and third rings are outlining the treatments which are currently in phase 1, 2 and 3 of trials. The symbols represent for which kind of group of patients the therapeutic agents are addressed and color stands for the type of the targeted mechanism (adapted form Cummings *et al.*[8]).

The pie chart depicted in Figure 1 provides a list of all therapeutic strategies in clinical trials as of January 2021 to combat this type of dementia. These treatments can be divided into three main categories: symptom-reducing small molecules, disease-modifying biologic, and disease-modifying small molecules[8].

System-reducing drugs aimed at reducing behavioral and neuropsychiatric symptoms and represent ~20% of the total therapeutic strategies currently under evaluation, while the remaining ~80% is represented by disease-modifying drugs intended to change the biology of AD[8]. About

~7% of the disease-modifying drugs are used to combat the hyperphosphorylation of Tau protein, while ~11% have Aβ species as primary targets[8].

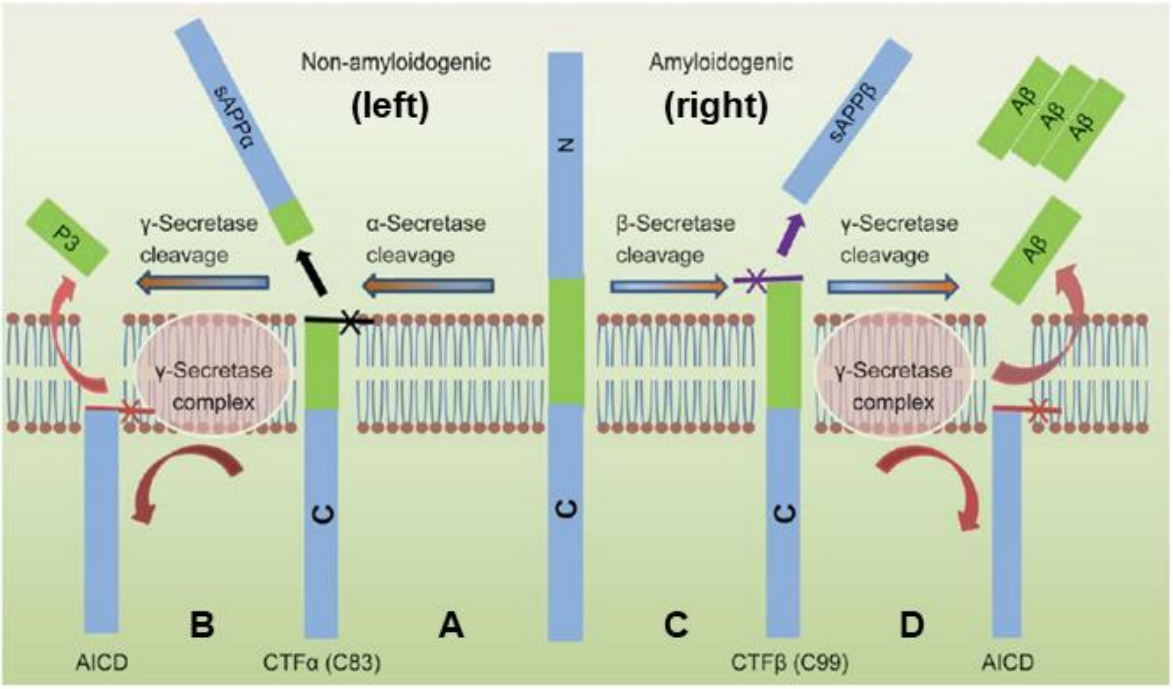

Figure 2. Schematic map showing the possible APP processing pathways: non-amyloidogenic (**left**) and amyloidogenic (**right**). In the non-amyloidogenic pathway, APP is cleaved by (**A**) α-secretase to form a soluble N-terminal fragment, sAPPα, and a C-terminal fragment, CTFα (C83). (**B**) The CTFα is further cleaved by γ-secretase yielding a soluble N-terminal fragment, P3 and AICID. In the amyloidogenic pathway, APP is cleaved first by (**C**) β-secretase, yielding a soluble N-terminal fragment sAPPβ and a membrane-bound C-terminal fragment, CTFβ (C99), which is then cleaved by (**D**) γ-secretase yielding the AICD domain, and a soluble N-terminal fragment, sAPPβ, representing the Aβ monomers that further undergo the amyloid cascade of reactions leading to the formation of soluble toxic species and to the accumulation of amyloid plaques in the extracellular space of the brain of patients suffering from AD (adapted from Chen *et al.*[3]).

The amyloid hypothesis states that the production of Aβ peptides occurs during the catabolic process of the amyloid precursor protein (APP)[3,5]. The processing of APP can occur in either a non-amyloidogenic or amyloidogenic pathway (Figure 2). The non-amyloidogenic processing occurs when the protein undergoes its normal biological functions (Figure 2 - left). The protein is first cleaved by an enzyme α-secretase to form a soluble N-terminal fragment (sAPPα) considered neuroprotective, which is believed to be involved in the enhancement of neurite growth and neuronal survival, and an 83 amino acid long C-terminal fragment (CTFα), which is instead preserved in the membrane[9]. The CTFα is further cleaved by a presenilin-containing γ-secretase enzyme yielding a soluble N-terminal fragment (P3) and APP intracellular domain (AICD) (Figure 2 – left B)[10]. In the amyloidogenic pathway, APP is cleaved first by a transmembrane aspartic

protease enzyme, β-secretase, yielding a soluble N-terminal fragment (sAPPβ) and a longer membrane-bound C-terminal fragment (CTFβ) comprised of 99 amino acids, compared to the one generated during the action of α-secretase, as the cut is performed closer to the N-terminus of APP (Figure 2 – right C)[11]. The β-site of APP is more enriched in neurons and may trigger the amyloidogenic processing pathway in the brain and diminishing neuronal survival[12]. The second cleavage along the pathway (Figure 2 – right D) is performed by γ-secretase but this time acted upon CTFβ, yielding the same AICD domain and N-terminal soluble fragment, longer than P3, representing Aβ monomers of various forms and lengths[13]. The exact role of AICD is not yet fully understood, but it is believed to be involved in nuclear signaling to associate with different proteins[13]. It was recently found that the resulting γ-secretase complexes are mainly comprised of several proteins[14], but these structures are still under investigation to better understand their aggregation mechanism. And although the monomers are requisite for neuronal function, they can further initiate the aggregation process that leads to the formation of highly ordered species which may or may not be toxic, and of fibrils that further accumulate in the extracellular space of the brain to form the amyloid plaques[3,6,15,16].

The following sections aim to provide information regarding the current knowledge of the aggregation mechanism of Aβ by discussing the dynamic evolution of Aβ species, with particular focus on their size, shape, and ability to self-assemble based on structural changes that are governed by a wide range of both intrinsic and extrinsic physico-chemical parameters. The discussion is then followed by the description of small molecules designed to inhibit several species and/or the self-assembly pathways and conclude with a brief overview of some of the most employed biophysical techniques that can monitor the kinetics of the aggregation process and the size and morphology of the species.

I.2. Current knowledge regarding the aggregation mechanism of Aβ peptides

As presented in the previous section, the amyloidogenic pathway begins when β-secretase acts on the active β-sites of APP, which consequently leads to the generation of Aβ monomers. These monomeric species are then capable to undergo a supramolecular nucleation-condensation polymerization reaction, or simply called the nucleation process, leading to the formation of

soluble toxic intermediates that can further disperse throughout the cells, the capillary vessels or into body fluids and fibrils responsible for the accumulation of the amyloid plaques found in the brains of patients suffering from AD[17–20].

Because native Aβ belong to a class of intrinsically disordered peptides (IDPs), they can undergo unfolded, partially folded and nucleus favored conformations (Figure 3) in strong equilibrium with each other[21,22]. Thus, the nucleation process is favored due to a specific conformation that further dictates the ability of these species to aggregate[17,22–25], but this aspect has generated numerous hypotheses and controversies regarding the aggregation mechanism.

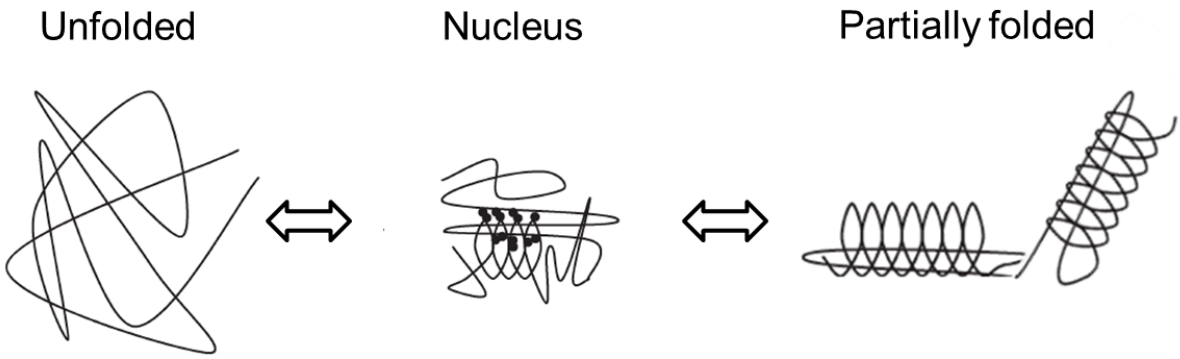

Figure 3. Possible equilibrium states during the nucleation–condensation mechanism of peptide folding. Folding is promoted by the generation of a critical nucleus which presents specific structure interactions so that further conformations can rapidly condense on the nucleus (adapted from Nölting *et al.*[22]).

According to the classical nucleation theory (CNT), early molecular studies of Aβ aggregation suggested that the process proceeded via a single-step nucleation reaction[20,25]. The CNT theory states that if a small group of monomers exhibits a high interfacial free energy with respect to water molecules, then the tendency to dissociate into single monomers increases[23,25,26]. But, as the species evolve in the course of aggregation, the size of the intermediates increases becoming more stable, and thus the formation tendency of the species would be favored via monomer addition because the aggregate dissociation becomes less significant and it would require a lot of energy to detach[21,23,26,27]. Due to the development of novel biophysical techniques along with the advancement in the computational methods of molecular dynamic (MD) simulations, the CNT model underwent many adjustments as it could not be fitted using the novel experimental data along with the gradual discovery of a wide range of aggregation intermediates[23,28].

In the early years of AD diagnosis, fibrils were the main therapeutic targets of AD because the formation of amyloid plaques represented one of the main hallmarks behind AD[19]. It was not until

1997 that Teplow and co-workers first introduced protofibrils as precursors for fibrils, while oligomers were considered to be just transient species along the aggregation pathway[29]. Only a year later, Klein's group introduced the amyloid oligomer hypothesis by showing that synthetic preparations of soluble Aβ oligomers, introduced as Aβ-derived diffusible ligands (ADDLs), are potent central nervous system (CNS) neurotoxins responsible for nerve cell death[18]. Later on, Lee's group showed that Aβ displayed amphiphilic characteristics in aqueous solution and that the C-terminal region was able to form a hydrophobic core in water[30]. It was further proposed by Bitan *et al.* that the nucleation proceeds through stable pentamers and hexamers, defined as paranuclei, on which monomers attach for further elongation. However, more recent studies suggest that dimers and trimers might be the smallest critical nuclei as they are able to adopt different types of β-sheet arrangements that are likely favored by a β-hairpin conformation[31,32]. It was also established that the formation of the nucleus is favored only above a certain concentration[33] but a consensus regarding the precise type and size of the critical nuclei has not yet been reached.

Based on these observations and discoveries, the oligomers have attracted much attention and became the primary therapeutic targets in the development of disease-modifying compounds able to modulate the aggregation process[34,35]. Over the last decade, it was also revealed that the aggregation occurs through a secondary nucleation mechanism where preformed aggregates can serve as catalytic surfaces for monomer addition leading to the formation of other oligomeric species[23,36,37]. Therefore, it is now universally accepted that the aggregation process proceeds through a multi-step chain of reactions, often referred to as the amyloid cascade of reactions, where monomers can begin to self-assemble over a specific concentration into high-ordered aggregates through at least one type of critical nucleus of a certain size which can be favored either through a specific conformation adopted by the monomers and/or by preformed aggregates such as protofibrils and fibrils[25,33,37,38].

I.2.1. Possible aggregation pathways and the dynamic evolution of Aβ species involved in the aggregation process

A schematic map of the aggregation process is depicted in Figure **4** where the current consensus regarding the aggregation mechanism and some of the questions that have yet to be answered are outlined. As shown in the figure, native Aβ monomers are in a dynamic equilibrium with their unfolded and/or partially folded conformations. At least one of these conformations (e.g.

β-hairpin) serves as an intermediate that favors the assembly of monomers into larger aggregates. The aggregation is generally characterized as a sigmoidal growth (blue solid line) of fibrils concentration until nearly all free aggregation-prone species are converted into a fibrillar form. This generic view is derived from experimental data obtained from the thioflavin T (ThT) fluorescence assay, which is currently the most widely used technique for assessing the kinetics rate and mechanisms of the aggregation process. Briefly, the ThT assay provides information regarding the accumulation of fibril mass as a function of time, and generally is characterized as a sigmoidal increase of the signal up until the maximum fibril yield is reached[39].

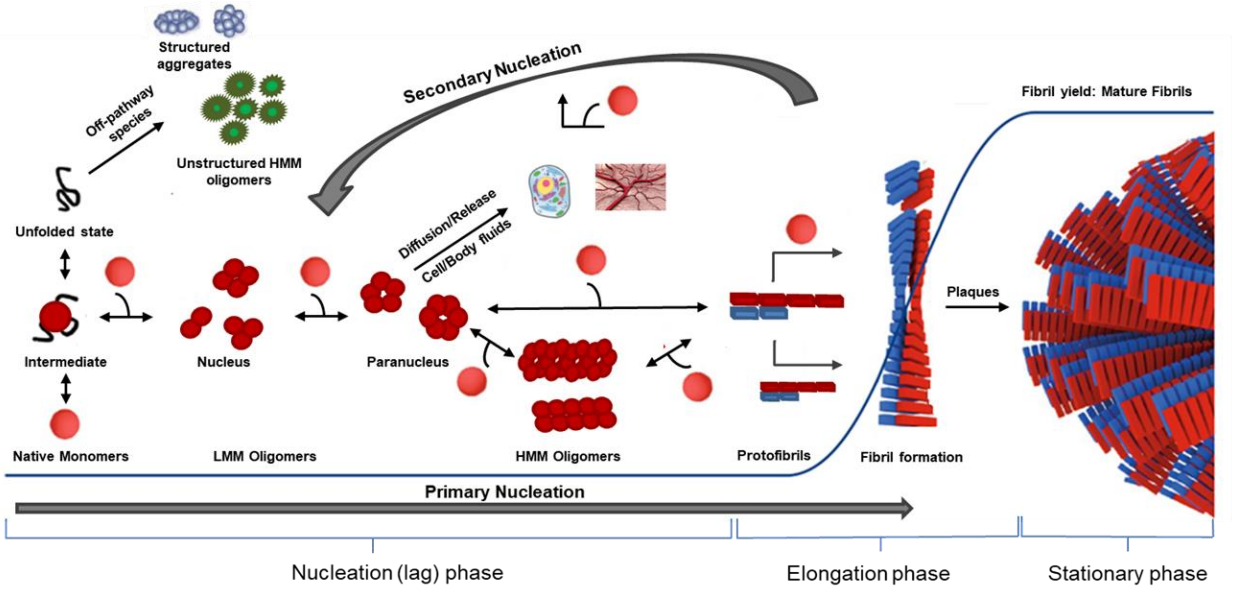

Figure 4. Schematic map outlining the current knowledge of the aggregation mechanism showing the main phases of the amyloid aggregation process: 1) The Nucleation or lag phase, where the oligomers and the protofibrils are formed; 2) the elongation phase where the fibrils are formed and finallky 3) the stationary phase and the deposition of mature fibrils (senile plaques). Adapted from Lee *et al.*[37], Törnquist *et al.*[23], Iadanza *et al.*[15], and Roychaudhuri *et. al.*[21].

The aggregation process first involves the lag phase related to the early stages of the aggregation, in which low molecular mass (LMM) oligomers are first generated through a favored conformation and they may or may not serve as critical nuclei along the aggregation pathway for the formation of high molecular mass (HMM) oligomers and larger aggregates. All the species formed during this nucleation step are believed to be in strong equilibrium with each other[40,41]. The process is then followed by an elongation phase, which can be translated from the slope generated during the ThT assay in which protofibrils and fibrils begin to form. As the elongation proceeds, fibrils may allow the formation of secondary nucleation sites that can serve as catalysts for monomer addition, especially if they are subjected to mechanical stress. The process then reaches a stationary phase

when all the aggregation-prone species are consumed, leading to a maximum fibrils yield characterized as a plateau of mature fibrils[15,23,39].

According to the current consensus there are two preferred nucleation pathways: primary and secondary nucleation. Primary nucleation can be defined as supramolecular nucleation where monomers self-assemble into fibrils via a specific critical nucleus by monomer addition without the contribution of preformed aggregates[23,42]. It can either occur homogeneously between the monomers or heterogeneously by the interaction with other particles or surfaces[27] such as metals[43,44], proteins[17,45], air-water interface[46], membranes[17]. Thus, primary nucleation occurs only during the lag phase.

Secondary nucleation is a supramolecular reaction in which monomers can interact with preformed aggregates creating a nucleus that further self-catalyzes the aggregation process, leading to generation of new Aβ species[47,48]. It is currently considered that secondary nucleation can only occur between monomers and aggregates generated by the same type of monomer[23]. Thus, secondary nucleation can be promoted only after the elongation phase has been reached or if seeds are present during the initial stages of the aggregation.

Another aspect that allows to outline the complexity of the aggregation process is related to the discovery of the off-pathway species, which mainly refers to species that do not follow the amyloid cascade of reaction[49,50]. These species are often characterized as unstructured and amorphous species, and are generally not recognized by conformational antibodies[37]. Therefore, these off-pathway species can be differentiated from on-pathway aggregates as they are often nontoxic and more stable, and can possibly be detected during the stationary phase.

So far, a wide range of on-pathway species were extensively described and reviewed in the literature[21,28,37,51,52]. They can be divided into four main categories of Aβ populations as follows: monomers, oligomers, protofibrils and fibrils.

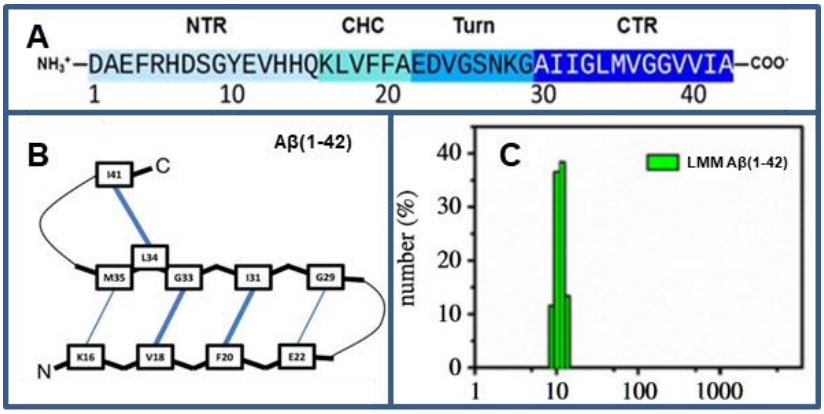

Figure 5. (**A**) Main characteristics of Aβ(1-42) peptide sequence: NTR (residues 1-16), CHC (residues 17–21), Turn (residues 22–29), and CTR (residues 30–42). These characteristics are generic also for other Aβ isoforms and variants (adapted from Chakraborty *et al.*[24]). (**B**) Example of a simulated β-Hairpin model for Aβ1−42 highlighting CHC and CTR interactions (adapted from Nasica-Labouze *et al.*[17]). (**C**) Example of the oligomer size distribution of LMM Aβ(1-42) obtained by DLS with a maximum centered around 10 nm (adapted from Liu *et al.*[53]).

Monomers are linear or truncate peptides comprised of 37-49 amino acids[3]. They are produced in the amyloidogenic pathway as a result of the sequential cleavage of APP by β- and γ-secretases and represent the starting point in the amyloid cascade of reactions[5,21]. Based on the current consensus, the Aβ sequence presents four main structural characteristics (Figure 5 A for Aβ(1-42) peptide): a randomly disordered N-terminal region (NTR) followed by a central hydrophobic cluster (CHC) which is in direct contact with the hydrophobic C-terminal region (CTR), followed by a turn that helps the monomer to stabilize into a β-hairpin like conformation (Figure 5 B), which is believed to serve as an intermediate that favors the formation of the nucleus[17,24]. In solution, monomers exhibit a disordered conformation[54]. Then, as the nucleation reaction proceeds, they can further self-assemble via the β-hairpin conformation to form highly-ordered species comprised of extended β-sheets, as revealed by a wide range of structural analyses accompanied by MD simulations[17,24,51,52,55]. It was also revealed that these species are in equilibrium with LMM oligomers shortly after the dissolution of the peptide[56,57] and, for this reason, they are often termed as LMM Aβ[58]. However, because their size is very similar, they are generally characterized together (Figure 5 C) as discussed more thoroughly after. It was also found that the monomers are non-toxic and in healthy persons they were found to be neuroprotective[16].

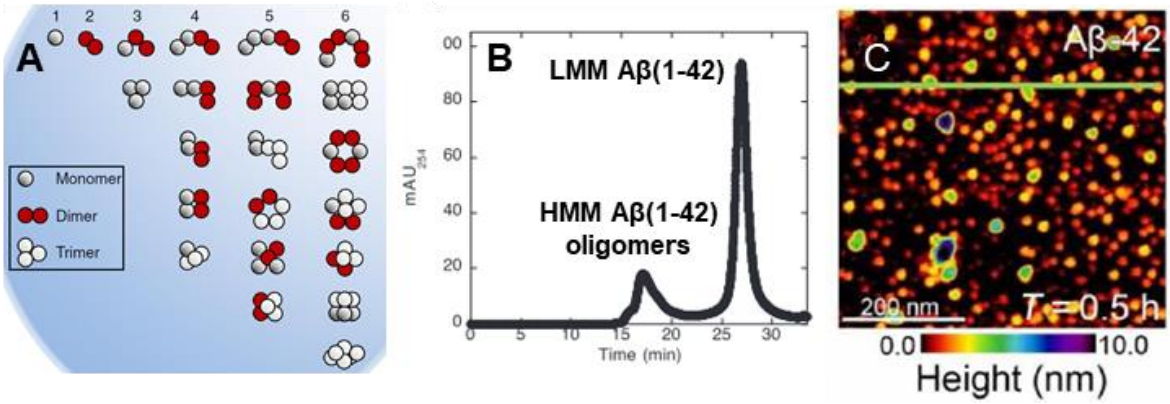

Figure 6. (**A**) Possible LMM oligomeric assemblies that may or may not serve as nuclei/paranuclei ranging from monomers to hexamers (adapted from Hayden *et al.*[51]). (**B**) Representative SEC separation of HMM Aβ(1-42) oligomers (eluting at 16 – 17 min) from LMM Aβ1–42 fraction (28 – 29 min) using a Superdex 75 column (adapted from Watanabe-Nakayama *et al.* [40]). (**C**) AFM image of spherical Aβ(1-42) oligomers having a mean diameter of 8.4 ± 2.1 nm (adapted from Nirmalraj *et al.*[59]).

An oligomer can be defined as a reaction product which contains at least two monomers[27]. They can be divided in two categories: LMM oligomers (≤ 6 mers) and HMM oligomers (≥7 mers). The LMM oligomers are considered to be critical nuclei. Due to their small similar size and high propensity to aggregate, a wide variety of LMM oligomers can be formed during the lag phase. In Figure 6 A, several possible LMM oligomeric assemblies are proposed based on the addition of monomers, dimers and tetramers and are generally less structured than fibrils. Thus, not all these structures can represent critical nuclei.

A critical nucleus can be defined as the most thermodynamically unstable species, presenting the highest Gibbs free energy along the aggregation pathway, which grows at a lower rate than more structured high-order aggregates and is generally favored by a β-hairpin conformation adopted by the monomers or by the presence of seeds such as protofibrils and fibrils[23,25,36]. On this basis, very few methods can provide accurate information regarding their nature, and only some of them are suitable form monitoring their evolution in real time. For example, dynamic light scattering (DLS) allowed to estimate the size (hydrodynamic radius, R_h) of the LMM Aβ between 1.4 and 10 nm[29,53,60–62]. However, light scattering techniques can be rapidly biased by the formation of larger objects and the smaller transient oligomers become less detectable[29,63]. On the other hand, imaging techniques such as electron microscopy (EM) or atomic force microscopy (AFM) cannot follow in real time the aggregation process and are difficult to implement for the detection of LMM species due to their small size[17,63]. However, some studies by EM and AFM revealed the presence of granular species having a size between 1 and 5 nm and were attributed to the LMM species[36,56].

On the other hand, HMM oligomers are considered to be metastable species and are believed to be either unstructured and stable off – pathway species, or structured aggregates which may serve as building blocks for protofibrils or may dissociate back into monomers capable of promoting the nucleation pathway[40]. Many types of oligomers reported in the literature and prepared in vitro resemble to the ones detected in the brain and biological fluids, or have been isolated from the brain of transgenic mice such as ADDLs, globulomers, Aβ*40 (40 kDa) or Aβ*56 (56 kDa)[18,28,64]. The mass of HMM oligomers was found to be within the range of 40 kDa – 1 MDa[28,34], and can be better evaluated using imaging methods as compared to LMM oligomers. They are often characterized as large spherical aggregates having a diameter of 5 – 25 nm by AFM[21,36,59] or as short prefibrillar filaments of about 5 nm width and up to 100 nm long by EM[40,65], looking like the protofibril structure. Depending on their nature, oligomers can have various toxic effects upon the nerves and cells and are often associated with selective neuronal death, calcium homeostasis, oxidative stress, Tau hyperphosphorylation, synapse deterioration, receptor redistribution and insulin resistance, making them primary therapeutic targets in AD[18,66–68]. In addition, they can be also detected in body fluids, such as cerebrospinal fluid (CSF) and blood plasma, and they can accumulate in the extracellular part of the brain by surrounding the amyloid plaques[69–71].

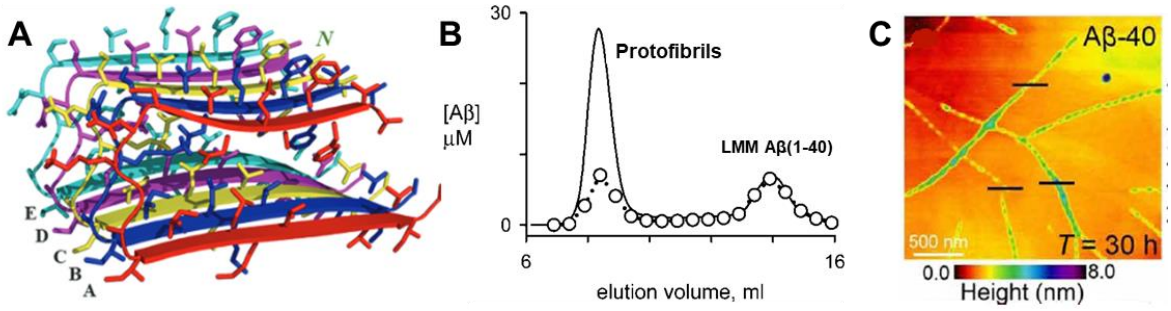

Figure 7. (**A**) Extended β-sheet Aβ(1-42) protofibril model (PDB: 2BEG) characterized by β-strand-turn conformations (CHC residues: 18-26; Turn residues: 27-30; CTR residues: 31-42) arranged in a parallel alingement (adapted from Kaur *et al.*[72]). (**B**) Representative SEC separation of Aβ(1-40) protofibrils (eluting at 7 – 9 min) from LMM Aβ1–40 fraction (13 – 15 min) using a Superdex 75 column (adapted from Nichols *et al.*[62]). (**C**) AFM image of Aβ(1-40) protofibrils presenting a charcteristic nodular structure and having a mean height diameter of 3.9 ± 1.6 nm (adapted from Nirmalraj *et al.*[59]).

Protofibrils are metastable and prefibrillar species presenting a greater β-sheet content (Figure 7 A), and consequently a higher stability than oligomeric species[28,72]. They are the largest soluble intermediates that lead to fibrils and begin to form during the elongation step of the aggregation

process[41]. They can be much better monitored and characterized by using EM and AFM techniques compared to oligomeric species (Figure 7 C) and can be also detected and monitored by size exclusion chromatography (SEC) and DLS analyses[28,62,73]. It has also been shown that protofibrils can bind ThT but to a smaller extent than fibrils[41]. They can be prepared and isolated mainly by SEC (Figure 7 B) under specific conditions[28,62] and, generally, are not able to self-associate into fibrils in the absence of monomers[36], except under physiological salt conditions (e.g. 100 – 150 mM NaCl) where they can further self-elongate *via* a lateral-association mechanism and can also act as seeds for catalyzing the aggregation process[28,62,74]. During their elongation, the average R_h was found to be within the range of 50 – 240 nm[62,74]. While these metastable species present a smooth and curvilinear shape often characterized by a twist and are less rigid than fibrils, they present a width of 5 - 10 nm and lengths up to 200 nm using imaging techniques[28,62]. Up until recent years, protofibrils were not considered to be as toxic as the oligomeric populations, but recent finding suggests that at least some types of protofibrils are also involved in neurodegeneration leading to AD, and it is forecasted than in the following years they can become primary therapeutic targets as well[75].

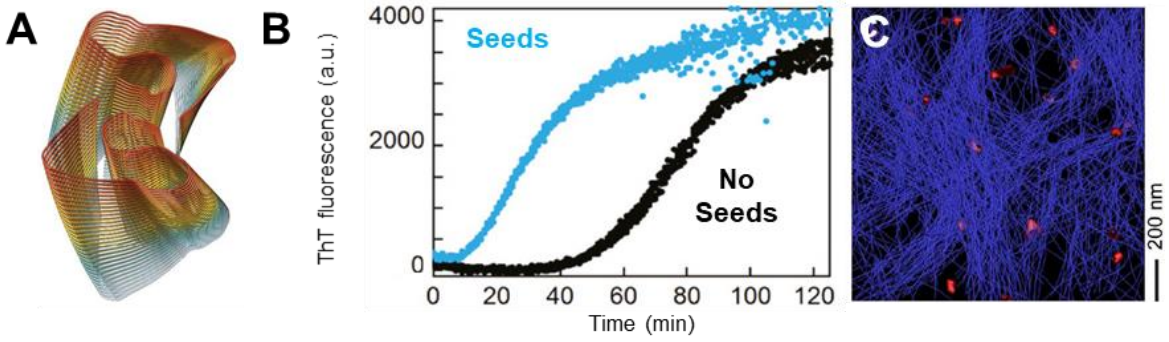

Figure 8. (**A**) 3D representation of an atomic model of the fibril obtained by cryo-EM characterized by a parallel cross-β structure of two interwined protofilaments and presenting an overall LS topology (adapted from Gremer *et al.*[76]). (**B**) ThT assay of Aβ(1-42) with (light blue symbols) or without (black symbols) 1 % of fragmented fibrils (seeds). Example of a secondary (seed-dependent) mechanism where fragmented fibrils are catalyzing the aggregation of the monomers (adapted from Linse[77]). (**C**) Representation of a 3D amyloid star fibril (blue) network in lipid vesicles (red). Fibrils presented a mean width distribution of 8.7 ± 1.4 nm and lipid vesicle diameter varied from 50 – 300 nm (adapted from Han *et al.*[78]).

Fibrils represent the end products of the aggregation process and, as protofibrils, they start to form mainly during the elongation phase. They represent the most stable species and have the most enriched β-sheet content compared to all the other soluble populations. Generally, they are comprised of 2 – 6 protofilament subunits and are more rigid than protofibrils and present a cross sectional diameter of 2 – 20 nm with lengths of more than 10 µm[28,62,76,79]. They were found to be

polymorphic as multiple types of fibrils, able to accumulate into different kinds of networks (Figure 8 C) and, as described in the literature, their formation depends on a wide range of physico-chemical parameters[17,80]. One recent structure was recently resolved by *cryo*-EM presenting a LS topology comprised of a parallel cross-β structure of two intertwined protofilaments (Figure 8 A)[76]. Fibrils are considered to be the main types of seeds (Figure 8 B) that favor the secondary nucleation mechanism[23,77]. According to the current consensus, the amyloid fibrils are no longer considered to be species of interest in the development of therapeutic strategies for combating AD, but rather are considered to be disease-relevant species due to their tendency to accumulate, leading to the formation of plaques surrounded by a halo of oligomers found in the brains of patients suffering of AD[6,15,23,27].

The most common isoforms produced by APP are Aβ(1-40) and Aβ(1-42), the latter being considered the core of the aggregation process as it was found to generate more toxic species[34,81]. However, mutations caused by abnormal processing of the APP can lead to the generation of truncated peptides of interest, such as E22G, H6N and D7N, even if they are less abundant than the common isoforms[82,83]. It is well known that Aβ(1-42) has the tendency to aggregate faster than Aβ(1-40)[61]. The difference in the oligomerization pathways of the two isoform centers around the two extra amino acids, Ile[41] and Ala[42], which Aβ(1-42) possess at the C-terminus[56]. Based on this finding, it is currently believed that the aggregation is driven by a hydrophobic effect and it proceeds through different types of critical nuclei[17,31,56]. It was also established that Aβ(1-42) derived species can induce more neuronal damage than that generated by Aβ(1-40)[81]. Some recent studies also suggest that that the size of Aβ(1-40) oligomers is higher than those generated by Aβ(1-42)[84] and that the ones generated by Aβ(1-40) are less abundant than the ones produced by Aβ(1-42)[59].

Beyond these aspects, the challenge to better understand the aggregation mechanism also arises from the difficulty of reproducing the results described in the literature due to different analyses conditions, biophysical techniques and a wide range of factors that may affect the process in various ways[17,63] and are described in more detail in the following subsections.

I.2.2. Factors affecting the aggregation process of Aβ peptides

The evolution of the Aβ species is quite complex since many types of intermediates were identified along the aggregation pathway. Further, their formation, size, shape, and toxicity are

strictly dependent on many factors governing the aggregation mechanism. These factors can be intrinsic or extrinsic, such as the nature of the peptide, concentration, pH, ionic strength, temperature, and incubation conditions[17,85]. In addition, other studies have shown that the nucleated aggregation is also governed by stochastic factors[86], making getting reproducible results a challenging task[87]. The following subsections aim to highlight how these factors affect the aggregation process.

I.2.2.1 Effect of Aβ intrinsic properties upon the aggregation process

The intrinsic factors are related to the structural features of the peptide sequence, therefore, they mainly relate to the nature of the peptide[85]. The main intrinsic aspects that influence the aggregation mechanism are the net charge of the peptide sequence[85], the chain length of the Aβ isoforms[56], mutations that occur at different amino acids positions[82] , and specific modifications that occur at different binding sites of the peptide.

I.2.2.1.1. Net charge of Aβ peptides chain

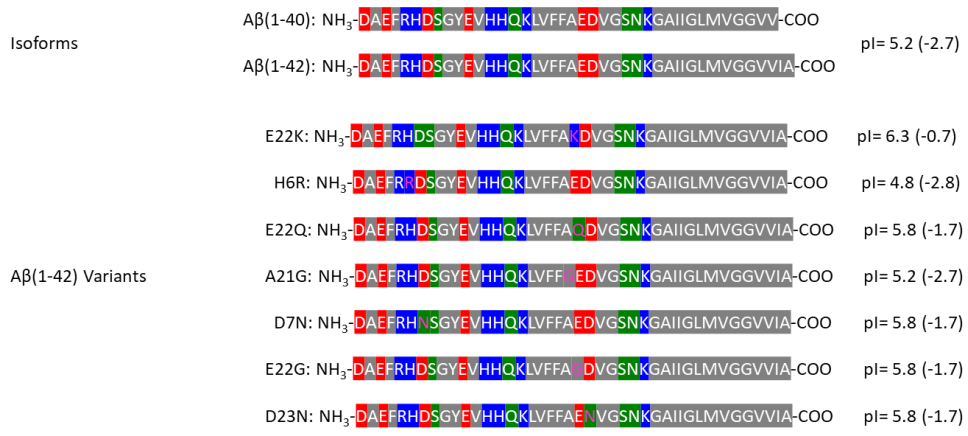

Figure 9. Peptide sequence of some of the most common isoforms and variants. The filled colors are related to the amino acid character: hydrophobic (grey), hydrophilic (green), negatively charged (red), positively charged (blue). The amino acid letter in pink represents the amino acid residue where the mutation occurred. The pI and the net charge (in brackets) values were calculated using BACHEM peptide calculator at pH 7.0 (https://www.bachem.com/knowledge-center/peptide-calculator/, accessed on July 2021).

A small percentage of familial forms of AD may suffer mutations in APP, leading to changes in the sequence of the common forms of Aβ peptides[3]. Mutations may occur especially during the early-onset of AD; however, they are not detected in all the patients suffering from this

dementia[3,82]. More than 30 mutations have been reported in the literature so far, and some of the most common variants of interest are the Dutch (E22Q), Flemish (A21G), Italian (E22K), Arctic (E22G), Iowa (D23N), English (H6R) and Tottori (D7N) mutants, which occur within the NTR and CHC regions of the peptide sequence[3,82]. Depending on the position where the mutation occurs, they can also affect the overall net charge of the peptide by reducing specific effects in the peptide chain while promoting others. Indeed, electrostatic attractions take place between Aβ monomers and aggregated species and increase the aggregation behavior of Aβ peptides[88]. For example, in the case of Aβ(1-42) mutations, the total net charge of the sequence chain of the E22K variant changed from -2.7 to -0.7 and to -1.7 for E22Q, E22G, D23N and D7N respectively, whereas for the H6R mutation the charge was only slightly affected and for A21G the net charge was unchanged. Thus, an increase in the electrostatic attractions can be expected for E22Q, E22G, D23N, D7N and E22K which could lead to an increase in aggregation behavior, the highest effect being foreseen for E22K, while no significant changes should be expected for H6R and A21G just by considering this factor.

I.2.2.1.2. Chain length of Aβ isoforms

As mentioned before, Aβ monomers generated from APP have typical lengths of 37-49 amino acid residues[3]. It was also reported that both the oligomer size distribution and the aggregation kinetics can be affected for Aβ isoforms that present different chain lengths.

In a study performed by Bitan *et al*[56], the authors employed a photo-induced cross-linking of unmodified proteins (PICUP) to trap the LMM oligomers formed during the aggregation process of Aβ(1-39), Aβ(1-40), Aβ(1-41), Aβ(1-42) and Aβ(1-43). Aβ peptides were first pretreated by SEC and then immediately subjected for the PICUP reaction. After the reaction was finalized, the cross-linked LMM Aβ peptides were analyzed by sodium dodecyl sulfate polyacrylamide gel electrophoresis (SDS-PAGE) analysis and, as can be seen in Figure 10 A, Aβ(1-39) and Aβ(1-40) were found to produce a monomer – tetramer equilibrium, as the bands produced strong intensities up to 17 kDa, while for Aβ(1-41), oligomers up to octamers were generated as the intensity increased up to ~30 kDa.

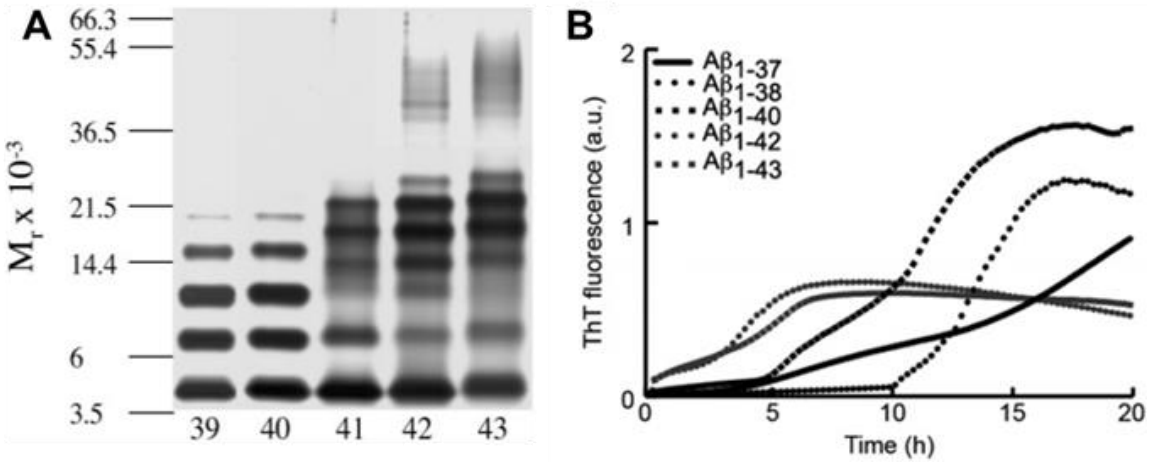

Figure 10. Examples of chain-length effect upon the aggregation process. (**A**) SDS-PAGE analysis of SEC-isolated cross-linked Aβ (1-39) – Aβ(1-43) (left to right). Experimental conditions: Sample: ~25 µM cross-linked Aβ; 10 mM phosphate buffer pH 7.4. Incubation: quiescent conditions at 25 °C. Gel lane: tris-tricine-10-20 % polyacrylamide (adapted from Bitan *et al.*[56]). (**B**) ThT fluorescence assay of Aβ isoforms of different lengths. Experimental conditions: Sample: 1 µM Aβ + 12 µM ThT; 50 mM Tris buffer / 1 mM EDTA, pH 7.5. Incubation: quiescent conditions at 25 °C. Fluorescence detection: λ_{Em}= 480 nm; λ_{Ex}= 430 nm (adapted from Vandersteen *et al.*[83]).

Finally, the bands of Aβ(1-42) and Aβ(1-43) showed also the formation of highly ordered species of 30-60 kDa. By combining these observations with other structural and morphological analyses, the authors were able to demonstrate that Val^{40} is not essential to produce the monomer – tetramer equilibrium, while Ile^{41} only mediates the initial oligomerization and Ala^{42} is responsible for the formation of stable pentamer or hexamer structures, which serve as paranuclei that further provide a template for the formation of larger aggregates[56]. However, other studies have suggested that the smallest critical nuclei are dimers and trimers, and a consensus regarding the exact critical nucleus size has not yet been reached[17,31].

In Figure 10 B**,** the ThT fluorescence assay performed by another group is depicted for several Aβ of different chain lengths[83]. The kinetics of the aggregation were faster with increasing the C-terminal length further suggesting that the process is driven by a hydrophobic effect. The authors also monitored the aggregation by imaging methods and showed that the fibril morphology of Aβ(1-37), Aβ(1-38), and Aβ(1-40) resulted in the formation of extended fibrils, while densely packed fibrillar networks were observed for Aβ(1-42) and Aβ(1-43). Based on these observations, the authors suggested that the highest fluorescence intensity plateau is detected for Aβ(1-37), Aβ(1-38), and Aβ(1-40) because the longer fibrils provide more access to the ThT dye[83].

I.2.2.1.3. In vitro modifications within the peptide sequence

Many modifications can occur within the Aβ sequence, such as N-terminal modifications, racemization, isomerization, oxidation, phosphorylation or glycosylation. Then, depending on the type, they can occur either in vitro or in vivo, or both[89]. The most common in vitro modifications are usually performed at the N-terminus of Aβ by tagging them with specific fluorophores used purposely to study the aggregation process at the physiological concentration[90].

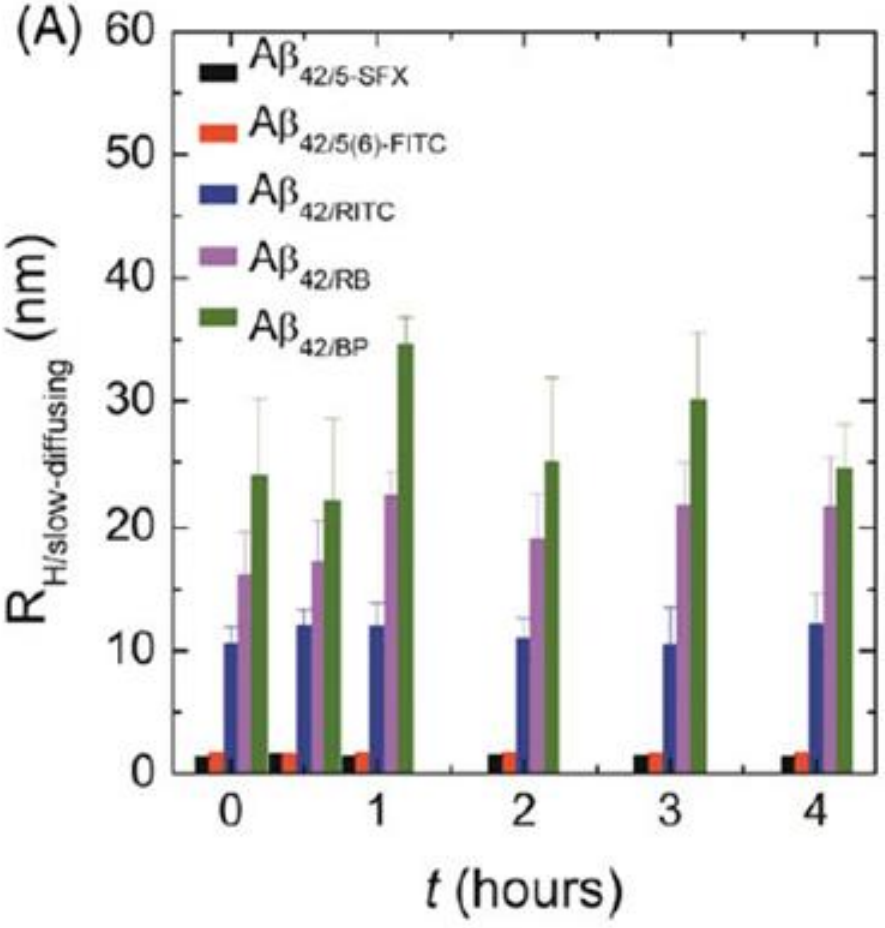

Figure 11. FCS monitoring of the hydrodynamic radius evolution of the oligomers obtained for different dyes at different selected time: 5-SFX – black bar, 5(6)-FITC – orange bar, RITC – blue bar, RB – violet bar and BP – green bar. Experimental conditions: Sample: 5 µM Aβ native/tagged mixtures (Labelling efficiency: Aβ42/BP - 46.2%; Aβ42/RB - 39.6%; Aβ42/RITC - 57.2%; Aβ42/5-SFX - 48.7%; Aβ42/5(6)-FITC - 59.8%; 10 mM phosphate buffer, 154 mM NaCl, pH 7.4. Incubation: quiescent conditions at 25 °C. FCS detection: 488 nm Argon multiline laser (BP, 5-SFX, 5(6)-FITC); 543-nm He-Ne laser (RB, RITC). Measurements were acquired by diluting the Aβ samples with the sample matrix to a concentration of 5 nM for each selected incubation time (adapted from Zheng *et al.*[91]).

Although several studies have pointed out that the fluorophores can affect the aggregation mechanism in various ways, these aspects are often disregarded[91–93]. In a study performed by Zheng *et al.,* fluorescence correlation spectroscopy (FCS) was used to monitor the influence of

hexanoic acid succinimidyl ester (5-SFX), fluorescein 5(6)-isothiocyanate (5(6)-FITC), rhodamine B isothiocyanate (RITC), N-hydroxysuccinimide rhodamine B ester (RB) and BODIPY® FL-C5 (BP) tags on the oligomerization of Aβ(1-42). The labeled peptides were incubated at a concentration of 5 µM and, diluted to a 5 nM concentration before each FCS measurement to measure the hydrodynamic radius (Figure 11). Shortly after the dissolutions, the systems containing BP, RB, RITC, 5-SFX, and 5(6)-FITC presented an initial R_h of 23.9, 16.2, 10.6, 1.7, and 1.3 nm, respectively. After 1 h of incubation, the R_h of BP, RB, RITC containing systems increased to 34.5, 22.4, and 11.9 nm, respectively, whereas for mixtures comprised of 5-SFX, 5(6)-FITC the R_h remained constant throughout the whole monitoring of the aggregation[91].

These results, show that fluorescent tags BP, RB, RITC, which present a hydrophobic character, increased the tendency to form HMM oligomers, while the more hydrophilic labels, 5-SFX and 5(6)-FITC, inhibited the oligomerization[91]. However, the authors did not perform a complete aggregation process and did not directly compare these systems with the native Aβ(1-42) to better understand the extent to which the overall aggregation mechanism was affected.

I.2.2.2. Effect of Aβ extrinsic factors upon the aggregation process

The extrinsic factors relate to the origin of the peptide[94], different pretreatment methods[56,95,96], incubation conditions[80], and physico-chemical parameters of the sample media, such as the concentration[97], the pH[98], the nature of the salt[99], the ionic strength[61], the temperature[100] and the influence of other species such as metals[17] or proteins[45], as well as the presence of stochastic factors that may lead to difficulties in obtaining repeatable results[86].

I.2.2.2.1. Origin of the peptide

The origin of the peptide represents one of the most important factors influencing the aggregation and primarily relates to the purity of the sample[101]. Generally, peptides can be either of synthetic origin, mainly produced by solid-phase peptide synthesis (SPPS), or they can be of recombinant origin, prepared using deoxyribonucleic acid (DNA)-based expressions[94].

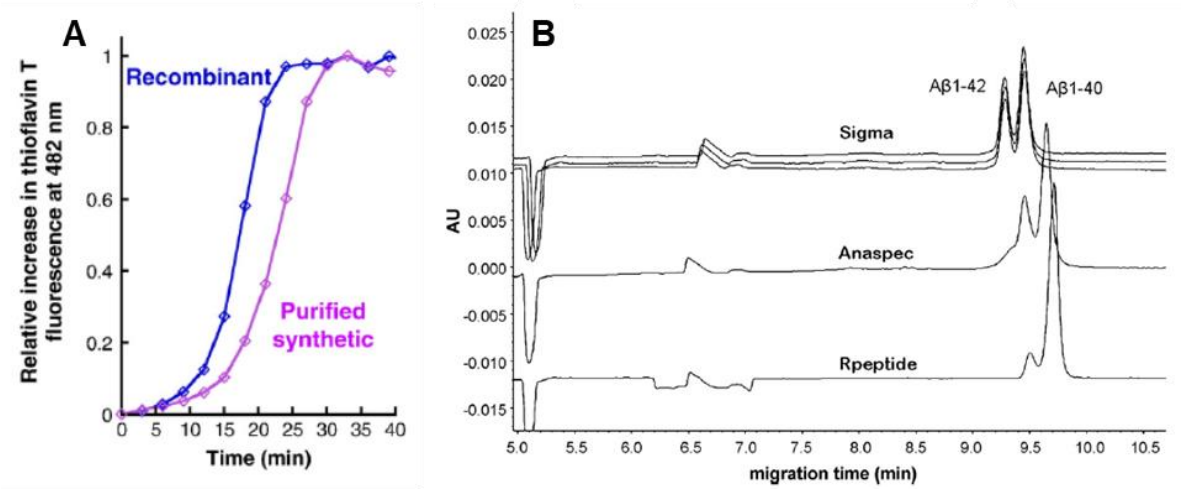

Figure 12. Effect of the origin of the peptide upon the aggregation process of Aβ peptides. (A) ThT fluorescence assay of synthetic and recombinant Aβ(1-42). Experimental conditions: Sample: 7.4 µM Aβ1–42 + 50 µM ThT, 10 mM phosphate buffer, 100 mM NaCl, pH 7.4. Incubation: quiescent conditions at 37 °C. Fluorescence detection: λEm= 482 nm; λEx=440 nm (adapted from Finder *et al.*[94]). (B) Comparison of CE-UV electropherograms of Aβ(1-40) and Aβ(1-42) acquired from different suppliers. Experimental condition: Sample: ~8 µM Aβ, 0.004% (m/v) NH4OH. Incubation: quiescent conditions at 6 ◦C. CE-UV: fused silica capillaries: 50 µm ID x 57 cm X 47 cm; BGE: 100 mM borate buffer + 3 mM DAB, pH 10; Voltage: + 16 kV; Injection: 34 mbar; Analyses were performed at 25 ◦C; UV detection at 214 nm (adapted from Verpillot *et al.*[102]).

Another study compared both types of origin to verify whether there are differences in the aggregation behavior[94]. To investigate this, the recombinant Aβ(1-42) was prepared by cytoplasmic expression in *Escherichia coli* and a commercial synthetic Aβ(1-42) peptide was repurified by reversed-phase high-performance liquid chromatography (RP-HPLC) to ensure a final purity of 97.1 %. The authors employed a ThT assay (Figure 12 A) for monitoring the aggregation process and observed that the recombinant peptide aggregated faster than the synthetic peptide but presented a similar fibrilization plateau[94].

It was also found that Aβ peptides can display different initial profiles when comparing different batches acquired from different suppliers. For instance, Verpillot *et al.* compared by capillary electrophoresis (CE) both Aβ(1-40) and Aβ(1-42) isoforms of two synthetic origins obtained from Sigma-Aldrich and Anaspec, and one origin which was prepared using recombinant protocols, purchased from Rpeptide. All peptides presented a TFA salt form and equimolar mixtures of the two isoforms obtained from each supplier were prepared[102]. Despite thorough sample preparation and dissolution under the same conditions, all the origins presented different peak areas during CE separation, as shown in the electropherograms of Figure 12 B. In the case of the Rpeptide origins, the peak area of Aβ(1-42) was very low compared to the other isoform. The authors stated that the Aβ(1-42) obtained from Rpeptide was probably less soluble compared to

the other origins further suggesting the possibility that it was initially aggregated, while the ones purchased from Anaspec exhibited other minor peaks suggesting that the sample was impure. It follows that the origins obtained from Rpeptide and Sigma-Aldrich were more pure compared to the Anaspec batches and that the Sigma-Aldrich samples appeared to be more suitable compared to those obtained from Rpeptide since the peak area between the two isoforms was more similar[102]. Therefore, Aβ peptides may behave differently from batch to batch and it follows that highly pure raw material, preferably not already aggregated, should be purchased or prepared prior to both the pretreatment step and the aggregation study[101,102].

I.2.2.2.2. Pretreatment methods for obtaining aggregate-free Aβ peptides

Another very important aspect is related to the need of obtaining aggregate-free formulations before performing aggregation studies[58]. These formulations are often termed LMM Aβ as they represent mixtures of monomers and LMM oligomers that are in strong equilibrium with each other[58]. Table 1 presents a brief overview of several pretreatment protocols described in the literature, outlining the isoforms, the pretreatment types including the important steps for each protocol.

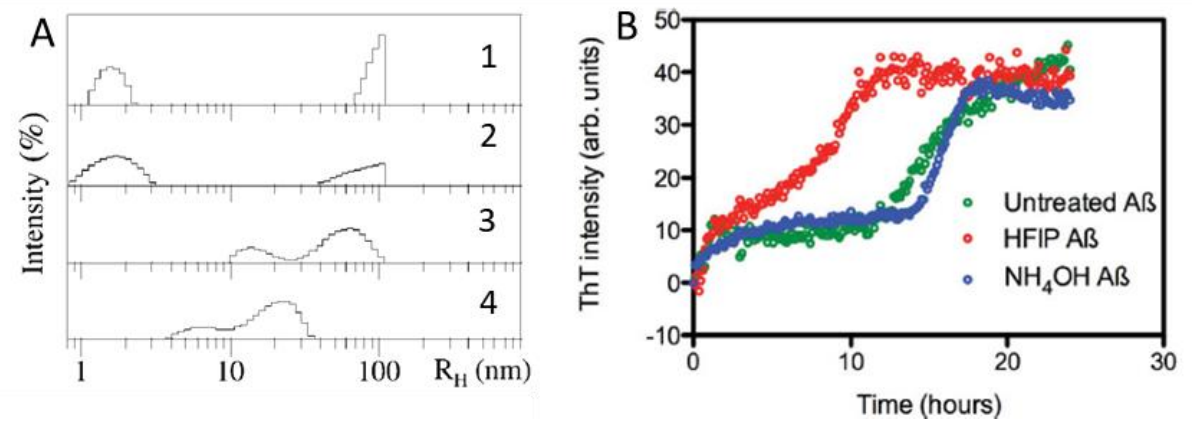

Figure 13. Effect of sample pretreatment upon the aggregation process of Aβ peptides. (A) DLS analysis LMM Aβ(1-40) and LMM Aβ(1-42) isolated by SEC and MWCO filtration. Layers: 1 (Aβ40-SEC), 2 (Aβ40-MWCO), 3 (Aβ42-SEC), 4 (Aβ42-MWCO). Experimental conditions: Sample: ~25 µM Aβ; 10 mM phosphate buffer pH 7.4. Incubation: quiescent conditions at 25 °C. DLS: Argon ion laser operating at 514 nm; θ= 90°; Analyses were performed at 25 ◦C (adapted from Teplow *et al.*[56]). (B) ThT fluorescence assay of different sample preparations of Aβ(1-42): HFIP pretreated Aβ(1-42) (red), NH_4OH pretreated Aβ(1-42) (blue), untreated Aβ(1-42) (green). Experimental conditions: Sample: 5 µM Aβ(1-42) + 30 µM ThT, phosphate buffered saline (36.89 mM NaCl, 2.68 mM KCl, 6.39 mM Na_2PO_4, 1.47 mM KH_2PO_4), pH 7.4. Incubation: agitated conditions at 37 °C. Fluorescence detection: λ_{Em}= 485 nm; λ_{Ex}= 440 nm (adapted from Breheney *et al.*[95]).

The pretreatment methods can be divided in two categories: physical and chemical disaggregation protocols. Physical disaggregation protocols mainly include SEC[36] and filtration by using a suitable molecular weight cut-off (MWCO)[56], usually of about 10 kDa[56,58]. On the other hand, chemical disaggregation methods may include the use of aqueous (e.g. NH_4OH[103], NaOH[80]) or organic solvents (e.g. HFIP[104], TFA[105], DMSO[106] or ACN[107]) media. Depending on the type of aggregation study, more than one type of pretreatment protocols can be employed[104,108,109]. However, numerous studies have shown that pretreatment methods can affect the aggregation behavior of Aβ peptides in different ways[56,95,96,110].

Teplow and co-workers were among the first to introduce SEC and MWCO as physical disaggregation protocols[56,58]. In one of their studies[56], the authors compared by DLS the LMM fractions of both Aβ(1-40) and Aβ(1-42), obtained using the latter mentioned disaggregation protocols, and observed that in the case of Aβ(1-40) the R_h was about 1 – 2 nm with some low abundant large aggregates of ~100 nm with no significant difference between SEC (Figure 13 A1) and MWCO (Figure 13 A2) pretreatments. SEC isolated LMM Aβ(1-42) presented distributions of 10 – 20 nm and centered around 60 nm (Figure 13 A3), while the ones isolated by MWCO filtration presented a small distribution of about 6 – 7 nm (Figure 13 A4). Whereas the peak comprised of HMM aggregates observed for SEC prepared formulations was not present, suggesting that MWCO is a better disaggregation alternative especially for the more aggregation-prone Aβ peptides[56].

Another study which compared two chemical disaggregation protocols noted that they can have a significant impact upon the initial aggregation state[95]. The authors monitored the aggregation process using ThT fluorescence assay (Figure 13 B) of Aβ(1-42) that was pretreated either by HFIP and NH_4OH solution and compared with the raw material as well. It can be observed that HFIP pretreatment resulted in a much shorter lag phase and a faster fibrillization plateau, whereas the aqueous pretreatment provided a similar but smoother profile compared to the untreated raw material. The authors combined these data with other scattering techniques, and showed that HFIP presented a greater proportion of oligomeric and fibrillar species, while NH_4OH solution exhibited a more homogeneous formulation consisting primarily of LMM Aβ[95].

In any case, in addition to the effect upon the aggregation behavior of Aβ peptides, all these protocols present different drawbacks and advantages. Physical disaggregation methods may allow a much better separation of LMM Aβ from larger aggregates compared to the chemical protocols[58],

but the main disadvantages are related to the long procedural times and the high loss of raw material which can be more than 70%[58,104]. Larger aggregates that present a variable stability might interact with the column matrix and dissociate into LMM Aβ fractions during SEC separation[28]. On the other hand, chemical disaggregation protocols generally require less preparation time for aggregate-free formulations compared to physical separations, but the disaggregation efficiency depends on the nature of the organic solvent or on the aqueous media[95,103]. For example, ACN was found to generate spontaneous aggregation and therefore it is not a suitable solvent for the disaggregation protocols[107,111]. DMSO can have a great efficiency in monomerizing β-sheet structures but it is extremely difficult to remove, thus it is generally employed in parallel with other protocols such as SEC or it can be diluted up to unsignificant amounts with the sample matrix after the disaggregation is complete[28,58,111]. Among all the disaggregation methods, one of the most adopted is the pretreatment with ammonia because the protocol is faster and more efficient compared to other methods[95,103].

In general, the ThT assay is the most suitable technique to investigate the aggregation state of the peptides[95,112]. However, to ensure an accurate study, the purity and the aggregation state of the raw material must be optimal enough, otherwise the pretreatment step cannot be efficient as discussed in the previous subsection.

Table 1. Disaggregation methods for obtaining LMM Aβ peptides

Entry	β-Amyloid		Pretreatment		Refs
	Name	Origin	Type	Steps	
1	• Aβ(1-39) • Aβ(1-40) • Aβ(1-41) • Aβ(1-42) • Aβ(1-43)	• Synthesis: Automated SPPS Fmoc chemistry • Purification: RP-HPLC > 97% purity	SEC	• Dissolve 350 - 500 µg of peptide in DMSO (2 mg/mL) • Sonication 1 minute • Centrifugation 10 minutes at r.t 16,000 xg • Sample is then injected onto the column (Superdex 75 - 10 mM phosphate buffer pH7.4)	56,58
2	• Aβ(1-42)	• Lyophilized Aβ(1-42) from Yale University , New Haven, CT, USA	SEC	• 1 mg of peptide dissolved in 50 µL of DMSO • Addition of 800 µL of ultra-pure water + 10 µL of 2 M Tris, pH 7.6 • Centrifugation at 600 g for 4 min at 4 °C • Supernatant injected on the column (Superdex 75 - 10 mM Tris-HCl pH 7.4)	36
3	• Aβ(1-39) • Aβ(1-40) • Aβ(1-41) • Aβ(1-42) • Aβ(1-43)	• Synthesis: Automated SPPS Fmoc chemistry • Purification: RP-HPLC > 97%	MWCO	• Dissolve Aβ in H_2O (4 mg /mL) • Add 1 M NaOH for pH > 10.5 • Dilution with 20 mM sodium phsophate buffer (pH 7.4) at 2 mg/mL Aβ • Sonication for 1 minute and filter (Microcon-10 kDa) • Storage at -80 °C	56,58
4	• Aβ(1-40)	• Donated by Pharmacia (Nerviano, Italy)	ACN / Na_2CO_3	• Peptide dissolved in ACN/300 mM Na2CO3 pH 10.5 (50:50 v/v) (100 µM) • Sample aliquoted, freeze-dried and stored at -20 °C • Aliquots dissolved in 100 µL of 20 mM phosphate buffer, pH 7.4 (100 µM) • Sonication for 3 min • Centrifugation at 14 437 x g for 10 min	113
5	• Aβ(1-42)	• Provided by Core Protein Laboratory of Wake Forest University (Dr. M. O. Lively)	ACN / Na_2CO_3	• Peptide dissolved in ACN/300 mM Na2CO3 pH 10.5 (50:50 v/v) (100 µM) • Sample aliquoted, freeze-dried and stored at -20 °C • Aliquots dissolved in 100 µL 20 mM phosphate buffer, pH 7.4) (100 µM) • Sonication for 3 min • Centrifugation at 3326 x g for 20 min	107

6	• Aβ(1-42)	• Aβ (1-42) (TFA salt) from American Peptide (Sunnyvale, CA, USA)	NH_4OH	• Peptide dissolved in 0.16% NH_4OH (~ 443 µM) • Incubated for 10 min at 20°C • Lyophilization • Storage at −20°C until further use • Dried peptide was reconstituted in 20 mM phosphate buffer pH 7.4 (100 µM) at 20°C	103
7	• Aβ(1-40)	• Aβ(1-40) (human sequence) from Sigma, Roboscreen or rPeptides	NH_4OH without lyophilization	• Dissolve peptide in 0.1% NH_4OH (200 µM Aβ) • Split in 20 µL aliquots • Storage at −30°C.	114
8	• Aβ(1-37) • Aβ(1-38) • Aβ(1-39) • Aβ(1-40) • Aβ(1-42)	• Lyophilized peptides from Anaspec (Le Perrey en Yvelines, France), Sigma (St. Louis, MO, USA) and Rpeptide (Bogart, GA, USA).	NH_4OH without lyophilization	• Peptide dissolved in 0.10 or 0.16% NH_4OH (2 mg/mL) • Sample aliquoted and stored at -20 °C	102
9	• Aβ(1-42)	• Aβ(1-42) (TFA salt) from American Peptide	NH_4OH	• Peptide dissolved in 0.16% NH_4OH (~ 443 µM) • Incubated for 10 min at 20 °C • Lyophilization • Storage at −20 °C • Dried peptide was reconstituted in 20 mM phosphate buffer pH 7.4 (100 µM) at 20 °C	115
10	• Aβ(1-42)	• Lyophilized Aβ(1-42) from Anaspec	NH_4OH	• Peptide dissolved in 0.16% NH_4OH (~ 443 µM) • Sample separated into aliquots • Aliquots freeze-dried • Aliquots stored at −20 °C	106
11	• Aβ(1-40) • Aβ(1-42)	• Aβ(1-40) from W.M Keck Foundation Biotechnology Research Laboratory • Aβ(1-42) from rPeptide (Bogart, GA)	TFA / HFIP	• Peptides dissolved in TFA/ HFIP • Evaporation of solvents under N_2 stream • Dried peptide reconstituted in 10 mM Tris buffer pH 7.8 • Kept on ice or refrigerated at 4 °C before analysis	109
12	• Aβ(1-40)	• Aβ(1-40) lyophilized powder from Anaspec	HFIP / NaOH	• Peptide dissolved in HFIP (1 M) • Stock solution was aliquoted (62.5 µg Aβ) • Slow evaporation of HFIP overnight • Aliquots stored at -80 °C until further use • Aliquots reconstituted in 5 mM NaOH stock solution before dilution with buffer	96

13	• Aβ (1-42)	• Recombinant Aβ(1-42) from Isoloid Germany	HFIP / NaOH	• Peptide dissolved in HFIP, aliquoted and lyophilized • Aliquots reconstituted in 2 mM NaOH at (~ 221 µM) • Aliquots diluted in HBS (20 mM HEPES, 150mM NaCl, pH 7.4 and directly used	104
14	• Aβ(1-40) • Aβ(1-42)	• Dry synthetic peptides from Keck laboratories, Yale	HFIP / NaOH	• Peptides dissolved in (HFIP) and incubated at 25 °C for 1 h • Sample was aliqouted into equal amounts • Aliqouts dried using a speed-vac • Before use: aliqouts dissolved in 15 mM NaOH • Aliquots sonicated on ice bath for 15 min • Aliquots centrifuged at 16 000 x g for 20 min (~ 866 µM) • Diluted fivefold with 10 mM PBS (150 mM NaCl, pH 7.4) • Aliquots sonicated for 1 min • Aliquots centrifuged at 13000 rpm for 20 min.	116
15	• Aβ(1-42)	• Lyophilized solids from Biopeptide Co., LLC (USA)	HFIP/NaOH	• Peptide dissolved in HFIP and dried • Peptide disolved in 10 mM NaOH at (0.5 mM) • Solution diluted with 100 mM HEPES buffer (pH 5.0) to pH 6.8 • Centrifugation at 16,000 x g for 10 min • Solutions adjusted to desired conc. in buffer	117
16	• Aβ(1-40)	• Lyophilized powder from Anaspec	HFIP / NaOH	• Peptide dissolved in HFIP (1000 µM) • Stock solution was aliquoted (0.0625 mg peptide) • Slow evaporation of HFIP overnight • Aliquots stored at -80 °C until further use • Aliquots reconstituted in 5 mM NaOH stock solution	118
17	• Aβ(1-40)	• Donated by Pharmacia (Nerviano, Italy)	HFIP / DMSO	• Peptide dissolved in 1 mM HFIP • Sample freeze-dried and stored at -20 °C • Peptide HFIP film dissolved in DMSO (5mM) • Sample divide in two aliquots • Aliquots diluted with 20 mM phosphate buffer, pH 7.4 (100 µM) • Sonication for 3 min • Centrifugation at 14 437 x g for 10 min	113

18	• Aβ(1-42)	• Lyophilized Aβ(1-42) from Anaspec	HFIP / DMSO	• Peptide dissolved in HFIP (~221 µM) and dried • Peptide film disolved in DMSO • Sonication for 10 min • Solution diluted with 20 mM PBS buffer (137 mM NaCl, pH 7.4) (50 µM Aβ)	106
19	• Aβ(1-40) • Aβ(1-42)	• E coli human recombinant Aβ(1–40) Ultra Pure HFIP and Aβ(1-42) - Ultra Pure HFIP from rPeptide	HFIP / DMSO / Desalting column	• Defreeze 0.5 mg Aβ-HFIP at r.t. for 10 min • Dissolve in 500 µL HFIP • Vortex 1 min with or without mixing specific volumes of Aβ(1-42):Aβ (1-40) - (0:10), (1:9), (3:7) and (10:0) • Evaporate HFIP under N or Ar gas • Resdisolve Aβ/HFIP films in 500 µL DMSO • Vortex 1 min • Sample injected onto the column (GE Healthcare Hitrap Desalting column 17-1408-01 - 10 mM 50 mM Tris / 1 mM EDTA buffer pH 7.4) • Fractions stored at- 20 °C	108
20	• Aβ(1-40)	• Aβ(1-40) lyophilized powder from Anaspec	NaOH / SEC	• Peptide reconstituted in 50 mM NaOH (~ 462 µM) • Sample is then injected onto the column (Superdex 75 HR10/30 - 40 mM Tris-HCl buffer pH 8.0) • Aliquots were flash frozen, shipped overnight on dry ice and used immeadiately or stored at -80 °C	96

I.2.2.2.3. Incubation conditions

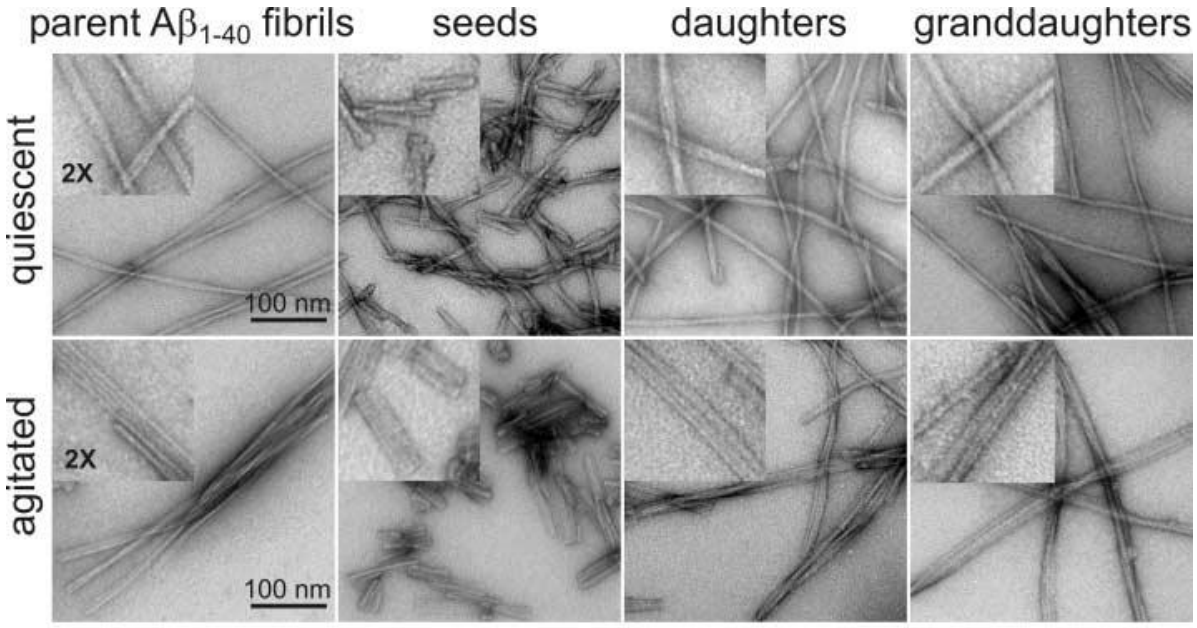

Figure 14. TEM images of amyloid fibrils formed by the Aβ(1-40) peptide formed under quiescent (upper layer) or agitated (bottom layer) conditions. Experimental conditions: Sample: 210 μM Aβ(1-40); 10 mM phosphate buffer, 0.01% NaN_3, pH 7.53. Incubation: quiescent or gentle agitated conditions at 24 °C; Parent fibrils: 21 – 68 days; Daughter/Granddaughter fibrils: 3 – 8 days. STEM analysis: 3 nm carbon films on 200 mesh copper grids. Voltage: 100 kV. Probe diameter: 1 nm. Current: 2 pA. Electron dose: 10^3 e/nm^2 (adapted from Petkova *et al.*[80]).

Another factor that alters the aggregation behavior of Aβ peptide is represented by the incubation conditions and can be categorized in two types, quiescent or agitated environments, the latter being employed at different rates depending on the aggregation study[80,97].

In a study performed by Petkova *et al.*, the authors investigated what effect the incubation conditions have on the aggregation process of Aβ(1-40)[80]. To do so, the authors first independently grown the parent fibrils under both incubation conditions for a period 21 – 68 days. Then they produced two new generations of fibrils for shorter incubation periods of 3 – 8 days, denoted as daughter and granddaughters, by seeding new Aβ(1-40) solutions with the corresponding parent fragmented fibrils which were sonicated a few minutes prior to the dissolution. The parent fibrils generated under quiescent conditions were larger (12 nm in width and 50 to 200 nm in length) as compared to those obtained under agitated conditions (filaments having a width of 5.5 nm). The most important observation was finally related to that the morphological characteristics of the corresponding fragmented parent fibrils, which were preserved in the new generated daughter fibrils[80].

I.2.2.2.4. Peptide concentration

The most predominant Aβ isoforms are Aβ(1-40) and Aβ(1-42), the former of which is the most abundant in biological fluids[17]. The Aβ levels have been found to be in the nanomole range in the CSF, presenting a ratio of ~3:1 between the two isoforms and in sub-nanomole concentrations in blood plasma, the peptides being highly soluble under physiological conditions in the body fluids[17,42,119].

To the present knowledge, no reports were published on the exact Aβ levels in the human brain, for example in the hippocampus and the cortex[120]. A recent study performed an all-atom MD simulation for Aβ(1-42) dimers, trimers, and tetramers and, by assuming an initial concentration of 0.8 nM of Aβ it was revealed that it would take approximately 62 years for toxic species to form, at an age that is very close to the age of the AD onset[120].

When performing aggregation studies, the Aβ concentration varies primarily within the nM - μM range depending on the limit of detection (LOD) of the techniques available nowadays[63,112]. Generally, the biophysical techniques that allow the monitoring of the aggregation at a close-physiological concentration, especially during the nucleation stage of the process, are fluorophore-based fluorescence methods[33,97,112].

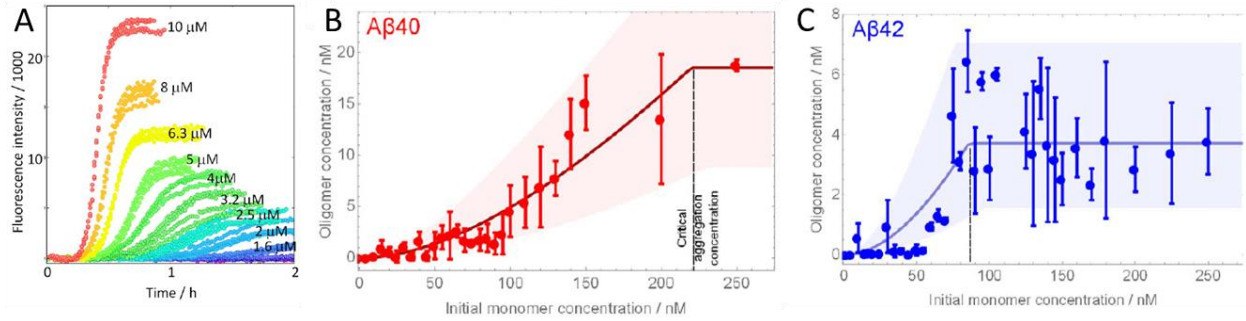

Figure 15. Effect of sample concentration upon the aggregation process of Aβ peptides. (A) ThT fluorescence assay of Aβ(1-42)-A2V mutant at different concentrations. Experimental conditions: Sample: 1.6 - 10 μM Aβ(1-42)-A2V + 6 μM ThT, 20 mM sodium phosphate buffer, 200 μM EDTA, 0.02% NaN_3, pH 8. Incubation: quiescent conditions at 37 °C. Fluorescence detection: λ_{Em}= 480 nm; λ_{Ex}=440 nm (adapted from Meisl *et al.*[97]). Determination of the CAC for Aβ(1-40) and Aβ(1-42) single-molecule fluorescence measurements. Experimental conditions: Sample: (B) 0 - 250 nM AlexaFluor488-Aβ40:AlexaFluor647-Aβ40 (50:50 %) and (C) 0 - 250 nM AlexaFluor488-Aβ42:AlexaFluor647-Aβ42 (50:50 %); SSPE buffer (150 mM NaCl, 10 mM $Na_2H_2PO_4$ x H_2O, 10 mM Na_2EDTA, 0.01% NaN_3, pH 7.4). Incubation: agitated conditions (200 rpm) at 37 °C. Single-molecule fluorescence spectroscopy: Two-colour coincidence detection with dual excitation mode in 488 and 633 nm; Analyses were performed at 20 ◦C (adapted from Iljina *et al.*[33]).

It has been well established since the beginning of the molecular studies of the Aβ aggregation mechanism that the aggregation proceeds in a concentration-dependent manner[61]. An example is

shown in Figure 15 A**,** in which the aggregation process of the Aβ(1-42)-A2V mutant was monitored by ThT assay over a concentration range of 1.6 – 10 μM[97]. It can be observed that all three main phases are affected. The lag phase is shortened while the elongation and the stationary phase are occurring much faster, suggesting that both the aggregation kinetics and the fibrilization rate are promoted by increasing the Aβ concentration[97].

According to the current consensus, the critical nucleus formation can only occur above a critical aggregation concentration (CAC)[33]. It can be simply defined as the minimum required concentration at which LMM critical nuclei or paranuclei such as dimers – hexamers are able to begin associating with Aβ monomers allowing the conversion into highly ordered species and eventually fibrils[33].

In a study performed by Iljina *et al.*, the authors investigated which was the CAC for both Aβ(1-40) and Aβ(1-42) using a specific single-molecule fluorescence technique that offers a two-color coincidence detection by allowing a dual excitation mode at 488 and 633 nm, respectively[33]. To do so, equimolar fluorophore-based independent mixtures of AlexaFluor488-Aβ40:AlexaFluor647-Aβ40 (Figure 15 B) and AlexaFluor488-Aβ42:AlexaFluor647-Aβ42 (Figure 15 C) were prepared and analyzed at different concentrations within the range of 0 – 250 nM, and measurements were recorded for each concentration after an incubation period of 3 days at 37 °C, a time considered optimal as the abundance of formed high-ordered Aβ species was constant up to longer incubation times. Based on the obtained results, the authors further performed a thorough statistical modelling approach, and estimated a CAC of 222 ± 10 nM for Aβ(1-40), and 86 ± 10 nM for Aβ(1-42)[33].

However, it is noteworthy to mention that these experiments were performed using labelled Aβ peptides and, as they were found to change the aggregation behavior of native peptides[91–93], it is still unclear whether the estimated CAC values were affected by the use of fluorophores.

I.2.2.2.5. pH of the system

Since the beginning of the mechanistic studies, it was observed that Aβ aggregation is strongly dependent on the pH[61] and its effect was further explored in recent years[43,98]. Most studies were performed at the physiological pH (7.4), still it remains important to evaluate the aggregation process over a wider pH range because different types of media may exist in various parts of the

body, such as in certain endosomes and lysosomes compartments where the acidic pH is predominant[51].

An in-depth study of the pH effect upon the aggregation mechanism of Aβ peptides was performed by Kobayashi *et al.*, in which the authors monitored the aggregation over a wide range of pH by ThT assay for an incubation period of 96 h (Figure 16 A and B) and performed in silico simulations based on the obtained results, further accompanied by structural analyses.

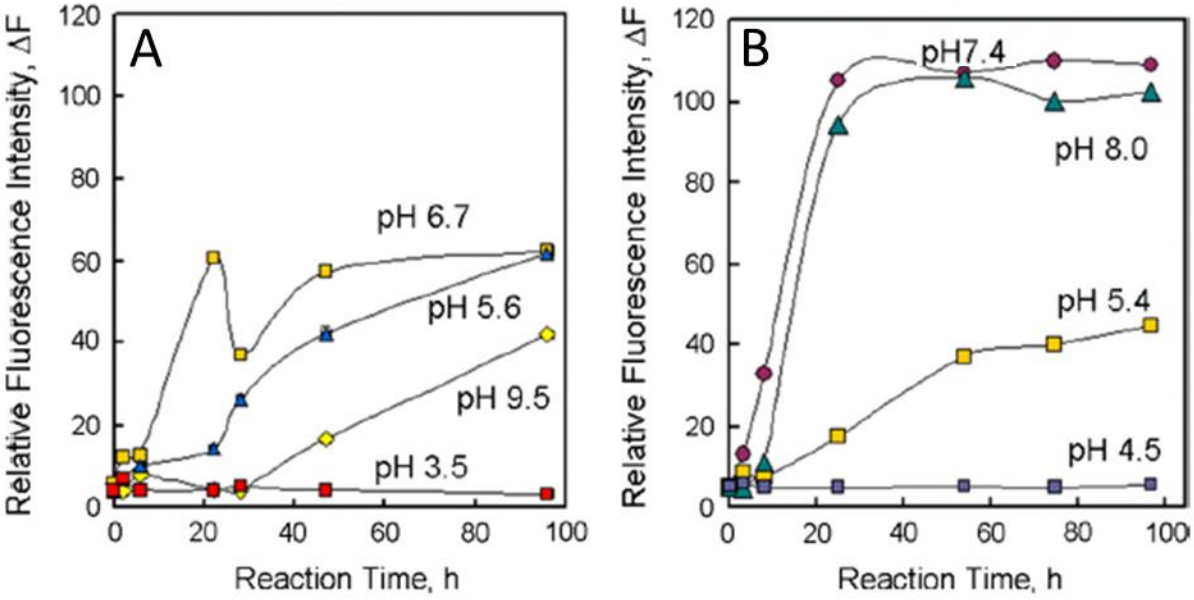

Figure 16. Effect of sample pH upon the aggregation process of Aβ peptides. ThT fluorescence assay of Aβ(1-42) at wide range of pH: (A) pH 3.5, pH 5.6, pH 6.7, pH 9.5 and (B) pH 4.5, pH 5.4, pH 7.4, pH 8.0. Experimental conditions: Sample: 25 µM Aβ(1-42) + 7 µM ThT; 10 mM Na_2HPO_4 for pH 3.5; 10 mM K_2HPO_4 for pH 4.5, 5.4 and 5.6; 10 mM Tris–HCl for pH 6.7, 7.4, 8.0 and 9.5. Incubation: quiescent conditions at 37 °C. Fluorescence detection: λ_{Em}= 490 nm; λ_{Ex}=455 nm (adapted from Kobayashi *et al.*[98]).

At first, all the ThT assay profiles showed that Aβ(1-42) was initially unaggregated. As can be seen in Figure 17, no aggregation was observed for pH 3.5 and 4.5. As for pH values of 5.4- 5.6, the aggregation progressed slowly from the beginning reaching a plateau after 50 h. At pH 6.7, the aggregation was more pronounced presenting two peaks and reaching a plateau after 50 h, while for the aggregations monitored at pH 7.4 and 8.0, the profiles presented similar short lag phases and similar fibril yield; the kinetics at pH 8.0 being slightly retarded. At pH 9.5, a 28 h lag phase was observed followed by an elongation phase without reaching a plateau after 96 h of incubation. According to these data, combined with the structural analysis and modelling simulations, the authors were then able to determine that at a pH < 6 and >9.5, the aggregation does not occur because the monomers do not undergo the necessary conformational changes that lead to the toxic

β-sheet structures, while at pH values between 6 and 9.5, monomers can aggregate due to specific conformational changes that occur mainly within the CHC region, and that pH 7.4 promoted the most the aggregation of the Aβ peptides. However, it is noteworthy to mention that, depending on the desired pH, different sample matrices were used to ensure certain pH values and it cannot be excluded that changes in the nature of the sample media had an impact on the obtained results[61,99].

I.2.2.2.6. Salts and ionic strength of the system

Aggregation kinetics are known to be accelerated when increasing the amount of salt present in the sample media, and studying the aggregation at physiological salt concentration (e.g. 150 mM NaCl) is important to better understand how the mechanism proceeds in the brains of patients suffering from AD[61,62].

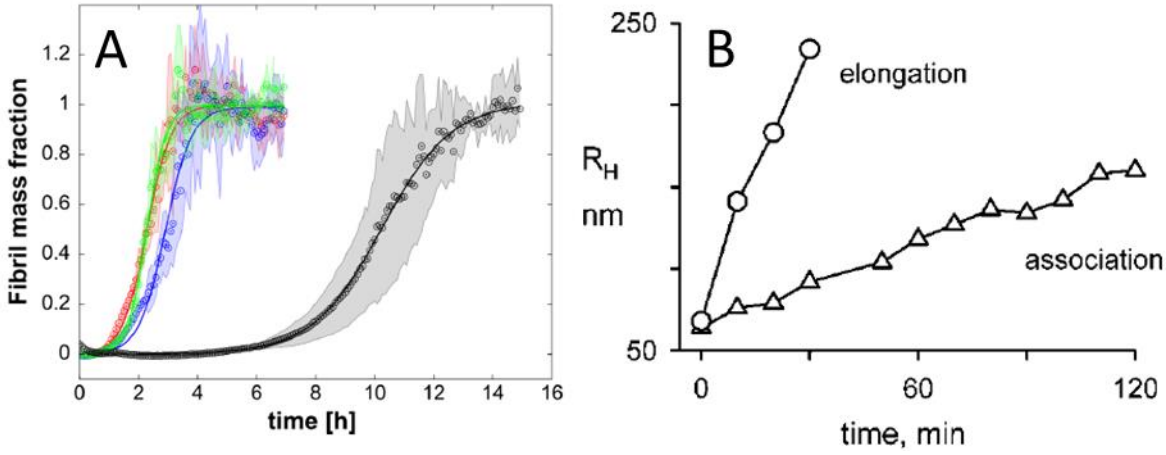

Figure 17. Effect of ionic strength of the sample upon the aggregation process of Aβ peptides. (A) ThT fluorescence assay of Aβ(1-40) in the absence (black) and the presence of 150 mM NaCl (blue), NaF (red) and LiCl (green). Experimental conditions: Sample: 20 µM Aβ(1-40) + 40 µM ThT; 10 mM phosphate buffer, 0.02 % NaN_3, pH 7.2. Incubation: quiescent conditions at 37 °C. Fluorescence detection: λ_{Em}= 482 nm; λ_{Ex}= 440 nm (adapted from Abelein *et al.*[99]). (B) Evolution of the hydrodynamic radius of Aβ(1-40) protofibrils by monomer elongation and by protofibril association monitored with DLS. Experimental conditions: Sample (elongation): 1.3 µM Aβ(1-40) protofibrils (Aβ residue units) + 30 µM LMM Aβ(1-40); 50 mM Tris-EDTA, pH 8.0; Sample (association): 1.3 µM Aβ(1-40) protofibrils (Aβ residue units); 50 mM Tris-EDTA, 150 mM NaCl, pH 8.0 Incubation: agitated conditions at 37 °C. DLS: Argon ion laser operating at 514 nm; θ= 90°; Analyses were performed at 25 ◦C (adapted from Nichols *et al.*[62]).

In their study, Abelein *et al.* evaluated the influence of different salts upon the aggregation process of Aβ(1-40)[99]. Here, the changes in the aggregation behavior, in the presence and the absence of 150 mM NaCl, NaF, and LiCl, were monitored by ThT fluorescence assay (Figure 17 A). It was observed that all the salts significantly reduced the nucleation phase without affecting the final fibril yield, with NaF and LiCl only slightly increasing the kinetics of the aggregation compared to NaCl. Moreover, the authors also observed that by maintaining a constant high ionic

strength while varying the concentrations of Aβ(1-40), the presence of the salt did not affect the concentration-dependence of the aggregation compared with the concentration-dependent experiments performed in the absence of the salt. By combining these results with other structural and morphological analyses, the authors were finally able to show that a high salt concentration is able to increase the rate of reaction of Aβ(1-40) by promoting a surface-catalyzed secondary nucleation reaction that is favored due to the reduction of the electrostatic repulsions between the monomers and the fibrils surface[99].

It was also showed that the presence of physiological ionic strength also changes the mechanism of protofibrils assembly[62,74]. In general, protofibrils cannot self-assemble in the absence of monomers, or at least under simple media conditions[74]. In a study performed by Nichols *et al.*, the authors showed via monitoring by DLS (Figure 17 B) the R_h evolution of Aβ(1-40) protofibrils in the presence of monomers without high ionic strength conditions and in the absence of monomers under physiological salt conditions[62]. First, LMM Aβ (R_h 1.4 ± 0.2 nm) were pretreated by SEC and protofibrils were prepared by vortexing using the aggregate-free formulation and then separated using the same method. The smallest observed protofibrils presented an average R_h of about 60 nm. Furthermore, when incubating 1.3 µM protofibrils with 30 µM LMM Aβ, the elongation led to the formation of larger aggregates of about 250 nm within only 30 min of incubation, whereas when protofibrils were incubated in the absence of monomers and in the presence of 150 nM NaCl, the elongation occurred much slowly reaching a R_h of ~150 nm after 120 min of incubation. These data were eventually correlated by ThT assays, SEC-coupled with multiangle light scattering (MALS), and other morphological analyses, and the authors hypothesized that the protofibril elongation in the absence of monomeric species may occur via a lateral self-association mechanism which can lead to formation of fibrils[62]. This mechanism was further investigated by another group where the authors also proposed a mathematical model for the association of protofibrils favored by the presence of salts, but in the absence of monomers[74]. Overall, these results suggested that the ionic strength represents a strong factor influencing the aggregation process, which may have a significant impact on the kinetics of Aβ peptide formation, more specifically upon the formation of different species.

I.2.2.2.7. Temperature of the system

The temperature variation has also been reported to have strong influence upon the aggregation kinetics and mechansim[100,121,122]. Depending on the health of a person, the local temperature in the brain can vary from 33.4 to 42.0 °C, though most of the aggregation studies are performed at 37 °C[100].

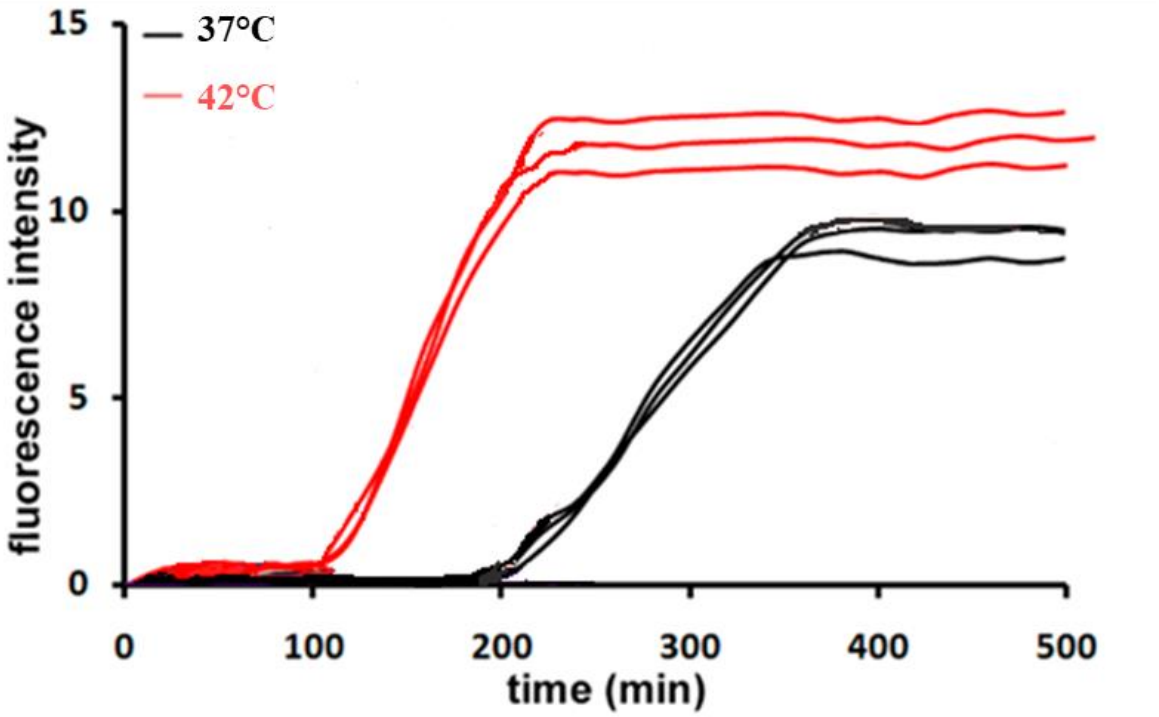

Figure 18. Temperature effect upon the aggregation process of Aβ peptides. (A) Availability/exposure of the 17-24 KLVFFAED (CHC/Turn) residue of the Aβ sequence at various temperatures in the presence of 4G8 monoclonal antibody obtained by UV-Vis spectroscopy. Sample: 5 µM Aβ(1-42) + 1 mg/mL 4G8; 13 mM sodium phosphate buffer, 0.02% NaN_3, pH 7.4. Incubation: Quiescent conditions at 32-42 °C (with 1°C intervals). UV-Vis detection at 405 nm (B) ThT fluorescence assay of Aβ(1-42) in the absence and in the presence of different nanoparticles at 37 and 42 °C. Experimental conditions: Sample: 5 µM Aβ(1-42) + 10 µM ThT ± 5 µM nanoparticles; 13 mM sodium phosphate buffer, 0.02% NaN_3, pH 7.4. Incubation: agitated conditions (700 rpm) at 37 °C. Fluorescence detection: λ_{Em}= 480 nm; λ_{Ex}= 440 nm (adapted from Ghavami *et al.*[100]).

In a study performed by Ghavami *et al.*, the authors investigated the effect of the temperature upon Aβ(1-42) at 37°C and 42 °C, respectively[100] by ThT assay (Figure 18). A shortened lag phase was observed for Aβ(1-42) at the higher temperature, suggesting that the kinetics of the process were accelerated, in agreement with previous reports from the literature[121,122].

I.2.2.2.8. Influence of metals and proteins upon the aggregation process

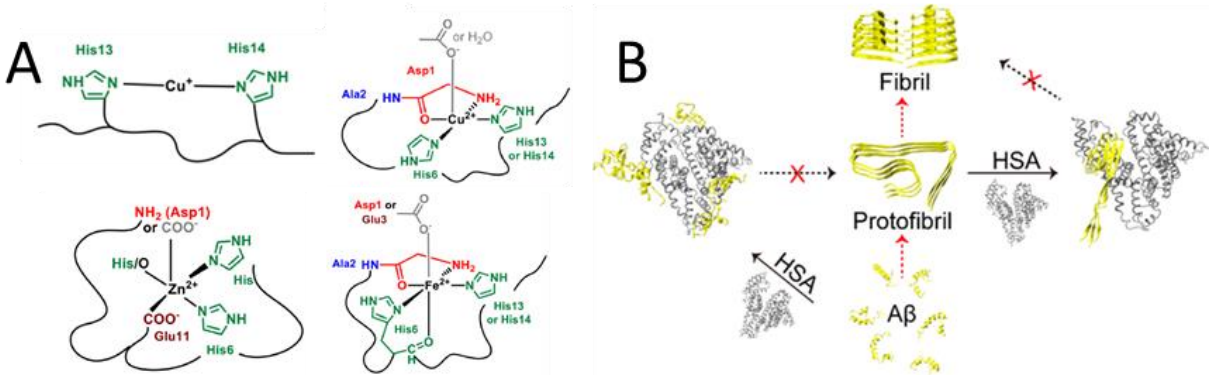

Figure 19. Influence of metals and proteins upon the Aβ aggregation process.(A) Possible coordination spheres of Cu, Zn and Fe within the NTR region of the Aβ peptide sequence for a pH range of 6-8 (adapted from Nasica-Labouze *et al.*[17]). (B) Influence of HSA upon the aggregation process Aβ(1-40). HSA can prevent monomers and protofibrils to HSA with extensive molecular dynamics simulations. HSA potentially interacts with multiple monomers to yield nonfibrillar oligomers. HSA tends to block the addition of monomers to protofibrils preventing the formation of fibrils (adapted from Zhao *et al.*[45]).

The impact of extrinsic species such as small molecules, metals and proteins have been found to affect the aggregation process of Aβ peptides in various ways[17,43].

Several metals such as Cu, Zn, Fe, Mn, Cr, Mo are essential for the health of the organism and generally their transport into the brain takes place in the synaptic cleft[43]. Some of these metals are involved in several processes that relate to dementia[123]. According to the current knowledge, there are four metals of interest in AD that affect the aggregation process of Aβ peptides, and the extent to which they change the aggregation behavior of the amyloidogenic peptides depends on their oxidation state and the resulting beta-amyloid metal complexes (Aβ-M^{+}) interactions with other species in the brain: Cu (Cu^{2+}/Cu^{+}), Zn (Zn^{2+}), Fe (Fe^{2+}/Fe^{3+}) and Ca (Ca^{2+})[17,43,124]. Based on a wide range of extensive studies, it is currently assumed that metal binding domain occurs within the first 16 amino acid residues within the Aβ peptide, representing the NTR region of their sequence and the soluble neuroprotective P3 peptide released during the processing of APP in the non-amyloidogenic pathway. In addition, depending on the nature and the oxidation state of the metal, they can adopt different coordination spheres[3,17,43]. A common structural feature of Aβ-M^{+} complexes is that they can occur *via* supramolecular interactions with the imidazole moieties belonging to the His residues found at the positions 6, 13 and 14 within the Aβ sequence (Figure 19 A)[17]. However, studying metal influence upon AD pathology can be very difficult. For example, Fe^{2+} and Cu^{+} require anaerobic conditions and for this reason their influence upon the aggregation cannot be monitored using most of the available techniques, whereas Fe^{3+} is not really soluble in

buffers and precipitates as a hydroxide[17,43]. Therefore, the most widely studied metal states are Zn^{2+}, Cu^{2+} and Ca^{2+}[43,124] but all the above-mentioned metals were found to alter the aggregation process of Aβ peptides, leading to an abnormal redistribution in other compartments of the brain and eventually to cell death. Because these are subject to a wide range of complicated mechanisms, their action upon the amyloid cascade of reaction is strictly dependent on all the factors influencing the aggregation, as thoroughly described in the previous subsections[43,123]. These aspects are also better reviewed elsewhere[17,43,123,124].

As in the case of metals, proteins were also found to alter the aggregation behavior of Aβ, leading to complicated mechanisms in the brain[17,125]. Some of the most common examples are Apolipoprotein-E and Cathepsin D, which are often present in the senile plaques of patients suffering from AD[125]. However, another protein known to inhibit the Aβ aggregation is the human serum albumin (HSA)[126], which is not produced in the brain but in the liver, and then released in body fluids such as CSF and blood plasma[17,45].

Given the importance of HSA, a recent study reported an extensive MD simulation approach on the protein binding with both monomers and protofibrils of Aβ(1-40) **(**Figure 19 B) based on the current consensus in the literature[45]. The authors suggested that HSA may bind the monomers mainly at the CTR region, but secondary interactions could also occur in NTR/CHC. Following this mechanism, HSA is able to destabilize the preferred conformations of the monomers that favor the formation of oligomeric aggregates. While, in the case of protofibrils, the main interactions with HSA occur in the CHC region, destabilizing β-sheet arrangements, and to a smaller extent in the CTR by blocking the monomer addition and overall preventing the formation of fibrils[45]. On this basis, the author noted that their findings are extremely valuable in developing and improving disease-modifying biologic therapeutics based on HSA[35,45,127].

I.2.2.2.9. Effect of stochastic factors upon repeatability of the experiments

Along with all the factors described in the previous subsections, evidence that the aggregation can be influenced by stochastic events affecting the repeatability of the results have also emerged[86,87].

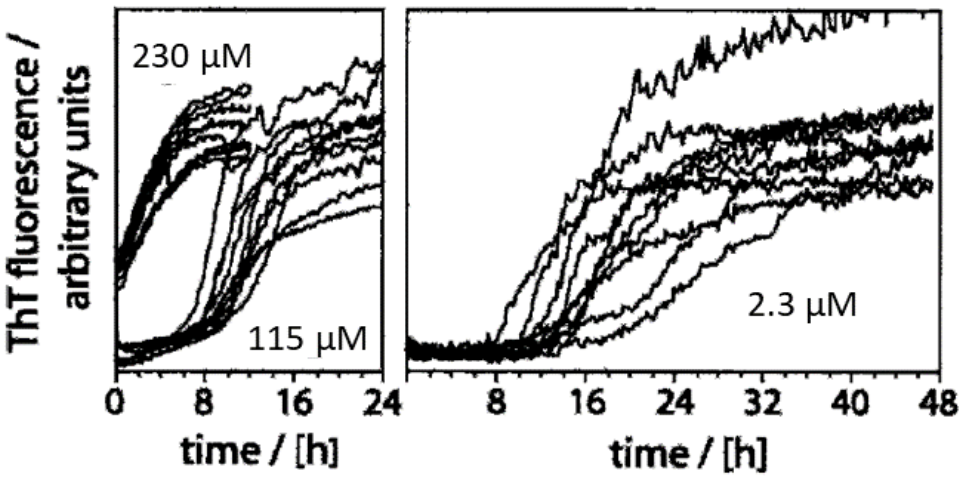

Figure 20. Kinetic repeatability of several Aβ(1-40) aliquots monitored by ThT fluorescence assay at 2.3, 115 and 230 µM. Experimental conditions: Sample: 2.3, 115 or 230 µM Aβ(1-40) + 20 µM ThT; 50 mM sodium phosphate buffer, pH 7.4. Incubation: quiescent conditions at 37 °C. Fluorescence detection: λ_{Em}= 490 nm; λ_{Ex}= 450 nm (adapted from Hortschansky *et al.*[86]).

One of the first reports on the existence of stochastic factors was made by Hortschansky and co-workers[86]. Despite careful sample preparation, the authors monitored via ThT assay (Figure 20) the aggregation process of Aβ(1-40) by checking several aliquots of the same batch at concentrations of 2.3, 115 and 230 µM, respectively. Initially, a reduction in the lag-phase was observed in a concentration-dependent manner, which is in agreement with the aspects described in subsection I.2.2.2.4, while it could also be observed that, at a concentration of 115 µM, the lag phase presented an increase in the intensity before reaching the elongation phase. Then, at a concentration of 230 µM, the process was saturated, as only part of the slope and the fibrillization plateau were recorded, suggesting a spontaneous aggregation. Even though, the main observation lies in the lack of repeatability of the tested aliquots for each concentration, where all the 3 phases were affected. Ultimately, based on these results, the authors suggested that the nucleation process, in addition to being influenced by common physicochemical factors, is also affected by a stochastic factor altering the aggregation mechanism[86].

In a very recent report, Faller and Hureau described their experience in obtaining reproducible results[87]. It was stated that, depending on the type of aggregation experiment, the results were either completely different or very similar. Therefore, the authors suggested that multiple aspects should be taken into consideration to achieve repeatable results. First, the pretreatment of the peptide should be thoroughly performed in order to obtain LMM Aβ without any presence of aggregates that could seed the process, by choosing a suitable method as described in subsection

I.2.2.2.2. Secondly, the sample dissolution should be performed all the time in the same manner, preferably by different investigators, and suitable tools such as low-binding tips, plates and vials should be employed to avoid peptide adhesion on the vessel walls. Experimental conditions should also be adapted with care. For example, when performing the ThT assay, it should be ensured that the concentration of the fluorophore is not a limiting factor, as the stationary phase could be recorded before the aggregation is completed. Then, if possible, it is recommended to use multiple batches acquired from different suppliers to ensure the robustness of the study. Ultimately, it is also important for the referees to verify that the authors have taken these careful steps in their study, but comprehend that some variations between experiments can occur, and as long as the results are statistically relevant, they should treat the study with indulgence[87]. In any case, since the aggregation process of Aβ peptides is highly sensitive, a complete control of the experimental condition is required because no variations in the physico-chemical parameters, such as pH, concentration, temperature, ionic strength, and buffer should occur between repetitions and, to evaluate the influence of each of these factors, only one of them should be varied per time, while the others must be kept constant[87,97].

I.2.3. Co-aggregation of Aβ peptides

The investigation of more complex biological Aβ systems, as in the case of their co-aggregation, is an important aspect since several isoforms and mutations were found to be generated during the final cleavage of APP[3,82]. The most important isoforms are Aβ(1-40) and Aβ(1-42), the former being the most abundant in biological fluids[17]. This section aims to introduce and briefly describe the current knowledge regarding the co-aggregation of these two Aβ isoforms.

Since the beginning of the aggregation studies, it was revealed by Snyder *et. al.* that the kinetics and the formation of aggregate species during the Aβ(1-42) process can be inhibited by Aβ(1-40)[61], and to a smaller extent by the NTR and CHC Aβ fragments of the sequence such as Aβ(1-28), suggesting that a selective inhibition of the process requires all important segments of the sequence. Furthermore, by monitoring the turbidity of the sample, the authors observed that at a ratio of Aβ(1-40):Aβ(1-42) of 3:1, the aggregation kinetics were faster compared to Aβ(1-40) alone, whereas at an equimolar ratio, the aggregation was nearly spontaneous[61]. However, the exact extent to which the aggregation was retarded and/or inhibited was unclear as the total Aβ

concentration was not kept constant, but only the concentration of Aβ(1-42) was fixed at 45 µM while that of Aβ(1-40) was varied depending on the studied ratio[61].

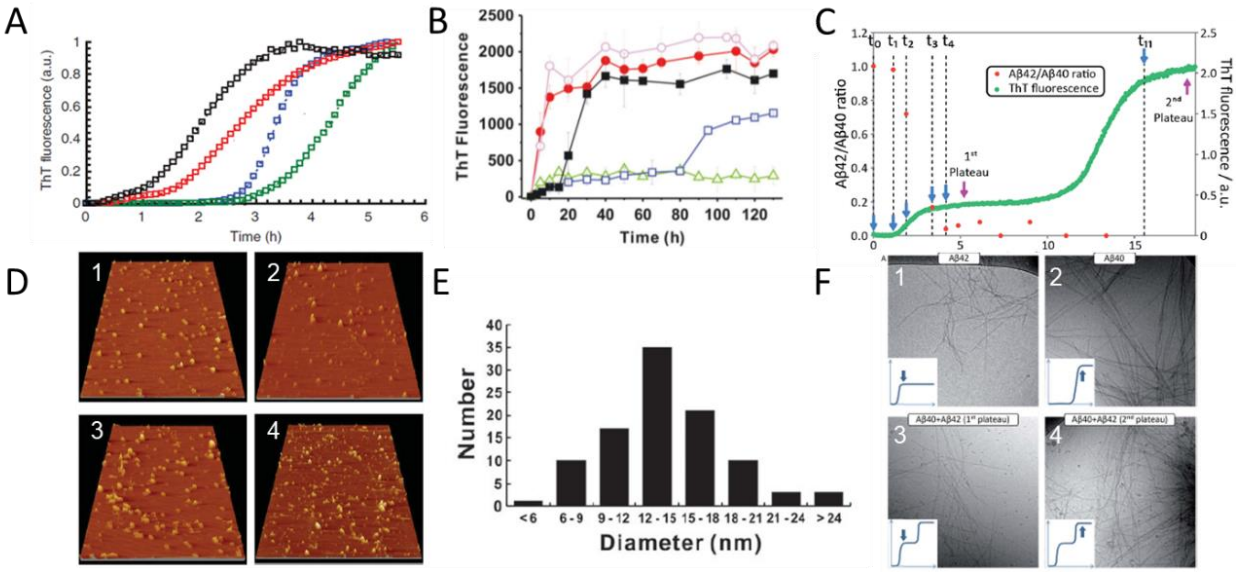

Figure 21. Effect of mixing Aβ(1:40) and Aβ(1-42). Monitoring the co-aggregation of Aβ(1-40):Aβ(1-42) by (A) ThT fluorescence and (D) AFM at different ratios. ThT assay: 0:10 (50 µM Aβ42) - black symbols; 7:3 (35 µM Aβ40 + 15 µM Aβ42) – red symbols; 9:1 (45 µM Aβ40 + 5 µM Aβ42) – green symbols; 10:0 (50 µM Aβ40) – blue symbols. Experimental conditions: Sample: 50 µM total Aβ + 12 µM ThT; 50 mM Tris–HCl, 1 mM EDTA, pH 7.5. Incubation: quiescent conditions at 25 °C. Fluorescence detection: λ_{Em}= 480 nm, λ_{Ex}= 440 nm. AFM measurements were taken after 1.5 h of incubation at 25 °C: 1 (10:0); 2 (9:1); 3 (7:3); 4 (0:10). The samples AFM sample did not contain ThT (adapted from Kuperstein *et al.*[128]). Kinetic evaluation of several Aβ(1-40):Aβ(1-42) ratios by (B) ThT fluorescence and (E) the oligomer size distributions obtained by TEM for the equimolar mixture after 140 h of aggregation. ThT assay: 0:10 (50 µM Aβ42) – red solid circles; 1:9 (5 µM Aβ40 + 45 µM Aβ42) – pink open circles; 5:5 (25 µM Aβ40 + 25 µM Aβ42) – green open triangles; 9:1 (45 µM Aβ40 + 5 µM Aβ42) – blue open squares; 10:0 (50 µM Aβ40) – black solid squares. Experimental conditions: Sample: 50 µM total Aβ + 5 µM ThT; 10 mM phosphate buffer pH 7.4. Incubation: agitated conditions at 25 °C. Fluorescence detection: λ_{Em}= 485 nm, λ_{Ex}= 442 nm. TEM analysis: 400-mesh Formvar carbon coated copper grids; Grids were negatively stained with 2 % uranyl acetate 5 min after sample deposition and then rinsed with water; Samples did not contain ThT; Voltage: 75 kV. Analyses were performed at 25 °C (adapted from Chang *et al.*[129]). Monitoring the aggregation kinetics and fibril formation of an equimolar Aβ(1-40):Aβ(1-42) mixture by (C) ThT assay/MALDI-TOF MS and (F) *cryo*-TEM. Each of the 11 times points correspond to the moments where a small amount of sample was taken and subjected to MS analysis. The remaining concentration of the equimolar ratio was estimated by MS (red solid circles). Aβ(1-40) was entirely native while Aβ(1-42) contained ^{15}N isotope for a proper discrimination between the homo- and heteromolecular species during the MS analyses. Experimental conditions: Sample: 3 µM total Aβ (1.5 µM Aβ40 + 1.5 µM Aβ42) + 5 µM ThT; 20 mM sodium phosphate buffer, 200 µM EDTA, 0.02 % NaN_3, pH 7.4. Incubation: quiescent conditions at 25 °C. Fluorescence detection: λ_{Em}= 480 nm, λ_{Ex}= 440 nm. *cryo*-TEM analysis: lacey carbon filmed copper grids; Grids were placed in liquid ethane; before each analysis Voltage: 120 kV. Analyses were performed at -180 °C. For the *cryo*-TEM, the total Aβ concentration was 3 µM (1.5 µM Aβ40 + 1.5 µM Aβ42) and did not contain ThT (adapted from Cukalevski *et al.*[46]).

With the advancement and improvement of biophysical techniques, the co-aggregation of Aβ peptides and their corresponding mutants was investigated more extensively over recent years, especially for the most abundant isoforms Aβ(1-40) and Aβ(1-42)[33,46,128–134]. Two independent

groups have studied the co-aggregation mechanism of the two isoforms at different ratios of Aβ(1-40):Aβ(1-42) with a major focus on the kinetics of process and the size and morphology of the generated species[128,129]. The main differences between the two studies were mainly related to the different origins of the peptide, purchased[128] or synthesized[129], the pretreatment steps involving either a combination of HFIP, DMSO followed by a separation through a desalting column[128] or a dissolution in DMSO followed by a dilution in the incubation buffer[129], and the sample matrix, which consisted of 50 mM Tris–HCl, 1 mM EDTA, pH 7.5[128] or 10 mM phosphate buffer pH 7.4[129]. Both studies kept the total Aβ concentration constant at 50 μM for all the studied Aβ(1-40):Aβ(1-42) ratios[128,129].

First, the aggregation process of the mixtures was monitored by ThT assay[128,129]. Kuperstein *et al.*[128] studied four different Aβ(1-40):Aβ(1-42) ratios of 10:0, 9:1, 7:3, and 0:10, respectively (Figure 21 A), while Chang *et al.*[129] extended their study to include the equimolar ratio and the 1:9 ratio (Figure 21 B) without investigating the 7:3 system. The former observed that there was a strong dependence on the kinetics of the aggregation with respect to the Aβ ratios, without exhibiting a significant effect upon the final fibril yield[128]. Most interestingly, it was found that, at a ratio of 9:1, the process was slightly retarded compared to Aβ(1-40)[128] and, strikingly, despite the differences in the sample preparation, Chang *et al.* observed the same kinetic effect when comparing the 9:1 ratio with the Aβ(1-40) independent experiment, but to a larger extent than depicted in the study performed by Kuperstein *et al.*[129]; while, for the rest of the systems, the kinetics were retarded in a ratio-dependent manner by increasing the Aβ(1-40) content[128,129]. Another interesting aspect related to the equimolar ratio (Figure 21 B - green open triangles) observed by the authors is the lag phase of ~6 h and a significantly reduced fibrilization plateau as compared to all the other systems, suggesting that a smaller number of fibrils were formed[129].

A more thorough investigation of the kinetics of the equimolar mixtures for these two isoforms was performed by Cukalevski *et al.*[46]. The aggregation was monitored simultaneously by ThT assay and a more advanced mass spectrometry (MS) technique (Figure 21 C)[46]. For better discrimination between the isoforms during the MS analysis, the authors used ^{15}N-Aβ(1-42) while Aβ(1-40) was in its native state[46]. It was observed that the fibrillization occurred in a two-step sigmoidal increase, suggesting that two different processes occur simultaneously in the sample[46], contrary to what was observed by Chang *et al.* during their aggregation study. However, it is noteworthy to mention that both analyses and experimental conditions were very different between

the studies[129]. Initially, a short lag phase of about 1 h was followed by a first intermediate plateau lasting for about 11 hours[46]. According to MS measurements, the total Aβ concentration, in terms of monomer consumption, decreased very fast and reached a minimum shortly after the first plateau was recorded[46]. The MS analysis revealed that Aβ(1-42) was consumed during this incubation time, while the signal of Aβ(1-40) was still stable, further demonstrating that the first sigmoidal step belongs to the aggregation process of Aβ(1-42)[46]. After approximately 12 h of incubation, the second transition started to occur and stabilized as a secondary fibrilization plateau after ~16 h[46]. According to the MS analysis, the second transition corresponded to the consumption of Aβ(1-40) early stage species as no MS signals corresponding to Aβ(1-40) were detected at the t_{11} measurement, showing that the secondary fibrillization plateau belongs to the formation of Aβ(1-40) fibrils[46].

Depending on the ratio, some morphological differences of the species were also described[128,129]. Notably, Kuperstein *et al.* performed both TEM and AFM analyses for some selected incubation times, which they further correlated with some thorough toxicity studies[128]. The authors showed that no fibrils were present at the moment of the dissolution in all of the studied ratios[128]. The mature Aβ(1-42) fibrils were thus characterized as densely packed fibrillar networks[128]. For the Aβ(1-40) independent experiment 9:1 ratio, the fibrils exhibited a similar morphology but with a regular twisting pattern compared with those generated by Aβ(1-42)[128]. At the 7:3 ratio, the authors stated that the first aggregates started to appear after 9 h along with multiple types of fibrils that could not be discriminated from each other, and that these observations were not in agreement with the ThT assay for which a fibrilization plateau was observed only after 4 h (Figure 21 A – red symbols)[128]. According to the authors, a plausible explanation would be due to the formation of ThT binding species for the 7:3 ratio[128]. By using AFM analysis, it was also revealed that the oligomeric species were generated for all the studied ratios after an incubation time of 1.5 h (Figure 21 D), which coincides with the time corresponding to the highest detected synapto-toxicity of the 0:10 and 1:9 ratios[128]. The authors hypothesized that the oligomeric species are not necessarily toxic species, but that the toxicity may be generated by a preferred organization within the tested cells, as no toxicity was observed at that time for Aβ(1-40) alone nor for the 9:1 mixture[128]. However, a clear morphological comparison between the oligomers generated during the studied ratios has not been performed in their study[128]. A more detailed characterization of these species was performed using TEM correlated with dot blot

analysis in the study published by Chang *et al.*[129]. For the Aβ(1-40) enriched ratios, 10:0 and 9:1 oligomers were distinct and presented a low abundance compared to the other ratios, while the protofibrils generated during the 9:1 ratio presented a very low abundance and were found to be very similar to those generated during the Aβ(1-40) aggregation process, although they also contained shorter protofibrils of length 20 – 90 nm, that were predominant in the Aβ(1-42) enriched ratios of 1:9 and 0:10, respectively[129]. No differences were observed between the mature fibrils generated in the two Aβ(1-40) enriched ratios[129], whereby the fibrils were described as long and straight with characteristic lengths ranging from 100 nm to more than 1 μm[129]. The most striking results were observed in the case of the equimolar mixtures, in which dispersed spherical oligomeric populations of 9 – 20 nm in diameter, with a maximum centered around 12 – 15 nm (Figure 21 E) at both initial and end points of the aggregation, were observed, suggesting that these species are off-pathway and present the highest rate of toxicity[129]. After 120 h of incubation, protofibrils were present in a similar abundance compared to those generated during the aggregation Aβ(1-40) enriched mixture, while no significant fibrils formation occurred, in agreement with the observations from the ThT assay (Figure 21 B, green open triangles)[129]. However, this is in contrast to what was reported by Cukalevski *et al.*[46]. In their study, the authors compared the equimolar mixture with the Aβ(1-40) and Aβ(1-42) independent aggregation experiments by taking the measurements at similar incubation times (Figure 21 F) and by using a more sophisticated *cryo*-TEM technique[46]. According to the authors, Aβ(1-40) fibrils were large, straight, and thick with a characteristic node-to-node distance of 162 ± 21 nm (Figure 21 F1)[46], while Aβ(1-42) fibrils were more densely packed, shorter, and twisted compared to the ones generated during the Aβ(1-40) process, characterized by a node-to-node distance of 31 ± 17 nm (Figure 21 F2)[46]. Performing the morphological analyses on the equimolar mixture revealed that the fibrils formed during the first plateau were very similar to those formed during the Aβ(1-42) aggregation (Figure 21 F3), having a characteristic node-to-node distance of 39 ± 17 nm, while the analysis performed after the appearance of the secondary plateau, presented two sets of fibrils with a node-to-node distance of 39 ± 17 nm (Figure 21 F4) and 199 ± 28 nm (Figure 21 F4), for the first and the second sets of fibrils, respectively; the latter resembling the ones formed during the Aβ(1-40) independent experiment[46]. The authors further suggested that, at least during the equimolar co-aggregation process, independent but not mixed fibrils can form[46].

The formation of Aβ co-nuclei from MS measurements was also observed by Cukalevski *et al.*, as different mass signals than those detected for Aβ(1-40) and ^{15}N-Aβ(1-42)[46] were recorded. To gain more insights regarding the dynamics of the co-aggregation process of Aβ peptides, the authors further correlated these results with other in-depth structural investigations and theoretical calculations[46]. Based on their findings, they proposed that during the co-aggregation of Aβ(1-40) and Aβ(1-42), the nucleation proceeds with the formation of both homomolecular nuclei (Aβ40-Aβ40 and Aβ42-Aβ42) and heteromolecular co-nuclei (Aβ40-Aβ42) that self-associate into separate homomolecular fibrils, since Aβ(1-40) fibrils were found to be unable to seed the aggregation process of Aβ(1-42) and viceversa[46]. This supports the previous observations of Kuperstein *et al.*, where the content of Aβ40-Aβ40, Aβ42-Aβ42 and Aβ40-Aβ42 nuclei was assessed by MS during the co-aggregation of Aβ(1-40):Aβ(1-42) for the following ratio: 9:1 (81%, 1% and 18%), 7:3 (49%, 9% and 42%), 1:1 (25%, 25% and 50%)[128]. In addition, Chang *et al.* proposed some possible aggregation pathways depending on the studied ratio[129].

Although it is more widely accepted that Aβ peptides can only be seeded by fibrillar species obtained from the same isoform[23,46,132], some reports have also suggested that cross-seeing may occur to a certain extent[130] or that heteromolecular fibrils might form during the co-aggregation of Aβ peptides[131].

In conclusion, it is now accepted that Aβ(1-40) is able to inhibit the aggregation process Aβ(1-42), playing an important neuroprotective role during the amyloid cascade of reactions[46,134]. Thus, the toxicity is ratio-dependent and it has been found to increase in the following order: Aβ(1-40) enriched ratios > Aβ(1-42) enriched ratios > Aβ(1-40):Aβ(1-42) equimolar ratio[128–130,134]. Nonetheless, a clear consensus regarding the co-aggregation mechanism has not yet been reached, especially because the extent to which early stages species are inhibited has not yet been accurately described. Therefore, there is a strong demand in the development of novel biophysical techniques that can allow a simple and fast analysis for real-time monitoring of the dynamics of the Aβ peptides co-aggregation, more specifically directed toward the size, shape, and evolution of the oligomeric and protofibrillar intermediates.

I.3. Disease-modifying small molecules designed for inhibiting the aggregation process of Aβ peptides

As presented in section 1, there are three main types of therapeutic strategies to combat AD: system-reducing small molecules, disease-modifying biologic, and disease-modifying small molecules[35]. Most of the strategies directed towards the inhibition of the aggregation mechanism of the Aβ peptides are therapeutics based on small molecules[17,35]. Such compounds may be represented either by short peptides that mimic specific fragments of the Aβ sequence[135] or compounds designed to target specific aggregation sites of the species[35].

Until 1998, year when the amyloid oligomer hypothesis has emerged[18], fibrils were considered the main therapeutic targets for AD[19]. Nowadays, the most common therapeutic strategies are: i) compounds that can inhibit the formation of fibrils[19,136]; ii) small molecules that inhibit the formation of toxic oligomers by accelerating fibril formation[17,137]; iii) small molecules that inhibit the self-assembly process: β-hairpin modulators[32,138].

Inhibitors that are able to reduce the fibrils fragmentation, and thus block secondary-nucleation sites that occur on the surface of the fibril, are also of great importance[23]. Nonetheless, these therapeutics are based on disease-modifying biological species as the molecular Chaperon domain[23], or monoclonal antibodies such as aducanumab[7,8].

I.3.1. Small molecules that inhibit the formation of fibrils

As mentioned before, fibrils are no longer considered the main species of interest in the development of AD. However, their importance cannot be overlooked as they represent the end products of the aggregation process of Aβ peptides and their accumulation leads to the formation of extracellular deposits known as amyloid plaques, which are further capable of blocking the communication between neurons and cells[6,15,135]. Some of the most novel strategies are drugs that can interact with oligomers by preventing them from further self-associating into fibrils[17]. Some examples belong to a class of polyphenol derivatives such as ε-Viniferin glucoside and epigallocatechin gallate, but most of these drugs have failed during clinical trials[17].

Historically, one of the first important family of small molecules that can inhibit fibril formation are represented by short peptides that can act as β-sheet breakers[135]. One type of such inhibitor is iAβ5p (Ac-LPFFD-NH_2) (Figure 22 A) and was first reported by Soto *et al*[19].

Structurally, it resembles a part of the CHC fragment of the Aβ sequence, which is known to aggregate on its own[19,100]. The authors showed that this inhibitor can bind the Aβ peptides to destabilize the β-sheet enriched structures and consequently prevent the formation of fibrils[19,135]. Therefore, there has been increasing interest in this type of small peptides over the years and especially since other studies reported the development of various structures resembling that of iAβ5p precursor[139–141].

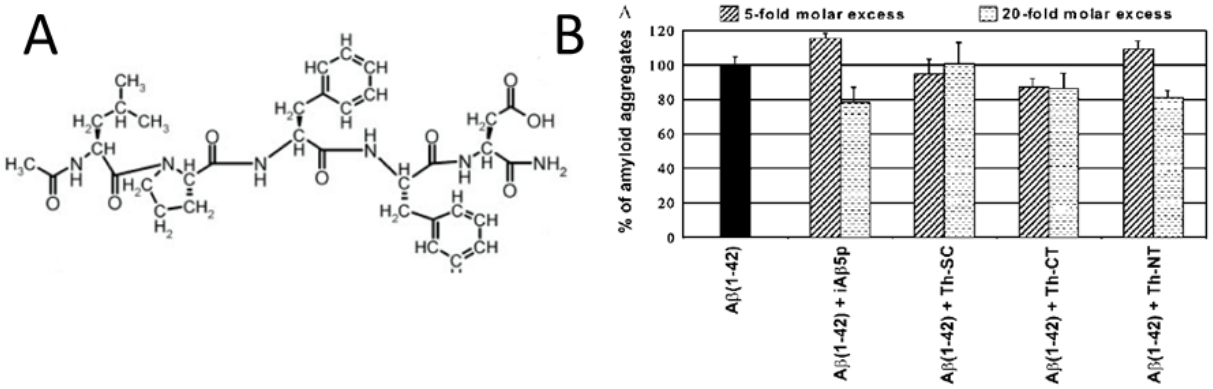

Figure 22. Monitoring the inhibition effect of iAβ5p and some of its precursors upon the aggregation process of Aβ(1-42): (A) Chemical structure of iAβ5p (adapted from Adessi *et al.*[135]). (B) Effect upon the fibrillization inhibition monitored by ThT assay in the presence and in the absence of iAβ5p, Th-SC, Th-NT and Th-CT respectively. Experimental conditions: Sample: 100 μM Aβ(1-42) (with or without inhibitor) + 10 μM ThT; 20 mM phosphate buffer, pH 7.4. Incubation: quiescent conditions at 37 °C. Fluorescence detection: λ_{Em}= 480 nm; λ_{Ex}= 440 nm (adapted from Debona *et al.*[139]).

In one of these studies, De Bona *et al.* developed three new trehalose conjugates capable of inhibiting the aggregation: Ac-LPFFN(Th)-NH2 (Th-SC), Th-Succinyl-LPFFD-NH2 (Th-NT), and Ac-LPFFD-Th (Th-CT), respectively[139]. Afterwards, for a proper comparison, they used the iAβ5p precursor in their experiments. The authors first monitored the aggregation by ThT assay, and then compared the overall fibril yield (Figure 22 B) obtained using a molar excess of 5 and 20-fold that of the studied inhibitors, with respect to the one obtained for the Aβ(1-42) independent experiment. It was revealed that Th-SC had little effect on the fibrillization in either ratio, whereas Th-NT presented a similar behavior compared to iAβ5p. The most promising results were obtained for iAβ5p and Th-NT, which showed an approximately 20% reduction in the fibril plateau during the 20-fold molar excess experiments and for the Th-SC, which instead presented the same degree of fibril inhibition at both studied ratios. Combining these results with other morphological and toxicological analyses, the authors further suggested that the novel derivatives might also have an impact on the nucleation stage of the process[139].

I.3.2. Small molecules that accelerate the formation of fibrils

This class of compounds is able to reduce the life-time of preformed oligomers by increasing the fibrillization rate of the aggregation process[17]. One type of such compound is represented by TRO (Figure 23 A), a natural product generally found in the liver of sharks and dogfish that belongs to a class of compounds known to preserve the integrity of cell membranes[137].

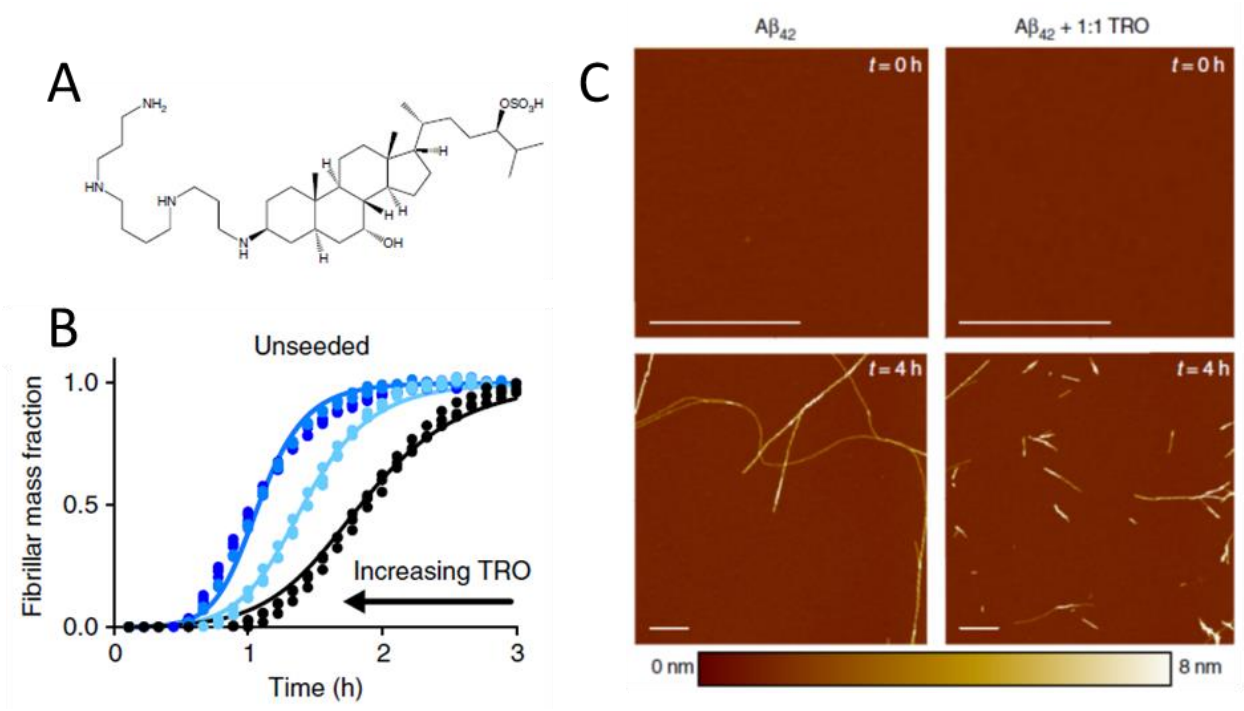

Figure 23. Monitoring the inhibition effect of TRO upon the aggregation process of Aβ(1-42). (A) Chemical structure of TRO. Inhibition was monitored by (B) ThT assay at three different Aβ(1-42):TRO ratios of 1:1 (dark blue), 5:1 (medium blue) and 10:1 (light blue) respectively, and (C) by taking AFM measurements 0 and 4 h of incubation for Aβ(1:42) and the equimolar ratio. Experimental conditions: Sample: 2 µM Aβ(1-42) + 20 µM ThT ± 2, 10 or 20 µM TRO; 5 mM sodium phosphate, 200 µM EDTA, 150mM NaCl, pH 8.0. Incubation: quiescent conditions at 37 °C. Fluorescence detection: λ_{Em}= 480 nm, λ_{Ex}= 440 nm. AFM analysis: mica subtrates were positively functionalized with 0.05% (v/v) (3-aminopropyl) triethoxysilane; Samples did not contain ThT; Tapping mode with scan rates <0.5 Hz; Analyses were performed at 25 °C (adapted from Limbocker *et al.*[137]).

A recent study employed the use of trodusquemine (TRO) upon the aggregation of Aβ(1-42) to evaluate its inhibition effect[137]. The authors first monitored the aggregation of Aβ(1-42) by ThT assay (Figure 23 B) in the presence and absence of TRO at three different ratios of 1:1, 1:5 and 1:10, respectively. Interestingly, the highest accelerating effect was observed for 1:1 and 1:5 Aβ(1-42):TRO ratios when the process was unseeded. Then, the authors performed these experiments also in the presence of seeded Aβ(1-42), where fragmented fibrils of the corresponding isoform were used to catalyze the aggregation process and a more clear discrimination in the kinetics of

the studied ratios was observed, showing that the aggregation process is accelerated in the order of decreasing the Aβ(1-42):TRO ratio. The most promising results were observed for the equimolar system. In addition, the authors performed measurements by AFM for Aβ(1-42) alone and the equimolar ratio (Figure 23 C) shortly after the dissolution and after 4 h of incubation. At *t* = 0 h, no predominant aggregates or fibrils were detected in either case. After 4 h of incubation, Aβ(1-42) fibrils presented average heights of 4.2 ± 0.2 nm, widths of 12 ± 1 nm, and lengths of 1.81 ± 0.12 μm, while those generated in the presence of TRO showed higher cross-sectional diameters characterized by average heights of 6.3 ± 0.3 nm and widths of 15 ± 1 nm, while their average lengths were significantly reduced to 0.63 ± 0.06 μm. These results were further confirmed by TEM analysis. Eventually, by correlating these results with other in-depth structural and toxicological analyses and theoretical calculations, the authors were able to demonstrate that TRO is likely to enhance the aggregation kinetics by increasing both the rate of secondary-nucleation and elongation, consequently reducing the binding and the toxicity of preformed oligomers, classifying these natural compounds as suitable for combating AD[137].

I.3.3. Small molecules that inhibit the self-assembly process: β-hairpin modulators

As most of the presented previous strategies directed toward the amyloid cascade of reactions have proven not to be completely efficient because many of them failed different phases of clinical trials, new strategies that can efficiently inhibit the aggregation process of Aβ peptides are in high demand[7,17]. According to recent structural and mechanistic information, new studies have shown that the self-assembly process could be favored by a β-hairpin conformation that could represent the key intermediate behind the generation of critical nuclei[17,55]. On this basis, research is now driven toward the development of β-hairpin modulators able to inhibit the aggregation by blocking the nucleus formation and consequently the self-assembly motifs from the onset of the aggregation[17,32,138].

Recent examples of this class of inhibitors include a type of foldamers presenting different repetitive units of 4-amino-(methyl)-1,3-thiazole-carboxylic acid (ATC), as shown in Figure 24 A.

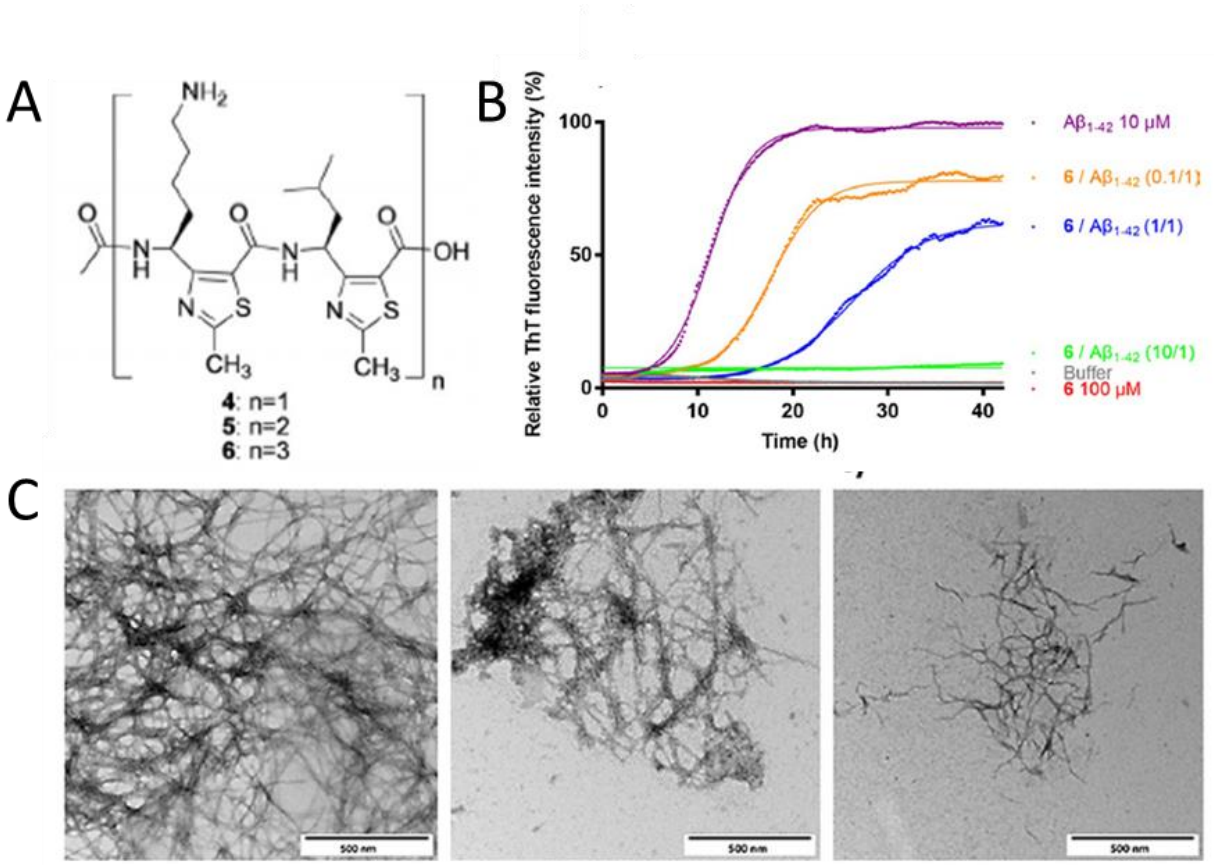

Figure 24. Monitoring the inhibition effect of ATC foldamers upon the aggregation process of Aβ(1-42): (A) General structure of ATC foldamers. Monitoring the aggregation by (B) ThT assay with or without inhibitor at an Aβ(1-42):ATC ratio of 1:0 (violet), 1:0.1 (orange), 1:1 (blue) and 1:10 (green) and by (C) TEM by taking measurements for the Aβ(1-42):ATC ratios of 1:0 (left), 1:1 (center) and 1:10) (right) after 42 h of incubation. Experimental conditions: Sample: 10 µM Aβ(1-42) + 40 µM ThT ± 1, 10 or 100 µM ATC; 10 mM Tris-HCl, 100 mM NaCl, 0.5% (v/v) DMSO, pH 7.4. Incubation: quiescent conditions at 37 °C. Fluorescence detection: λ_{Em}= 485 nm; λ_{Ex}=440 nm. TEM analysis: 400-mesh Formvar carbon coated copper grids; Grids were negatively stained with 2 % uranyl acetate 2 min after sample deposition and then rinsed with water; Voltage: 80 kV. Analyses were performed at 25 °C (adapted from Kaffy *et al.*[138]).

In this study, the authors first monitored by ThT assay the influence of all the synthesized foldamers at four different Aβ(1-42):ATC ratios of 1:0, 1:0.1, 1:1, and 1:10, respectively[138]. The most promising results were observed in the case of the foldamer ATC 6 (Figure 24 B) bearing three repetitive units as there was a significant inhibition of both the nucleation phase and the final fibrils yields in an increasing ATC concentration manner. Moreover, for the ratio of 1:10, the fibrillization was completely inhibited. The authors further investigated the morphologies of the generated fibrils by TEM measurements (Figure 24 C) of Aβ(1-42) alone and in the presence of ATC 6 at a ratio of 1:1 and 1:10 after 42 h of incubation. Aβ(1-42) fibrils were characterized by highly dense packed networks[138] resembling other descriptions from the literature[46,83,128]. Those

obtained during the equimolar ratio exhibited a significant reduction in the fibrillar material and were shorter and twisted around by large aggregates while, at the excess ratio, they were significantly thin suggesting a very high inhibition compared to the control Aβ(1-42) experiment[138]. The authors further confirmed these results with other CE analyses and suggested that these helical ATC foldamers might be able to destabilize Aβ preferential folding by interacting with the peptide in the CHC and CTR regions. Finally, the authors proposed that these structures may be modified to inhibit other amyloidogenic peptides or proteins since a significant inhibition of human islet amyloid polypeptide, known to be involved in the development of type 2 diabetes, was observed as well in their study[138].

I.4. Biophysical techniques employed for evaluating kinetics, size distribution and morphology of Aβ species

A wide range of biophysical techniques can be found in the literature that were applied for the study of the amyloid cascade of reactions. Among these techniques, structural characterization methods such as circular dichroism (CD)[17,83], X-ray diffraction[15,17], infrared (IR) spectroscopy[17,108], nuclear magnetic resonance (NMR)[17,46] or advanced MS techniques[15,31] are employed to characterize the formed species, to monitor conformational changes or to determine possible binding modes with different extrinsic species. While the kinetics and the mechanism of the aggregation are mainly evaluated by ThT assay[79,112], likewise CE can also be used[103,114]. Alternatively, the most common tools for evaluating the size (R_h) distribution of the species are DLS[29,142] and FCS[91,143] whereas PAGE[143] and SEC-MALS[29,63] are used to get the mass distribution. Further, the morphology of the species is generally assessed by imaging methods such as EM and AFM[36,63], the latter methods have provided most of the actual information on the aggregation behavior of Aβ peptides. However, a single method is not enough to unravel the overall information regarding the aggregation mechanism, as each of these techniques present several limitations despite the useful quantitative and/or qualitative data that they are able to provide. Therefore, all these methods are complementary to each other and are often employed together to gain more insights on the aggregation process of Aβ peptides. Nonetheless, only a few of these methods can be used to monitor the aggregation in real time, providing information about kinetics, size, and the shape of the species.

Table 2 provides some examples of biophysical techniques employed so far to evaluate the aggregation process of Aβ peptides, listing the studied isoforms, the analysis, and sample specifications.

Table 2. Biophysical techniques employed for studying the aggregation process of Aβ peptides.

Entry	β-Amyloid		Biophysical technique		Sample specifications			Ref.
	Name	Origin	Type	Analysis specifications	Concentration (µM)	Matrix	Temperature (°C)	
1	• Aβ(1-40) • Aβ(1-42)	• Lyophilized powder recombinant Aβ from AlexoTech AB	AFM	• Freshly cleaved mica mica substrates • Resonance frequency ~150 kHz • Analyses were performed at 25 °C	27 for Aβ(1-40) and 29.3 for Aβ(1-42)	50 mM sodium phosphate buffer, pH 7.4	25	[144]
2	• Aβ(1-42)	• Lyophilized Aβ(1-42) from Yale University, New Haven, CT, USA	AFM	• Freshly cleaved mica substrates functinaized with 0.05 % (v/v) APTES • resonance frequency: 96-168 kHz • Analyses were performed at 25 °C	20	10 mM Tris-HCl, pH 7.4	37	[36]
3	• Aβ(1-40)	• Aβ (1-40) (human sequence) from Sigma, Roboscreen or rPeptides	CE-LIF	• fs capillaries 50 um X 53 cm X 70 cm • BGE: 10 mM ThT, 50 mM ammonium acetate, pH 4.7 • Injection: 0.5 psi for 10 s • Diode laser: 190 nm / λ_{Em} = 485nm • Voltage: 25 kV	100	Ringer solution	35	[114]
4	• Aβ(1-42)	• Lyophilized Hylite Fluor 488 Aβ(1-42) powder from Bachem	CE-LIF	• fs capilaries 50 µm ID × 50 cm X 40 cm • BGE: 80 mM phosphate buffer pH 7.4 • Ar-ion laser • λEx = 488 nm / λEm = 520 nm • Injection: 3.44 kPa • Voltage: +16 kV	5	20 mM phosphate buffer, pH 7.4	37	[106]

5	• Aβ(1-42)	• Aβ (1-42 (TFA salt) - American Peptide (Sunnyvale, CA, USA)	CE-UV	• fs capillaries: 50 µm ID × 80 cm x 10.2 cm • BGE: 80 mM phosphate / 9 mM DAB buffer pH 7.4 • Voltage: −30 kV • Injection: 3.44 kPa for 10 s • UV detection: 190 nm	100	20 mM phosphate buffer, pH 7.4	20	[103]
6	• Aβ(1-40) • Aβ(1-42)	• Aβ(1-40) donated by Pharmacia (Nerviano, Italy) • Aβ(1-42) synthesized at the Core Protein Laboratory of Wake Forest University (Dr. M. O. Lively)	CE-UV	• Fs capillaries 50 µm ID X 53 cm X 48.5 cm • BGE : 80 mM phosphate buffer pH 7.4 • Injection: 50 mbar for 8 s • UV detection: 200 nm • Voltage: 16 kV	100	20 mM phosphate buffer, pH 7.4	25	[113]
7	• Aβ(1-40) • Aβ(1-42)	• Synthesis: Automated SPPS Fmoc chemistry • Purification: RP-HPLC >97%	DLS	• Operation: 514 nm • Scaterring angle 90° • Analyses were performed at 25 °C	15 - 40	10 mM phosphate buffer, pH 7.4	25	[56]
8	• Aβ(1-42)	• Synthesis: Automated SPPS Fmoc chemistry • Purification: RP-HPLC	DLS	• Coherent 304 argon ion laser	220	HFIP DMSO H_2O/0.1% TFA 2-Pr	r.t.	[61]

9	• Aβ(1-39) • Aβ(1-40) • Aβ(1-41) • Aβ(1-42) • Aβ(1-43)	• Synthesis: Automated SPPS Fmoc chemistry • Purification: RP-HPLC >97%	PICUP - SDS/PAGE	• 1 µL of 1 mM Ru(Bpy) + 1 µL of 20 mM APS in 1 mM sodium phosphate at pH 7.4 + 18 µL peptide • Irradiation with visible light • Reaction quenched immediately with 10 µL of tricine sample buffer containing 5% (β -ME) • Peptide sample was loaded on the lane of a tris- tricine-10-20 % polyacrylamide gel	15 - 40	10 mM phosphate buffer, pH 7.4	r.t.	[56]
10	• Aβ(1-42)	• Aβ (1-42) (TFA salt) from American Peptide (Sunnyvale, CA, USA)	SDS/PAGE	• Tris-glycine-17% polyacrylamide gel • Voltage: 80 V for 10 min and then at 200 V for 45 min	100 ± inhibitor	20 mM phosphate buffer, pH 7.4	20	[103]
11	• Aβ(1-40)	• Synthesis: Automated SPPS Fmoc chemistry • Purification: RP-HPLC 97% purity	STEM	• 3 nm carbon films on 200 mesh copper grid • Accelerating voltage: 100 kV • Probe diameter: 1 nm • Current: 2 pA • Electron dose: 103 e/nm2	210	10 mM phosphate buffer pH 7.53 + 0.01% NaN3	37	[80]
			TEM	• Lacy Formvar/carbon films on 200 mesh copper grid • grids tained with 1 % uranyl acetate				
12	• Aβ(1-42)	• Aβ (1-42) (TFA salt) - American Peptide (Sunnyvale, CA, USA)	TDA	• Fs 50 µm ID X 50 cm X 39.8 cm • BGE: 20 mM phosphate buffer, pH 7.4 • Mobilization pressure: 68.9 mbar • Injection: 3.44 kPa for 15 s • UV detection: 190 nm	100	Buffer - (20 mM phosphate buffer pH 7.4)	r.t.	[103]

13	• Aβ(1-42)	• Aβ (1-42) (TFA salt) from American Peptide	ThT fluorescence assay	• λEx = 440 nm / λEm = 485 nm	10 Aβ(1-40) + 40 ThT ± inhibitors	10 mM Tris-HCl buffer, 100 mM NaCl, pH 7.4	25	[115]
14	• Aβ(1-40) • Aβ(1-42)	• E coli human recombinant Aβ from rPeptide	ThT fluorescence assay	• λEx = 440 nm / λEm = 480 nm	50 Aβ + 12 ThT	50 mM Tris-HCl, 1 mM EDTA, pH 7.4	25	[108]

I.4.1. Fluorescent dyes used for evaluating the aggregation process of Aβ peptides

The most employed techniques used to monitor the kinetics and to evaluate the aggregation mechanism of Aβ peptides are fluorophore-based fluorescence methods, especially because they allow an accurate evaluation of the process at close-physiological concentrations, the most notable being the ThT fluorescence assay[33,97,112].

In general, there are two types of fluorophores that can be employed for studying the aggregation process: i) intrinsic dyes such as FITC, RITC, RB, Alexa Fluor or HiLyte Fluor derivatives[91,93,106], and ii) extrinsic dyes such as ThT, congo red (CR), 1-anilinonaphthalene-8-sulfonic acid (ANS) or dicyanomethylene-4H-pyran (DCMP) derivatives[112,148,149]. Most of the techniques that involve the use of intrinsic dyes are FCS, fluorescence anisotropy, and SMFS, whereas extrinsic dyes are primarily used when performing fluorescence assays[33,91,150].

As discussed in subsection I.2.2.1.3, intrinsic dyes are covalently bonded to different amino acid residues, and most of the labeling reactions are performed at the N-terminal Asp[1]. Depending on the aim of the study, they can be used either 100% labelled[57,106] or as a mixture with the corresponding native Aβ isoform[91,93]. Using covalently attached dyes is of a great importance as they can provide information regarding the evolution of all the species during the aggregation process at physiological or close-physiological concentrations[90,151]. However, peptide labelling is believed to alter the aggregation behavior of the native peptides[91–93].

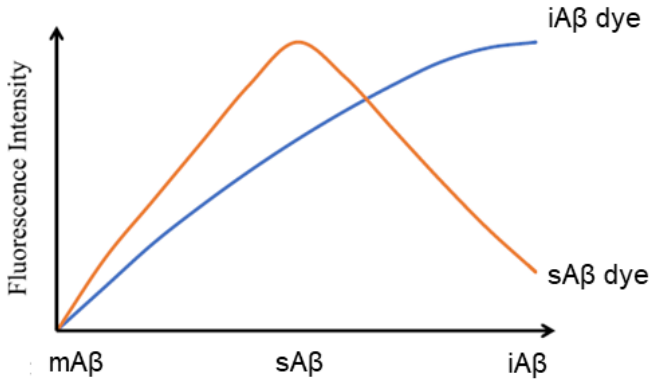

Figure 25. Schematic diagram of fluorescence intensities of Aβ-targeting fluorophores: monomeric Aβ aggregates (mAβ), oligomeric/protofibrillar Aβ aggregates (sAβ), and insoluble fibrillar Aβ aggregates (iAβ); Dye fluorescence intensity pattern of sAβ (orange) and iAβ (blue) (adapted from Lee *et al.*[151]).

On the other hand, extrinsic fluorophores are more widely employed when performing fluorescence assays, because they present a much simpler analysis and data interpretation of the obtained results as compared to other fluorescence-based methods such as FCS or SMF. Depending on the nature of the target species, they can be either dyes capable of detecting soluble aggregates (sAβ) such as oligomers and protofibrils[117,148], or dyes that are capable of recognizing insoluble aggregates (iAβ)[39], more specifically fibrils. By assuming that oligomers and protofibrils are on-pathway species, the fluorescence intensity of targeted sAβ should present a bell-shaped profile (Figure 25 A – orange line), while for the iAβ dyes, the recorded intensities are increasing during the aggregation course up until a maximum fluorescence plateau is reached (Figure 25 A – blue line). Dyes that can detect sAβ come with many drawbacks. In particular, during the nucleation and elongation phase, the sample is highly heterogeneous in nature as it is composed of a mixture of monomer, oligomers, protofibrils, and, to a certain extent, fibrils. Therefore, the sAβ can have a broad molecular mass range since various species, differing in size and structure, are present in the sample, especially the oligomeric populations that are unstable and transient in nature[56]. For this reason, it is highly difficult to isolate or prepare *in vitro* oligomeric species that present the same nature as those extracted from the brain and, consequently, designing dyes that can target a specific intermediate remains challenging. One of the most promising class of dyes that exhibit a high affinity for binding oligomers belongs to ANS derivatives, but have also been found to detect protofibrils up to a certain extent[149]. A very recent study presented the design of a novel DCMP derivative found to be highly selective towards the detection of protofibrils, but it is also capable of binding oligomers to a certain degree[148]. Therefore, it is important to mention that there are currently no available extrinsic dyes that can target with a selectivity of 100% a specific sAβ species[148,149,151]. However, although they are very difficult to be employed when performing full monitoring of the aggregation process, they are of great importance when drug-screening experiments are performed to verify the specific inhibition properties of the investigated therapeutics[137]. Compared to sAβ binding dyes, fluorophores that can detect iAβ are generally targeting enriched cross-β sheet structures[19,39]. The main species bearing this type of arrangement are highly rigid and stable fibrils, but some of them can also detect soluble and metastable protofibrils to a smaller extent because they also present an extended β-sheet content[39,41]. Because these species are more stable compared to soluble intermediates, the fluorescence detection of iAβ

is simpler and more accurate. Nonetheless, for most of the commercially available extrinsic dyes, the exact impact upon the aggregation process of Aβ peptides is not extensively described[90,112,151].

I.4.2. Monitoring the kinetics and the evolution of the species generated during the aggregation process of Aβ peptides

The most widely used tool for assessing the kinetics and the aggregation mechanism of Aβ peptides is the ThT fluorescence assay[23,39,79,112]. ThT is an extrinsic dye that presents a high selectivity toward the detection of fibrils, but can also bind protofibrils to a small degree[41]. It is characterized by a blue shift in the emissions spectrum starting from a wavelength of 510 nm in its free state, to 480 nm when attached to the fibril[39,152].

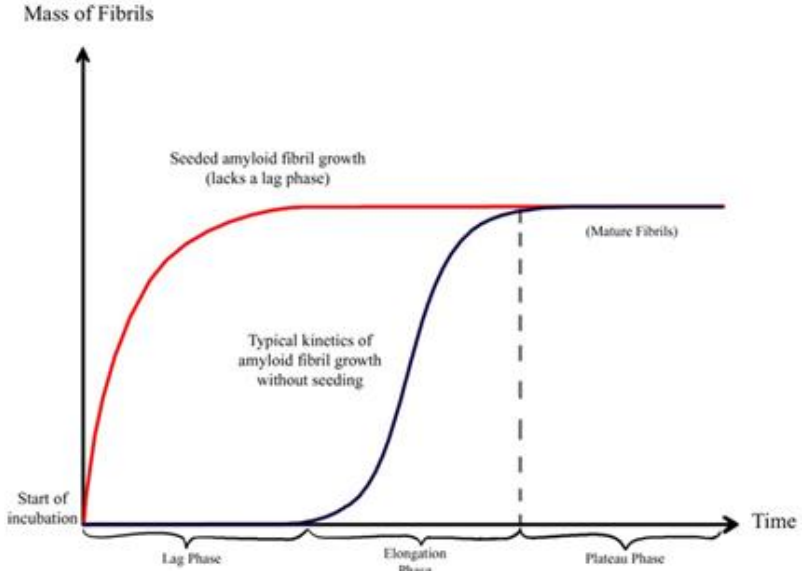

Figure 26. Schematic ThT fluorescence diagram during the monitoring of Aβ aggregation process with or without the presence of seeds. Without the presence of seeds the ThT profiles presence three phases: lag, elongation and plateau characterized by a sigmoidal shape (blue line). In the presence of seed a polynomial increase of the signal is observed lacking the lag phase (red line) (adapted from Ow *et al.*[153]).

A great advantage is that, for a given ThT concentration, the signal is linearly dependent on the fibrils generated during the aggregation process of a specific system[39,112] and, therefore, this analysis allows information to be derived about the mass accumulation of fibrils as a function of time (Figure 26 B). For this reason, it is highly important to evaluate morphological and structural differences between fibrils if different biological systems or Aβ isoforms are examined[83,112]. Another noteworthy aspect is related to the fact that the ThT concentration should not be limiting as the final fibril yield could be recorded before the aggregation has been completed[87]. It has also

been found that the optimal concentration of ThT should be within the range of 5 – 50 μM[46,97,145,154]. Above this range, quenching of the ThT-bound fibrils may occur due to the excess of ThT and may begin to affect the aggregation process of Aβ peptides[97,154]. As presented in more details in subsection I.2.1., the ThT fluorescence profile presents three important phases. During the lag (nucleation) phase, oligomeric species are mainly predominant. The profile is followed by a slope that corresponds to the elongation phase in which protofibrils and fibrils are the most abundant species, and it ends when the plateau phase is reached, corresponding to a final fibril yield, because the aggregation-prone species are no longer available to participate in the process. When the process is unseeded (Figure 26 B – blue line), all the three phases can be observed if LMM Aβ represents the starting material and the profile is depicted as a sigmoidal increase of the signal. When the LMM Aβ are seeded with species that are able to catalyze the reaction (Figure 26 B – red line), such as fragmented fibrils, the process generally lacks the lag phase leading to a polynomial increase of the signal by promoting the elongation from the beginning of the aggregation. This behavior can also be observed when studying the aggregation at high concentrations of the peptide[36,86]. Besides these important advantages, the ThT assay also presents some drawbacks. The major pitfall is that only the fibrillar species are detected[112]. Therefore, to properly monitor the evolution of the early-stage species, other biophysical methods should be employed in parallel for a more thorough investigation of the aggregation process. The ThT-fibril interaction and emission can be strongly affected by different parameters of the sample. For example, at acidic pH, ThT gets protonated leading to a significant decrease of the fluorescence signal[155]. Caution should also be taken when performing drug screening experiments, because small molecules that present similar structures to ThT can interact together and lead to the quenching of the fluorescence signal[156]. Nevertheless, the ThT assay remains the most employed method for evaluating the kinetics of the process, probing the aggregation mechanism of Aβ peptides, and performing drug screening assays because it provides robust data that can be further applied in the kinetic amyloid model[27]. These aspects are better described elsewhere[23,27,79].

Another technique that received a lot of attention during the last two decades is CE, especially for its ability to electrokinetically separate Aβ species[103]. Different CE modes have been explored for monitoring the aggregation process of Aβ peptides, such as capillary gel electrophoresis[96], and capillary zone electrophoresis which, in this study, is simply denoted as CE, the latter being the

most employed[103,106,113,114,138,145]. The majority of the studies used either UV[103,113,138] or laser induced fluorescence (LIF)[106,114,145] detection.

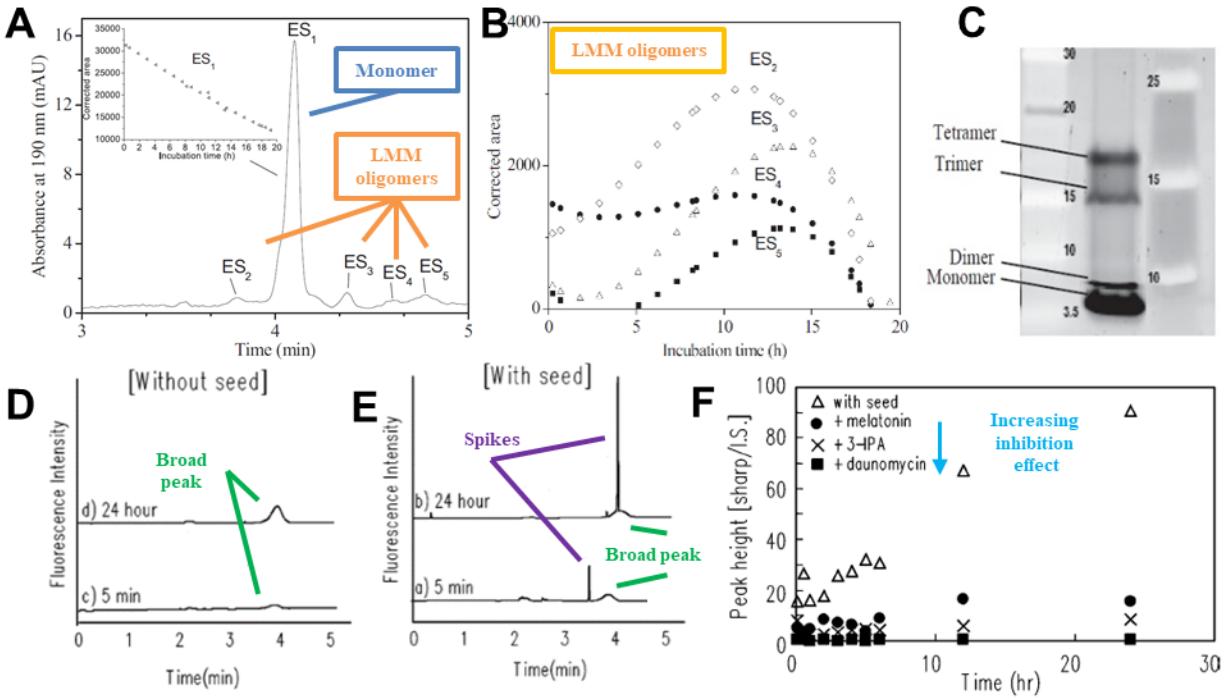

Figure 27. Monitoring the aggregation of Aβ(1-42) by CE-UV and correlated with SDS PAGE analysis. (A) Electropherogram of LMM Aβ(1-42) shortly after the peptide dissolution; inset depicts the evolution of the monomer peak. (B) LMM Aβ(1-42) oligomers evolution during the aggregation course. (C) SDS-PAGE analysis of LMM Aβ(1-42) shortly after the dissolution. Experimental conditions: Sample: 100 µM Aβ(1-42); 20 mM phosphate buffer, pH 7.4. Incubation: quiescent conditions at 20 ◦C. CE-UV: fs capillaries: 50 µm ID × 365 µm OD x 80 cm x 10.2 cm; BGE: 80 mM phosphate + 9 mM DAB buffer, pH 7.4; Voltage: -30 kV; Injection: 34.4 for 10 s; Analyses were performed at 20 ◦C; UV detection at 190 nm. SDS-PAGE: Gel lane: tris-glycine-17% polyacrylamide (adapted from Brinet *et al.*[103]). Monitoring the aggregation of Aβ(1-42) by CE-LIF after 5 min and 24 h (D) in the absence and (E) the presence of seeds and (F) by studying the inhibition properties of melatonin, 3-IPA and daunomycin. Experimental conditions: Sample: 130 µM Aβ(1-42) ± Aβ(1-42) fibrils ± 3 mM of inhibitor; 20 mM phosphate buffer, pH 7.4. Incubation: quiescent conditions at 25 ◦C. CE-LIF: fs capillaries: 50 µm ID x 30 cm total length; BGE: 10 µM ThT + 0.2 M Gly-NaOH buffer, pH 9.5; Voltage: +10 kV; Injection: 20 psi for 5 s; Analyses were performed at 25 ◦C; LIF: He-Cd laser; Fluorescence detection: λEm= 482 nm, λEx= 450 nm (adapted from Kato *et al.*[145]).

One of most interesting examples of CE-UV was reported by Brinet *et al.*, where the authors reported an improved analysis for studying the aggregation process of Aβ(1-42)[103]. The authors employed the use of 1,4-diaminobutane (DAB) in the background electrolyte (BGE) for tunning the electroosmotic flow (EOF)[103]. Under these conditions, the electropherogram presented four low abundant peaks separated from the major peak (Figure 27 A)[103]. To better understand the nature of the peaks, SDS-PAGE was employed to verify the aggregation state of the sample shortly after the dissolution[103]. The analysis revealed that the LMM Aβ(1-42) was mainly comprised of a

monomer – tetramer equilibrium (Figure 27 B) and the size was further assed by TDA showing a R_h of 1.8 ± 0.1 nm, which was found to be in agreement with other reports from the literature[16]. On this basis, the authors suggested that the small peaks corresponded to LMM oligomers, while the major peak was attributed to the monomer (Figure 27 A)[103]. By monitoring the course of aggregation, the evolution of the early stage species (Figure 27 C) presented a bell-shaped profile, characteristic for sAβ species (Figure 25 A – orange line), which disappeared after 20 h of aggregation, while the monomer peak area decreased linearly until it reached the same time of aggregation (Figure 27 A - insert)[103]. This outlines that in CE, the kinetics of the aggregation can be evaluated based on the monomer consumption, in contrast to ThT assay where the kinetics are determined in terms of fibril accumulation[103,112]. Furthermore, after more than 8 h of incubation, the authors observed the formation of later migrating peaks corresponding to large sAβ species of >50 kDa, and spikes, which in CE are often attributed to insoluble aggregates, such as fibrils, that manage to enter the capillary during the injection[103,114,145,157]. Finally, the authors also evaluated the methylene blue effect upon the aggregation, an inhibitor known to inhibit the oligomerization by accelerating fibril formation. Here, a reduction of the later migrating peaks was observed accompanied by the appearance of a significant number of spikes, further suggesting that CE-UV is a suitable tool for drug screening[103]. Overall, this study represented one of the first CE-UV examples of a full-time monitoring of the aggregation process of Aβ peptides with particular focus on the evolution of the early stage species[103].

One of the first CE-LIF method applied to the aggregation process of Aβ peptides was developed by Kato *et al.*[145]. The authors designed the analysis by introducing the fluorescent dye in the BGE, so that the aggregation behavior of Aβ peptides would not be affected[145]. They first evaluated the aggregation by using ThT as a fluorescent dye, either when the process was unseeded (Figure 27 D) or seeded (Figure 27 E) with a small fraction of preformed Aβ(1-42) mature fibrils after both 5 min and 24 h of incubation, respectively[145]. In the non-seeded experiment, a broad peak was observed shortly after the aggregation was initiated and it appeared more pronounced after 24 h of incubation, whereas in the seeded experiment the peak area of the broad peak was higher and accompanied by a spike shortly after the dissolution, and both species were found to be more abundant after 24 h, thus suggesting that the aggregation was catalyzed[145]. The authors assumed that the broad peak was a precursor of the spike[145], but mostly likely it represents the protofibrils population since it is well known to be the only other Aβ species that ThT is able to

bind[112]. In Figure 27 F it is depicted the inhibition effect of three small molecules such as melatonin, 3-indolepropionic acid (3-IPA), and daunomycin, which are known to prevent fibrillization[145]. The experiments were performed in the presence of seeds and it was observed that the inhibition effect of fibrils enhanced in the latter mentioned order of the drug candidates with respect to the control seeded experiment, further showing proof of concept that CE-LIF can be a powerful technique for drug screening[145].

In principle, CE present several advantages. The first comes from the ability to separate and monitor the evolution of a wide sAβ species[103,109,145]. In general, this method presents a simple and fast analysis allowing a low sample consumption, normally in the range of nL per injection, which can be easily adapted for studying different biological systems without the need to perform manipulations of the sample such as vortexing, filtration or centrifugation, which may affect the aggregation of peptides or proteins. Another main advantage is that it helps preventing possible dissociation of the species, which typically occur through interactions with the column packing or gel phase when using chromatographic or other electrophoretic methods such as SEC or PAGE respectively[28,157]. In the UV detection mode, the main advantage is that native peptides can be used to allow a reliable interpretation of the aggregation mechanism[103], but the main drawback still remains the LOD, found to be around 0.3-0.5 μM[102]. For this reason, to properly monitor the evolution of the species, the starting concentration should be in the range of 50 – 100 μM, values that are very far from the Aβ levels found in biological fluids[42,103,107]. In contrast to UV, LIF detection mode can overcome this aspect because it is more sensitive and the LOD for Aβ peptides has been found to be around 0.1 nM[158]. However, this implies the use of intrinsically labelled dyes that are believed to alter the aggregation process[91]. A main advantage of LIF is that the use of fluorescent dyes in the BGE, such as ThT, can avoid altering the aggregation behavior of Aβ peptides, although this allows only the evaluation of fibrillar aggregates[114,145]. Therefore, it is very difficult to monitor the early stages as there are no available dyes that can selectively detect early stages species[151]. Another major drawback is that CE cannot allow a suitable discrimination between the nature of the species, thus, CE has been employed together with a wide range of techniques such as EM[109], SEC[96], ThT assay[138], MWCO filtration[113], SDS-PAGE[103], TDA[103] or IR[159], to provide complementary information related to the aggregation process.

I.4.3. Determination of the size distribution of Aβ species

The most common biophysical techniques used to assess the size distribution of the species in terms of R_h are DLS[29,142] and FCS[91,143], while in terms of molar mass distribution are PAGE[143] and SEC-MALS[29,63], which can be considered as alternative methods. PAGE techniques present a fast and cost-effective analysis, reason for which they are widely employed for detecting several types of Aβ species[143]. SDS-PAGE was one of the most common electrophoretic methods used to characterize Aβ oligomers obtained from brain tissues or prepared in vitro until SDS was found to be denaturant, causing the dissociation of HMM oligomers into smaller aggregates[63]. Due to this major disadvantage, this analysis is often employed in conjunction with oligomer cross-linking techniques, such as PICUP[56], or it can be replaced with native PAGE but, in this case, the resolution of HMM species is very low, so other methods such as SEC-MALS should be employed for a better comparison[63,143]. As discussed in subsection I.2.2.2.2., SEC is a suitable disaggregation method that allows the separation and isolation of LMM Aβ species, but it can also be used to obtain monomer-free aggregates such as protofibrils and HMM oligomers[28,29,40]. In one of their studies, Nichols *et al.* isolated protofibrils generated from Aβ(1-40) by SEC-MALS, which presented an initial molecular mass of 30 MDa that extended to maximum values of 57 MDa during elongation in the presence of monomers, and of 86 MDa by self-association promoted by the high ionic strength conditions[62]. In addition, Watanabe *et al.* also isolated HMM oligomeric species using SEC[40]. The authors did not employ MALS to evaluate the molar mass, but these species were characterized morphologically by TEM analysis and revealed short and relatively narrow structures of ~5 nm in diameter resembling that of protofibrils[40]. Despite its potential to separate different Aβ species, SEC also has several limitations. Indeed, this method requires a high initial concentration of the raw material such as 1 – 2 g/L in volumes of 0.1 – 1 mL which, by the end of the separation, can lead to losses of about 70% of the peptide[58,63,104]. In addition, larger aggregates may interact with the column matrix and dissociate into LMM Aβ fractions during SEC separation[28,143]. Furthermore, several fluorescence techniques have been also employed to assess the size distribution of Aβ species and it was shown that by SMFS, using an equimolar system of AlexaFluor488-Aβ:AlexaFluor647-Aβ, the CAC values for Aβ(1-40) and Aβ(1-42) were estimated to be 222 ± 10 nM and 86 ± 10 nM, respectively[33]. In another study, Jiang *et al.* monitored the evolution of Aβ(1-42) oligomers in the presence of a novel $[Ru(bpy)2(dpqp)]^{2+}$ dye

by using fluorescence anisotropy[150]. here, the authors observed an increase in the anisotropy signal after 5 h of incubation reaching a maximum after ~80 h of incubation and, by correlating these results with DLS, it was found that the initial LMM Aβ(1-42) formulation presented a R_h of ~5 nm and reached maximum values of ~35 nm after 25 h of incubation[150]. Among all the fluorescence-based biophysical techniques, FCS was most commonly employed. Nag *et al.* determined a R_h for Aβ monomers of ~0.9 nm for both rhodamine labeled Aβ(1-42) and acetylaminoethyl-5-naphthylamine-1-sulfonic acid (EDANS)-labelled Aβ(1-40), at a concentration of 150 nM[57]. Then, by using tetramethylrhodamine (TMR) labelled Aβ(1-40), Matsumura *et al.* observed the formation of 15–40 nm species after 2 h of incubation[160]. Garai *et al.* also studied the oligomerization of Aβ(1-40) by employing a N-terminal RB dye and it was observed that after only 1 h of incubation very large species of 20 – 100 nm were formed, which were very different from those described by Matsumura *et al.*[161]. It is possible that this difference resulted from the different sample conditions and/or because different rhodamine derivatives were used as dyes.

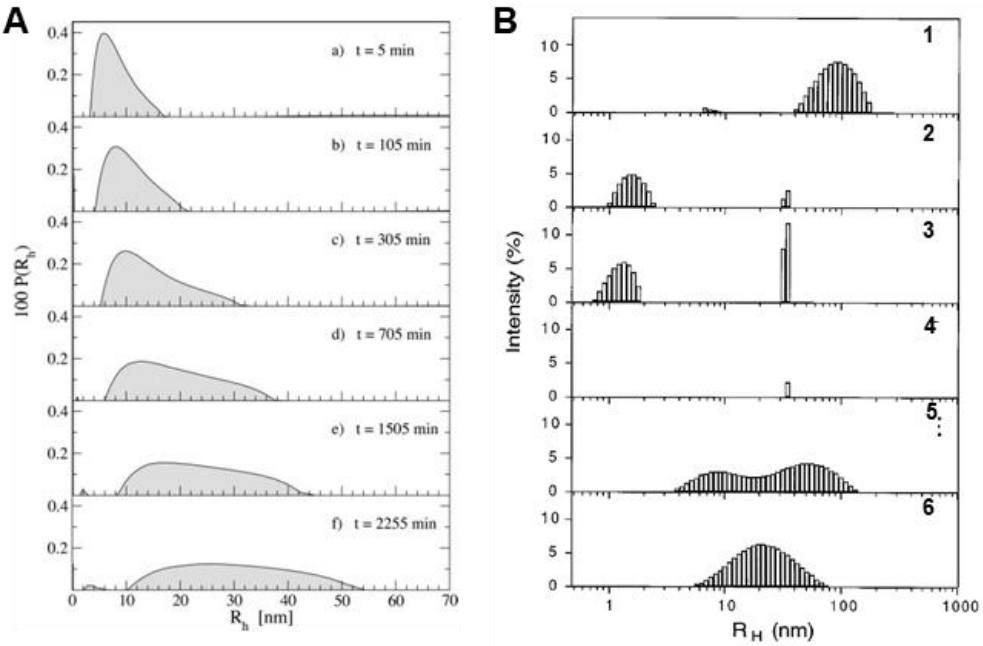

Figure 28. (A) Monitoring the aggregation process of Aβ(1-40) by DLS. Experimental conditions: Sample: 185 μM Aβ(1-40), 100 mM citrate buffer, pH 3.1. Incubation: quiescent conditions at 37 °C. DLS: Argon ion laser operating at 514.5 nm; θ= 90°; Analyses were performed at 0.05 ◦C (adapted from Carrotta *et al.*[142]). (B) DLS the size distribution determination of different Aβ(1-40) species: (1) Soluble Aβ(1–40) fraction obtained shortly after peptide dissolution; (2) The gel-included fraction of the supernatant obtained by SEC separation; (3) Aprotinin (6.5 kDa); (4) 0.1 M Tris-HCl buffer; (5) Supernatant of soluble Aβ(1–40) from (1) incubated at room temperature for 48 h; (6) The gel-excluded fraction of the supernatant obtained by SEC separation. Experimental conditions: Sample: Aβ(1-40), 100 mM Tris-HCl buffer, pH 7.4. Incubation: quiescent conditions at 25 °C. DLS: Argon ion laser operating at 514 nm; θ= 90°; Analyses were performed at 25 ◦C (adapted from Walsh *et al.*[29]).

A more advantageous technique for evaluating the R_h of Aβ species is DLS, primarily because it allows the use of unmodified native peptides. Many studies have revealed that LMM Aβ formulations present a R_h of 1.4 – 10 nm[29,53,56,60–62]. DLS was also employed to monitor the evolution of protofibrils[62], as presented in subsection I.2.2.2.6. What is interesting is that, despite the larger R_h values obtained for the protofibrils formed by monomer elongation, the largest protofibrillar species promoted by self-association presented a higher molar mass as discussed above[62].

Carrotta *et al.* performed a real-time monitoring of the R_h evolution of Aβ(1-40) under acidic conditions for a course of ~38 h by using DLS (Figure 28 A)[142]. Before the aggregation was initiated, the sample was filtered with a 0.2 µm filter and the final sample concentration was evaluated by measuring tyrosine absorbance at 276 nm[142]. After 5 min, the sample presented a R_h of 7 nm[142]. This result was confirmed on the basis of the observations provided by a previous study performed by Lomakin *et al.* under similar conditions, where the authors found a R_h of 7 nm shortly after the peptide dissolution[162]. As can be observed from the following measurements, the size distribution of the early stage species increased during the incubation time, where larger species formed at the expenses of the initial ones, further outlining that the polydispersity of the system increases as the aggregation proceeds[142].

In another study, Walsh *et al.* evaluated by DLS different Aβ species isolated by SEC (Figure 28 B)[29]. Prior to the analyses, the sample was filtered through a filter characterized by a porosity of 20 nm[29]. The buffer was found to be dust-free (Figure 28 B4), presenting some small distributions of ~35 nm which were disregarded from the interpretation of the results[29]. First, the Aβ (1-40) presented a size distribution of 40 – 200 nm shortly after dissolution (Figure 28 B1) [29]. Prior to SEC, the sample was incubated at room temperature for 48 h to obtain enough aggregated material[29]. The aggregated sample was then centrifuged and the supernatant showed a size distribution of 4 – 150 nm (Figure 28 B5)[29]. During the SEC fractionation of the supernatant, two distinct populations were isolated[29]. The gel-excluded peak (detected in the interstitial volume) was comprised of species having a molecular mass >670 kDa, while the ones detected in the gel-included fraction (between interstitial and dead volume) had a mass of 15 kDa, suggesting that LMM Aβ(1-40) presented a monomer – tetramer equilibrium during SEC fractionation[29]. The DLS analysis of the gel-included peak (Figure 28 B2) showed a size distribution of 1.8 ± 0.2 nm[29] and, by considering geometrical predictions, Aβ(1-40) (4.3 kDa) result to be in a dimeric equilibrium

for a R_h range of 1.5 – 2.1 nm[29]. By using also aprotinin (6.5 kDa) as a comparison, exhibiting a distribution of 1.6 ± 0.6 nm (Figure 28 B3), it was revealed that Aβ(1-40) actually presents a monomer – dimer equilibrium, in contrast to what was observed by SEC[29]. The gel-excluded peak showed a size distribution of 10 – 50 nm (Figure 28 B6), leading to the hypothesis that this fraction was mainly comprised of HMM oligomers and protofibrils[29].

Because the resolution in DLS is not so high, it is not easy to differentiate between different populations. Therefore, a difference in the molar mass by a factor of ~8 between the species is necessary for a proper discrimination of the species[63]. Another major drawback is that the scattering intensity is highly affected by the presence of large aggregates, making the data difficult to interpret[29,61]. Thus, it is important that the sample should be aggregate-free during the analysis, especially if a real-time monitoring of the process is required. In addition to this, DLS is highly sensitive to dust and, for this reason, at least the buffer (if not the entire sample) should be filtered prior to analysis[29,142,163]. It follows that DLS is a powerful complementary technique useful to give information related to the size distribution of different Aβ species.

I.4.4. Morphological characterization of Aβ species

The biophysical techniques employed for morphological characterizations of Aβ species are ultrastructural imaging methods such as EM and AFM[73]. Multiple EM methods such as TEM[29], SEM[73], STEM[80] and cryo-TEM[76] have been used both to characterize the species and to reveal important mechanistic information related to the aggregation process especially when employed in parallel with other techniques.

Due to their vast heterogeneity and high propensity to aggregate, it is quite difficult to distinguish between different types of oligomers[17]. LMM Aβ are approximatively characterized as quasicircular or granular structures of 3-5 nm in diameter by EM[40,56] (Figure 29 A) or as spherical nonfibrous oligomers of 1-5 nm in height by AFM[36,40] (Figure 29 D). Depending on their nature, HMM oligomers can be characterized as large spherical aggregates with a diameter of 5 – 25 nm by AFM[21,36,59] or as short prefibrillar filaments with a width of about 5 nm and up to 100 nm in length, sometimes resembling protofibril structures by using EM[40,65]. For example, in a study performed by Watanabe-Nakayama *et al.*, the authors isolated both LMM Aβ and HMM oligomers by SEC and monitored the aggregation process of these Aβ species by high resolution AFM and TEM analyses[40]. The authors revealed that some HMM oligomer formulations tended rather to

dissociate back into smaller aggregates that further elongated into fibrils[40]. Thus, when EM methods are combined with the 3D mapping obtained by AFM, a better understanding of the aggregation process and of the structural properties of different aggregates can be achieved[40,137].

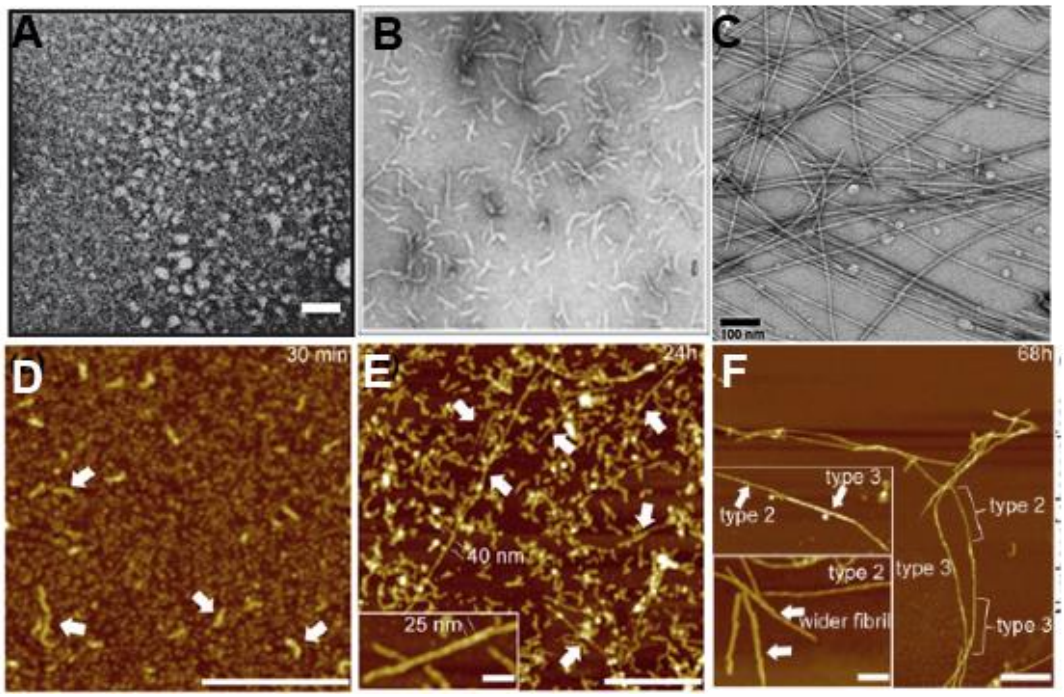

Figure 29. EM representative images obtained by (A) TEM of SEC isolated LMM Aβ(1-42) characterized as globular species having an average diameter of 3.7 ± 0.62 nm (adapted from Watanabe-Nakayama *et al.*[40]); EM of SEC isolated Aβ(1-40) protofibrils characterized as short, curly fibrils 6–10 nm in diameter and 5–160 nm in length (adapted from Walsh *et al.*[29]); (C) Cryo-TEM of Aβ(1-42) comprised of two intertwined protofilaments having diameters of ~7 nm and were >1 μm long (adapted from Gremer *et al.*[76]). Monitoring the aggregation process of Aβ(1-42) by AFM: Images recorded at (D) 0.5, (E) 24 and (F) 68 h of incubation. Experimental conditions: Sample: 20 μM Aβ(1-42), 10 mM Tris-HCl pH 7.4. Incubation: quiescent conditions at 37 °C. AFM analysis: mica substrates were functionalized with 0.05% (v/v) APTES; Tapping mode with scan rates ranging from 96 to 168 kHz; Analyses were performed at 25 °C (adapted from Jeong *et al.*[36]).

On the other hand, protofibrils and fibrils can be more thoroughly described due to their increased stability and larger size[28]. Protofibrils are generally characterized as short and flexible chains that exhibit widths of 5 - 10 nm and lengths up to 200 nm[28,36,62]. Historically, protofibrils were first described by Walsh *et al.* in 1997[29]. These species were isolated by SEC and further characterized by EM (Figure 29 B) as short, curly fibrils 6–10 nm in diameter, and 5–160 nm in length[29]. In contrast to protofibrils, fibrils are more rigid characterized as rod-like chains having a cross-sectional diameter of 2 – 20 nm and can reach lengths of more than 10 μm[28,62,76,79]. Generally, they are comprised of 2 – 6 protofilament subunits[28,76]. Fibril morphology was also found to be dependent on the nature of the peptide. Aβ(1-40) fibrils are generally described to be long and straight, while the ones generated by Aβ(1-42) are often characterized as densely packed

fibrillar networks[46,128,129]. A more thorough morphological distinction between the fibrils was described by Cukalevski *et al.* which in their study used *cryo*-TEM[46]. Here, the authors observed that Aβ(1-42) fibrils are short, twisted, and densely packed presenting a node-to-node distance of 31 ± 17 nm, while those generated by Aβ(1-40) are larger, straight, and thicker compared to the other Aβ isoform, presenting a node-to-node distance of 162 ± 21 nm[46]. It was revealed by NMR that Aβ fibrils can adopted either U-shaped or S-shaped conformations[164]. Recently, Gremer *et al.* employed both *cryo*-TEM and NMR, resolving a LS topology of Aβ(1-42) fibrils[76]. The fibrils were comprised of two intertwined protofilaments with a diameter of ~7 nm and were >1 μm long[76]; a 3D representation of the LS topology is presented in Figure 8 A. One of the first studies employing AFM for a full-time monitoring of the aggregation process of Aβ(1-42) was performed by Jeong *et al.*[36]. In this case, after 30 min of incubation, spherical oligomers 1.00 ± 0.30 nm in diameter (Figure 29 D) and short protofibrils were observed (Figure 29 D-white arrows)[36]. After 24 h of incubation, most of the oligomers transformed into protofibrils, which at that time presented an average cross-sectional diameter of 3.95 ± 0.64 nm and an average length of 115.42 ± 25.84 nm (Figure 29 E) and some of them were straight and on-pathway for fibril formation (Figure 29 E-white arrows and inset)[36]. After 68 h of incubation, three different types of fibrils were observed having characteristic cross-sectional diameters of 4.60 ± 0.56, 4.07 ± 0.46 and 7.54 ± 1.00 nm for type 1, 2, and 3, respectively (Figure 29 F)[36]. Furthermore, the authors also monitored the aggregation process in the presence of seeds, which in their case were protofibrils isolated by SEC, and at the end of the aggregation process two new types of fibrils were observed having a cross-sectional diameter of 7.29 ± 0.82 nm for type 4 composed of 2 protofilaments, and 9.17 ± 0.89 nm for type 5 comprising 3 protofilaments[36]. Moreover, the authors reported several secondary-nucleation events occurring on the surface of some of the fibrils[36]. These results outline the polymorphic nature of Aβ fibrils[36].

To conclude, both EM and AFM are powerful biophysical techniques for monitoring the aggregation and characterizing different species with a particular focus on high-ordered aggregates. Compared to classical EM techniques, AFM can acquire high resolution images at subnanometer level by drawing a 3D topographical map[63]. *Cryo*-TEM can characterize the species without the need of staining and are generally preserved at a temperature of −180 °C, allowing a 3D image reconstruction at the atomic level[73]. The main advantage of EM techniques is that they

allow a faster scanning speed, which is in the range of seconds, and larger scanning area compared to those obtained by AFM for which the analysis can take up to several minutes[73].

I.4.5. Taylor dispersion analysis as a promising tool for monitoring the aggregation of Aβ peptides

TDA was first described by Sir Geoffrey I. Taylor in 1953[165]. It allows the determination of the molecular diffusion coefficient (*D*) and consequently the R_h, based on the dispersion of an injected band of a solute in an open tube under Poiseuille laminar flow conditions[166]. Depending on the analysis conditions, TDA can size and quantify different particles and species ranging from 0.1 nm to ~1 µm[167].

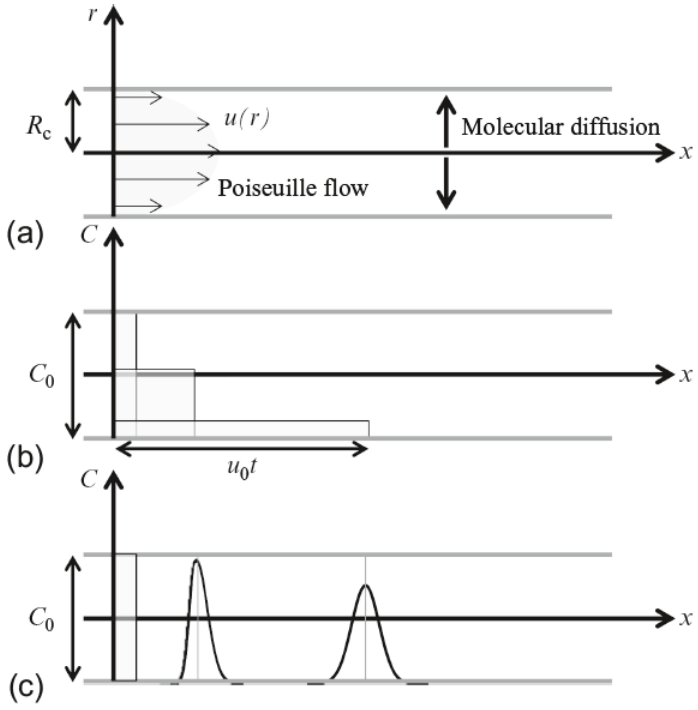

Figure 30. Principle of TDA. (A) *u(r)* in laminar flow conditions occurring in a cylindrical tube. (B) Concentration distribution characterized by a dispersive velocity profile in the case of when solutes move only by convection. (C) Concentration distribution characterized by the molecular diffusion of the molecules in the presence of *u(r)* (adapted from Chamieh *et al.*[166]).

The resulting dispersion stems from the interaction of the radial diffusion of solutes and the parabolic velocity profile of the Poiseuille laminar flow (*u(r)*) that occurs when the mobilization pressure is applied (Figure 30 A)[166]. In fact, if the solutes would move only by convention, the species present at the center would move very fast, while those near to the wall of the tube would have negligible velocity, resulting in a considerable spreading of the concentration distribution

(Figure 30 B)[166]. In reality, due to the combination of the parabolic velocity profile and the molecular diffusion of the solutes, the resulting Taylor dispersion is translated into a normal distribution of the concentration leading, experimentally, to Gaussian elution peaks, for samples that are monodisperse in size, as depicted in Figure 30 C[166]. Small molecules diffuse fast and the gaussian elution peak is narrow (Figure 30 C-left peak), while large molecules diffuse slowly resulting in a wider gaussian peak = (Figure 30 C-right peak)[166].

Experimentally, the determination of the peak variance, σ^2, allows the calculation of D from Eq. (1) and consequently the R_h from the Stokes-Einstein equation, Eq. (2)[166].

$$D = \frac{R_c^2 t_0}{24\sigma^2} \quad (1)$$

$$R_h = \frac{k_b T}{6\pi\eta D} \quad (2)$$

where R_c is the capillary radius (m), t_0 is the average elution time of the solute (s), σ^2 is the temporal peak variance (s^2), k_b is the Boltzmann constant (Pa m^3 K^{-1}), T is the analysis temperature (K), and η is the viscosity of the sample (Pa s).

The determination of σ^2 can be derived by performing a Gaussian fitting of the experimental peak when the samples are monodispersed in size. In the case of polydisperse samples, the elution profile is a sum of Gaussian peaks that can be deconvoluted by fitting with a sum of Gaussian functions which number should be defined before the fit or by applying the constrained regularized linear inversion (CRLI) algorithm which allows the fitting without any hypothesis on the number of Gaussian functions[168,169]. The conditions of validity of TDA as well as the data processing approaches for fitting the experimental taylorgrams are more thoroughly described in the Supporting Information sections of Chapters II, III, and IV.

TDA is an absolute method, thus, does not require calibration, allowing an absolute size determination of the solutes[163]. Modern TDA analysis is generally performed on commercially available CE instruments[163]. In general, it requires a low sample consumption which remains in the range of nL per injection[163]. Furthermore, compared to DLS, it requires no sample filtration because it is not sensitive to dust[163]. Hence, based on these aspects, TDA can be applied in various cases such as measurements of polymers[170], nanoparticles[167] , and protein-protein interactions[171]

but its main limitation is related to the difficulty to size or quantify solutes larger than 300 nm with the current experimental setup[167].

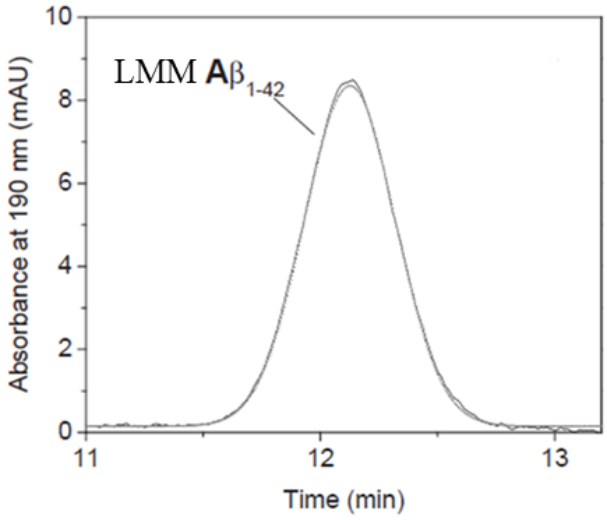

Figure 31. Taylorgram of LMM Aβ(1-42) shortly after the dissolution. Experimental conditions: Sample: 100 µM Aβ(1-42); 20 mM phosphate buffer, pH 7.4. Incubation: quiescent conditions at 20 ◦C. CE-UV: fs capillaries: 50 µm ID x 50 cm x 39.8 cm; BGE: 20 mM phosphate buffer, pH 7.4; Mobilization pressure: 68.9 mbar; Hydrodynamic injection: 34.4 mbar for 15 s; Analyses were performed at 20 ◦C; UV detection at 190 nm (adapted from Brinet *et al.*[103]).

To date, TDA has only been used once to evaluate the size of LMM Aβ(1-42)[103], but it has never been employed for a full-scale monitoring of the aggregation process of Aβ peptides. Specifically, in this study, the authors obtained a R_h of 1.8 ± 0.1 nm (Figure 31), which was then correlated with CE and SDS-PAGE[103]. This size is consistent with the R_h values measured for several LMM Aβ formulations and that fall in the range of 1.4 to 10 nm obtained using DLS[29,53,56,60–62].

Ultimately, considering that TDA is capable of detecting these initial intermediates, and because it offers several advantages as presented above, this technique may prove to be a powerful tool for monitoring the aggregation process of Aβ peptides, especially for assessing the evolution of the early stage species. Furthermore, since the main objective of this study is to apply TDA for evaluating the aggregation mechanism of these amyloidogenic peptides, the following chapters present and thoroughly describe how TDA can size, quantify, and speciate different Aβ intermediates in real-time, as well as how the data can be processed and interpreted.

I.5. References

1. Wechalekar, A. D., Gillmore, J. D. & Hawkins, P. N. Systemic amyloidosis. *Lancet* **387,** 2641–2654 (2016).
2. Ghiso, J. & Frangione, B. Amyloidosis and Alzheimer's disease. *Adv. Drug Deliv. Rev.* **54,** 1539–1551 (2002).
3. Chen, G. F., Xu, T. H., Yan, Y., Zhou, Y. R., Jiang, Y., Melcher, K. & Xu, H. E. Amyloid beta: Structure, biology and structure-based therapeutic development. *Acta Pharmacol. Sin.* **38,** 1205–1235 (2017).
4. *2019 Alzheimer's disease facts and figures*. *Alzheimer's Dement.* **15,** (2019).
5. Hardy, J. A. & Higgins, G. A. Alzheimer's disease: The amyloid cascade hypothesis. *Science (80-.).* **256,** 184–185 (1992).
6. Folch, J., Ettcheto, M., Petrov, D., Abad, S., Pedrós, I., Marin, M., Olloquequi, J. & Camins, A. Review of the advances in treatment for Alzheimer disease: strategies for combating β-amyloid protein. *Neurol. (English Ed.* **33,** 47–58 (2018).
7. McDade, E. & Bateman, R. J. Stop Alzheimer's before it starts. *Nature* **547,** 153–155 (2017).
8. Cummings, J., Lee, G., Zhong, K., Fonseca, J. & Taghva, K. Alzheimer's disease drug development pipeline: 2021. *Alzheimer's Dement. Transl. Res. Clin. Interv.* **7,** (2021).
9. Esch, F. S., Keim, P. S., Beattie, E. C., Blacher, R. W., Culwell, A. R., Oltersdorf, T., McClure, D. & Ward, P. J. Cleavage of amyloid β peptide during constitutive processing of its precursor. *Science (80-.).* **248,** 1122–1124 (1990).
10. Gu, Y., Misonou, H., Sato, T., Dohmae, N., Takio, K. & Ihara, Y. Distinct Intramembrane Cleavage of the β-Amyloid Precursor Protein Family Resembling γ-Secretase-like Cleavage of Notch. *J. Biol. Chem.* **276,** 35235–35238 (2001).
11. Joshi, G. & Wang, Y. Golgi defects enhance APP amyloidogenic processing in Alzheimer's disease. *BioEssays* **37,** 240–247 (2015).
12. Lu, D. C., Rabizadeh, S., Chandra, S., Shayya, R. F., Ellerby, L. M., Ye, X., Salvesen, G. S., Koo, E. H. & Bredesen, D. E. A second cytotoxic proteolytic peptide derived from amyloid β-protein precursor. *Nat. Med.* **6,** 397–404 (2000).
13. Goodger, Z. V., Rajendran, L., Trutzel, A., Kohli, B. M., Nitsch, R. M. & Konietzko, U. Nuclear signaling by the APP intracellular domain occurs predominantly through the amyloidogenic processing pathway. *J. Cell Sci.* **122,** 3703–3714 (2009).
14. Lu, P., Bai, X. C., Ma, D., Xie, T., Yan, C., Sun, L., Yang, G., Zhao, Y., Zhou, R., Scheres, S. H. W. & Shi, Y. Three-dimensional structure of human γ-secretase. *Nature* **512,** 166–170 (2014).
15. Iadanza, M. G., Jackson, M. P., Hewitt, E. W., Ranson, N. A. & Radford, S. E. A new era for understanding amyloid structures and disease. *Nat. Rev. Mol. Cell Biol.* **19,** 755–773 (2018).

16. Giuffrida, M. L., Caraci, F., Pignataro, B., Cataldo, S., De Bona, P., Bruno, V., Molinaro, G., Pappalardo, G., Messina, A., Palmigiano, A., Garozzo, D., Nicoletti, F., Rizzarelli, E. & Copani, A. B-Amyloid Monomers Are Neuroprotective. *J. Neurosci.* **29,** 10582–10587 (2009).

17. Nasica-Labouze, J., Nguyen, P. H., Sterpone, F., Berthoumieu, O., Buchete, N. V., Coté, S., De Simone, A., Doig, A. J., Faller, P., Garcia, A., Laio, A., Li, M. S., Melchionna, S., Mousseau, N., Mu, Y., Paravastu, A., Pasquali, S., Rosenman, D. J., Strodel, B., Tarus, B., Viles, J. H., Zhang, T., Wang, C. & Derreumaux, P. Amyloid β Protein and Alzheimer's Disease: When Computer Simulations Complement Experimental Studies. *Chem. Rev.* **115,** 3518–3563 (2015).

18. Lambert, M. P., Barlow, A. K., Chromy, B. A., Edwards, C., Freed, R., Liosatos, M., Morgan, T. E., Rozovsky, I., Trommer, B., Viola, K. L., Wals, P., Zhang, C., Finch, C. E., Krafft, G. A. & Klein, W. L. Diffusible, nonfibrillar ligands derived from Aβ1-42 are potent central nervous system neurotoxins. *Proc. Natl. Acad. Sci. U. S. A.* **95,** 6448–6453 (1998).

19. Soto, C., Kindy, M. S., Baumann, M. & Frangione, B. Inhibition of Alzheimer's amyloidosis by peptides that prevent β-sheet conformation. *Biochem. Biophys. Res. Commun.* **226,** 672–680 (1996).

20. Crespo, R., Rocha, F. A., Damas, A. M. & Martins, P. M. A generic crystallization-like model that describes the kinetics of amyloid fibril formation. *J. Biol. Chem.* **287,** 30585–30594 (2012).

21. Roychaudhuri, R., Yang, M., Hoshi, M. M. & Teplow, D. B. Amyloid β-protein assembly and Alzheimer disease. *J. Biol. Chem.* **284,** 4749–4753 (2009).

22. Nölting, B. & Agard, D. A. How general is the nucleation-condensation mechanism? *Proteins Struct. Funct. Genet.* **73,** 754–764 (2008).

23. Törnquist, M., Michaels, T. C. T., Sanagavarapu, K., Yang, X., Meisl, G., Cohen, S. I. A., Knowles, T. P. J. & Linse, S. Secondary nucleation in amyloid formation. *Chem. Commun.* **54,** 8667–8684 (2018).

24. Chakraborty, S. & Das, P. Emergence of Alternative Structures in Amyloid Beta 1-42 Monomeric Landscape by N-terminal Hexapeptide Amyloid Inhibitors. *Sci. Rep.* **7,** (2017).

25. Chatani, E. & Yamamoto, N. Recent progress on understanding the mechanisms of amyloid nucleation. *Biophys. Rev.* **10,** 527–534 (2018).

26. Erdemir, D., Lee, A. Y. & Myerson, A. S. Nucleation of crystals from solution: Classical and two-step models. *Acc. Chem. Res.* **42,** 621–629 (2009).

27. Linse, S. Monomer-dependent secondary nucleation in amyloid formation. *Biophys. Rev.* **9,** 329–338 (2017).

28. Jan, A., Hartley, D. M. & Lashuel, H. A. Preparation and characterization of toxic aβ aggregates for structural and functional studies in alzheimer's disease research. *Nat. Protoc.* **5,** 1186–1209 (2010).

29. Walsh, D. M., Lomakin, A., Benedek, G. B., Condron, M. M. & Teplow, D. B. Amyloid β-protein fibrillogenesis: Detection of a protofibrillar intermediate. *J. Biol. Chem.* **272,** 22364–22372 (1997).

30. Zhang, S., Iwata, K., Lachenmann, M. J., Peng, J. W., Li, S., Stimson, E. R., Lu, Y. A., Felix, A. M., Maggio, J. E. & Lee, J. P. The Alzheimer's peptide Aβ adopts a collapsed coil structure in water. *J. Struct. Biol.* **130,** 130–141 (2000).

31. Pujol-Pina, R., Vilaprinyó-Pascual, S., Mazzucato, R., Arcella, A., Vilaseca, M., Orozco, M. & Carulla, N. SDS-PAGE analysis of Aβ oligomers is disserving research into Alzheimer's disease: Appealing for ESI-IM-MS. *Sci. Rep.* **5,** (2015).

32. Tonali, N., Kaffy, J., Soulier, J. L., Gelmi, M. L., Erba, E., Taverna, M., van Heijenoort, C., Ha-Duong, T. & Ongeri, S. Structure-activity relationships of β-hairpin mimics as modulators of amyloid β-peptide aggregation. *Eur. J. Med. Chem.* **154,** 280–293 (2018).

33. Iljina, M., Garcia, G. A., Dear, A. J., Flint, J., Narayan, P., Michaels, T. C. T., Dobson, C. M., Frenkel, D., Knowles, T. P. J. & Klenerman, D. Quantitative analysis of co-oligomer formation by amyloid-beta peptide isoforms. *Sci. Rep.* **6,** (2016).

34. Lesné, S. E. Breaking the code of amyloid-β oligomers. *Int. J. Cell Biol.* (2013). doi:10.1155/2013/950783

35. Cummings, J., Lee, G., Ritter, A., Sabbagh, M. & Zhong, K. Alzheimer's disease drug development pipeline: 2019. *Alzheimer's Dement. Transl. Res. Clin. Interv.* **5,** 272–293 (2019).

36. Jeong, J. S., Ansaloni, A., Mezzenga, R., Lashuel, H. A. & Dietler, G. Novel mechanistic insight into the molecular basis of amyloid polymorphism and secondary nucleation during amyloid formation. *J. Mol. Biol.* **425,** 1765–1781 (2013).

37. Lee, S. J. C., Nam, E., Lee, H. J., Savelieff, M. G. & Lim, M. H. Towards an understanding of amyloid-β oligomers: Characterization, toxicity mechanisms, and inhibitors. *Chem. Soc. Rev.* **46,** 310–323 (2017).

38. Richard, T., Poupard, P., Nassra, M., Papastamoulis, Y., Iglésias, M. L., Krisa, S., Waffo-Teguo, P., Mérillon, J. M. & Monti, J. P. Protective effect of ε-viniferin on β-amyloid peptide aggregation investigated by electrospray ionization mass spectrometry. *Bioorganic Med. Chem.* **19,** 3152–3155 (2011).

39. Naiki, H., Higuchi, K., Hosokawa, M. & Takeda, T. Fluorometric determination of amyloid fibrils in vitro using the fluorescent dye, thioflavine T. *Anal. Biochem.* **177,** 244–249 (1989).

40. Watanabe-Nakayama, T., Ono, K., Itami, M., Takahashi, R., Teplow, D. B. & Yamada, M. High-speed atomic force microscopy reveals structural dynamics of amyloid β1-42 aggregates. *Proc. Natl. Acad. Sci. U. S. A.* **113,** 5835–5840 (2016).

41. Walsh, D. M., Hartley, D. M., Kusumoto, Y., Fezoui, Y., Condron, M. M., Lomakin, A., Benedek, G. B., Selkoe, D. J. & Teplow, D. B. Amyloid β-protein fibrillogenesis. Structure and biological activity of protofibrillar intermediates. *J. Biol. Chem.* **274,** 25945–25952 (1999).

42. Harper, J. D. & Lansbury, P. T. MODELS OF AMYLOID SEEDING IN ALZHEIMER'S DISEASE AND SCRAPIE:Mechanistic Truths and Physiological Consequences of the Time-Dependent Solubility of Amyloid Proteins. *Annu. Rev. Biochem.* **66,** 385–407 (2002).

43. Faller, P., Hureau, C. & Berthoumieu, O. Role of metal ions in the self-assembly of the Alzheimer's amyloid-β peptide. *Inorg. Chem.* **52,** 12193–12206 (2013).

44. Smith, D. G., Cappai, R. & Barnham, K. J. The redox chemistry of the Alzheimer's disease amyloid β peptide. *Biochim. Biophys. Acta - Biomembr.* **1768,** 1976–1990 (2007).

45. Zhao, M. & Guo, C. Multipronged Regulatory Functions of Serum Albumin in Early Stages of Amyloid-β Aggregation. *ACS Chem. Neurosci.* **12,** 2409–2420 (2021).

46. Cukalevski, R., Yang, X., Meisl, G., Weininger, U., Bernfur, K., Frohm, B., Knowles, T. P. J. & Linse, S. The Aβ40 and Aβ42 peptides self-assemble into separate homomolecular fibrils in binary mixtures but cross-react during primary nucleation. *Chem. Sci.* **6,** 4215–4233 (2015).

47. Cohen, S. I. A., Linse, S., Luheshi, L. M., Hellstrand, E., White, D. A., Rajah, L., Otzen, D. E., Vendruscolo, M., Dobson, C. M. & Knowles, T. P. J. Proliferation of amyloid- 42 aggregates occurs through a secondary nucleation mechanism. *Proc. Natl. Acad. Sci.* **110,** 9758–9763 (2013).

48. Meisl, G., Kirkegaard, J. B., Arosio, P., Michaels, T. C. T., Vendruscolo, M., Dobson, C. M., Linse, S. & Knowles, T. P. J. Molecular mechanisms of protein aggregation from global fitting of kinetic models. *Nat. Protoc.* **11,** (2016).

49. Lasagna-Reeves, C. A., Glabe, C. G. & Kayed, R. Amyloid-β annular protofibrils evade fibrillar fate in Alzheimer disease brain. *J. Biol. Chem.* **286,** 22122–22130 (2011).

50. Westlind-Danielsson, A. & Arnerup, G. Spontaneous in vitro formation of supramolecular β-amyloid structures, 'βamy balls', by β-amyloid 1-40 peptide. *Biochemistry* **40,** 14736–14743 (2001).

51. Hayden, E. Y. & Teplow, D. B. Amyloid β-protein oligomers and Alzheimer's disease. *Alzheimer's Res. Ther.* **5,** (2013).

52. Rahimi, F. & Bitan, G. in *Adv. Alzheimer's Res.* 291–374 (2014). doi:10.2174/9781608058525114020014

53. Liu, C., Huang, H., Ma, L., Fang, X., Wang, C. & Yang, Y. Modulation of β-amyloid aggregation by graphene quantum dots. *R. Soc. Open Sci.* **6,** (2019).

54. Kirkitadze, M. D., Condron, M. M. & Teplow, D. B. Identification and characterization of key kinetic intermediates in amyloid β-protein fibrillogenesis. *J. Mol. Biol.* **312,** 1103–1119 (2001).

55. Nguyen, P. H., Ramamoorthy, A., Sahoo, B. R., Zheng, J., Faller, P., Straub, J. E., Dominguez, L., Shea, J. E., Dokholyan, N. V., de Simone, A., Ma, B., Nussinov, R., Najafi, S., Ngo, S. T., Loquet, A., Chiricotto, M., Ganguly, P., McCarty, J., Li, M. S., Hall, C., Wang, Y., Miller, Y., Melchionna, S., Habenstein, B., Timr, S., Chen, J., Hnath, B., Strodel, B., Kayed, R., Lesné, S., Wei, G., Sterpone, F., Doig, A. J. & Derreumaux, P. Amyloid oligomers: A joint experimental/computational perspective on Alzheimer's disease, Parkinson's disease, type II diabetes, and amyotrophic lateral sclerosis. *Chem. Rev.* **121,** 2545–2647 (2021).

56. Teplow, D. B., Bitan, G., Lomakin, A., Benedek, G. B., Kirkitadze, M. D. & Vollers, S. S. Amyloid -protein (A) assembly: A 40 and A 42 oligomerize through distinct pathways. *Proc. Natl. Acad. Sci.* **100,** 330–335 (2003).

57. Nag, S., Sarkar, B., Bandyopadhyay, A., Sahoo, B., Sreenivasan, V. K. A., Kombrabail, M.,

Muralidharan, C. & Maiti, S. Nature of the amyloid-β monomer and the monomer-oligomer equilibrium. *J. Biol. Chem.* **286,** 13827–13833 (2011).

58. Bitan, G. & Teplow, D. B. in *Methods Mol. Biol.* **299,** 3–9 (2005).

59. Nirmalraj, P. N., List, J., Battacharya, S., Howe, G., Xu, L., Thompson, D. & Mayer, M. Complete aggregation pathway of amyloid β (1-40) and (1-42) resolved on an atomically clean interface. *Sci. Adv.* **6,** (2020).

60. Turner, J., Dyrks, T., Georgalis, Y., Saenger, W., Oakley, A. E., Lobbia, A., Kosciessa, U. & Thunecke, M. Aggregation of Aβ Alzheimer's disease-related peptide studied by dynamic light scattering. *J. Pept. Res.* **52,** 509–517 (1998).

61. Snyder, S. W., Ladror, U. S., Matayoshi, E. D., Krafft, G. A., Holzman, T. F., Barrett, L. W., Huffaker, H. J., Wang, G. T. & Wade, W. S. Amyloid-beta aggregation: selective inhibition of aggregation in mixtures of amyloid with different chain lengths. *Biophys. J.* **67,** 1216–1228 (1994).

62. Nichols, M. R., Moss, M. A., Reed, D. K., Lin, W. L., Mukhopadhyay, R., Hoh, J. H. & Rosenberry, T. L. Growth of β-amyloid(1-40) protofibrils by monomer elongation and lateral association. Characterization of distinct products by light scattering and atomic force microscopy. *Biochemistry* **41,** 6115–6127 (2002).

63. Bruggink, K. A., Müller, M., Kuiperij, H. B. & Verbeek, M. M. Methods for analysis of amyloid-β aggregates. *J. Alzheimer's Dis.* **28,** 735–758 (2012).

64. Lesné, S., Ming, T. K., Kotilinek, L., Kayed, R., Glabe, C. G., Yang, A., Gallagher, M. & Ashe, K. H. A specific amyloid-β protein assembly in the brain impairs memory. *Nature* **440,** 352–357 (2006).

65. Lashuel, H. A., Hartley, D. M., Petre, B. M., Wall, J. S., Simon, M. N., Walz, T. & Lansbury, P. T. Mixtures of wild-type and a pathogenic (E22G) form of Aβ40 in vitro accumulate protofibrils, including amyloid pores. *J. Mol. Biol.* **332,** 795–808 (2003).

66. Demuro, A., Mina, E., Kayed, R., Milton, S. C., Parker, I. & Glabe, C. G. Calcium dysregulation and membrane disruption as a ubiquitous neurotoxic mechanism of soluble amyloid oligomers. *J. Biol. Chem.* **280,** 17294–17300 (2005).

67. Longo, V. D., Viola, K. L., Klein, W. L. & Finch, C. E. Reversible inactivation of superoxide-sensitive aconitase in Aβ1-42-treated neuronal cell lines. *J. Neurochem.* **75,** 1977–1985 (2000).

68. De Felice, F. G., Wu, D., Lambert, M. P., Fernandez, S. J., Velasco, P. T., Lacor, P. N., Bigio, E. H., Jerecic, J., Acton, P. J., Shughrue, P. J., Chen-Dodson, E., Kinney, G. G. & Klein, W. L. Alzheimer's disease-type neuronal tau hyperphosphorylation induced by Aβ oligomers. *Neurobiol. Aging* **29,** 1334–1347 (2008).

69. Watanabe, M., Golde, T. E., Nakamura, T., Hirai, S., Younkin, S. G., Hosoda, K., Shoji, M., Cheung, T. T., Shaffer, L. M., Harigaya, Y. & Younkin, L. H. Amyloid-β protein levels in cerebrospinal fluid are elevated in early-onset Alzheimer's disease. *Ann. Neurol.* **36,** 903–911 (1994).

70. Mehta, P. D., Pirttila, T., Patrick, B. A., Barshatzky, M. & Mehta, S. P. Amyloid β protein 1-40 and 1-42 levels in matched cerebrospinal fluid and plasma from patients with

Alzheimer disease. *Neurosci. Lett.* **304,** 102–106 (2001).

71. Koffie, R. M., Meyer-Luehmann, M., Hashimoto, T., Adams, K. W., Mielke, M. L., Garcia-Alloza, M., Micheva, K. D., Smith, S. J., Kim, M. L., Lee, V. M., Hyman, B. T. & Spires-Jones, T. L. Oligomeric amyloid β associates with postsynaptic densities and correlates with excitatory synapse loss near senile plaques. *Proc. Natl. Acad. Sci. U. S. A.* **106,** 4012–4017 (2009).

72. Kaur, A., Shuaib, S., Goyal, D. & Goyal, B. Interactions of a multifunctional di-triazole derivative with Alzheimer's Aβ42 monomer and Aβ42 protofibril: A systematic molecular dynamics study. *Phys. Chem. Chem. Phys.* **22,** 1543–1556 (2020).

73. Siddiqi, M. K., Majid, N., Malik, S., Alam, P. & Khan, R. H. in *Subcell. Biochem.* **93,** 471–503 (2019).

74. Ghosh, P., Kumar, A., Datta, B. & Rangachari, V. Dynamics of protofibril elongation and association involved in Aβ42 peptide aggregation in Alzheimer's disease. in *BMC Bioinformatics* **11,** (2010).

75. Ono, K. & Tsuji, M. Protofibrils of amyloid-β are important targets of a disease-modifying approach for alzheimer's disease. *Int. J. Mol. Sci.* **21,** (2020).

76. Gremer, L., Schölzel, D., Schenk, C., Reinartz, E., Labahn, J., Ravelli, R. B. G., Tusche, M., Lopez-Iglesias, C., Hoyer, W., Heise, H., Willbold, D. & Schröder, G. F. Fibril structure of amyloid-β(1–42) by cryo–electron microscopy. *Science (80-.).* **358,** 116–119 (2017).

77. Linse, S. Mechanism of amyloid protein aggregation and the role of inhibitors. *Pure Appl. Chem.* **91,** 211–229 (2019).

78. Han, S., Kollmer, M., Markx, D., Claus, S., Walther, P. & Fändrich, M. Amyloid plaque structure and cell surface interactions of β-amyloid fibrils revealed by electron tomography. *Sci. Rep.* **7,** (2017).

79. Michaels, T. C. T., Šarić, A., Habchi, J., Chia, S., Meisl, G., Vendruscolo, M., Dobson, C. M. & Knowles, T. P. J. Chemical Kinetics for Bridging Molecular Mechanisms and Macroscopic Measurements of Amyloid Fibril Formation. *Annu. Rev. Phys. Chem.* **69,** 273–298 (2018).

80. Petkova, A. T., Leapman, R. D., Guo, Z., Yau, W. M., Mattson, M. P. & Tycko, R. Self-propagating, molecular-level polymorphism in Alzheimer's β-amyloid fibrils. *Science (80-.).* **307,** 262–265 (2005).

81. Dahlgren, K. N., Manelli, A. M., Blaine Stine, W., Baker, L. K., Krafft, G. A. & Ladu, M. J. Oligomeric and fibrillar species of amyloid-β peptides differentially affect neuronal viability. *J. Biol. Chem.* **277,** 32046–32053 (2002).

82. Van Dam, D. & De Deyn, P. P. Drug discovery in dementia: The role of rodent models. *Nat. Rev. Drug Discov.* **5,** 956–970 (2006).

83. Wenschuh, H., Hubin, E., Schymkowitz, J., Sarroukh, R., Vandersteen, A., Subramaniam, V., Broersen, K., Wildemann, D., De Baets, G., Raussens, V. & Rousseau, F. A comparative analysis of the aggregation behavior of amyloid-β peptide variants. *FEBS Lett.* **586,** 4088–4093 (2012).

84. Michaels, T. C. T., Šarić, A., Curk, S., Bernfur, K., Arosio, P., Meisl, G., Dear, A. J., Cohen, S. I. A., Dobson, C. M., Vendruscolo, M., Linse, S. & Knowles, T. P. J. Dynamics of oligomer populations formed during the aggregation of Alzheimer's Aβ42 peptide. *Nat. Chem.* **12,** 445–451 (2020).

85. Bemporad, F., Calloni, G., Campioni, S., Plakoutsi, G., Taddei, N. & Chiti, F. Sequence and structural determinants of amyloid fibril formation. *Acc. Chem. Res.* **39,** 620–627 (2006).

86. Hortschansky, P., Schroeckh, V., Christopeit, T., Zandomeneghi, G. & Fändrich, M. The aggregation kinetics of Alzheimer's beta-amyloid peptide is controlled by stochastic nucleation. *Protein Sci.* **14,** 1753–9 (2005).

87. Faller, P. & Hureau, C. Reproducibility Problems of Amyloid-β Self-Assembly and How to Deal With Them. *Front. Chem.* **8,** (2021).

88. Yang, X., Meisl, G., Frohm, B., Thulin, E., Knowles, T. P. J. & Linse, S. On the role of sidechain size and charge in the aggregation of Aβ42 with familial mutations. *Proc. Natl. Acad. Sci. U. S. A.* **115,** E5849–E5858 (2018).

89. Kummer, M. P. & Heneka, M. T. Truncated and modified amyloid-beta species. *Alzheimer's Res. Ther.* **6,** (2014).

90. Aliyan, A., Cook, N. P. & Martí, A. A. Interrogating Amyloid Aggregates using Fluorescent Probes. *Chem. Rev.* (2019). doi:10.1021/acs.chemrev.9b00404

91. Zheng, Y., Xu, L., Yang, J., Peng, X., Wang, H., Yu, N., Hua, Y., Zhao, J., He, J. & Hong, T. The effects of fluorescent labels on Aβ 42 aggregation detected by fluorescence correlation spectroscopy. *Biopolymers* **109,** (2018).

92. Jungbauer, L. M., Yu, C., Laxton, K. J. & LaDu, M. J. Preparation of fluorescently-labeled amyloid-beta peptide assemblies: The effect of fluorophore conjugation on structure and function. in *J. Mol. Recognit.* **22,** 403–413 (2009).

93. Wägele, J., De Sio, S., Voigt, B., Balbach, J. & Ott, M. How Fluorescent Tags Modify Oligomer Size Distributions of the Alzheimer Peptide. *Biophys. J.* **116,** 227–238 (2019).

94. Finder, V. H., Vodopivec, I., Nitsch, R. M. & Glockshuber, R. The Recombinant Amyloid-β Peptide Aβ1-42 Aggregates Faster and Is More Neurotoxic than Synthetic Aβ1-42. *J. Mol. Biol.* **396,** 9–18 (2010).

95. Breheney, K., Waddington, L. J., Streltsov, V. A., Ryan, T. M., Roberts, B. R., Nigro, J., Kirby, N., Mertens, H. D. T., Curtain, C., Caine, J. & Masters, C. L. Ammonium hydroxide treatment of Aβ produces an aggregate free solution suitable for biophysical and cell culture characterization. *PeerJ* **1,** e73 (2013).

96. Pryor, N. E., Moss, M. A. & Hestekin, C. N. Capillary electrophoresis for the analysis of the effect of sample preparation on early stages of Aβ1-40aggregation. *Electrophoresis* **35,** 1814–1820 (2014).

97. Meisl, G., Yang, X., Frohm, B., Knowles, T. P. J. & Linse, S. Quantitative analysis of intrinsic and extrinsic factors in the aggregation mechanism of Alzheimer-associated Aβ-peptide. *Sci. Rep.* **6,** (2016).

98. Kobayashi, S., Tanaka, Y., Kiyono, M., Chino, M., Chikuma, T., Hoshi, K. & Ikeshima, H. Dependence pH and proposed mechanism for aggregation of Alzheimer's disease-related amyloid-β(1-42) protein. *J. Mol. Struct.* **1094,** 109–117 (2015).

99. Abelein, A., Jarvet, J., Barth, A., Gräslund, A. & Danielsson, J. Ionic Strength Modulation of the Free Energy Landscape of Aβ40 Peptide Fibril Formation. *J. Am. Chem. Soc.* **138,** 6893–6902 (2016).

100. Ghavami, M., Rezaei, M., Ejtehadi, R., Lotfi, M., Shokrgozar, M. A., Abd Emamy, B., Raush, J. & Mahmoudi, M. Physiological temperature has a crucial role in amyloid beta in the absence and presence of hydrophobic and hydrophilic nanoparticles. *ACS Chem. Neurosci.* **4,** 375–378 (2013).

101. Zagorski, M. G., Yang, J., Shao, H., Ma, K., Zeng, H. & Hong, A. in *Methods Enzymol.* **309,** 189–204 (1999).

102. Verpillot, R., Otto, M., Klafki, H. & Taverna, M. Simultaneous analysis by capillary electrophoresis of five amyloid peptides as potential biomarkers of Alzheimer's disease. *J. Chromatogr. A* **1214,** 157–164 (2008).

103. Brinet, D., Kaffy, J., Oukacine, F., Glumm, S., Ongeri, S. & Taverna, M. An improved capillary electrophoresis method for in vitro monitoring of the challenging early steps of Aβ(1-42) peptide oligomerization: Application to anti-Alzheimer's drug discovery. *Electrophoresis* **35,** 3302–3309 (2014).

104. Ziehm, T., Buell, A. K. & Willbold, D. Role of Hydrophobicity and Charge of Amyloid-Beta Oligomer Eliminating d -Peptides in the Interaction with Amyloid-Beta Monomers. *ACS Chem. Neurosci.* **9,** 2679–2688 (2018).

105. Orlando, R., Jao, S.-C., Zagorski, M. G., Ma, K. & Talafous, J. Trifluoroacetic acid pretreatment reproducibly disaggregates the amyloid β-peptide. *Amyloid* **4,** 240–252 (1997).

106. Brambilla, D., Verpillot, R., Taverna, M., De Kimpe, L., Le Droumaguet, B., Nicolas, J., Canovi, M., Gobbi, M., Mantegazza, F., Salmona, M., Nicolas, V., Scheper, W., Couvreur, P. & Andrieux, K. New method based on capillary electrophoresis with laser-induced fluorescence detection (CE-LIF) to monitor interaction between nanoparticles and the amyloid-β peptide. *Anal. Chem.* **82,** 10083–10089 (2010).

107. Racchi, M., Verga, L., Carotti, A., De Lorenzi, E., Lanni, C., Catto, M., Colombo, R. & Caccialanza, G. CE can identify small molecules that selectively target soluble oligomers of amyloid β protein and display antifibrillogenic activity. *Electrophoresis* **30,** 1418–1429 (2009).

108. Rozenski, J., Pastore, A., Schymkowitz, J., Broersen, K., Jonckheere, W., Pauwels, K., Vandersteen, A. & Rousseau, F. A standardized and biocompatible preparation of aggregate-free amyloid beta peptide for biophysical and biological studies of Alzheimer's disease. *Protein Eng. Des. Sel.* **24,** 743–750 (2011).

109. Picou, R. A., Kheterpal, I., Wellman, A. D., Minnamreddy, M., Ku, G. & Gilman, S. D. Analysis of Aβ (1-40) and Aβ (1-42) monomer and fibrils by capillary electrophoresis. *J. Chromatogr. B Anal. Technol. Biomed. Life Sci.* **879,** 627–632 (2011).

110. Porzoor, A., Caine, J. M. & Macreadie, I. G. Pretreatment of chemically-synthesized Aβ42

affects its biological activity in yeast. *Prion* **8,** 404–410 (2014).

111. Shen, C. L. & Murphy, R. M. Solvent effects on self-assembly of beta-amyloid peptide. *Biophys. J.* **69,** 640–651 (1995).

112. Gade Malmos, K., Blancas-Mejia, L. M., Weber, B., Buchner, J., Ramirez-Alvarado, M., Naiki, H. & Otzen, D. ThT 101: a primer on the use of thioflavin T to investigate amyloid formation. *Amyloid* **24,** 1–16 (2017).

113. Caccialanza, G., Bellotti, V., Racchi, M., Lanni, C., Calligaro, A., Sabella, S., De Lorenzi, E., Govoni, S. & Quaglia, M. Capillary electrophoresis studies on the aggregation process ofβ-amyloid 1-42 and 1-40 peptides. *Electrophoresis* **25,** 3186–3194 (2004).

114. Denoroy, L. & Parrot, S. Advances and Pitfalls in the Capillary Electrophoresis Analysis of Aggregates of Beta Amyloid Peptides. *Separations* **5,** 2 (2017).

115. Kaffy, J., Piarulli, U., Fanelli, R., Vahdati, L., Lequin, O., Ongeri, S., Taverna, M., Bernadat, G., Brinet, D., Panzeri, S. & Correia, I. Synthesis and Characterization of Hairpin Mimics that Modulate the Early Oligomerization and Fibrillization of Amyloid β-Peptide. *European J. Org. Chem.* **2017,** 2971–2980 (2017).

116. Ryan, T. M., Kirby, N., Mertens, H. D. T., Roberts, B., Barnham, K. J., Cappai, R., Pham, C. L. L., Masters, C. L. & Curtain, C. C. Small angle X-ray scattering analysis of Cu2+-induced oligomers of the Alzheimer's amyloid β peptide. *Metallomics* **7,** 536–543 (2015).

117. Mantsyzov, A. B., Radko, S. P., Mitkevich, V. A., Khmeleva, S. A., Kiseleva, Y. Y., Makarov, A. A. & Kozin, S. A. Heparin Modulates the Kinetics of Zinc-Induced Aggregation of Amyloid-β Peptides. *J. Alzheimer's Dis.* **63,** 539–550 (2018).

118. Paracha, S. & Hestekin, C. Field amplified sample stacking of amyloid beta (1-42) oligomers using capillary electrophoresis. *Biomicrofluidics* **10,** (2016).

119. Ruiz, A., Pesini, P., Espinosa, A., Pérez-Grijalba, V., Valero, S., Sotolongo-Grau, O., Alegret, M., Monleón, I., Lafuente, A., Buendía, M., Ibarria, M., Ruiz, S., Hernández, I., San José, I., Tárraga, L., Boada, M. & Sarasa, M. Blood amyloid beta levels in healthy, mild cognitive impairment and Alzheimer's disease individuals: Replication of diastolic blood pressure correlations and analysis of critical covariates. *PLoS One* **8,** (2013).

120. Man, V. H., He, X., Ji, B., Liu, S., Xie, X. Q. & Wang, J. Molecular Mechanism and Kinetics of Amyloid-β42 Aggregate Formation: A Simulation Study. *ACS Chem. Neurosci.* **10,** 4643–4658 (2019).

121. Sabaté, R., Gallardo, M. & Estelrich, J. Temperature dependence of the nucleation constant rate in β amyloid fibrillogenesis. *Int. J. Biol. Macromol.* **35,** 9–13 (2005).

122. Kusumoto, Y., Lomakin, A., Teplow, D. B. & Benedek, G. B. Temperature dependence of amyloid -protein fibrillization. *Proc. Natl. Acad. Sci.* **95,** 12277–12282 (1998).

123. Ayton, S., Lei, P. & Bush, A. I. Metallostasis in Alzheimer's disease. *Free Radic. Biol. Med.* **62,** 76–89 (2013).

124. Wang, L., Yin, Y. L., Liu, X. Z., Shen, P., Zheng, Y. G., Lan, X. R., Lu, C. B. & Wang, J. Z. Current understanding of metal ions in the pathogenesis of Alzheimer's disease. *Transl. Neurodegener.* **9,** (2020).

125. Penke, B., Bogár, F., Paragi, G., Gera, J. & Fülöp, L. Key Peptides and Proteins in Alzheimer's Disease. *Curr. Protein Pept. Sci.* **20,** 577–599 (2019).

126. Milojevic, J., Costa, M., Ortiz, A. M., Jorquera, J. I. & Melacini, G. In vitro amyloid-β binding and inhibition of amyloid-β self-association by therapeutic albumin. *J. Alzheimer's Dis.* **38,** 753–765 (2014).

127. Boada, M., López, O. L., Olazarán, J., Núñez, L., Pfeffer, M., Paricio, M., Lorites, J., Piñol-Ripoll, G., Gámez, J. E., Anaya, F., Kiprov, D., Lima, J., Grifols, C., Torres, M., Costa, M., Bozzo, J., Szczepiorkowski, Z. M., Hendrix, S. & Páez, A. A randomized, controlled clinical trial of plasma exchange with albumin replacement for Alzheimer's disease: Primary results of the AMBAR Study. *Alzheimer's Dement.* **16,** 1412–1425 (2020).

128. Kuperstein, I., Broersen, K., Benilova, I., Rozenski, J., Jonckheere, W., Debulpaep, M., Vandersteen, A., Segers-Nolten, I., Van Der Werf, K., Subramaniam, V., Braeken, D., Callewaert, G., Bartic, C., D'Hooge, R., Martins, I. C., Rousseau, F., Schymkowitz, J. & De Strooper, B. Neurotoxicity of Alzheimer's disease Aβ peptides is induced by small changes in the Aβ42 to Aβ40 ratio. *EMBO J.* **29,** 3408–3420 (2010).

129. Chang, Y. J. & Chen, Y. R. The coexistence of an equal amount of Alzheimer's amyloid-β 40 and 42 forms structurally stable and toxic oligomers through a distinct pathway. *FEBS J.* **281,** 2674–2687 (2014).

130. Jan, A., Gokce, O., Luthi-Carter, R. & Lashuel, H. A. The ratio of monomeric to aggregated forms of Aβ40 and Aβ42 is an important determinant of amyloid-β aggregation, fibrillogenesis, and toxicity. *J. Biol. Chem.* **283,** 28176–28189 (2008).

131. Cerofolini, L., Ravera, E., Bologna, S., Wiglenda, T., Böddrich, A., Purfürst, B., Benilova, I., Korsak, M., Gallo, G., Rizzo, D., Gonnelli, L., Fragai, M., De Strooper, B., Wanker, E. E. & Luchinat, C. Mixing Aβ(1-40) and Aβ(1-42) peptides generates unique amyloid fibrils. *Chem. Commun.* **56,** 8830–8833 (2020).

132. Economou, N. J., Giammona, M. J., Do, T. D., Zheng, X., Teplow, D. B., Buratto, S. K. & Bowers, M. T. Amyloid β-Protein Assembly and Alzheimer's Disease: Dodecamers of Aβ42, but Not of Aβ40, Seed Fibril Formation. *J. Am. Chem. Soc.* **138,** 1772–1775 (2016).

133. Dammers, C., Schwarten, M., Buell, A. K. & Willbold, D. Pyroglutamate-modified Aβ(3-42) affects aggregation kinetics of Aβ(1-42) by accelerating primary and secondary pathways. *Chem. Sci.* **8,** 4996–5004 (2017).

134. Kwak, S. S., Washicosky, K. J., Brand, E., von Maydell, D., Aronson, J., Kim, S., Capen, D. E., Cetinbas, M., Sadreyev, R., Ning, S., Bylykbashi, E., Xia, W., Wagner, S. L., Choi, S. H., Tanzi, R. E. & Kim, D. Y. Amyloid-β42/40 ratio drives tau pathology in 3D human neural cell culture models of Alzheimer's disease. *Nat. Commun.* **11,** (2020).

135. Adessi, C. & Soto, C. Beta-sheet breaker strategy for the treatment of Alzheimer's disease. *Drug Dev. Res.* **56,** 184–193 (2002).

136. Ehrnhoefer, D. E., Bieschke, J., Boeddrich, A., Herbst, M., Masino, L., Lurz, R., Engemann, S., Pastore, A. & Wanker, E. E. EGCG redirects amyloidogenic polypeptides into unstructured, off-pathway oligomers. *Nat. Struct. Mol. Biol.* **15,** 558–566 (2008).

137. Limbocker, R., Chia, S., Ruggeri, F. S., Perni, M., Cascella, R., Heller, G. T., Meisl, G.,

Mannini, B., Habchi, J., Michaels, T. C. T., Challa, P. K., Ahn, M., Casford, S. T., Fernando, N., Xu, C. K., Kloss, N. D., Cohen, S. I. A., Kumita, J. R., Cecchi, C., Zasloff, M., Linse, S., Knowles, T. P. J., Chiti, F., Vendruscolo, M. & Dobson, C. M. Trodusquemine enhances Aβ 42 aggregation but suppresses its toxicity by displacing oligomers from cell membranes. *Nat. Commun.* **10,** (2019).

138. Kaffy, J., Berardet, C., Mathieu, L., Legrand, B., Taverna, M., Halgand, F., Van Der Rest, G., Maillard, L. T. & Ongeri, S. Helical γ-Peptide Foldamers as Dual Inhibitors of Amyloid-β Peptide and Islet Amyloid Polypeptide Oligomerization and Fibrillization. *Chem. - A Eur. J.* **26,** 14612–14622 (2020).

139. De Bona, P., Giuffrida, M. L., Caraci, F., Copani, A., Pignataro, B., Attanasio, F., Cataldo, S., Pappalardo, G. & Rizzarelli, E. Design and synthesis of new trehalose-conjugated pentapeptides as inhibitors of Aβ(1-42) fibrillogenesis and toxicity. *J. Pept. Sci.* **15,** 220–228 (2009).

140. Shamloo, A., Asadbegi, M., Khandan, V. & Amanzadi, A. Designing a new multifunctional peptide for metal chelation and Aβ inhibition. *Arch. Biochem. Biophys.* **653,** 1–9 (2018).

141. Giordano, C., Punzi, P., Lori, C., Chiaraluce, R. & Consalvi, V. β-sheet breaker peptides containing α,β- dehydrophenylalanine: Synthesis and in vitro activity studies. *Chempluschem* **79,** 1036–1043 (2014).

142. Carrotta, R., Manno, M., Bulone, D., Martorana, V. & San Biagio, P. L. Protofibril formation of amyloid β-protein at low pH via a non-cooperative elongation mechanism. *J. Biol. Chem.* **280,** 30001–30008 (2005).

143. Elizabeth Pryor, N., Moss, M. A. & Hestekin, C. N. Unraveling the early events of amyloid-ß protein (Aß) aggregation: Techniques for the determination of Aβ aggregate size. *Int. J. Mol. Sci.* **13,** 3038–3072 (2012).

144. Lindberg, D. J., Wranne, M. S., Gilbert Gatty, M., Westerlund, F. & Esbjörner, E. K. Steady-state and time-resolved Thioflavin-T fluorescence can report on morphological differences in amyloid fibrils formed by Aβ(1-40) and Aβ(1-42). *Biochem. Biophys. Res. Commun.* **458,** 418–423 (2015).

145. Kato, M., Hori, Y., Toyo'oka, T., Enokita, M., Kinoshita, H., Hashimoto, T. & Iwatsubo, T. Analytical Method for β-Amyloid Fibrils Using CE-Laser Induced Fluorescence and Its Application to Screening for Inhibitors of β-Amyloid Protein Aggregation. *Anal. Chem.* **79,** 4887–4891 (2007).

146. Varesio, E., Rudaz, S., Krause, K. H. & Veuthey, J. L. Nanoscale liquid chromatography and capillary electrophoresis coupled to electrospray mass spectrometry for the detection of amyloid-β peptide related to Alzheimer's disease. *J. Chromatogr. A* **974,** 135–142 (2002).

147. Picou, R., Moses, J. P., Wellman, A. D., Kheterpal, I. & Gilman, S. D. Analysis of monomeric Aβ (1-40) peptide by capillary electrophoresis. *Analyst* **135,** 1631–1635 (2010).

148. Lv, G., Sun, A., Wang, M., Wei, P., Li, R. & Yi, T. A novel near-infrared fluorescent probe for detection of early-stage Aβ protofibrils in Alzheimer's disease. *Chem. Commun.* **56,** 1625–1628 (2020).

149. Younan, N. D. & Viles, J. H. A Comparison of Three Fluorophores for the Detection of

Amyloid Fibers and Prefibrillar Oligomeric Assemblies. ThT (Thioflavin T); ANS (1-Anilinonaphthalene-8-sulfonic Acid); and bisANS (4,4′-Dianilino-1,1′-binaphthyl-5,5′-disulfonic Acid). *Biochemistry* **54,** 4297–4306 (2015).

150. Jiang, B., Aliyan, A., Cook, N. P., Augustine, A., Bhak, G., Maldonado, R., Smith McWilliams, A. D., Flores, E. M., Mendez, N., Shahnawaz, M., Godoy, F. J., Montenegro, J., Moreno-Gonzalez, I. & Martí, A. A. Monitoring the Formation of Amyloid Oligomers Using Photoluminescence Anisotropy. *J. Am. Chem. Soc.* **141,** 15605–15610 (2019).

151. Lee, D., Kim, S. M., Kim, H. Y. & Kim, Y. Fluorescence Chemicals to Detect Insoluble and Soluble Amyloid-β Aggregates. *ACS Chem. Neurosci.* **10,** 2647–2657 (2019).

152. LeVine, H. Quantification of β-sheet amyloid fibril structures with thioflavin T. *Methods Enzymol.* **309,** 274–284 (1999).

153. Ow, S. Y. & Dunstan, D. E. A brief overview of amyloids and Alzheimer's disease. *Protein Sci.* **23,** 1315–1331 (2014).

154. Xue, C., Lin, T. Y., Chang, D. & Guo, Z. Thioflavin T as an amyloid dye: Fibril quantification, optimal concentration and effect on aggregation. *R. Soc. Open Sci.* **4,** (2017).

155. Hackl, E. V., Darkwah, J., Smith, G. & Ermolina, I. Effect of acidic and basic pH on Thioflavin T absorbance and fluorescence. *Eur. Biophys. J.* **44,** 249–261 (2015).

156. Kroes-Nijboer, A., Lubbersen, Y. S., Venema, P. & van der Linden, E. Thioflavin T fluorescence assay for β-lactoglobulin fibrils hindered by DAPH. *J. Struct. Biol.* **165,** 140–145 (2009).

157. Picou, R. A., Schrum, D. P., Ku, G., Cerqua, R. A., Kheterpal, I. & Gilman, S. D. Separation and detection of individual Aβ aggregates by capillary electrophoresis with laser-induced fluorescence detection. *Anal. Biochem.* **425,** 104–112 (2012).

158. Mai, T. D., Pereiro, I., Hiraoui, M., Viovy, J. L., Descroix, S., Taverna, M. & Smadja, C. Magneto-immunocapture with on-bead fluorescent labeling of amyloid-β peptides: towards a microfluidized-bed-based operation. *Analyst* **140,** 5891–5900 (2015).

159. Bisceglia, F., Natalello, A., Serafini, M. M., Colombo, R., Verga, L., Lanni, C. & De Lorenzi, E. An integrated strategy to correlate aggregation state, structure and toxicity of Aß 1–42 oligomers. *Talanta* **188,** 17–26 (2018).

160. Matsumura, S., Shinoda, K., Yamada, M., Yokojima, S., Inoue, M., Ohnishi, T., Shimada, T., Kikuchi, K., Masui, D., Hashimoto, S., Sato, M., Ito, A., Akioka, M., Takagi, S., Nakamura, Y., Nemoto, K., Hasegawa, Y., Takamoto, H., Inoue, H., Nakamura, S., Nabeshima, Y. I., Teplow, D. B., Kinjo, M. & Hoshia, M. Two distinct amyloid β-protein (Aβ) assembly pathways leading to oligomers and fibrils identified by combined fluorescence correlation spectroscopy, morphology, and toxicity analyses. *J. Biol. Chem.* **286,** 11555–11562 (2011).

161. Garai, K., Sahoo, B., Sengupta, P. & Maiti, S. Quasihomogeneous nucleation of amyloid beta yields numerical bounds for the critical radius, the surface tension, and the free energy barrier for nucleus formation. *J. Chem. Phys.* **128,** (2008).

162. Lomakin, A., Chung, D. S., Benedek, G. B., Kirschner, D. A. & Teplow, D. B. On the nucleation and growth of amyloid β-protein fibrils: Detection of nuclei and quantitation of

rate constants. *Proc. Natl. Acad. Sci. U. S. A.* **93,** 1125–1129 (1996).

163. Moser, M. R. & Baker, C. A. Taylor dispersion analysis in fused silica capillaries: A tutorial review. *Anal. Methods* **13,** 2357–2373 (2021).

164. Grasso, G., Rebella, M., Muscat, S., Morbiducci, U., Tuszynski, J., Danani, A. & Deriu, M. A. Conformational dynamics and stability of u-shaped and s-shaped amyloid β assemblies. *Int. J. Mol. Sci.* **19,** (2018).

165. Taylor, G. I. Dispersion of soluble matter in solvent flowing slowly through a tube. *Proc. R. Soc. London. Ser. A. Math. Phys. Sci.* **219,** 186–203 (1953).

166. Chamieh, J. & Cottet, H. in *Colloid Interface Sci. Pharm. Res. Dev.* 173–192 (2014). doi:10.1016/B978-0-444-62614-1.00009-0

167. Chamieh, J., Leclercq, L., Martin, M., Slaoui, S., Jensen, H., Østergaard, J. & Cottet, H. Limits in Size of Taylor Dispersion Analysis: Representation of the Different Hydrodynamic Regimes and Application to the Size-Characterization of Cubosomes. *Anal. Chem.* **89,** 13487–13493 (2017).

168. Chamieh, J., Biron, J. P., Cipelletti, L. & Cottet, H. Monitoring Biopolymer Degradation by Taylor Dispersion Analysis. *Biomacromolecules* **16,** 3945–3951 (2015).

169. Cipelletti, L., Biron, J. P., Martin, M. & Cottet, H. Measuring Arbitrary Diffusion Coefficient Distributions of Nano-Objects by Taylor Dispersion Analysis. *Anal. Chem.* **87,** 8489–8496 (2015).

170. Ibrahim, A., Meyrueix, R., Pouliquen, G., Chan, Y. P. & Cottet, H. Size and charge characterization of polymeric drug delivery systems by Taylor dispersion analysis and capillary electrophoresis. *Anal. Bioanal. Chem.* **405,** 5369–5379 (2013).

171. Høgstedt, U. B., Schwach, G., van de Weert, M. & Østergaard, J. Taylor Dispersion Analysis as a promising tool for assessment of peptide-peptide interactions. *Eur. J. Pharm. Sci.* **93,** 21–28 (2016).

Chapter II

Research Article 1

Unraveling the Speciation of β-Amyloid Peptides during the Aggregation Process by Taylor Dispersion Analysis

Chapter II. Article 1. Unraveling the speciation of β-amyloid peptides during the aggregation process by Taylor dispersion analysis

This chapter was published in *Anal. Chem*., 2021, *93*, (*16*), 6523–6533.
https://doi.org/10.1021/acs.analchem.1c00527

Mihai Deleanu,[1] Jean-François Hernandez,[1] Luca Cipelletti,[2,3] Jean-Philippe Biron,[1] Emilie Rossi,[4] Myriam Taverna,[3,4] Hervé Cottet,*[1] Joseph Chamieh *[1]

[1] IBMM, Université Montpellier, CNRS, ENSCM, 34095 Montpellier, France
[2] Laboratoire Charles Coulomb (L2C), Université Montpellier, CNRS, Montpellier, France.
[3] Institut Universitaire de France (IUF), 75231 Paris, France
[4] Université Paris-Saclay, CNRS, Institut Galien Paris-Saclay, 92296, Châtenay-Malabry, Fr.

* CORRESPONDING AUTHORS
Tel: +33 4 6714 3920, Fax: +33 4 6763 1046. E-mail: joseph.chamieh@umontpellier.fr
Tel: +33 4 6714 3427, Fax: +33 4 6763 1046. E-mail: herve.cottet@umontpellier.fr

II. Abstract

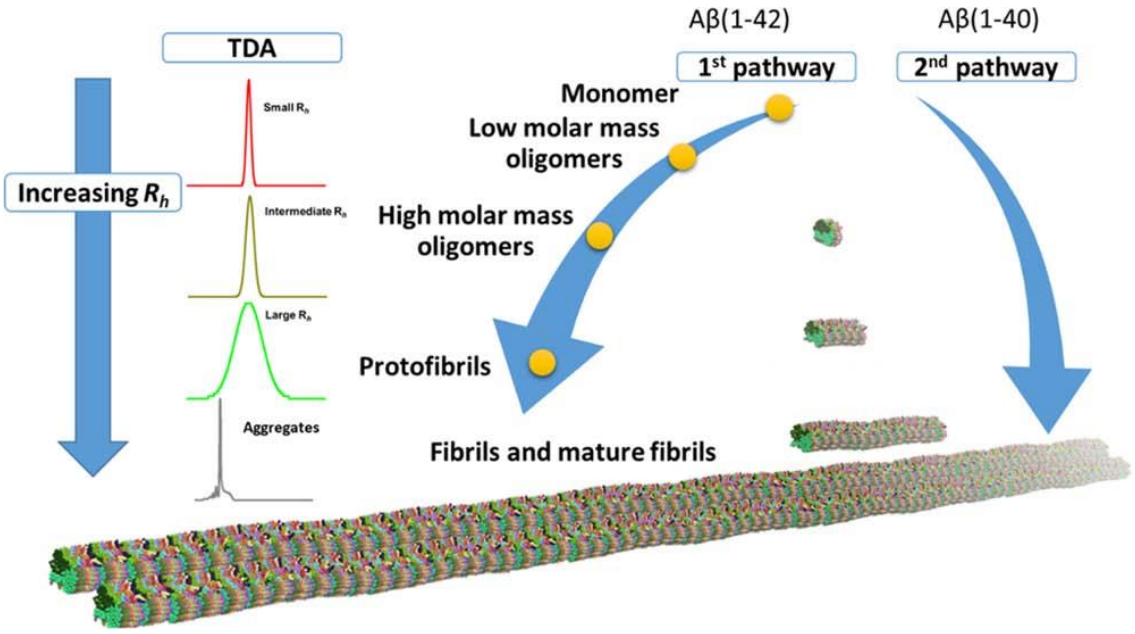

Aggregation mechanisms of amyloid β peptides depend on multiple intrinsic and extrinsic physicochemical factors (e.g., peptide chain length, truncation, peptide concentration, pH, ionic strength, temperature, metal concentration, etc.). Due to this high number of parameters, the formation of oligomers and their propensity to aggregate make the elucidation of this physiopathological mechanism a challenging task. From the analytical point of view, up to our knowledge, few techniques are able to quantify, in real time, the proportion and the size of the different soluble species during the aggregation process. This work aims at demonstrating the efficacy of the modern Taylor dispersion analysis (TDA) performed in capillaries (50 µm i.d.) to unravel the speciation of β-amyloid peptides in low-volume peptide samples (~100 µL) with an analysis time of ~3 min per run. TDA was applied to study the aggregation process of Aβ(1-40) and Aβ(1-42) peptides at physiological pH and temperature, where more than 140 data points were generated with a total volume of ~1 µL over the whole aggregation study (about 0.5 µg of peptides). TDA was able to give a complete and quantitative picture of the Aβ speciation during the aggregation process, including the sizing of the oligomers and protofibrils, the consumption of the monomer, and the quantification of different early- and late-formed aggregated species.

II.1. Introduction

Alzheimer's disease (AD) is the result of a slow degeneration of neurons. It starts in the hippocampus (which lies in the medial temporal lobes of the brain and is responsible for long-term memory) and then extends to the rest of the brain. This fatal neurodegenerative disorder is characterized by progressive cognitive and functional impairment and memory loss[1.] Currently, there is no cure for AD; however, there is extensive research to reveal its risk factors and the mechanisms leading to this dementia. Indeed, more than 95000 articles including more than 19000 reviews dealing with Alzheimer's disease were published just in the last decade (number of articles obtained on PubMed between 2010 and 2020 by searching "Alzheimer's disease").

For many years, AD was thought to be mainly associated with the formation of extracellular senile plaques composed primarily of amyloid β peptides (Aβ) and hyperphosphorylated neurofibrillary tangles of tau protein[2]. Consequently, research toward AD curative treatments has been driven largely by the amyloid cascade hypothesis. This hypothesis developed in the 1990s relies on the fact that Aβ peptides (Aβ1-40 and mainly Aβ1-42) released by amyloid β precursor protein (APP) enzymatic cleavage, readily self-assemble to form amyloid species with an evolving morphology and size (oligomers of increasing size, protofibrils and then fibrils) through a highly complicated process, finally accumulating into plaques, which were believed to be the major pathogenic forms of Aβ[3,4]. More recently, production of soluble amyloid β oligomers[5] and inflammation[6] have also emerged as important early steps in the pathogenesis of Alzheimer's disease. The "amyloid-β oligomer hypothesis", which is still under debate, states that the main reason behind AD is the formation of soluble oligomers of Aβ[7–10] considered to be more toxic than plaques and causing selective nerve cell death[10–12]. Indeed, soluble Aβ oligomers (AβO) are believed to be more toxic[13] than fibrils, which precipitate as plaques, because they are able to spread across neuronal tissue and they are supposed to mediate neurotoxicity and synaptic loss through binding to membrane receptors, including the prion protein[14,15]. To assess its validity and to develop new drug candidates against AD targeting the soluble oligomers, new analytical methodologies able to finely monitor, quantify, and characterize these oligomeric species are required. However, in contrast to fibrils, which have low solubility and are highly stable, the soluble oligomers are fragile, metastable, transient,[16] highly polydisperse in size, and therefore

more difficult to detect and study in real time[16].

When studied in vitro, the aggregation mechanisms leading to the oligomers and then to fibrils depend on multiple physicochemical factors that can be intrinsic[17] (e.g., chain length, truncation, net charge, and hydrophobicity) and extrinsic, such as concentration[18,19], pH, temperature, incubation conditions[20], buffer ionic strength, and salt composition[21]. The influence of metals and other proteins has also been reported[10]. Due to this high number of parameters the elucidation of the aggregation mechanism is a challenging task. The detection of fibrils during the early stages of the aggregation process can be realized by multiple analytical techniques and specifically by fluorescence using the ThT assay[22]. However, the ThT assay is mainly insensitive to Aβ oligomeric species[23]. In contrast, other analytical techniques such as size-exclusion chromatography (SEC)[24,25], atomic force microscopy (AFM)[26,27], capillary electrophoresis[28], mass spectrometry[29–31], and dynamic light scattering (DLS) [32], to name a few are able to detect the presence of oligomers. However, some of the aforementioned methods require a large sample volume (e.g., SEC), others are very sensitive to the presence of the large fibrils (or particles) making the detection of the small oligomers a difficult task (e.g., DLS). Few of these methods are able to follow in real time the aggregation process in a medium representative of the in vivo conditions. Furthermore, some of these techniques require a sample pretreatment before the analysis[25], which may alter the form of the species present in the sample. Thus, new methods able to rapidly determine the size of aggregates in the range 1−100 nm are highly required to better understand the real-time mechanism of oligomer formation.

In this context, Taylor dispersion analysis[33–35] (TDA) appears as a very promising alternative analytical method. Indeed, TDA is an absolute method (no calibration needed) allowing for the determination of the molecular diffusion coefficient, D, and of the hydrodynamic radius, R_h, of a solute, including for mixtures, without any bias in the size, the contribution of the small and the large solutes being proportional to their mass abundance in the mixture[36]. TDA is based on the dispersion of an injected band under a laminar Poiseuille flow. Its implementation in narrow bore capillaries (typically ∼50 μm i.d.) presents several advantages[37–40] such as a low sample consumption, a short analysis time, a wide range of sizing (from angstrom to submicron), and a straightforward analysis without any sample pretreatment or filtration[41–43].

In this work, TDA was applied to study the aggregation process of two Aβ sequences Aβ(1-40) and Aβ(1-42) at physiological pH (7.4) and temperature (37 °C) by providing a direct

determination of all possible forms of Aβ amyloid according to the incubation time. TDA was able to provide a complete picture of the Aβ speciation during the in vitro aggregation process, including the consumption of the monomer and the formation of oligomers, protofibrils, and fibrils.

II.2. Materials and methods

II.2.1. Materials.

Synthesized amyloid β(1-40) (denoted as Aβ(1-40) in this work) was prepared as described in the "Solid-Phase Synthesis of the Aβ(1-40)" section in the Supporting Information (Figure SI.1 shows a scheme of the synthesis protocol, while Figure SI.2 shows the chromatographic and mass spectrometry analysis of the synthesized peptide). Commercial amyloid β 1-40 (batch number 1658309, >95%) (denoted as cAβ(1-40) in this work) was purchased from Anaspec. Amyloid β(1-42) (Aβ(1-42), batch number 1071428, >95%) was purchased from Bachem (Bubendorf, Switzerland). Thioflavin T, sodium dihydrogen phosphate, tris(hydroxymethyl)aminomethane, hydrochloric acid fuming 37%, sodium chloride, and sodium hydroxide were purchased from Sigma-Aldrich (France). Fmoc protected amino acids, coupling reagents hexafluorophosphate azabenzotriazole tetra-methyl uronium (HATU) and benzotriazol-1-yl-oxytripyrrolidinophosphonium hexafluorophosphate (PyBOP) were purchased from Iris Biotech (Germany). The ChemMatrix H-Val-O-Wang resin was purchased from PCAS Biomatrix (Canada). Dimethylformamide, acetic anhydride, piperidine, dichloromethane, methanol, acetonitrile, trifluoroacetic acid, and diethyl ether were acquired from Carlo Erba (Italy), Sigma-Aldrich (Merck, Germany), Acros Organics (Thermo Fisher-Scientific, Germany), or Honeywell Riedel-de Haën (Fisher-Scientific, Illkirch, France), and all were of analytical grade. N,N-diisopropylethylamine, 1,1,1,3,3,3-hexafluoro-2-propanol, triisopropylsilane (TIS), and tetra-n-butylammonium bromide were purchased from Alfa Aesar (Thermo Fisher-Scientific, Germany) or Fluorochem (U.K.). Ultrapure water used for all buffers was prepared with a Milli-Q system from Millipore (France).

II.2.2. Peptide pretreatment.

Both Aβ(1-40) and Aβ(1-42) were first pretreated independently, as described elsewhere[28,44]. Briefly, Aβ(1-40) and Aβ(1-42) were dissolved in 0.10% (m/v) and 0.16% (m/v) NH4OH aqueous solutions, respectively, to reach a final peptide concentration of 2 mg/ mL. The peptide solutions were then incubated at room temperature for 10 min, separated into several aliquots and freeze-dried. The aliquot volume was calculated to obtain 10 nmol of peptides in each Eppendorf tube. The lyophilized peptide aliquots were stored at -20 °C until further use.

II.2.3. ThT fluorescence assay

To check the initial state of aggregation of the studied peptides, the ThT fluorescence assay was used by adapting the protocol described in ref 45. Briefly, peptides were dissolved at a concentration of 1 mM in a1% NH4OH aqueous solution, then diluted with 10 mM Tris−HCl + 100 mM NaCl buffer (pH 7.4) to a final concentration of 0.2 mM. A volume of 10 μL of the latter peptide solution was withdrawn and put in a Costar 96-well black polystyrene plate along with 189 μLof 40 μM ThT in the Tris−HCl saline buffer solution. The fluorescence was monitored at room temperature for 24 h using a Berthold TriStar LB 941 instrument (Germany) (an excitation wavelength of 430 nm and emission wavelength of 485 nm). Control wells were prepared by replacing the 10 μL of peptide solution with 10 μL of a 0.2% NH4OH aqueous solution prepared by diluting a 1% NH4OH aqueous solution with 10 mM Tris−HCl + 100 mM NaCl buffer (pH 7.4). Five wells were prepared for each solution.

II.2.4. Peptide aggregation study by Taylor dispersion analysis

TDA was performed on an Agilent 7100 (Waldbronn, Germany) capillary electrophoresis system using bare fused silica capillaries (Polymicro Technologies) having 40 cm × 50 μm i.d. dimensions and a detection window at 31.5 cm. New capillaries were conditioned with the following flushes: 1 M NaOH for 30 min and ultrapure water for 30 min. Between each analysis, the capillaries were rinsed with 20 mM phosphate buffer, pH 7.4 (2 min). Samples were injected

hydrodynamically on the inlet end of the capillary (44 mbar, 3 s, injected volume is about 7 nL corresponding to 1% of the capillary volume to the detection point). Experiments were performed using a mobilization pressure of 100 mbar. The temperature of the capillary cartridge was set at 37 °C. The vial carrousel was thermostated using an external circulating water bath from Bioblock (France). The solutes were monitored by UV absorbance at 191 nm. The mobile phase was a 20 mM phosphate buffer, pH 7.4 (viscosity at 37 °C is 0.7×10^{-4} Pa s)[28]. Peptide samples were dissolved in 100 µL of 20 mM phosphate buffer, pH 7.4, to reach a final concentration of 100 µM and were immediately transferred to a vial and incubated at 37 °C in the capillary electrophoresis instrument's carrousel. The aggregation was conducted by injecting the sample (Vinj ≈ 7 nL) every 7 min in the case of Aβ(1-42) and every 30 min in the case of Aβ(1-40). The total number of TDA runs for each sample was about 150, corresponding to a total sample volume of 1050 nL (1.05 µL). To avoid sample evaporation, the vial cap was changed three times a day. The taylorgrams were recorded with Agilent Chemstation software and then exported to Microsoft Excel for subsequent data processing.

II.2.5. Dynamic light scattering

Complementary dynamic light scattering data were acquired using a standard setup by Brookhaven Instruments Co. (BI-900AT), equipped with a 150 mW laser with an *in vacuo* wavelength λ = 532.5 nm. Frozen, dehydrated samples were thawed at room temperature. At time t_{ag} = 0, a volume of 100 µL of 20 mM phosphate buffer, pH 7.4, filtered through a 0.22 µm Millipore filter was added to the thawed powder, setting the Aβ(1-42) concentration to 100 µM. The sample was injected in a nuclear magnetic resonance (NMR) tube and placed in the setup immediately after mixing. Measurements were performed as a function of tag by alternating runs at scattering angles θ = 90 and 45° (run duration: 240 and 360 s, respectively). The sample was thermostated at 37.0 ± 0.1 °C.

The CONTIN algorithm[46,47] embedded in Brookhaven software was used to extract *PI(D)*, the intensity-weighted distribution of the diffusion coefficients D of the scatterers, which was then converted to the mass-weighted distribution of hydrodynamic radii R_h, $PM(R_h)$, using custom software. In performing the conversion, it was assumed that the peptides aggregate by forming cylindrical structures resulting from the stacking of dimer units (see the Results and Discussion

section and Figure 6). This allowed us to calculate the mass and scattered intensity (to within an inessential multiplicative constant) of the aggregates, as a function of their hydrodynamic radius, obtained via HYDROPRO software.[48] Knowledge of $M(R_h)$ and $I(R_h)$ allowed for re-expressing $PI(D)$as $PM(R_h)$, using standard probability distribution transformation laws and the Stokes−Einstein relationship $R_h = k_B T/(6\pi\eta D)$, with k_B Boltzmann's constant, T = 310.15 K, and η = 0.7 mPa s the solvent viscosity.

II.3. Results and discussion

II.3.1. ThT assay and the initial state of the peptide samples

The aggregation of Aβ peptides is a highly complex process that is dependent on, and very sensitive to, the initial conditions of peptide preparation. The initial presence of aggregates (or seeds of aggregates) can drastically influence the aggregation process. Therefore, the peptides were treated upon reception with an ammonium hydroxide solution before freeze drying and storage[28]. The aim of this step is to dissociate any aggregated peptide and to start the kinetic studies from the very early steps, with a nonaggregated sample. To confirm the success of this step, samples were submitted to the ThT fluorescence assay[49]. Figure SI.3 shows the fluorescence kinetic curves of the studied peptide batches: the synthesized Aβ(1-40), the commercial cAβ(1-40), Aβ(1-42), and a control run. Only the commercial cAβ(1-40) was found to be initially aggregated, despite the ammonium hydroxide treatment, since it showed an initial relatively high fluorescence signal and nearly no lag phase. In contrast, the synthesized Aβ(1-40) and the commercial Aβ(1-42) peptides were assumed to be free of aggregates since their initial fluorescence intensity was low and in the same order of magnitude as the control run. These results show the importance of using clean (nonaggregated) samples for kinetic studies.

II.3.2. Processing of the taylorgrams

Briefly, the band broadening resulting from the Taylor dispersion is easily quantified via the temporal variance (σ^2) of the elution profile. For that, a fit of the experimental peak with a Gaussian function allows for the determination of σ^2 and the calculation of the molecular diffusion coefficient, D, and consequently the hydrodynamic radius, R_h. The reader may refer to the

Supporting Information for the theoretical aspects, equations, and more details on data processing.

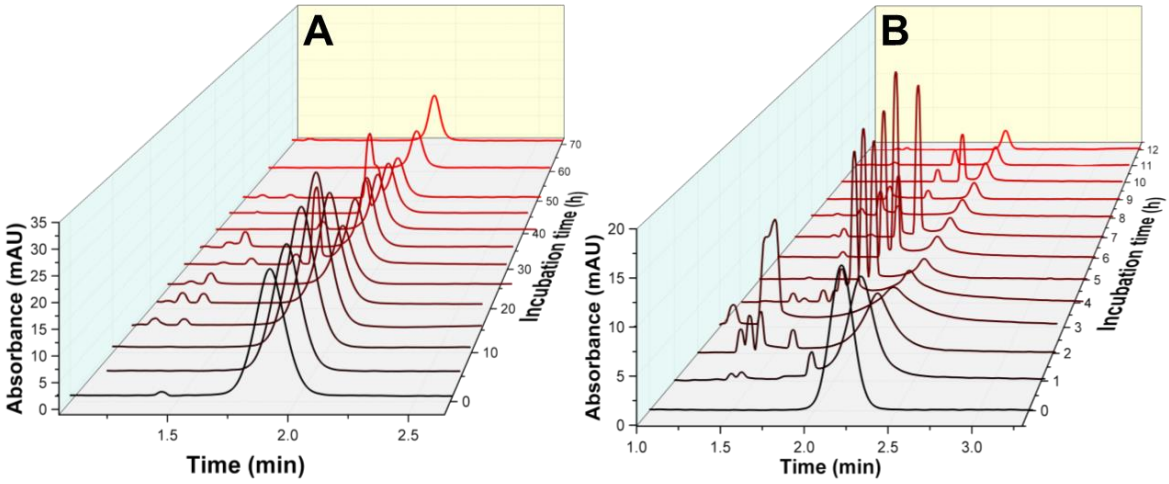

Figure 1. Three-dimensional overview of the obtained taylorgrams during the aggregation process of Aβ(1-40) (A) and Aβ(1-42) (B) at different incubation times. Experimental conditions: sample: 100 µM; 20 mM phosphate buffer, pH 7.4. Incubation: quiescent conditions at 37 °C. Fused silica capillaries: 50 µm i.d. × 40 cm × 31.5 cm. Mobile phase: 20 mM phosphate buffer, pH 7.4. Mobilization pressure: 100 mbar. Injection: 44 mbar for 3 s, Vi ≈ 7nL (Vi/Vd ≈ 1%). Analyses were performed at 37 °C. UV detection at 191 nm.

The peptides were incubated at 37 °C in a 20 mM phosphate buffer at pH 7.4. The aggregation was followed for 72 and 12.5 h for Aβ(1-40) and Aβ(1-42), respectively. Figure 1 shows the taylorgrams recorded at selected incubation times for Aβ(1-40) (Figure 1A) and Aβ(1-42) (Figure 1B) while all experimental taylorgrams, for all incubation times tag, are shown in Figures SI.4 and SI.5. Importantly, the elution profile evolved faster in the case of Aβ(1-42) as compared to Aβ(1-40), suggesting a faster aggregation kinetics for this peptide. A second observation is that, for both studied peptides, the main peak observed at an elution time of $t_0 \approx 2$ min, which represents the Aβ monomer at $t_{ag} = 0$, tended to broaden and to decrease in intensity during the aggregation process. This indicates the appearance of larger species and the decrease in the concentration of the soluble species in the sample. At the end of the aggregation experiment, only a small sharp peak was observed (with a size corresponding to a small molecule/ion of about 0.4 nm, smaller than the size of the peptide monomer ~1.8 nm), indicating the disappearance of the soluble peptides, probably transformed into insoluble and larger aggregates that were not entering in the capillary, leading to the decrease in the peak area. At intermediate incubation times (e.g., t_{ag} between 0.5 and ~11 h for Aβ(1-42)) the left side of the elution profile displayed spikes (very sharp peaks appearing before the main elution peak at elution times between 0.9 and 1.7 min), demonstrating the presence of very large species that are out of the Taylor regime[50,51] and rather belong to the so-called

convective regime. In addition to the convective regime[50], large aggregates such as Aβ fibrils can also generate spikes, as seen in capillary electrophoresis and/or the hydrodynamic flow of bacterial aggregates[52].

In general, the obtained elution profiles were not Gaussian meaning that the sample was polydisperse in size. All taylorgrams were fitted on the basis of the right-side elution profile (i.e., $t > t_0$, with t_0 the peak time) to get rid of the spikes that are present on the left side. The deconvolution of the right side of the taylorgram provides valuable information on the aggregation process. Indeed, a complex mixture of components was obtained, composed of varying proportions of the Aβ monomer, intermediate oligomers (R_h lower than 50 nm), protofibrils (R_h between 50 and 150 nm), small molecules (salts, counterions, etc.), and fibrils/insoluble aggregates (typical dimensions having an average diameter of ~7−10 nm and lengths up to several micrometers were reported for fibrils,[53−55] they are detected as spikes on the taylorgrams). Except for the fibrils and other insoluble aggregates, all components in the mixture could be sized and quantified by TDA. For that, all of the elution profiles were deconvoluted using two different approaches to extract the size and proportion of the different populations. A first fitting approach consisted in using a finite number of Gaussian curves (n =1− 4). The second fitting approach used the constrained regularized linear inversion (CRLI) algorithm, which does not require any hypothesis on the number of populations and allows obtaining a continuous distribution of the diffusion coefficient or of the hydrodynamic radius[56].

Figure SI.6 shows two typical examples of deconvolution of a TDA profile for Aβ(1-40) (Figure SI.6A) and Aβ(1-42) (Figure SI.6B), at selected incubation times t_{ag} = 25.52 h and t_{ag} = 1.98 h, respectively. In these examples, four Gaussian functions were used to fit the elution profile, with low residues for the curve fitting on the right side of the profile (see the upper part of each figure). When a lower number of Gaussian functions ($n \leq 3$) was used, the residues were much higher (see Figure SI.7). It is worth noting that a constraint was added to the fitting procedure on the value of the peak variance of the monomer population, allowing it to vary within 5% with respect to that at t_{ag} = 0 h (initial size of the monomers). Figures SI.8 and SI.9 show the Gaussian peaks extracted from the 4-Gaussian fit for the four populations and for both peptides, together with their respective areas as a function of the incubation time.

II.3.3. Monitoring Aβ(1-40) and Aβ(1-42) aggregation by TDA

Figure 2 shows the monitoring of Aβ(1-40) (Figure 2A) or Aβ(1-42) (Figure 2B) aggregation using the aforementioned data processing. The lower panels of Figure 2 represent the evolution of the peak area of each population (proportional to its mass abundance), while the middle and upper panels represent the evolution in the size (R_h) of these populations.

The populations were classified by size into four groups. In the first group, some small molecules (R_h = 0.3−0.4 nm) were detected (blue down triangles). Their sizes, as well as their abundance (peak area), were constant throughout the aggregation, and their presence seems, therefore, not related to the aggregation process. The second population (red boxes) had a size of 1.99 ± 0.09 nm for Aβ(1-40) and 1.94 ± 0.12 nm for Aβ(1-42) and was attributed to the monomeric and small oligomeric forms of the peptides (up to dodecamers, see the next section). The third population was attributed to higher molar mass oligomers with R_h between 4 and 50 nm. The average size of this population over the whole aggregation process was 24.9 ± 10.3 nm for Aβ(1-40) and 10.8 ± 6.1 nm for Aβ(1-42). The fourth population with R_h > 50 nm was attributed to soluble protofibrillar structures with an average size of 119 ± 49 nm for Aβ(1-40) and 110 ± 39 nm for Aβ(1-42).

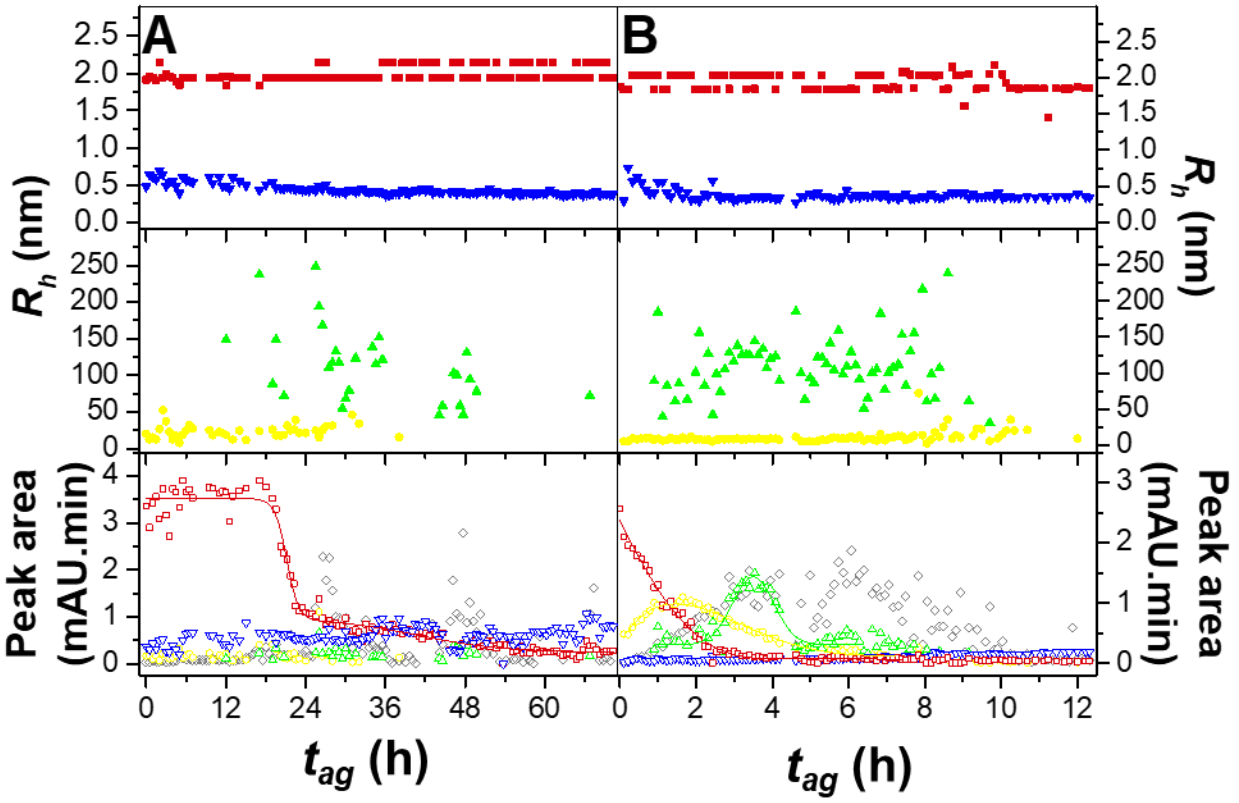

Figure 2. Hydrodynamic radius and peak area evolution of the different populations observed during the aggregation process of Aβ(1-40) (A) and Aβ(1-42) (B) using a 4-Gaussian fitting of the taylorgrams. Closed symbols are for the hydrodynamic radius: small molecules (blue triangle down solid), monomer and low molar mass oligomers (red box solid), higher molar mass oligomers (yellow circle solid), and soluble protofibrils (green triangle up solid). Open symbols correspond to the peak area of each species: small molecules (blue triangle down open), monomers and low molar mass oligomers (red box), higher molar mass oligomers (yellow circle open), soluble protofibrils (green triangle up open), and fibrils (gray diamond open) (spikes). The straight lines are guides for the eyes. Experimental conditions as in Figure 1.

For Aβ(1-40), only the monomeric and low molar mass oligomer populations were significantly present in the sample (see open red boxes in Figure 2A), as compared to the high molar mass oligomers and protofibril populations (open yellow circles and open green triangles, respectively), which were much less abundant. The red traces in Figure 2A showed that Aβ(1-40) was essentially in its monomeric form and remained so up to tag ~ 18 h. Afterward, the peak area of the monomeric population rapidly dropped to reach a lower plateau at tag ~ 24 h. It is important to note that despite the disappearance of the monomeric form, no other soluble species yielded a significant signal in TDA. Indeed, the aggregation of Aβ(1-40) displayed a threshold-type behavior, which indicates that the rate-determining step for aggregation is the formation of multimeric seeds. In other words, our results seem to indicate that Aβ(1-40) goes through a secondary nucleation mechanism where monomers add to already present fibrils to elongate them

and to produce larger fibrils, without going through intermediate species in accordance with what is discussed in the literature[57,58]. To confirm this hypothesis, a slight manual shaking of the vial was done at 25, 48, and 70 h, to resuspend any precipitate/fibrils that may have sedimented. After each remixing, a significant increase of the peak area of the "spikes" (gray open diamonds in the lower part of Figure 2A) was transiently observed, proving the presence of insoluble species in the sample that suspend upon shaking and then tend to decant.

The aggregation process for Aβ(1-42) displayed a different pathway as compared to that of Aβ(1-40). For Aβ(1-42) the proportion of monomeric and low molar mass oligomeric populations decreased rapidly, while the higher molar mass oligomeric species increased to reach a maximum at t_{ag} = 1.6 h, after the disappearance of the monomeric species. Subsequently, the protofibrils proportion increased to reach a maximum at t_{ag} = 3.5 h, and finally, the spikes (nondiffusing species in suspension) increased to reach a maximum at t_{ag} = 5.6 h. From these observations, it is evident that TDA experiments give a clear picture of the early stages of the aggregation process of Aβ(1-42) that goes through primary nucleation leading to intermediate species and successively an elongation step producing protofibrils and then fibrils.

The results for Aβ(1-40) and Aβ(1-42) obtained by fitting the taylorgram to n-Gaussians were compared to the evolution of the R_h distributions obtained by CRLI[56], as shown in the Supporting Information (Figures SI.10−SI.13). Continuous distributions of the hydrodynamic radius for each run (Figures SI.10 and SI.11) were obtained by the CRLI algorithm, allowing for a full and quantitative characterization of the aggregation process. The CRLI analysis confirmed the two different pathways that were inferred for the aggregation of Aβ(1-40) and Aβ(1-42) on the basis of the *n*-Gaussians fits.

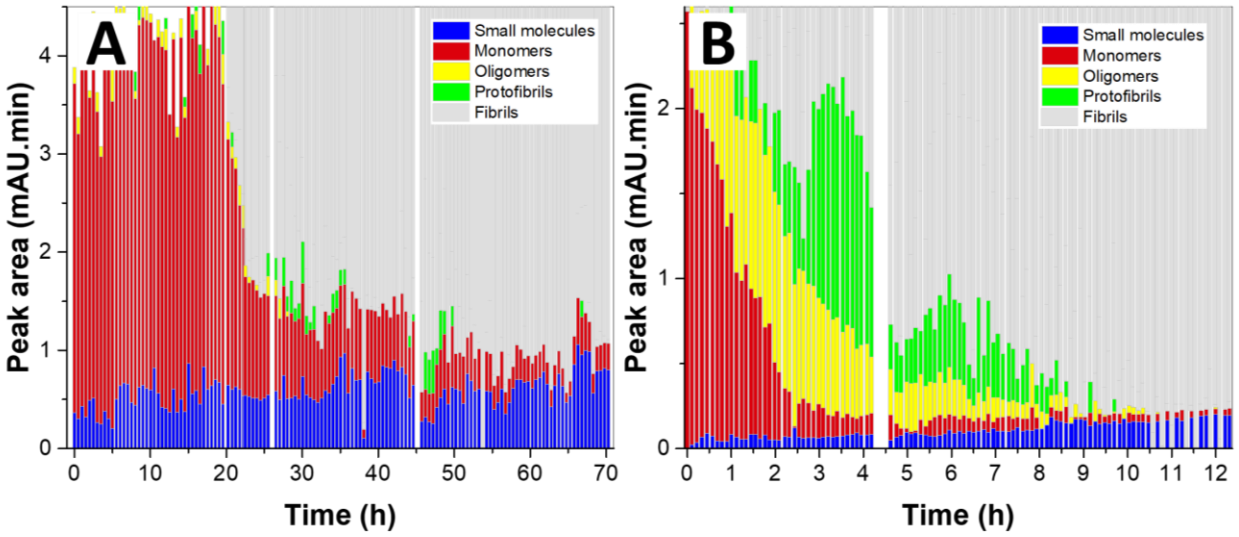

Figure 3. Stacked bar graphs showing the speciation of Aβ(1-40) (A) and Aβ(1-42) (B) at each analyzed incubation time obtained by TDA. Experimental conditions as in **Figure 1**. Four populations are distinguished: "small molecules" for R_h ~ 0.4 nm; "monomers" for the monomer and the low molar mass oligomers with R_h ~ 1.9 nm; "oligomers" for high molar mass oligomers with R_h between 4 and 50 nm; and "protofibrils" for large diffusion soluble species with R_h between 50 and 150 nm. Each population is represented by the corresponding peak area obtained by 4-Gaussian curve fitting. The population in gray represents the fibrils that are not quantified by TDA and are just represented by the difference.

Another way to qualitatively and visually assess the entire aggregation process and the speciation of the amyloid peptides during the aggregation process is shown in Figure 3, which displays a stacked bar representation of the peak area of each population. The gray region represents the insoluble species that can enter the capillary and appear as spikes as well as those that precipitate and no longer enter into the capillary at the injection step, lowering the total observed peak area over the incubation time. From this figure, one can clearly distinguish the two different aggregation pathways[32,59].

To confirm these observations, the ThT assay was realized in the same conditions as the TDA analysis. The ThT assay is best known to detect the amyloid fibrillary structures, which are formed at the expense of the soluble ones causing a decrease in their proportion. As seen in Figure SI.14, the ThT assay curve superimposes on the concentration evolution of the insoluble species determined by TDA, demonstrating that TDA faithfully captures the lag phase and the time to reach the plateau of the aggregation process. Additionally, TDA allowed for a quantitative estimation of the intermediate steps of the aggregation, especially in the case of Aβ(1-42), a feature difficult to obtain[57] with other techniques such as SEC[25].

II.3.4. Discussion on the size of the Aβ species during the aggregation process

Regarding the size of the aggregated forms, it was suggested from combined results obtained by NMR, Fourier transform infrared spectroscopy (FTIR), and AFM, that Aβ(1-42) rapidly forms low molar mass oligomers upon solubilization[60]. The predominant forms ranged from dimers to dodecamers[59,61] including some assemblies (from tetramers to octamers) called "paranuclei" [32], which were in equilibrium with the lower molar mass oligomers. Several methods were used in the literature to identify the nature of these oligomers. Ion mobility MS allows us to get the structural information relative to the oligomeric molar mass distribution[29]; however, the separation is obtained in the gas phase, which can perturb the oligomeric distribution. Further, an ion suppression effect may also occur for quantitative analysis in complex mixtures[62]. Real-time aggregation monitoring methods such as dynamic light scattering (DLS) are very difficult to apply to detect the presence of small oligomers in polydisperse samples, especially in the presence of large aggregates. TDA has the advantage of being less sensitive to the presence of very large aggregates[36,63] allowing the detection of the early stage species, without bias in the mass-weighted size distribution. For the sake of comparison, DLS experiments were realized on the Aβ(1-42) sample in the same conditions as in TDA. From the obtained size distributions, $P_M(R_h)$, we integrated over four intervals, so as to obtain the mass-weighted relative contribution of four classes of aggregates, with $R_h < 5$ nm, 5 nm $< R_h <$ 50 nm, 50 nm $< R_h <$ 500 nm, and $R_h > 500$ nm, respectively (see Materials and Methods for details).

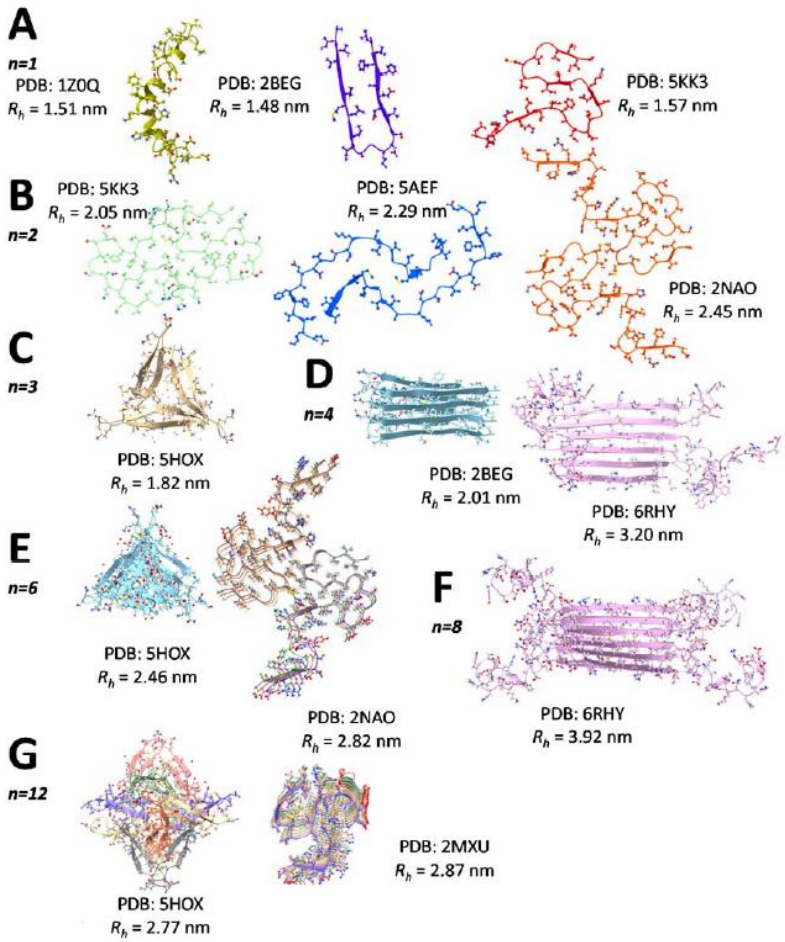

Figure 4. Schematic representation of the monomeric Aβ(1-42)(A) and small-oligomer conformations from dimmers to dodecamers (B−G represent dimers, trimers, tetramers, hexamers, octamers, and dodecamers, respectively). The 3D structures were realized using the UCSF ChimeraX software [67] and were adapted from the structure found in the literature (PDB codes 1Z0Q,[64] 2BEG,[68] and 5KK3[66]). The arrangement of the monomers in the oligomeric form was adapted from the literature (PDB codes 5AEF,[69] 2NAO,[70] 5HOX,[71] 6RHY,[72] and 2MXU[73]). The R_h values were calculated by introducing the generated PDB files for each structure into the HYDROPRO software.[48] It is worth noting that the R_h calculation takes into account all possible orientations of the molecular structure relative to the flow direction.

Figure SI.15 shows the time evolution of the (mass-weighted) fractions of the four classes of aggregates thus obtained. The data shown in the figure correspond to the average of results obtained by processing separately data collected at scattering angles θ = 90 and 45°; x and y error bars indicate the half-difference between the corresponding pairs of data at 90 and 45°. In contrast to TDA results, dimers and small oligomers, corresponding to R_h < 5 nm, are not detected by DLS, because their scattered intensity is much weaker than that of larger species. On the other hand, DLS detects large aggregates, including objects up to several hundred nm, which are beyond the range accessible to TDA. Aggregates with R_h > 500 nm are detected as early as at t_{ag} = 500 s. Their

relative contribution increases significantly for tag > 1200 s (0.33 h), at the expenses of both intermediate (50 nm < R_h < 500 nm) and smaller (5 nm < R_h < 50 nm) aggregates. These results show that DLS is a powerful technique able to follow in real time the evolution of the larger size species. However, in contrast to TDA, the sensitivity of DLS toward the smaller size species is quite limited. Thus, TDA and DLS are complementary methods.

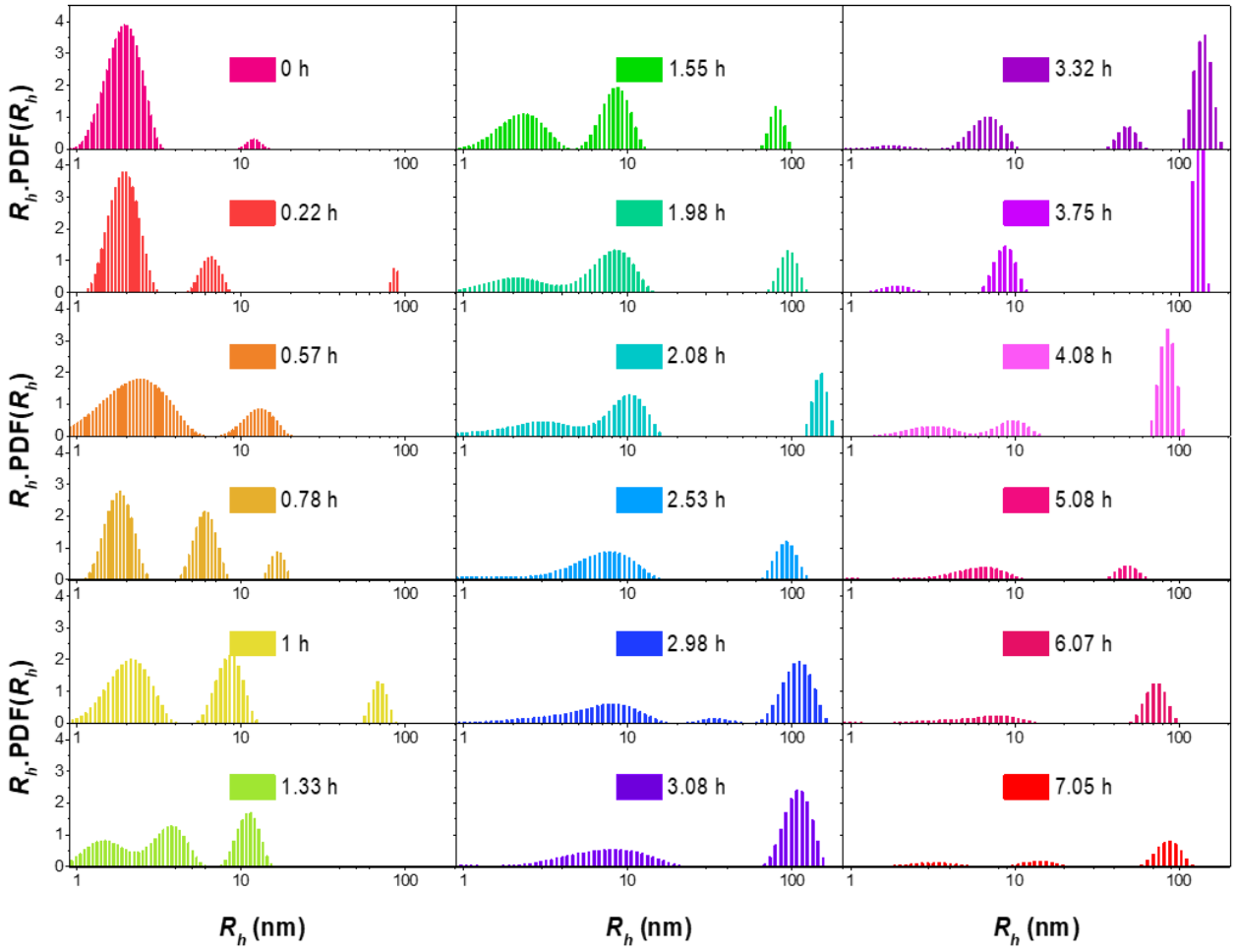

Figure 5. Size distributions of Aβ(1-42) obtained by CRLI analysis of the experimental taylorgrams as a function of the incubation time t_{ag} = 0−7 h. Experimental taylorgrams and conditions as in Figure 1.

To propose possible oligomeric structures that fit with the size of each population found by TDA, molecular simulation was performed based on Aβ(1-42) monomers (folded and unfolded)[64] and oligomer[65,66] structures found in the literature (low and high molar mass, from 2 to 360 monomer units). Different three-dimensional (3D) molecular structures were constructed using UCSF ChimeraX software[67] that were next loaded into HYDROPRO+[48] software to calculate the

hydrodynamic properties. The 3D structures were adjusted so that the calculated translational diffusion coefficients equal the experimental values obtained by TDA for each population. Figures 4 and 6 display possible conformations for small and large oligomers thus obtained.

Different Aβ(1-42) monomer structures were considered, based on the structures published by Tomaselli *et al.*[64] (PDB code 1Z0Q), Lührs *et al.*[68] (PDB code 2BEG), and Colvin *et al.*[66] (PDB code 5KK3). The results show hydrodynamic radii around 1.5 nm for the different conformations (see Figure 4, monomer structures). The average hydrodynamic radii of the "monomer and small oligomers" population obtained by TDA on all runs over the whole Aβ(1-42) aggregation study (t_{ag} = 12.5 h, n = 110 TDA runs) was 1.94 nm (relative standard deviation (RSD) = 5.9%) and the initial size at t_{ag} = 0 h was 1.84 nm. To correlate the observed experimental size with oligomeric structures, different proposed oligomeric structures from the literature, ranging from dimers to dodecamers with different conformations were used and computed to get the hydrodynamic radii (Figure 4) (PDB codes 5AEF[69], 2NAO[70], 5HOX[71], 6RHY[72], and 2MXU[73]). The latter structures were determined by electron cryo-microscopy[69], solid-state NMR[70,73], X-ray crystallography[71], and NMR.[72] The combination of our results and those from the literature suggest that the monomer and small oligomers population at t_{ag} = 0 h was mainly composed of monomers and dimers[74]. The weight-average R_h obtained by TDA is sensitive to the mass proportion of all of the soluble species present in the mixture. The CRLI analysis brings additional information about the polydispersity of each population mode (see Figure 5). However, due to the low difference in R_h of the various small species (monomers/dimers/trimers) neither the CRLI nor the Gaussian fitting approaches were able to resolve these small species. CRLI shows that the size distribution of the monomer and small oligomers population at t_{ag} = 0 h ranges between 1 and 3 nm and is centered around 1.9 nm. The polydispersity in size of this mode increases with increasing incubation times. This population becomes negligible after t_{ag} ~ 2−4 h. Several reports[75–77] suggested the presence of a critical nucleus size, which is the minimum size that enables the extension of amyloid fibrils. To our knowledge, no consensus was reached on the exact size of the nuclei, while other reports stated that the nucleation was heterogeneous.[78,79] However, aggregation numbers between 2 and 14 were reported[75–77,80,81], which according to this work would correspond to a size distribution between 1.8 and ~3 nm, and thus the first oligomer size population found by TDA.

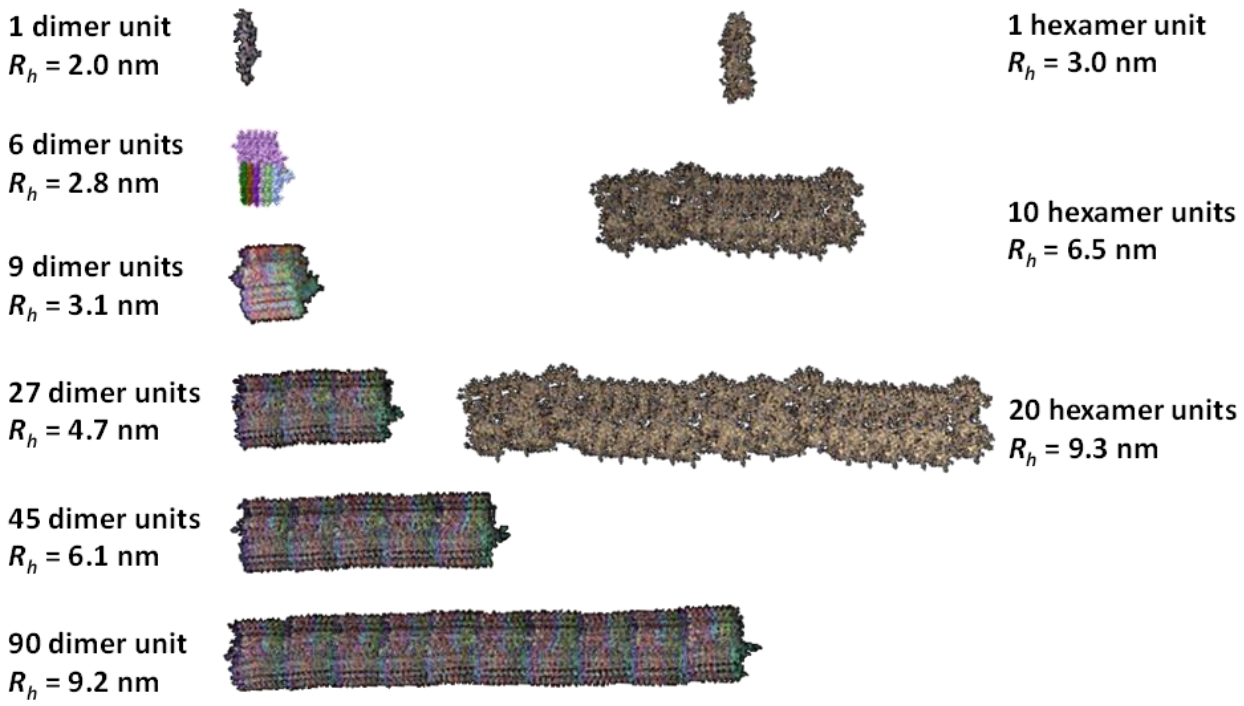

Figure 6. Schematic side view representation of possible conformations for the "high molar mass oligomeric Aβ(1-42)" population. The arrangement of the monomers in the oligomeric form was based on the structures described by Colvin *et al.*[66] and in Tran *et al.*[65].The 3D structures were realized using UCSF ChimeraX software[67] and were adapted from the structure published in ref [64] (PDB code 1Z0Q) for the hexameric structures and in ref [66] (PDB code 5KK3) for the dimeric structures. The Rh values were calculated by introducing the generated PDB files for each structure into HYDROPRO software[48]. The dimer, the hexamer, the dodecamer, and the octadecamer, which size is lower than 4 nm, are represented for the sake of comparison.

To identify the structure beneath the distribution of the "high molar mass oligomer" population, the same approach was applied by constructing 3D models and calculating their hydrodynamic radii. In fact, several NMR[66,70] or cryo-EM[82] studies have shown that the fibril core of Aβ(1-42) consisted of a dimer, each monomer containing four β-strands in an S-shaped amyloid fold arrangement (Figure SI.16). On these grounds, protofibrillar and fibrillar structures were constructed, using the PDB file code 5KK3,[66] to get structures having a parallel superposition of dimers and ranging from 1 dimer unit (disc shaped with a width of ~6.4 nm and a length of ~0.9 nm) up to 720 dimer units (cylinder shaped with a width of ~6.4 nm and a length of ~345 nm). The calculated size for the constructed oligomers is given in Table SI.1 and in Figure 6. From the TDA analysis, the minimum size calculated for the high molar mass oligomer distribution based on the results obtained on the simulated structures in Figure 6 was 5.1 nm and corresponded to an oligomer having 33 dimer units (~300 kDa) and dimensions of 17 nm in length and 3.2 nm in radius. The maximum size was 36 nm corresponding to ~700 dimer units (~6300 kDa) and

dimensions of ~335 nm in length and 3.2 nm in radius. Further, over the whole aggregation process (110 TDA runs), the average size was 10.7 nm corresponding to a cylinder-shaped oligomer having ~115 dimer units (~1035 kDa) with a 57 nm length and a 3.2 nm radius. The CRLI analysis on the TDA runs of Aβ(1-42) aggregation (Figure 5) showed that the high molar mass oligomer population, centered around 10 nm, was present at t_{ag} =0 h at a very low concentration as compared to that of the monomer and small oligomers population. These observations are in agreement with data obtained on Aβ(1-42) by fluorescence correlation spectroscopy (FCS) where stable micelle-like oligomers with a size of $R_h \approx 7-11$ nm and having 28−88 mers were observed.[83] The abundance of this population then increased with the incubation time to reach a maximum at 2h, and finally became negligible after about 7 h.

Further, both the deconvolution using *n* Gaussian functions and the CRLI analysis showed that a larger-sized population, appeared after 1 h and reached a maximum at 3 h, and then became negligible after 7 h. We attributed this population to protofibrils since they are still soluble. Indeed, TDA has shown that this population had a size (R_h) ranging between 50 and 240 nm with an average value of 113 nm over the whole aggregation process (n = 110 TDA runs). If the same calculations were naively applied as done for the high molar mass oligomers, structures having a length between 500 nm and up to 8.5 μm would be obtained, with an average length around 2.2 μm. The number of dimer units in these estimated elongated structures would range between 1200 and 18000 (average of 4650) (with a molar mass per unit length of about 19 kDa/nm). Nevertheless, one should keep in mind that TDA cannot give reliable information about the shape of these assemblies, only the R_h distribution is obtained. Other techniques such as AFM would be more suited for looking at the molecular structure.[84,85] Despite this limitation, which is common to all methods based on the determination of the diffusion coefficient (or R_h), the present work demonstrates that TDA in combination with molecular simulations can rapidly and advantageously propose a limited number of possible molecular conformations that are consistent with the experimental data.

Finally, reports from the literature found that toxic Aβ oligomers had a molar mass higher than 50 kDa[86,87], which corresponded to oligomers having more than ~11 monomer units. One of the most toxic reported oligomers was identified to be Aβ*56 (56 kDa)[88] corresponding to a dodecamer. Based on the calculations described in this work, a dodecamer would have an R_h around 2.8 nm, if it is formed by the superposition of dimers or of monomers (as depicted in ref

[73]). The size of the dodecamer would increase to 3.4 nm if constituted by the superposition of two hexamers. According to another report[10], the toxicity of Aβ(1-42) oligomers decreases with increasing size, and toxic oligomers are likely in the range of 8−24-mers, having an R_h between 3 and 4.2 nm, as calculated in this work. From the CRLI analysis in Figure 5, this fraction of potentially toxic oligomers appears after 30 min and then tends to decrease in proportion with the aggregation time as the oligomer size increases.

II.4. Conclusions

This work demonstrates that TDA can be used for the straightforward monitoring of the aggregation of Aβ amyloid peptides. Further, using an appropriate data treatment of the taylorgrams, one can assess the aggregation pathway by obtaining quantitative data on the proportion and the size of the different aggregated forms. To our knowledge, there is no other real-time aggregation monitoring method reported in the literature allowing us to obtain such information in one single analysis. It is worth noting that a low volume was used for each aggregation study (total volume of 1 µL of a 100 µM peptide solution) with an unprecedented large number of data points during the aggregation process (about 10 points/h) leading to a large amount of valuable data.

The results obtained in this work tend to confirm the aggregation pathway of Aβ(1-40) which goes from the monomeric state directly to a fibrillary structure, in contrast to Aβ(1-42), which goes through different intermediate states (oligomers and protofibrils) before reaching the fibrils, in agreement with previous works.[58,60] In addition, TDA data gave new insights for the identification of the formed oligomers in the early stages of the aggregation process, including the characterization of the size and abundance evolution of disease-relevant amyloid peptides in solution. The strength of the data processing described in this work lies in its ability to distinguish the small, potentially toxic oligomers in a polydisperse mixture of larger oligomers, protofibrils, and fibrils. In the future, it will be interesting to investigate experimental conditions mimicking the in vivo environment, such as lower concentrations of the peptides (in the 100 nM range), mixtures of different amyloid peptides, and the physicochemical properties (ionic strength, pH, and composition) mimicking the cerebrospinal fluid.

ASSOCIATED CONTENT (SI) *Supporting Information

The Supporting Information is available free of charge at https://pubs.acs.org/doi/10.1021/acs.analchem.1c00527. Experimental procedure for the synthesis; theoretical aspects and data processing of TDA; raw TDA data; ThT assay results; DLS results; and modelization data (PDF).

AUTHOR INFORMATION

Corresponding Authors

Hervé Cottet − IBMM, ENSCM, Université Montpellier, CNRS, 34095 Montpellier, France; orcid.org/0000-0002-6876-175X; Phone: +33 4 6714 3427; Email: herve.cottet@umontpellier.fr; Fax: +33 4 67631046;

Joseph Chamieh − IBMM, ENSCM, Université Montpellier, CNRS, 34095 Montpellier, France; orcid.org/0000-0003-4209-1337; Phone: +33 4 6714 3920; Email: joseph.chamieh@umontpellier.fr; Fax: +33 4 67631046.

Authors

Mihai Deleanu − IBMM, ENSCM, Université Montpellier, CNRS, 34095 Montpellier, France.

Jean-François Hernandez − IBMM, ENSCM, Université Montpellier, CNRS, 34095 Montpellier, France.

Luca Cipelletti − Laboratoire Charles Coulomb (L2C), Université Montpellier, CNRS, 34095 Montpellier, France; Institut Universitaire de France (IUF), France; orcid.org/0000-0003-2956-7580.

Jean-Philippe Biron − IBMM, ENSCM, Université Montpellier, CNRS, 34095 Montpellier, France.

Emilie Rossi − Université Paris-Saclay, CNRS, Institut Galien Paris-Saclay, 92296 Châtenay-Malabry, France.

Myriam Taverna − Université Paris-Saclay, CNRS, Institut Galien Paris-Saclay, 92296 Châtenay-Malabry, France; Institut Universitaire de France (IUF), France; orcid.org/0000-0002-3656-8293.

Complete contact information is available at:
https://pubs.acs.org/10.1021/acs.analchem.1c00527

NOTES

The authors declare no competing financial interest.

ACKNOWLEDGMENTS

L.C. and M.T. gratefully acknowledge support from the Institut Universitaire de France (IUF).

II.5. References

1. *2019 Alzheimer's disease facts and figures*. *Alzheimer's Dement.* **15,** (2019).
2. Folch, J., Ettcheto, M., Petrov, D., Abad, S., Pedrós, I., Marin, M., Olloquequi, J. & Camins, A. Review of the advances in treatment for Alzheimer disease: strategies for combating β-amyloid protein. *Neurol. (English Ed.* **33,** 47–58 (2018).
3. Hardy, J. A. & Higgins, G. A. Alzheimer's disease: The amyloid cascade hypothesis. *Science (80-.).* **256,** 184–185 (1992).
4. Liu, P. P., Xie, Y., Meng, X. Y. & Kang, J. S. History and progress of hypotheses and clinical trials for alzheimer's disease. *Signal Transduct. Target. Ther.* **4,** (2019).
5. Forloni, G. & Balducci, C. Alzheimer's Disease, Oligomers, and Inflammation. *J. Alzheimer's Dis.* **62,** 1261–1276 (2018).
6. Heppner, F. L., Ransohoff, R. M. & Becher, B. Immune attack: The role of inflammation in Alzheimer disease. *Nat. Rev. Neurosci.* **16,** 358–372 (2015).
7. Terry, R. D. The pathogenesis of Alzheimer disease: An alternative to the amyloid hypothesis. *J. Neuropathol. Exp. Neurol.* **55,** 1023–1025 (1996).
8. Hayden, E. Y. & Teplow, D. B. Amyloid β-protein oligomers and Alzheimer's disease. *Alzheimer's Res. Ther.* **5,** (2013).
9. Selkoe, D. J. & Hardy, J. The amyloid hypothesis of Alzheimer's disease at 25 years. *EMBO Mol. Med.* **8,** 595–608 (2016).
10. Sengupta, U., Nilson, A. N. & Kayed, R. The Role of Amyloid-β Oligomers in Toxicity, Propagation, and Immunotherapy. *EBioMedicine* **6,** 42–49 (2016).
11. Lambert, M. P., Barlow, A. K., Chromy, B. A., Edwards, C., Freed, R., Liosatos, M., Morgan, T. E., Rozovsky, I., Trommer, B., Viola, K. L., Wals, P., Zhang, C., Finch, C. E., Krafft, G. A. & Klein, W. L. Diffusible, nonfibrillar ligands derived from Aβ1-42 are potent central nervous system neurotoxins. *Proc. Natl. Acad. Sci. U. S. A.* **95,** 6448–6453 (1998).
12. Mastroeni, D., Nolz, J., Khdour, O. M., Sekar, S., Delvaux, E., Cuyugan, L., Liang, W. S., Hecht, S. M. & Coleman, P. D. Oligomeric amyloid β preferentially targets neuronal and not glial mitochondrial-encoded mRNAs. *Alzheimer's Dement.* **14,** 775–786 (2018).
13. Walsh, D. M., Klyubin, I., Fadeeva, J. V., Cullen, W. K., Anwyl, R., Wolfe, M. S., Rowan, M. J. & Selkoe, D. J. Naturally secreted oligomers of amyloid β protein potently inhibit hippocampal long-term potentiation in vivo. *Nature* **416,** 535–539 (2002).
14. Salazar, S. V. & Strittmatter, S. M. Cellular prion protein as a receptor for amyloid-β oligomers in Alzheimer's disease. *Biochem. Biophys. Res. Commun.* **483,** 1143–1147 (2017).
15. König, A. S., Rösener, N. S., Gremer, L., Tusche, M., Flender, D., Reinartz, E., Hoyer,

W., Neudecker, P., Willbold, D. & Heise, H. Structural details of amyloid β oligomers in complex with human prion protein as revealed by solid-state MAS NMR spectroscopy. *J. Biol. Chem.* **296,** (2021).

16. Guerrero-Muñoz, M. J., Castillo-Carranza, D. L., Sengupta, U., White, M. A. & Kayed, R. Design of metastable β-sheet oligomers from natively unstructured peptide. *ACS Chem. Neurosci.* **4,** 1520–1523 (2013).

17. Bemporad, F., Calloni, G., Campioni, S., Plakoutsi, G., Taddei, N. & Chiti, F. Sequence and structural determinants of amyloid fibril formation. *Acc. Chem. Res.* **39,** 620–627 (2006).

18. Ghosh, P., Kumar, A., Datta, B. & Rangachari, V. Dynamics of protofibril elongation and association involved in Aβ42 peptide aggregation in Alzheimer's disease. in *BMC Bioinformatics* **11,** (2010).

19. Jeong, J. S., Ansaloni, A., Mezzenga, R., Lashuel, H. A. & Dietler, G. Novel mechanistic insight into the molecular basis of amyloid polymorphism and secondary nucleation during amyloid formation. *J. Mol. Biol.* **425,** 1765–1781 (2013).

20. Petkova, A. T., Leapman, R. D., Guo, Z., Yau, W. M., Mattson, M. P. & Tycko, R. Self-propagating, molecular-level polymorphism in Alzheimer's β-amyloid fibrils. *Science (80-.).* **307,** 262–265 (2005).

21. Watanabe-Nakayama, T., Ono, K., Itami, M., Takahashi, R., Teplow, D. B. & Yamada, M. High-speed atomic force microscopy reveals structural dynamics of amyloid β1-42 aggregates. *Proc. Natl. Acad. Sci. U. S. A.* **113,** 5835–5840 (2016).

22. PS, V. & CULLING, C. Fluorescent stains, with special reference to amyloid and connective tissues. *Arch. Pathol.* **68,** 487–498 (1959).

23. Bieschke, J., Zhang, Q., Powers, E. T., Lerner, R. A. & Kelly, J. W. Oxidative metabolites accelerate Alzheimer's amyloidogenesis by a two-step mechanism, eliminating the requirement for nucleation. *Biochemistry* **44,** 4977–4983 (2005).

24. Yang, T., Li, S., Xu, H., Walsh, D. M. & Selkoe, D. J. Large soluble oligomers of amyloid β-protein from alzheimer brain are far less neuroactive than the smaller oligomers to which they dissociate. *J. Neurosci.* **37,** 152–163 (2017).

25. Michaels, T. C. T., Šarić, A., Curk, S., Bernfur, K., Arosio, P., Meisl, G., Dear, A. J., Cohen, S. I. A., Dobson, C. M., Vendruscolo, M., Linse, S. & Knowles, T. P. J. Dynamics of oligomer populations formed during the aggregation of Alzheimer's Aβ42 peptide. *Nat. Chem.* **12,** 445–451 (2020).

26. Rosensweig, C., Ono, K., Murakami, K., Lowenstein, D. K., Bitan, G. & Teplow, D. B. Preparation of stable Amyloid β-protein oligomers of defined assembly order. *Methods Mol. Biol.* **849,** 23–31 (2012).

27. Zhou, Y., Liu, J., Zheng, T. & Tian, Y. Label-Free SERS Strategy for in Situ Monitoring and Real-Time Imaging of Aβ Aggregation Process in Live Neurons and Brain Tissues. *Anal. Chem.* **92,** 5910–5920 (2020).

28. Brinet, D., Kaffy, J., Oukacine, F., Glumm, S., Ongeri, S. & Taverna, M. An improved capillary electrophoresis method for in vitro monitoring of the challenging early steps of Aβ(1-42) peptide oligomerization: Application to anti-Alzheimer's drug discovery. *Electrophoresis* **35,** 3302–3309 (2014).

29. Kaffy, J., Piarulli, U., Fanelli, R., Vahdati, L., Lequin, O., Ongeri, S., Taverna, M., Bernadat, G., Brinet, D., Panzeri, S. & Correia, I. Synthesis and Characterization of Hairpin Mimics that Modulate the Early Oligomerization and Fibrillization of Amyloid β-Peptide. *European J. Org. Chem.* **2017,** 2971–2980 (2017).

30. Ionuţ Iuraşcu, M., Cozma, C., Tomczyk, N., Rontree, J., Desor, M., Drescher, M. & Przybylski, M. Structural characterization of β-amyloid oligomer-aggregates by ion mobility mass spectrometry and electron spin resonance spectroscopy. *Anal. Bioanal. Chem.* **395,** 2509–2519 (2009).

31. Hu, J. & Zheng, Q. Applications of Mass Spectrometry in the Onset of Amyloid Fibril Formation: Focus on the Analysis of Early-Stage Oligomers. *Front. Chem.* **8,** (2020).

32. Teplow, D. B., Bitan, G., Lomakin, A., Benedek, G. B., Kirkitadze, M. D. & Vollers, S. S. Amyloid -protein (A) assembly: A 40 and A 42 oligomerize through distinct pathways. *Proc. Natl. Acad. Sci.* **100,** 330–335 (2003).

33. Chamieh, J. & Cottet, H. in *Colloid Interface Sci. Pharm. Res. Dev.* 173–192 (2014). doi:10.1016/B978-0-444-62614-1.00009-0

34. Taylor, G. Conditions under which dispersion of a solute in a stream of solvent can be used to measure molecular diffusion. *Proc. R. Soc. London. Ser. A. Math. Phys. Sci.* **225,** 473–477 (1954).

35. Taylor, G. Dispersion of soluble matter in solvent flowing slowly through a tube. *Proc. R. Soc. London. Ser. A. Math. Phys. Sci.* **219,** 186–203 (1953).

36. Cottet, H., Biron, J. P. & Martin, M. Taylor dispersion analysis of mixtures. *Anal. Chem.* **79,** 9066–9073 (2007).

37. Bello, M. S., Rezzonico, R. & Righetti, P. G. Use of Taylor-Aris dispersion for measurement of a solute diffusion coefficient in thin capillaries. *Science (80-.).* **266,** 773–776 (1994).

38. Sharma, U., Gleason, N. J. & Carbeck, J. D. Diffusivity of solutes measured in glass capillaries using Taylor's analysis of dispersion and a commercial CE instrument. *Anal. Chem.* **77,** 806–813 (2005).

39. Cottet, H., Martin, M., Papillaud, A., Souaïd, E., Collet, H. & Commeyras, A. Determination of dendrigraft poly-L-lysine diffusion coefficients by Taylor dispersion analysis. *Biomacromolecules* **8,** 3235–3243 (2007).

40. d'Orlyé, F., Varenne, A. & Gareil, P. Determination of nanoparticle diffusion coefficients by Taylor dispersion analysis using a capillary electrophoresis instrument. *J. Chromatogr. A* **1204,** 226–232 (2008).

41. Chamieh, J., Merdassi, H., Rossi, J. C., Jannin, V., Demarne, F. & Cottet, H. Size characterization of lipid-based self-emulsifying pharmaceutical excipients during lipolysis using Taylor dispersion analysis with fluorescence detection. *Int. J. Pharm.* **537,** 94–101 (2018).

42. Urban, D. A., Milosevic, A. M., Bossert, D., Crippa, F., Moore, T. L., Geers, C., Balog, S., Rothen-Rutishauser, B. & Petri-Fink, A. Taylor Dispersion of Inorganic Nanoparticles and Comparison to Dynamic Light Scattering and Transmission Electron Microscopy. *Colloids Interface Sci. Commun.* **22,** 29–33 (2018).

43. Pedersen, M. E., Østergaard, J. & Jensen, H. Flow-induced dispersion analysis (FIDA) for protein quantification and characterization. *Methods Mol. Biol.* **1972,** 109–123 (2019).

44. Verpillot, R., Otto, M., Klafki, H. & Taverna, M. Simultaneous analysis by capillary electrophoresis of five amyloid peptides as potential biomarkers of Alzheimer's disease. *J. Chromatogr. A* **1214,** 157–164 (2008).

45. Botz, A., Gasparik, V., Devillers, E., Hoffmann, A. R. F., Caillon, L., Chelain, E., Lequin, O., Brigaud, T. & Khemtemourian, L. (R)-α-trifluoromethylalanine containing short peptide in the inhibition of amyloid peptide fibrillation. *Biopolymers* **104,** 601–610 (2015).

46. Provencher, S. W. CONTIN: A general purpose constrained regularization program for inverting noisy linear algebraic and integral equations. *Comput. Phys. Commun.* **27,** 229–242 (1982).

47. Provencher, S. W. A constrained regularization method for inverting data represented by linear algebraic or integral equations. *Comput. Phys. Commun.* **27,** 213–227 (1982).

48. Ortega, A., Amorós, D. & García De La Torre, J. Prediction of hydrodynamic and other solution properties of rigid proteins from atomic- and residue-level models. *Biophys. J.* **101,** 892–898 (2011).

49. Naiki, H., Higuchi, K., Hosokawa, M. & Takeda, T. Fluorometric determination of amyloid fibrils in vitro using the fluorescent dye, thioflavine T. *Anal. Biochem.* **177,** 244–249 (1989).

50. Chamieh, J., Leclercq, L., Martin, M., Slaoui, S., Jensen, H., Østergaard, J. & Cottet, H. Limits in Size of Taylor Dispersion Analysis: Representation of the Different Hydrodynamic Regimes and Application to the Size-Characterization of Cubosomes. *Anal. Chem.* **89,** 13487–13493 (2017).

51. Cottet, H., Biron, J. P. & Martin, M. On the optimization of operating conditions for Taylor dispersion analysis of mixtures. *Analyst* **139,** 3552–3562 (2013).

52. Zheng, J. & Yeung, E. S. Mechanism of microbial aggregation during capillary electrophoresis. *Anal. Chem.* **75,** 818–824 (2003).

53. Schmidt, M., Sachse, C., Richter, W., Xu, C., Fändrich, M. & Grigorieff, N. Comparison of Alzheimer Aβ(1-40) and Aβ(1-42) amyloid fibrils reveals similar protofilament structures. *Proc. Natl. Acad. Sci. U. S. A.* **106,** 19813–19818 (2009).

54. Sachse, C., Fändrich, M. & Grigorieff, N. Paired β-sheet structure of an Aβ(1-40) amyloid fibril revealed by electron microscopy. *Proc. Natl. Acad. Sci. U. S. A.* **105,** 7462–7466 (2008).

55. Yusko, E. C., Prangkio, P., Sept, D., Rollings, R. C., Li, J. & Mayer, M. Single-particle characterization of Aβ oligomers in solution. *ACS Nano* **6,** 5909–5919 (2012).

56. Cipelletti, L., Biron, J. P., Martin, M. & Cottet, H. Measuring Arbitrary Diffusion Coefficient Distributions of Nano-Objects by Taylor Dispersion Analysis. *Anal. Chem.* **87,** 8489–8496 (2015).

57. Arosio, P., Knowles, T. P. J. & Linse, S. On the lag phase in amyloid fibril formation. *Phys. Chem. Chem. Phys.* **17,** 7606–7618 (2015).

58. Chen, Y.-R. & Glabe, C. G. Distinct Early Folding and Aggregation Properties of Alzheimer Amyloid-β Peptides Aβ40 and Aβ42. *J. Biol. Chem.* **281,** 24414–24422 (2006).

59. Economou, N. J., Giammona, M. J., Do, T. D., Zheng, X., Teplow, D. B., Buratto, S. K. & Bowers, M. T. Amyloid β-Protein Assembly and Alzheimer's Disease: Dodecamers of Aβ42, but Not of Aβ40, Seed Fibril Formation. *J. Am. Chem. Soc.* **138,** 1772–1775 (2016).

60. Fu, Z., Aucoin, D., Davis, J., Van Nostrand, W. E. & Smith, S. O. Mechanism of Nucleated Conformational Conversion of Aβ42. *Biochemistry* **54,** 4197–4207 (2015).

61. Bitan, G., Lomakin, A. & Teplow, D. B. Amyloid β-Protein Oligomerization. *J. Biol. Chem.* **276,** 35176–35184 (2001).

62. Heyman, H., Zhang, X., Tang, K., Baker, E. S. & Metz, T. O. Conventional and advanced separations in mass spectrometry-based metabolomics: Methodologies and applications. *Encycl. Spectrosc. Spectrom.* 376–384 (2016). doi:10.1016/B978-0-12-409547-2.12132-8

63. Hawe, A., Hulse, W. L., Jiskoot, W. & Forbes, R. T. Taylor dispersion analysis compared to dynamic light scattering for the size analysis of therapeutic peptides and proteins and their aggregates. *Pharm. Res.* **28,** 2302–2310 (2011).

64. Tomaselli, S., Esposito, V., Vangone, P., Van Nuland, N. A. J., Bonvin, A. M. J. J., Guerrini, R., Tancredi, T., Temussi, P. A. & Picone, D. The α-to-β conformational transition of Alzheimer's Aβ-(1-42) peptide in aqueous media is reversible: A step by step conformational analysis suggests the location of β conformation seeding. *ChemBioChem* **7,** 257–267 (2006).

65. Tran, L., Basdevant, N., Prévost, C. & Ha-Duong, T. Structure of ring-shaped Aβ42 oligomers determined by conformational selection. *Sci. Rep.* **6,** (2016).

66. Colvin, M. T., Silvers, R., Ni, Q. Z., Can, T. V., Sergeyev, I., Rosay, M., Donovan, K. J., Michael, B., Wall, J., Linse, S. & Griffin, R. G. Atomic Resolution Structure of Monomorphic Aβ42 Amyloid Fibrils. *J. Am. Chem. Soc.* **138,** 9663–9674 (2016).

67. Goddard, T. D., Huang, C. C., Meng, E. C., Pettersen, E. F., Couch, G. S., Morris, J. H. & Ferrin, T. E. UCSF ChimeraX: Meeting modern challenges in visualization and analysis.

Protein Sci. **27,** 14–25 (2018).

68. Lührs, T., Ritter, C., Adrian, M., Riek-Loher, D., Bohrmann, B., Döbeli, H., Schubert, D. & Riek, R. 3D structure of Alzheimer's amyloid-β(1-42) fibrils. *Proc. Natl. Acad. Sci. U. S. A.* **102,** 17342–17347 (2005).

69. Schmidt, M., Rohou, A., Lasker, K., Yadav, J. K., Schiene-Fischer, C., Fändrich, M., Grigorieff, N. & Petsko, G. A. Peptide dimer structure in an Aβ(1-42) fibril visualized with cryo-EM. *Proc. Natl. Acad. Sci. U. S. A.* **112,** 11858–11863 (2015).

70. Wälti, M. A., Ravotti, F., Arai, H., Glabe, C. G., Wall, J. S., Böckmann, A., Güntert, P., Meier, B. H. & Riek, R. Atomic-resolution structure of a disease-relevant Aβ(1-42) amyloid fibril. *Proc. Natl. Acad. Sci. U. S. A.* **113,** E4976–E4984 (2016).

71. Kreutzer, A. G., Hamza, I. L., Spencer, R. K. & Nowick, J. S. X-ray Crystallographic Structures of a Trimer, Dodecamer, and Annular Pore Formed by an Aβ17-36 β-Hairpin. *J. Am. Chem. Soc.* **138,** 4634–4642 (2016).

72. Ciudad, S., Puig, E., Botzanowski, T., Meigooni, M., Arango, A. S., Do, J., Mayzel, M., Bayoumi, M., Chaignepain, S., Maglia, G., Cianferani, S., Orekhov, V., Tajkhorshid, E., Bardiaux, B. & Carulla, N. Aβ(1-42) tetramer and octamer structures reveal edge conductivity pores as a mechanism for membrane damage. *Nat. Commun.* **11,** (2020).

73. Xiao, Y., Ma, B., McElheny, D., Parthasarathy, S., Long, F., Hoshi, M., Nussinov, R. & Ishii, Y. Aβ(1-42) fibril structure illuminates self-recognition and replication of amyloid in Alzheimer's disease. *Nat. Struct. Mol. Biol.* **22,** 499–505 (2015).

74. Cohen, S. I. A., Linse, S., Luheshi, L. M., Hellstrand, E., White, D. A., Rajah, L., Otzen, D. E., Vendruscolo, M., Dobson, C. M. & Knowles, T. P. J. Proliferation of amyloid- 42 aggregates occurs through a secondary nucleation mechanism. *Proc. Natl. Acad. Sci.* **110,** 9758–9763 (2013).

75. Cohen, S. I. A., Vendruscolo, M., Welland, M. E., Dobson, C. M., Terentjev, E. M. & Knowles, T. P. J. Nucleated polymerization with secondary pathways. I. Time evolution of the principal moments. *J. Chem. Phys.* **135,** (2011).

76. Knowles, T. P. J., Waudby, C. A., Devlin, G. L., Cohen, S. I. A., Aguzzi, A., Vendruscolo, M., Terentjev, E. M., Welland, M. E. & Dobson, C. M. An analytical solution to the kinetics of breakable filament assembly. *Science (80-.).* **326,** 1533–1537 (2009).

77. Lee, C. T. & Terentjev, E. M. Mechanisms and rates of nucleation of amyloid fibrils. *J. Chem. Phys.* **147,** (2017).

78. Srivastava, A. K., Pittman, J. M., Zerweck, J., Venkata, B. S., Moore, P. C., Sachleben, J. R. & Meredith, S. C. β-Amyloid aggregation and heterogeneous nucleation. *Protein Sci.* **28,** 1567–1581 (2019).

79. Shea, D., Hsu, C. C., Bi, T. M., Paranjapye, N., Childers, M. C., Cochran, J., Tomberlin, C. P., Wang, L., Paris, D., Zonderman, J., Varani, G., Link, C. D., Mullan, M. & Daggett, V. α-Sheet secondary structure in amyloid β-peptide drives aggregation and toxicity in

Alzheimer's disease. *Proc. Natl. Acad. Sci. U. S. A.* **116,** 8895–8900 (2019).

80. Ahmed, M., Davis, J., Aucoin, D., Sato, T., Ahuja, S., Aimoto, S., Elliott, J. I., Van Nostrand, W. E. & Smith, S. O. Structural conversion of neurotoxic amyloid-B 1-42 oligomers to fibrils. *Nat. Struct. Mol. Biol.* **17,** 561–567 (2010).

81. Ghosh, P., Vaidya, A., Kumar, A. & Rangachari, V. Determination of critical nucleation number for a single nucleation amyloid-β aggregation model. *Math. Biosci.* **273,** 70–79 (2016).

82. Gremer, L., Schölzel, D., Schenk, C., Reinartz, E., Labahn, J., Ravelli, R. B. G., Tusche, M., Lopez-Iglesias, C., Hoyer, W., Heise, H., Willbold, D. & Schröder, G. F. Fibril structure of amyloid-β(1–42) by cryo–electron microscopy. *Science (80-.).* **358,** 116–119 (2017).

83. Novo, M., Freire, S. & Al-Soufi, W. Critical aggregation concentration for the formation of early Amyloid-β (1-42) oligomers. *Sci. Rep.* **8,** (2018).

84. Mastrangelo, I. A., Ahmed, M., Sato, T., Liu, W., Wang, C., Hough, P. & Smith, S. O. High-resolution atomic force microscopy of soluble Aβ42 oligomers. *J. Mol. Biol.* **358,** 106–119 (2006).

85. Nirmalraj, P. N., List, J., Battacharya, S., Howe, G., Xu, L., Thompson, D. & Mayer, M. Complete aggregation pathway of amyloid β (1-40) and (1-42) resolved on an atomically clean interface. *Sci. Adv.* **6,** (2020).

86. Lacor, P. N., Buniel, M. C., Furlow, P. W., Clemente, A. S., Velasco, P. T., Wood, M., Viola, K. L. & Klein, W. L. Aβ oligomer-induced aberrations in synapse composition, shape, and density provide a molecular basis for loss of connectivity in Alzheimer's disease. *J. Neurosci.* **27,** 796–807 (2007).

87. Velasco, P. T., Heffern, M. C., Sebollela, A., Popova, I. A., Lacor, P. N., Lee, K. B., Sun, X., Tiano, B. N., Viola, K. L., Eckermann, A. L., Meade, T. J. & Klein, W. L. Synapse-binding subpopulations of Aβ oligomers sensitive to peptide assembly blockers and scFv antibodies. *ACS Chem. Neurosci.* **3,** 972–981 (2012).

88. Lesné, S., Ming, T. K., Kotilinek, L., Kayed, R., Glabe, C. G., Yang, A., Gallagher, M. & Ashe, K. H. A specific amyloid-β protein assembly in the brain impairs memory. *Nature* **440,** 352–357 (2006).

Chapter II. Supporting information of Article 1

This part was published as SI in *Anal. Chem*., 2021, *93*, (*16*), 6523–6533.
https://doi.org/10.1021/acs.analchem.1c00527

Mihai Deleanu,[1] Jean-François Hernandez,[1] Luca Cipelletti,[2,3] Jean-Philippe Biron,[1]

Emilie Rossi,[4] Myriam Taverna,[3,4] Hervé Cottet,*[1] Joseph Chamieh *[1]
[1] IBMM, Université Montpellier, CNRS, ENSCM, 34095 Montpellier, France
[2] Laboratoire Charles Coulomb (L2C), Université Montpellier, CNRS, Montpellier, France.
[3] Institut Universitaire de France (IUF), 75231 Paris, France
[4] Université Paris-Saclay, CNRS, Institut Galien Paris-Saclay, 92296, Châtenay-Malabry, Fr.

* CORRESPONDING AUTHORS
Tel: +33 4 6714 3920, Fax: +33 4 6763 1046. E-mail: joseph.chamieh@umontpellier.fr
Tel: +33 4 6714 3427, Fax: +33 4 6763 1046. E-mail: herve.cottet@umontpellier.fr

II.SI.1. Solid-phase peptide synthesis of Aβ(1-40)

II.SI.1.1. Instrumentation and sample analysis

Sample preparation for chromatographic analysis: every sample was dissolved in a 1:1 mixture of water and ACN before being loaded onto a chromatographic column. In the case of amyloidogenic segments, the peptide was first dissolved in 200 µL of HFIP, kept at 4 °C overnight and then diluted with 600 µL of 1:1 mixture of water and ACN. During synthesis, the quality of the advancing peptide was regularly checked after a small cleavage: a small portion of the peptide-resin was cleaved by treatment with a small amount of TFA (500 µL) and one drop of TIS for 1 hour at room temperature. The resin was then removed by filtration and the filtrate was evaporated under a N_2 stream. The residue was taken off in 600 µL of H_2O:ACN (50:50; v/v) and then subjected to analysis.

Chromatography:

The RP-HPLC analyses were carried out on a Waters Alliance 2690 instrument using a Merck Chromolith SpeedROD RP-18e reverse phase analytical column (50 × 4.6 mm) and a linear elution gradient starting from 100% A (H_2O + 0.1% TFA) to 100% B (ACN + 0.1% TFA) in 5 min at a

flow rate of 3 mL/min (named grad 5).

The LC/MS analyses were carried out on a Waters Alliance 2690 coupled to a Micromass ZQ spectrometer (electrospray ESI+ ionization mode) equipped with a C18 Chromolith Flash column (25 x 4.6 mm) at a flow rate of 3 mL/min following a linear elution gradient from 100% A (H_2O + 0.1% HCOOH) to 100% B (ACN + 0.1% HCOOH) in 2.5 or 5 min.

II.SI.1.2. General Description of solid phase peptide synthesis

Aβ(1-40) (H-DAEFRHDSGYEVHHQKLVFFAEDVGSNKGAIIGLMVGGVV-OH) was prepared by fast conventional SPPS using a *Fmoc* orthogonal strategy as depicted in Figure SI.1. The platform is comprised of a digital vortex connected to a filtration system as described elsewhere[1]. All steps were performed at 500 rpm at room temperature. The solid support was a ChemMatrix H-Val-O-Wang resin with a loading of 0.44 mmol/g. Amino acid side chain protection was as follows: Lys (Boc); Asn, Gln and His (Trt); Asp, Glu, Tyr and Ser (tBu); Arg (Pbf). Fresh and cold 0.5 M Fmoc-L-AA(PG)-OH and 0.5 M coupling reagent solutions in DMF were used for the coupling reaction. The main coupling reagent used during the synthesis was HATU. PyBOP was used for the couplings of Val24, Gln15 and His14 based on previous observations (data not shown) of unwanted guanidinylation occurring during some HATU couplings. Capping was performed with Ac_2O/DCM (50:50; v/v) and Fmoc removal was made using Pip/DMF (20:80; v/v). Between each step, the suspension was filtered, and the resin was washed with DMF. Cycle was repeated until all the required amino acids were coupled. The synthesis was monitored using HPLC and LC-MS by performing small cleavages of the peptide-resin as described above after coupling 13, 27 and 40 amino acids. The final cleavage of the peptide from the resin support was performed using a TFA/H_2O/TIS (95:2.5:2.5; v/v) cocktail and TBAB was added for preventing/reversing methionine oxidation. The crude peptide was treated with HFIP for avoiding any aggregation prior to analysis and purification.

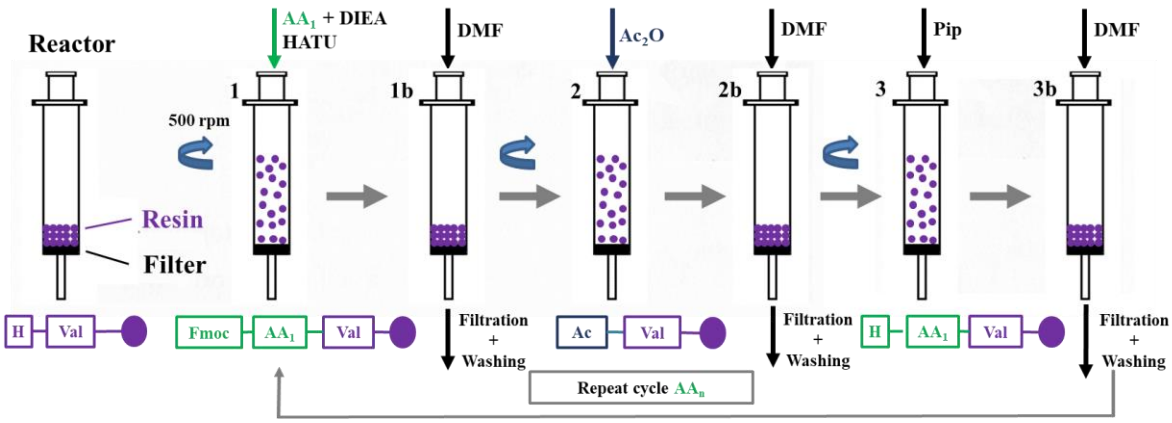

Figure SI.1. Schematic representation of the experimental setup of fast conventional SPPS of Aβ(1-40). Steps: 1. Coupling (2x 5 min): 5 eq. of AA + 5 eq. of HATU + 10 eq of DIEA; 1b. Washing: 3x DMF; 2. Capping (1x 1.5 min): Ac_2O/DCM (50/50; v/v); 2b. Washing: 3x DMF 3. Deprotection (2x 1.5 min): Pip/DMF (20/80; v/v); 3b. Washing: 5x DMF. All steps were performed at 500 rpm.

II.SI.1.3. Experimental Procedure

The resin H-Val-O-Wang ChemMatrix resin (341 mg; 0.15 mmol) was swollen in DMF for 30 min. Couplings were generally performed twice for 5 min by suspending the resin in a solution of 0.5 M Fmoc-AA(PG)-OH in DMF (1.5 mL; 5 eq.; 0.75 mmol) together with DIEA (260 µL, 10 eq.; 1.5 mmol). The 0.5 M HATU solution in DMF (1.5 mL; 5 eq.; 0.75 mmol) was added 1 min after the agitation started. In the case of Val and Ile couplings, the first coupling was performed for 10 min. For coupling Val24, Gln15 and His14, a DMF solution of 0.5 M PyBOP (1.5 mL; 5 eq.; 0.75 mmol) was used instead of HATU and the coupling was performed twice for 15 min. Resin was then filtered and washed three times with DMF. Capping was performed once for 1.5 min using DIEA (130 µL; 5 eq.; 0.75 mmol) and Ac_2O/DCM (1.5 mL; 50/50; v/v). The resin was filtered and washed again three times with DMF. Deprotection was carried out twice for 1.5 min by treatment with Pip/DMF (20:80; v/v). The resin was washed five times with DMF before starting the next coupling. Before the final cleavage, the resin was washed twice with DMF, twice with MeOH and twice with DCM and then dried under vacuum for 4 hours. The final cleavage of the peptide was achieved by suspending the dried resin (900 mg) in TFA/H_2O/TIS (9 mL; 95:2.5:2.5; v/v) under magnetic stirring for 1.5 hours and TBAB (68.5 mg; 0.21 mmol) was added 15 minutes before the end of this step. The resin was filtered and washed with TFA and DCM and the filtrate was evaporated under vacuum. The crude residue was taken off in Et_2O to precipitate the peptide, then the suspension was centrifuged for 10 min at 3000 rpm and the supernatant was

decanted. The latter step was performed three times. The residue containing the peptide was dried under vacuum overnight and 200 mg of crude Aβ(1-40) were obtained.

II.SI.1.4. Peptide Purification and Isolation

Purifications were performed by preparative HPLC equipped with a DeltaPak C4 column (100 x 40 mm, 15 µm, 300 Å) and with a DeltaPak C18 column (100 x 40 mm, 15 µm, 100 Å) at a wavelength of 214 nm. A mobile phase gradient elution consisting of A (H_2O + 0.1 % TFA) and B (ACN + 0.1 % TFA) was applied at a flow rate of 28 mL/min. Aβ(1-40) (200 mg; 0.05 mmol) was dissolved in 7 mL HFIP and was kept overnight under a N_2 stream. Immediately before purification, the solution was half-diluted with 0.1% aqueous TFA and filtered through a 0.1 µm aqueous filter. The filter was washed with the same volume of 0.1% aqueous TFA. The peptide was purified by first loading it onto a C4 column (5 runs of 40 mg each). The elution gradient was 5 % B to 35 % B in 40 min and the peptide eluted at 27 % B. The fractions containing the peptide in sufficient purity were mixed and freeze-dried overnight to yield 45 mg of white solid, which was subjected to a second purification step using a C18 column. The elution gradient was 5%B to 15 % B in 15 min and 15 % B to 45 % B in 40 min. The peptide eluted at 34 % B. The final fractions were freeze dried and 12 mg of Aβ(1-40) with a purity ≥95 % were obtained and stored at -20 °C until further use.

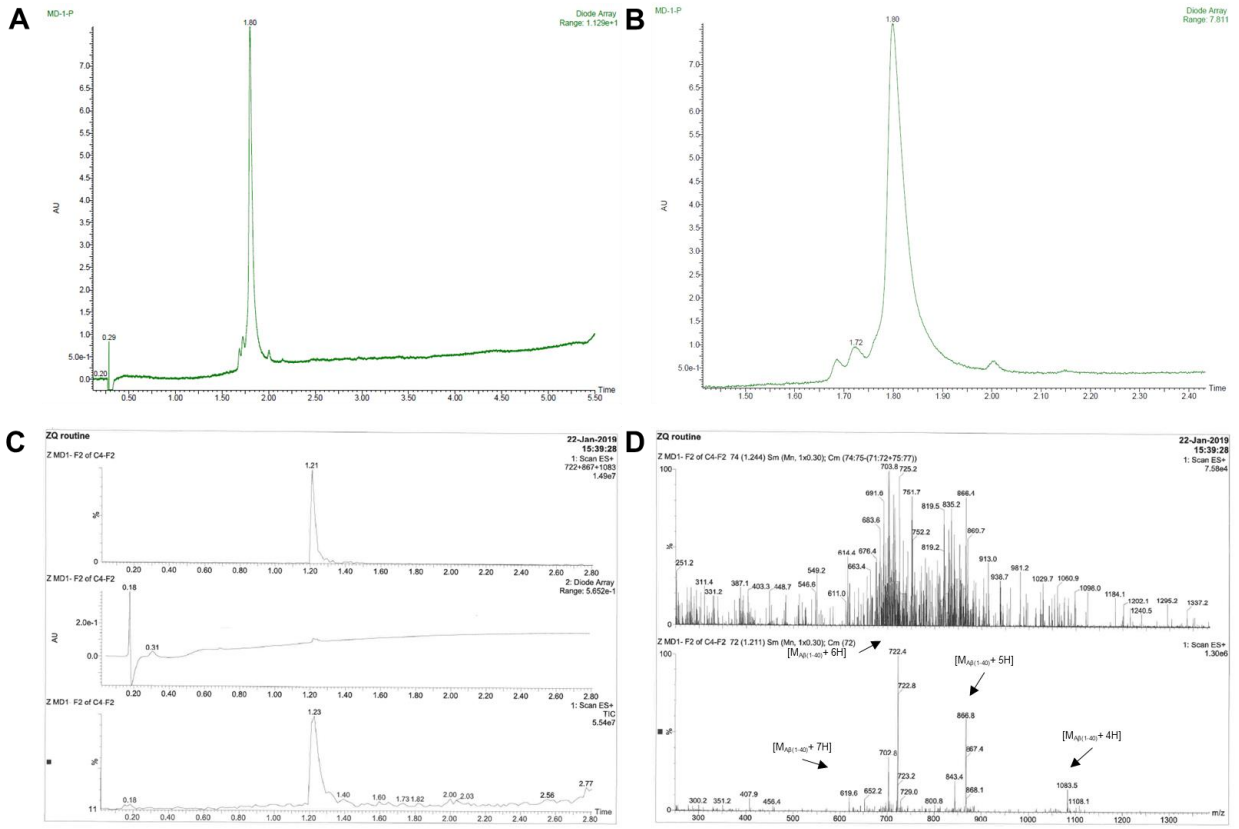

Figure SI.2. (A, B) HPLC-UV and (C,D) LC-MS analyses of the Aβ(1-40) batch used in this study. Experimental conditions: Sample: 800 µL H_2O:ACN:HFIP (37.5:37.5:25 v:v). HPLC: Chromolith SpeedROD RP-18e reverse phase analytical column: 50 × 4.6 mm; Linear elution gradient: 100% A (H_2O + 0.1% TFA) to 100% B (ACN + 0.1% TFA) in 5 min. Flow rate: 3 mL/min; UV detection at 214 nm. LC-MS: Chromolith RP-18e Flash column: 25 x 4.6 mm; Linear elution gradient: 100% A (H_2O + 0.1% HCOOH) to 100% B (ACN + 0.1% HCOOH) in 2.5 min; Flow rate: 3 mL/min; UV detection at 214 nm.

II.SI.2. ThT Fluorescence assay

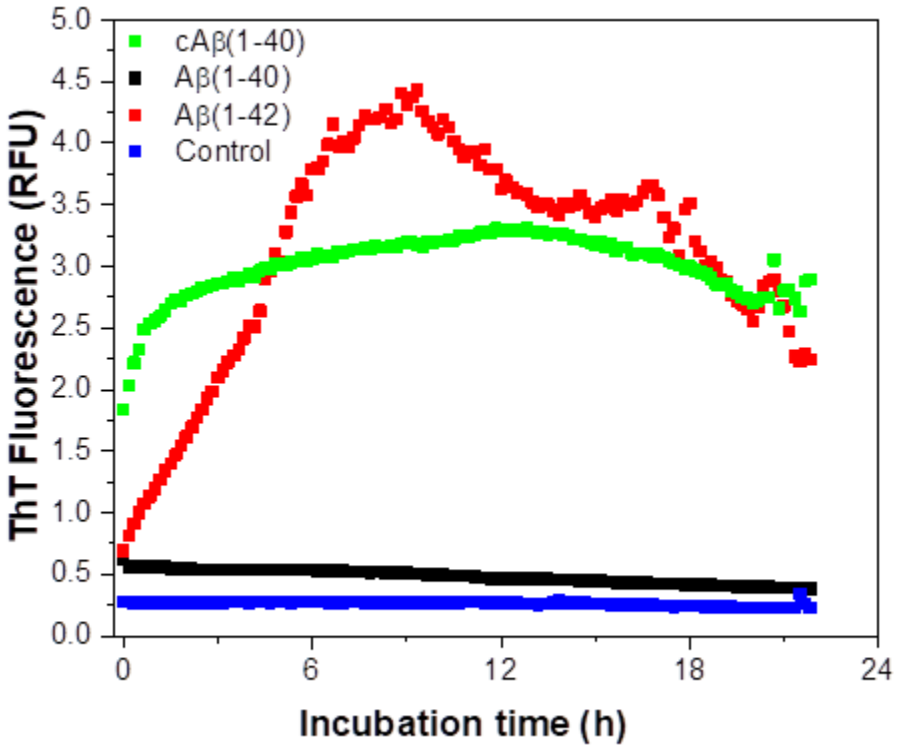

Figure SI.3. ThT fluorescence data of the aggregation of the studied peptides Aβ(1-40) and Aβ(1-42), cAβ(1-40) sample and a control run. Experimental conditions: Sample: 10 µM Aβ peptide (or sample matrix without the peptide for the control) + 38 µM ThT; 9 mM Tris-HCl + 91 mM NaCl, pH 7.4. Incubation: quiescent conditions at 25 °C. λ_{Em}= 485 nm; λ_{Ex}=430 nm.

II.SI.3. TDA: theoretical and data processing

Conditions of validity of TDA. The band broadening resulting from Taylor dispersion is easily quantified via the temporal variance of the elution profile. The diffusion coefficient D (m^2 s^{-1}) and the hydrodynamic radius R_h (m) are determined using Eq. SI.(1) and Eq. SI.(2), respectively:

$$D = \frac{R_c^2 t_0}{24\sigma^2} \qquad \text{SI.(1)}$$

$$R_h = \frac{k_b T}{6\pi\eta D} \qquad \text{SI.(2)}$$

where *Rc* is the capillary radius (m), t_0 is the average elution time (s), σ^2 is the temporal variance of the peak (s^2), k_B is the Boltzmann constant, T the temperature (K) and η the viscosity of the carrier liquid (Pa.s). It is noteworthy that Eq. SI.(1) is valid when the peak appearance time t_0 is higher than the characteristic diffusion time of the solute on a distance equal to the capillary radius as verified by Eq. (3)[2,3]:

$$\tau = \frac{Dt_0}{R_c^2} \geq 1.25 \qquad \text{SI.(3)}$$

where τ is an adimensional characteristic time. Axial diffusion should also be negligible compared to convection as verified by Eq. (4)[2,3]:

$$P_e = \frac{uR_c}{D} \geq 40 \qquad \text{SI.(4)}$$

where P_e is the Péclet number and u is the linear mobile phase velocity (m/s).

Data processing of the taylorgrams. The taylorgram $S(t)$ of a sample mixture containing n different components of individual diffusion coefficient D_i can be expressed as a sum of n individual Gaussian contributions $S_i(t)$, all centered at the same elution time t_0:

$$S(t) = \sum_{i=1}^{n} S_i(t) = \sum_{i=1}^{n} \frac{A_i}{\sigma_i\sqrt{2\pi}} e^{-\frac{1}{2}\frac{(t-t_0)^2}{\sigma_i^2}} \qquad \text{SI.(5)}$$

where A_i is a coefficient that is proportional to the concentration in species i and that depends on the response coefficient of the species i, at the specific detection wavelength. The diffusion coefficient of the species i is directly related to the standard deviation σ_i according to

$$D_i = \frac{R_c^2 t_0}{24\sigma_i^2} \qquad \text{SI.(6)}$$

Different approaches can be used to obtain information about the size distribution of the species in the mixture from the taylorgram *S(t)*.[4-6]

A first approach is based on a direct curve fitting with the sum of *n* Gaussian curves according to Eq. (5), when the total number of species, *n*, is limited ($n \leq 4$). The curve fitting was conducted using the Least Significant Difference method using the "GRG nonlinear" algorithm in Microsoft Excel.

A second approach is based on Constrained Regularized Linear Inversion (CRLI)[5] which aims at finding the probability density function $P_D(D)$ that fits the taylorgram according to the following equation:

$$s(t) = c\int_0^\infty P_D(D)\sqrt{D}\exp\left[-\frac{(t-t_0)^2 12D}{R_c^2 t_0}\right]dD \qquad \text{SI.(7)}$$

with $c = \left[\int_0^\infty P_D(D)\sqrt{D}dD\right]^{-1} = \left[\overline{D^{1/2}}\right]^{-1}$ a normalization factor and $P_D(D)$ the mass-weighted probability distribution function (PDF) of the diffusion coefficient. The main advantage of this approach, as compared to the first one, is that there is no need to hypothesize on the number of populations under the experimental distribution. For more details on that approach, the reader may refer to original publications [4,5].

II.SI.4. Experimental Taylorgrams

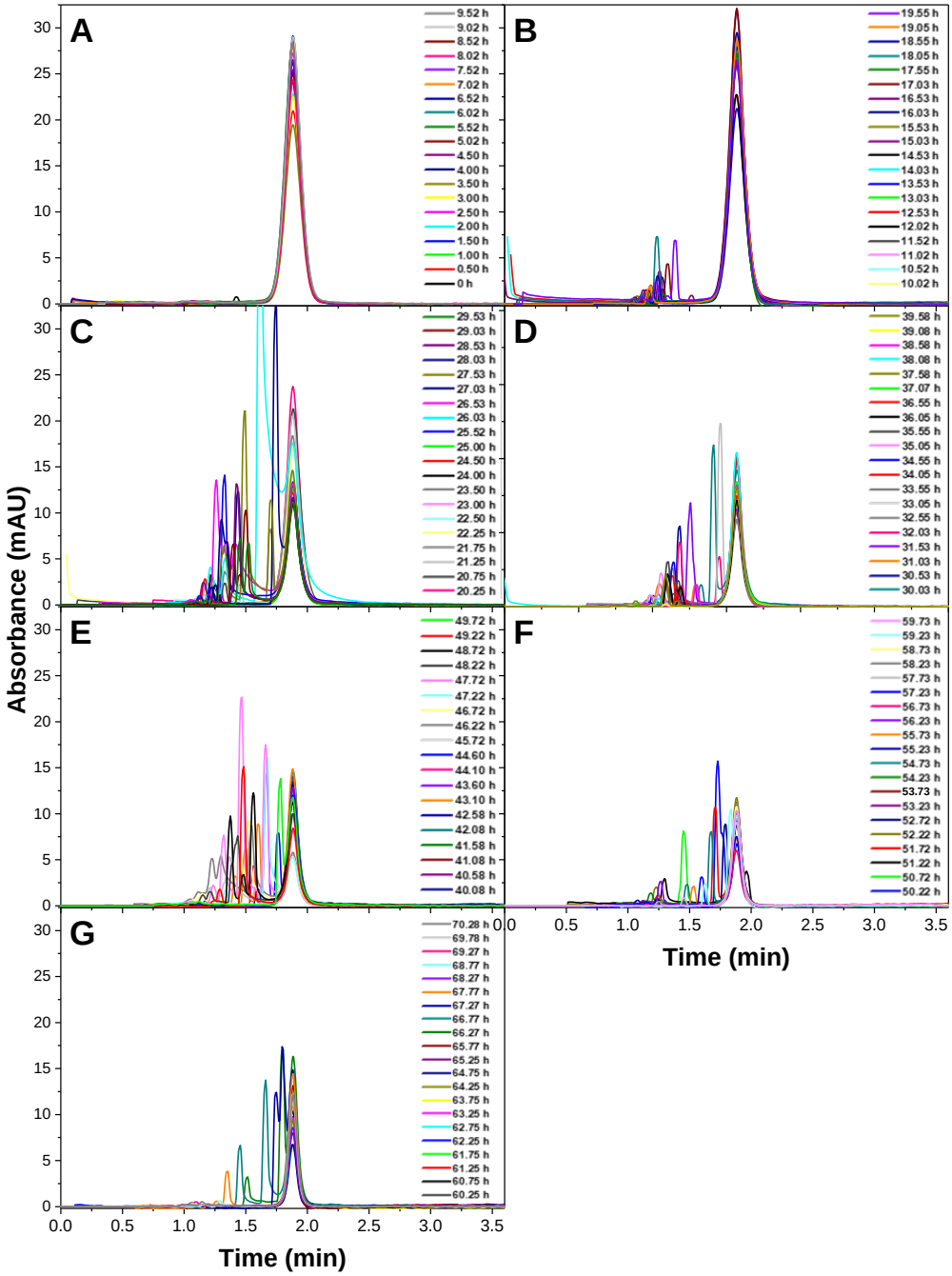

Figure SI.4. Experimental taylorgrams obtained for Aβ(1-40) aggregation monitoring over an incubation period of 70h. 0-10 h(A). 10 – 20 h (B). 20 – 30h (C). 30–40 h(D). 40 – 50 h (E). 50 – 60 h (F). 60 – 70 h (G). Experimental conditions: Sample: 100 µM Aβ(1-40) in 20 mM phosphate buffer pH 7.4. Incubation: quiescent conditions at 37 °C. Fused silica capillary: 50 µm i.d. × 40 cm × 31.5 cm. Eluent: 20 mM phosphate buffer, pH 7.4. Mobilization pressure: 100 mbar. Injection: 44 mbar for 3 s (*Vinj* = 7 nL, corresponding to 1% of capillary volume to injection point). Analyses were performed at 37 °C. UV detection at 191 nm.

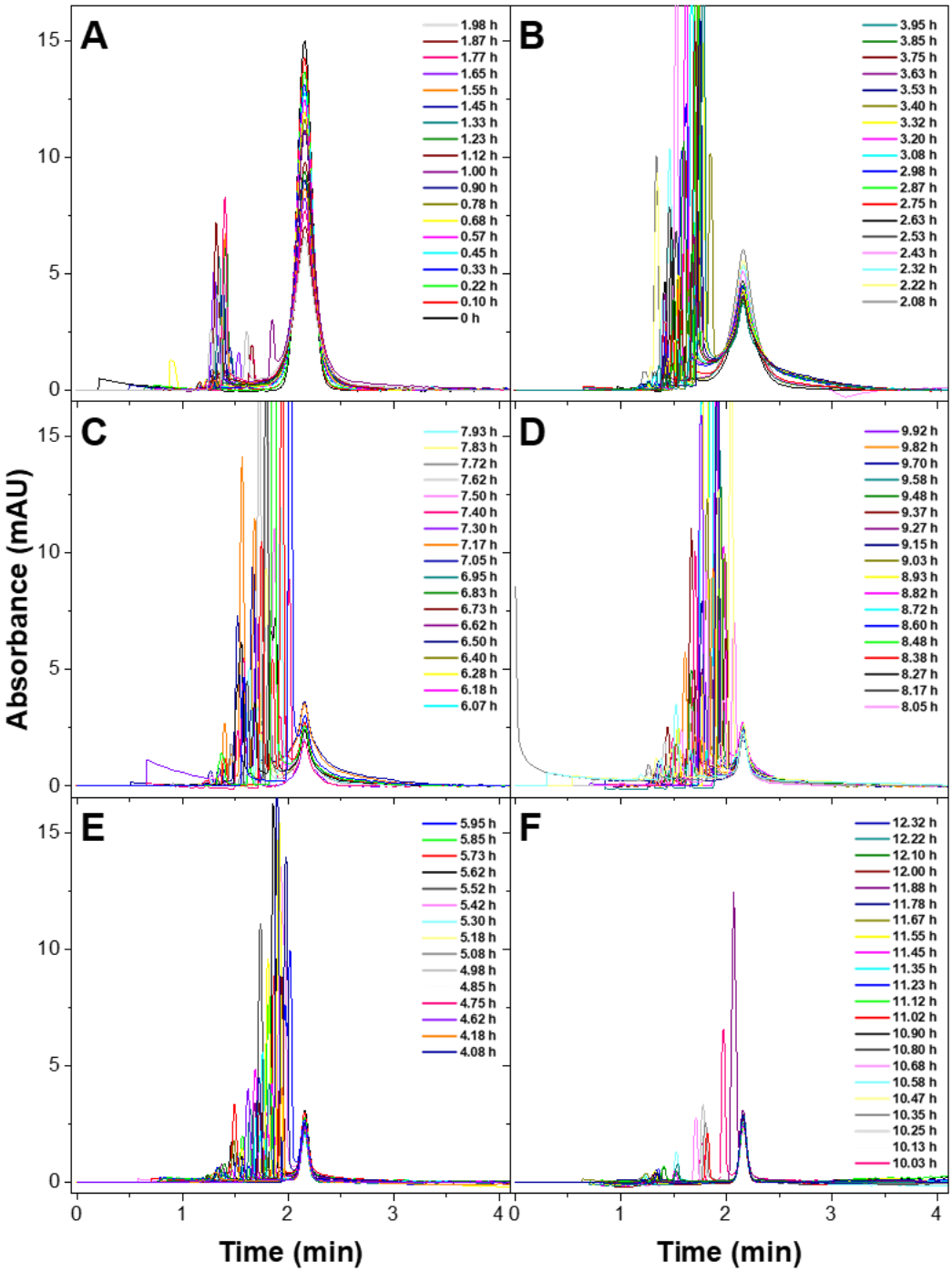

Figure SI.5. Experimental taylorgrams obtained for Aβ(1-42) aggregation monitoring over an incubation period of 12.5 h. (A) 0–2h. (B) 2 – 4 h. (C) 4–6h. (D) 6 –8 h.(E) 8 – 10h. (F) 10 – 12.5 h Experimental conditions: Sample: 100 µM Aβ(1-42) in 20 mM phosphate buffer pH 7.4. Incubation: quiescent conditions at 37 °C. Fused silica capillary: 50 µm i.d. × 40 cm × 31.5 cm. Eluent: 20 mM phosphate buffer, pH 7.4. Mobilization pressure: 100 mbar. Injection: 44 mbar for 3 s (*Vinj* = 7 nL, corresponding to 1% of capillary volume to injection point). Analyses were performed at 37 °C. UV detection at nm.

II.SI.5. Data treatment by Taylor dispersion analysis

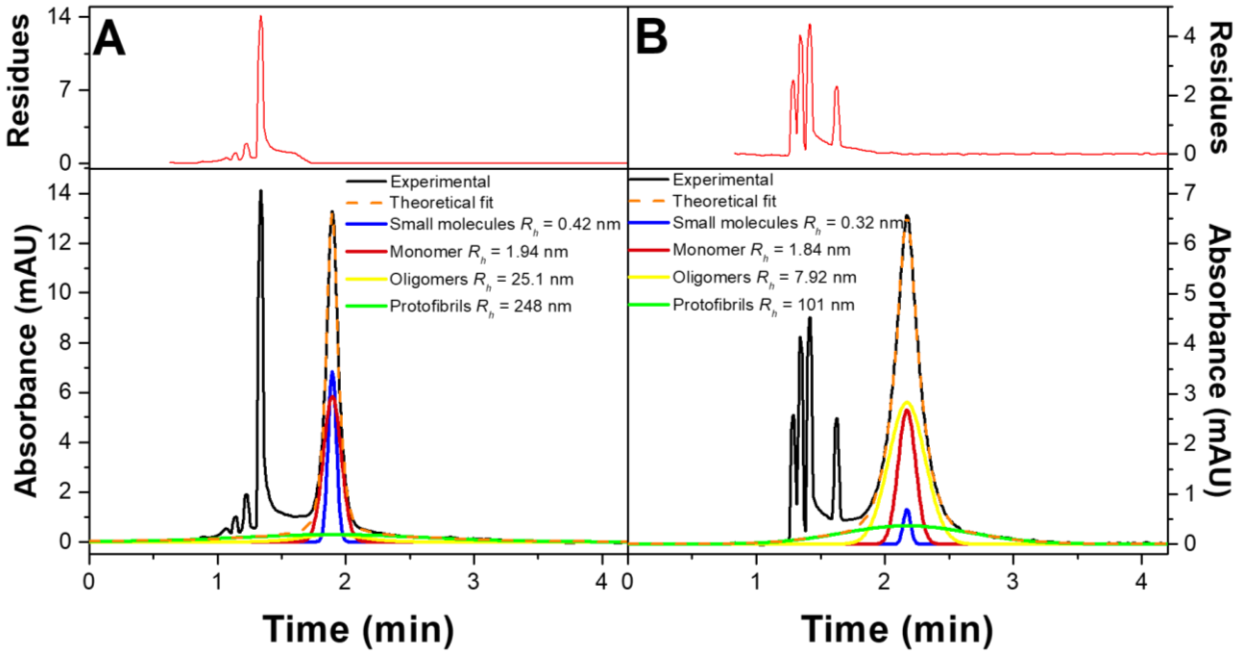

Figure SI.6. Data processing of the experimental taylorgrams for (A) Aβ(1-40) at t=25.52 h and (B) Aβ(1-42) at t=1.98. The lower graph represents the experimental data (black) fitted with the sum of four Gaussian peaks (dashed orange) which are individually represented on the graph. The residuals plot in the upper part of the graphs is the difference between the experimental data and the theoretical fit. Experimental conditions: Sample: 100 µM; 20 mM phosphate buffer pH 7.4. Incubation: quiescent conditions at 37 °C. Fused silica capillaries: 50 µm i.d. × 40 cm × 31.5 cm. Mobile phase: 20 mM phosphate buffer, pH 7.4. Mobilization pressure: 100 mbar. Injection: 44 mbar for 3 s. Analyses were performed at 37 °C. UV detection at 191 nm. Baseline treatment was performed in Microcal Origin. The experimental fitting of the taylorgrams was performed by using Equation 5 in Microsoft Excel.

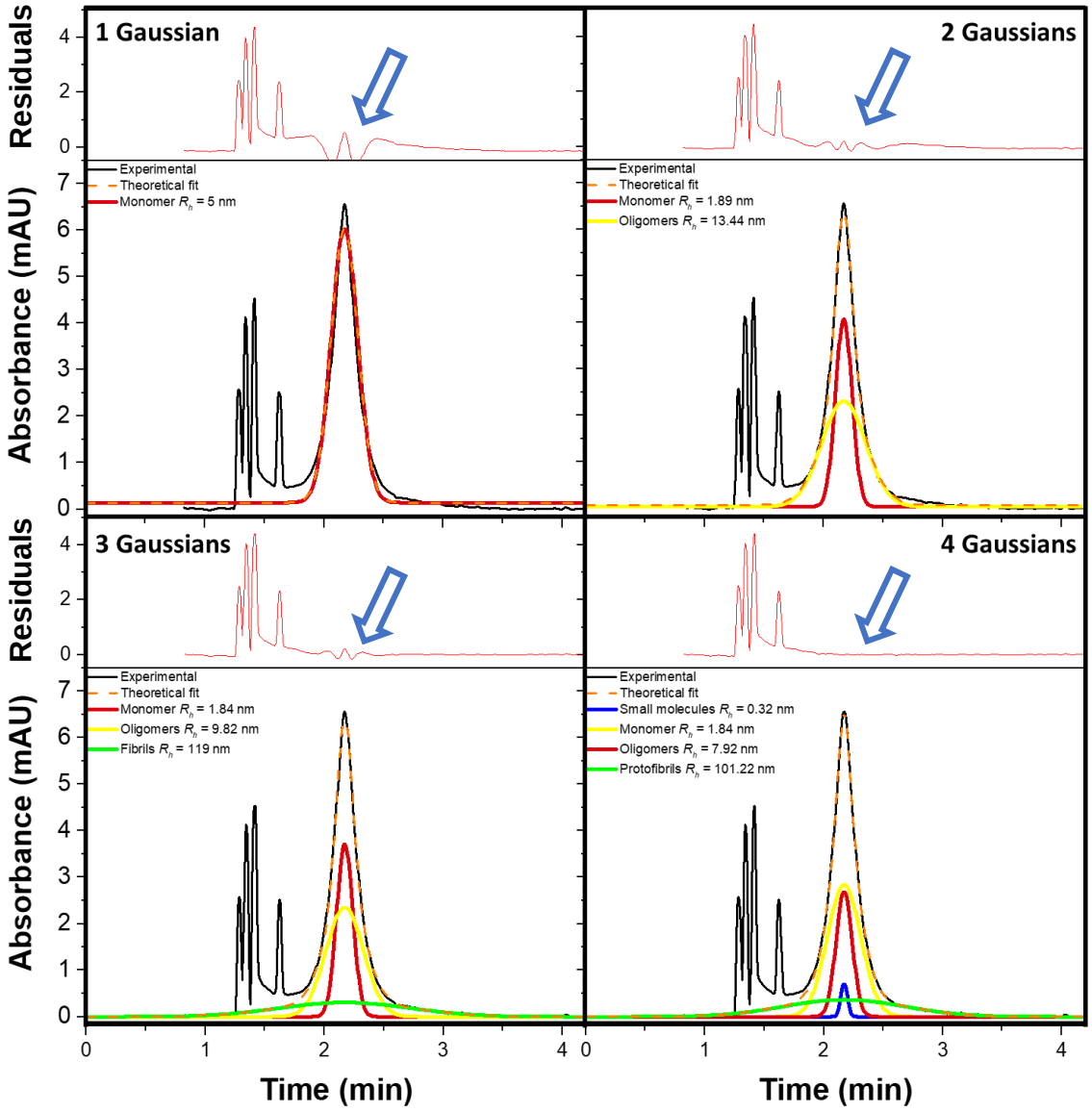

Figure SI.7. Data processing of the experimental taylorgrams for Aβ(1-42) at t=1.98 h, using 1, 2, 3 or 4 Gaussian functions. The lower part in each graph represents the experimental data (black) fitted with the sum of *n* Gaussian peaks (dashed orange) which are individually represented on the graph. The residuals plot in the upper part of the graphs is the difference between the experimental data and the theoretical fit. Experimental conditions as in **Figure SI.8**. Baseline treatment was performed in Microcal Origin. The experimental fitting of the taylorgrams was performed using Equation 5 in Microsoft Excel.

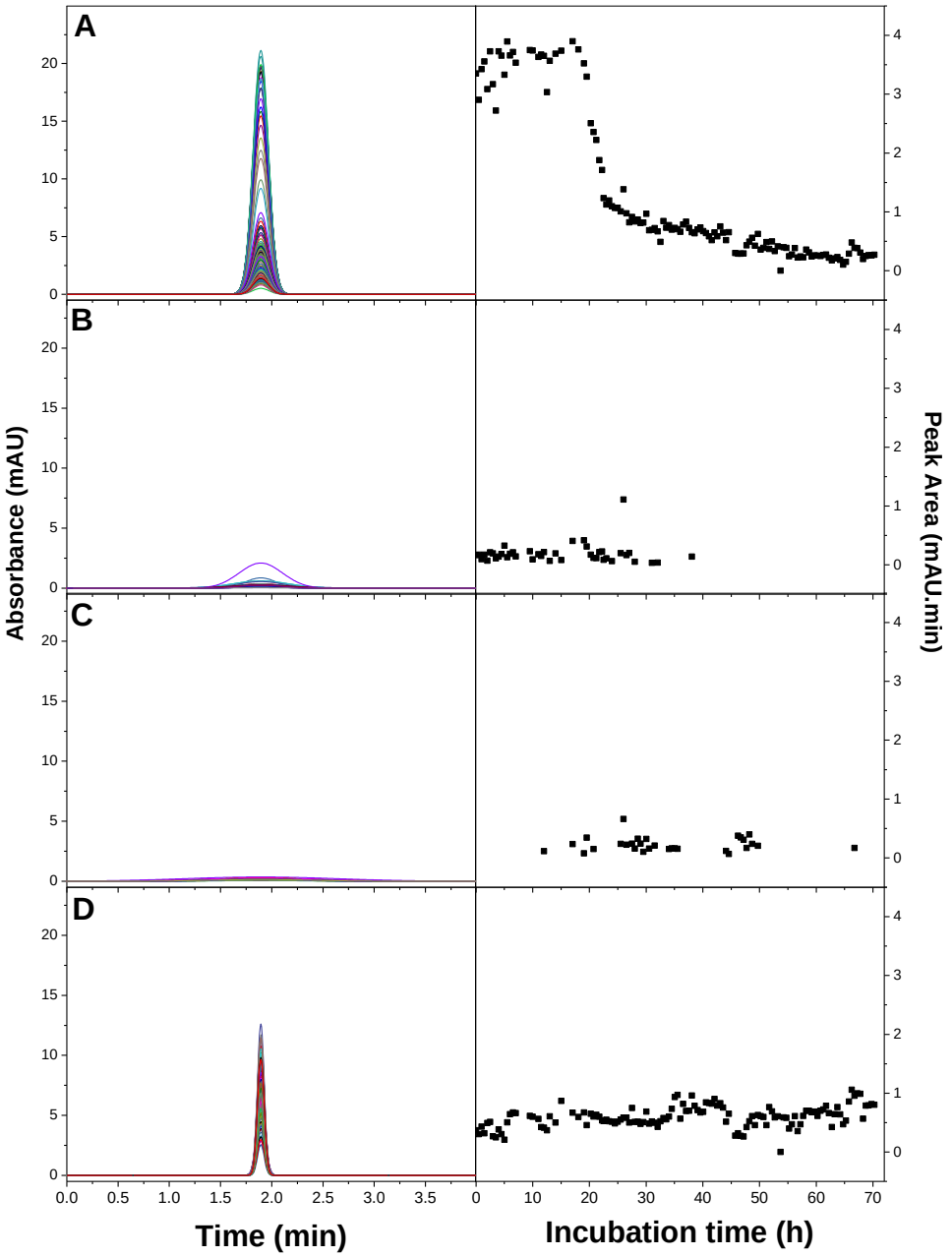

Figure SI.8. Extracted Gaussian peaks from the finite *n* Gaussian fitting for the four populations of Aβ(1-40) with their respective area as a function of incubation time. (A) Monomers and low molar mass oligomers; (B) higher molar mass oligomers; (C) protofibrils; (D) small molecules

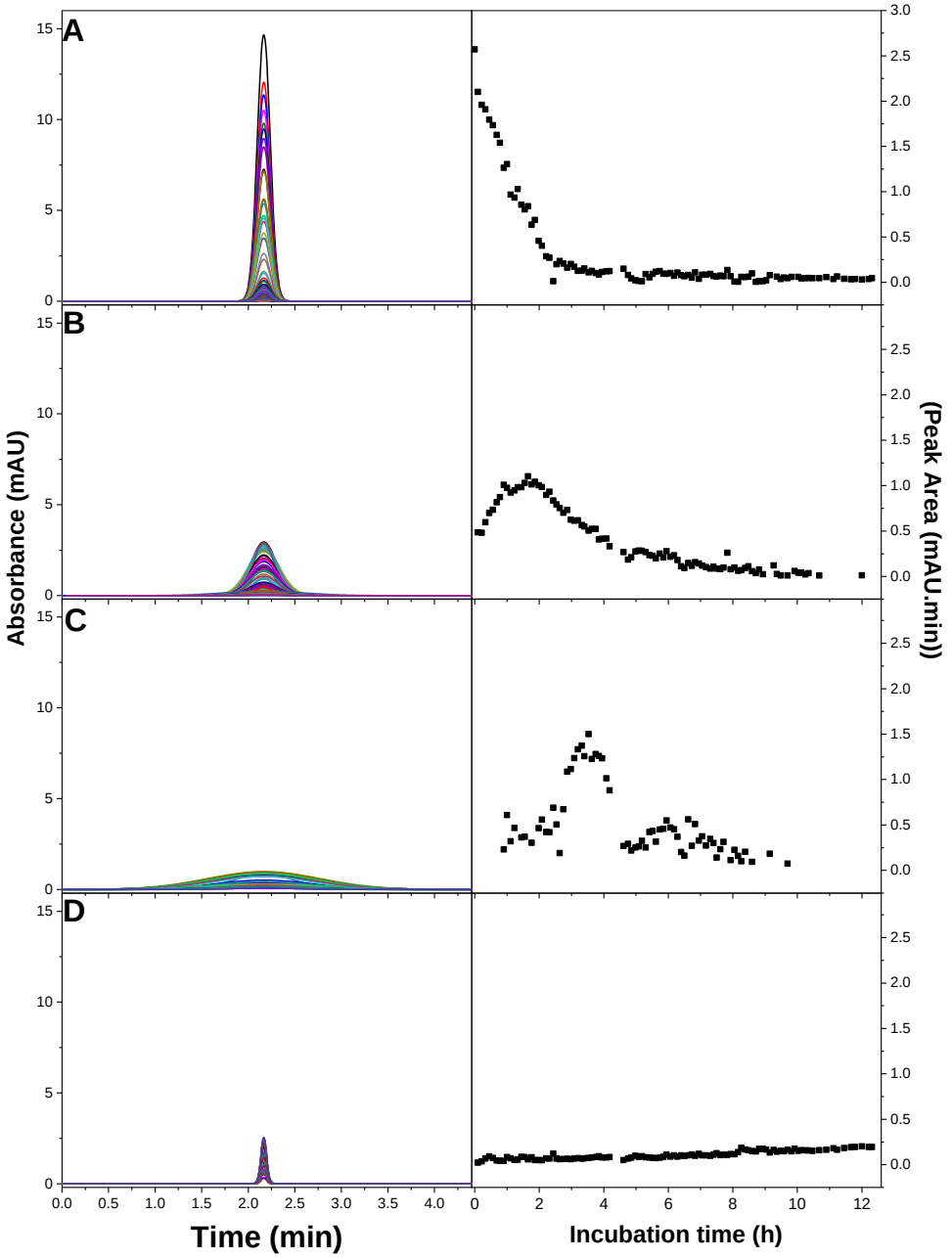

Figure SI.9. Extracted Gaussian peaks from the finite *n* Gaussian fitting for the four populations of Aβ(1-42) with their respective area as a function of incubation time. (A) Monomers and low molar mass oligomers; (B) higher molar mass oligomers; (C) protofibrils; (D) small molecules

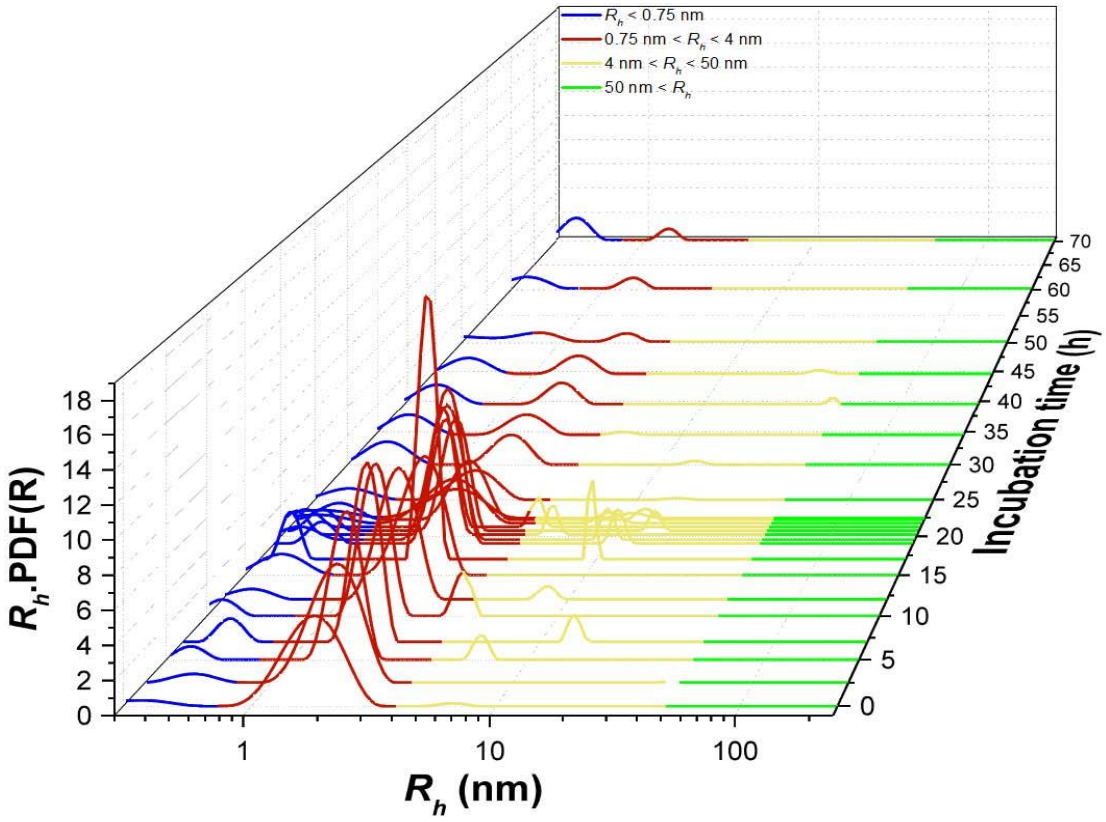

Figure SI.10. Hydrodynamic radius distribution as obtained by CRLI for the designated incubation times of Aβ(1-40). The distributions were divided into four color coded populations for better visual comparison: Blue line: small molecules R_h < 0.75 nm; red line: Monomer and small oligomers 0.75 nm < R_h < 4 nm; yellow line: High molar mass oligomers 4 nm < R_h < 50 nm; green line: Protofibrils R_h > 50 nm

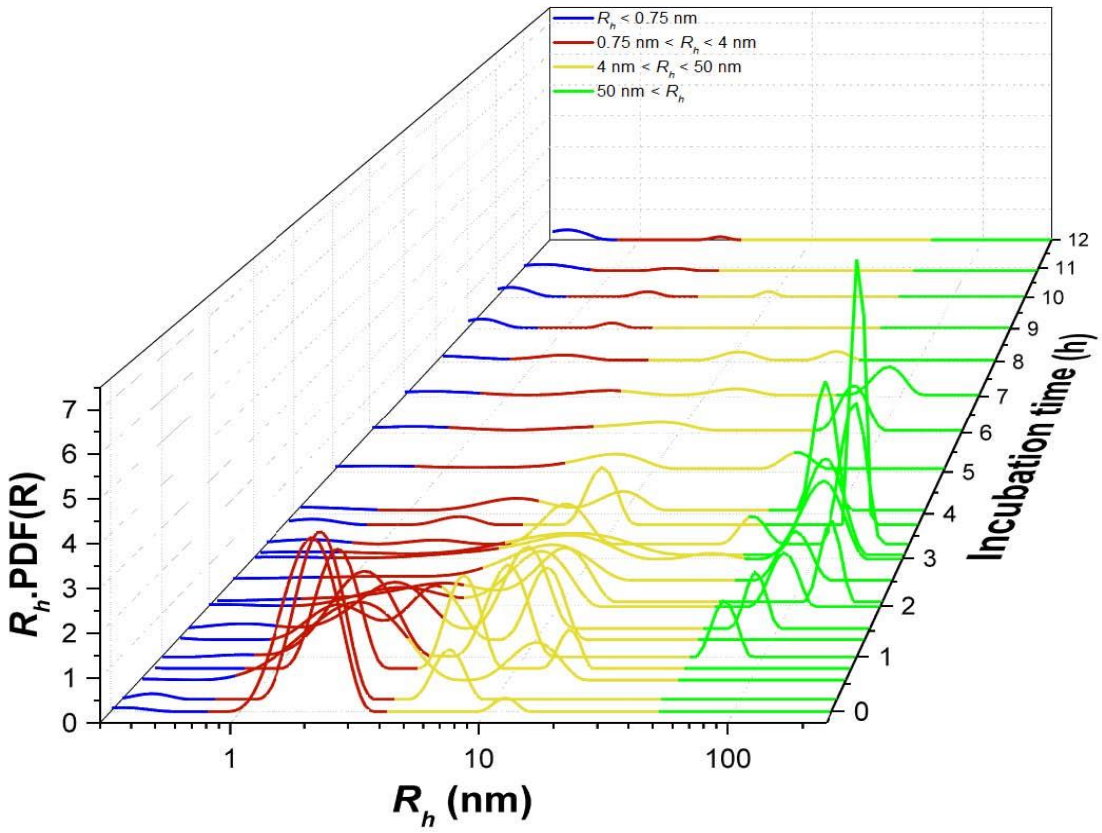

Figure SI.11. Hydrodynamic radius distribution as obtained by CRLI for the designated incubation times of Aβ(1-42). The distributions were divided into four color coded populations for better visual comparison: Blue line: small molecules R_h < 0.75 nm; red line: Monomer and small oligomers 0.75 nm < R_h < 4 nm; yellow line: High molar mass oligomers 4 nm < R_h < 50 nm; green line: Protofibrils R_h > 50 nm

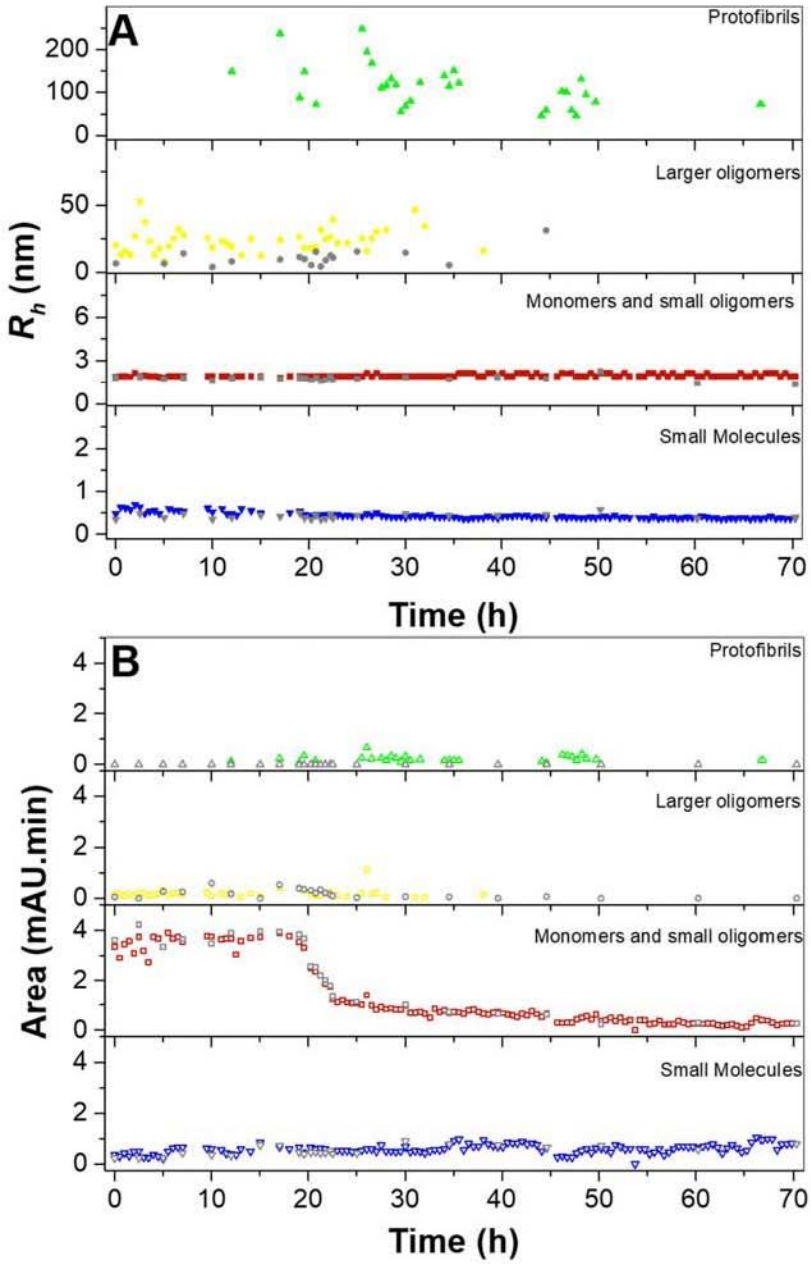

Figure SI.12. Comparison between data processing approaches for Aβ(1-40). (A) Obtained R_h value for each population as a function of incubation time; (B) relative peak area for each population as a function of the incubation time. Colored symbols are obtained using the 1st approach (limited number of Gaussian functions), grey symbols are obtained with the 2nd approach (CRLI).

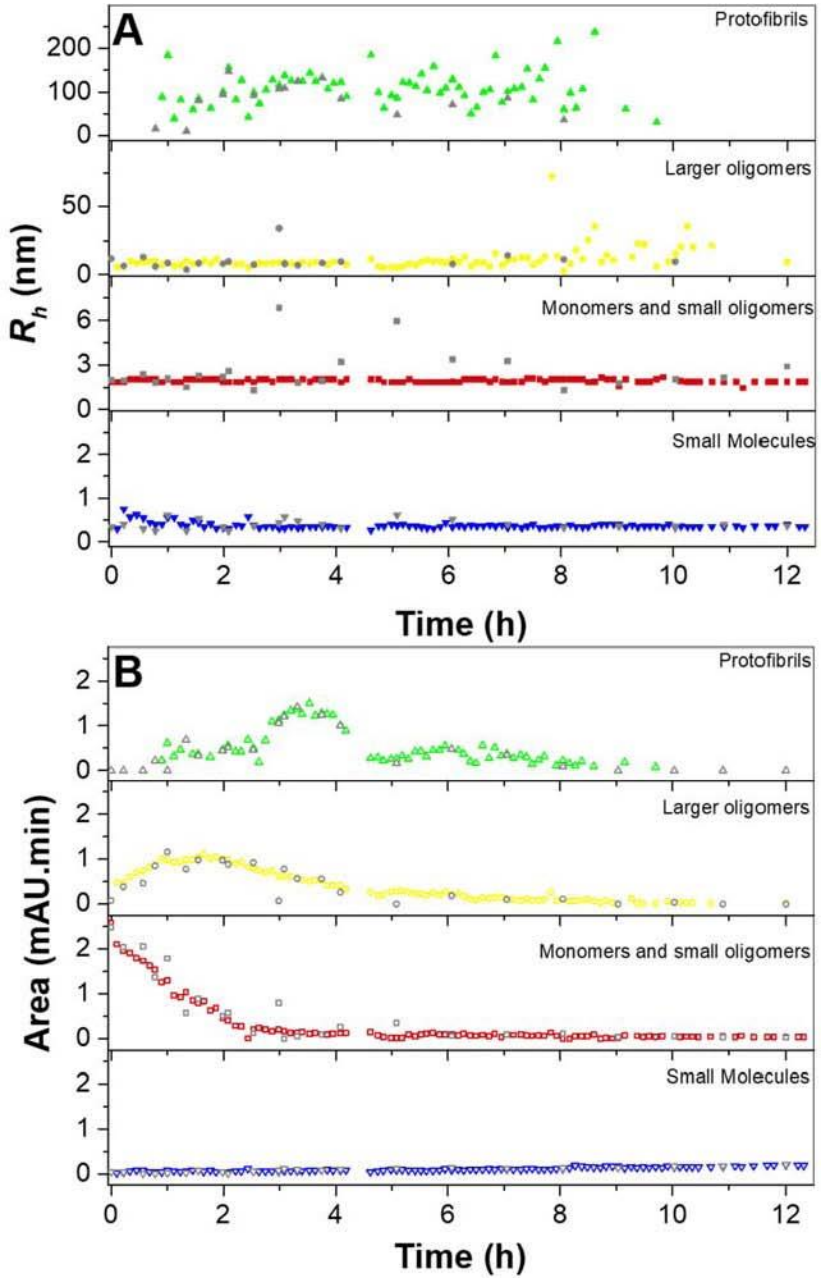

Figure SI.13. Comparison between data processing approaches for Aβ(1-42). (A) Obtained R_h value for each population as a function of incubation time; (B) relative peak area for each population as a function of the incubation time. Colored symbols are obtained using the 1st approach (limited number of Gaussian functions), grey symbols are obtained with the 2nd approach (CRLI).

II.SI.6. Comparison with ThT assay

To confirm the TDA observations, the ThT assay was realized in the same conditions as the TDA analysis. The estimated concentration expressed in µmol of monomer per L of solution is presented in Figure SI.14. The latter concentrations were estimated by supposing that all present species in the sample had the same detector response factor. This response factor was calculated from the first TDA run where only the monomer population was present. The decrease in the concentration of soluble species was attributed to the formation of insoluble species which are generally detected with the ThT assay. As seen in Figure SI.14, the ThT assay plot overlays the concentration evolution of the insoluble species suggesting that TDA alone is enough to estimate the lag phase and the time to reach the plateau of the aggregation process. In Figure SI.14B the ThT assay had the same shape as the insoluble Aβ(1-42) species but the time was not the same, thus the aggregation study was repeated by TDA. Results show different aggregation kinetics for all repetitions on both peptides, however the aggregation pathway remained the same, *i.e.* no intermediate species for Aβ(1-40) in contrast to Aβ(1-42). Figure SI.14C shows another repetition of the aggregation study by TDA of Aβ(1-42) where faster kinetics were observed as compared to Figure SI.16B. However, the population evolutions with incubation time were the same as the other repetition confirming that the kinetics of the aggregation process are controlled by a stochastic nucleation[7]. Another important observation is that in all cases it seems that the concentrations of monomeric species and insoluble aggregates follow specular sigmoidal shapes that cross at the half time of the ThT increase and at almost 50 % of each.

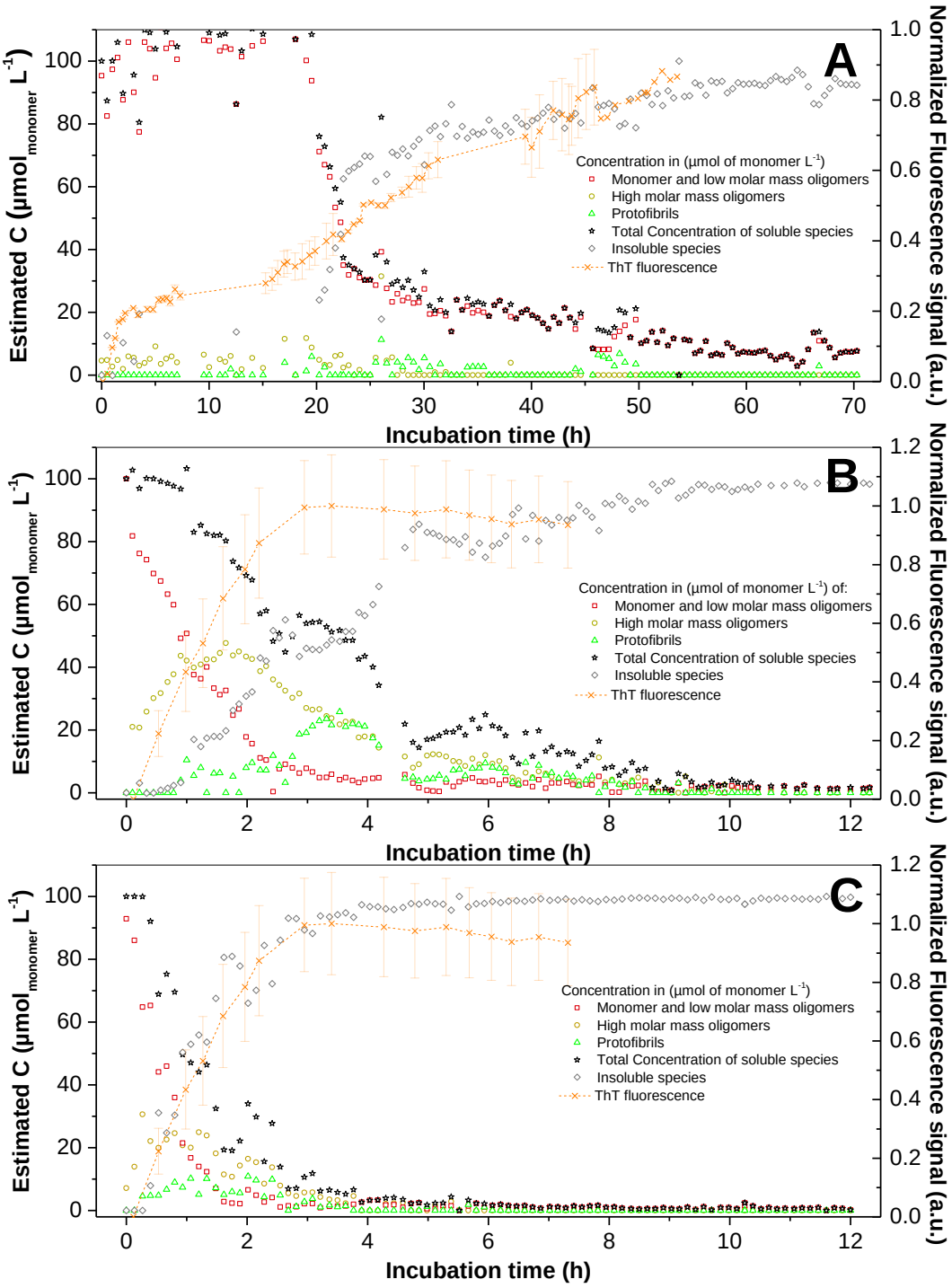

Figure SI.14. Estimated concentration evolution of all species and the ThT fluorescence assay at 37°C in the same buffer as the TDA analysis (phosphate buffer 20 mM pH 7.4) during the aggregation process of (A) Aβ(1-40) (B) Aβ(1-42) 1st repetition and (C) Aβ(1-42) 2nd repetition. Experimental ThT fluorescence assay conditions: Sample: 100 µM Aβ peptide + 38 µM ThT; 19.2 mM phosphate buffer, pH 7.4. Incubation: quiescent conditions at 37 °C. Fluorescence detection: λ_{Em}= 485 nm; λ_{Ex}=430 nm.

II.SI.7. Dynamic light scattering

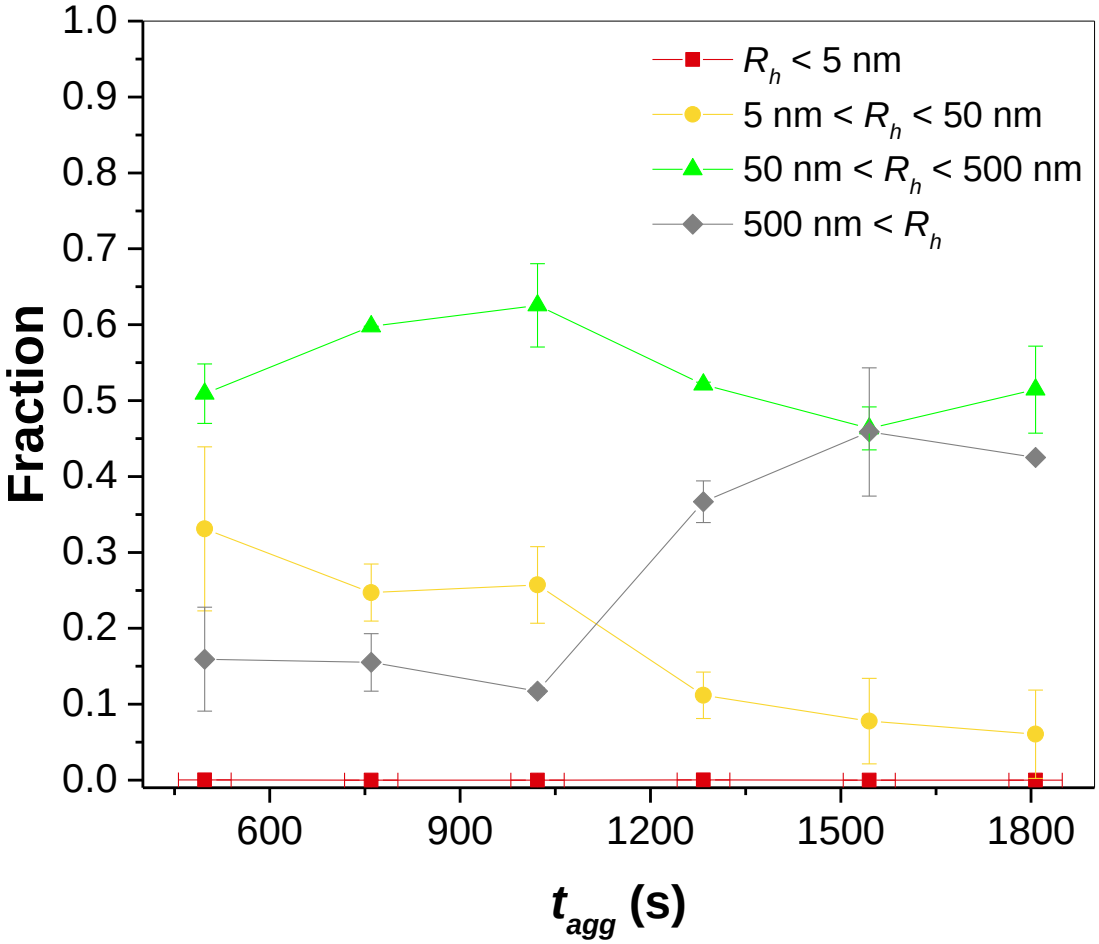

Figure SI.15: Time evolution of four classes of Aβ 42 aggregates, as measured by dynamic light scattering. Error bars quantify the difference between data obtained by analyzing runs at scattering angles of 45° and 90°.

II.SI.8. Modelization data

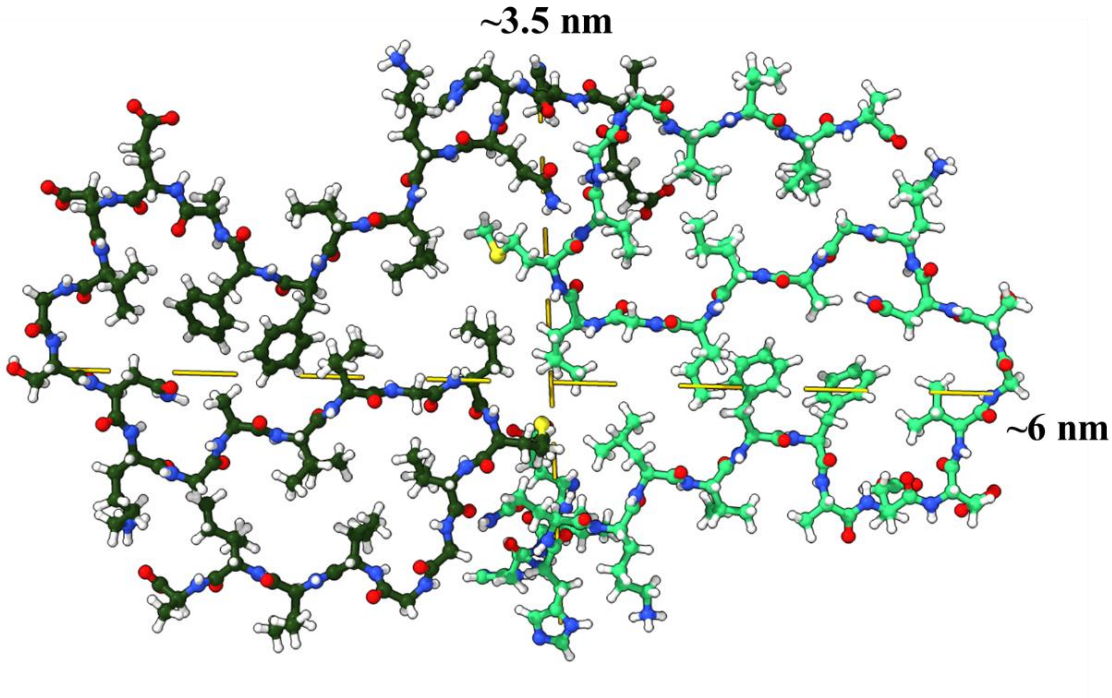

Figure SI.16. Structure of Aβ(1-42) as described in[8] showing the S shape conformation of the monomers, dimensions were measured in Chimera X[9].

Table SI.1. Calculated size of the constructed structures of Aβ(1-42) oligomers using HYDROPRO software[10] or by using the equations of Perrin[11].

n dimer	R_h HYDROPRO (nm)	L = 2*l* (nm)	*R* (nm)	MM (g mol^{-1})	R_h Cylinder (nm)	R_h Prolate (nm)	R_h Oblate (nm)
1	2.0	6.48	0.44	9028.08			2.1
9	3.1	6.48	2.24	81252.72	2.9	2.6	
27	4.7	14.5	3.24	243758.16	5.2	4.5	
45	6.1	23.1	3.24	406263.6	6.6	5.7	
90	9.2	44.7	3.24	812527.2	9.6	8.5	
135	11.7	65.8	3.24	1218790.8	12.3	10.9	
180	14.4	88.0	3.24	1625054.4	14.9	13.3	
360	23.2	174	3.24	3250108.8	24.1	21.9	
720	40.0	343	3.24	6500217.6	40.0	36.8	

Perrin[11] described in its seminal work how to estimate the hydrodynamic radius of macromolecules depending on their shape. If the macromolecule is an oblate ellipsoid (disc shaped) then equation

SI.(8) should be used, if it is prolate ellipsoid (football shaped) then equation SI.(9) should be used and if it is cylindrical then equation SI.(10) should be used:

$$D_{oblate} = \frac{k_B T}{6\pi\eta \dfrac{\left(l^2 - R^2\right)^{1/2}}{\tan^{-1}\left(\left(\dfrac{l^2 - R^2}{R^2}\right)^{1/2}\right)}} \Rightarrow R_{h,Oblate} = \frac{\left(l^2 - R^2\right)^{1/2}}{\tan^{-1}\left(\left(\dfrac{l^2 - R^2}{R^2}\right)^{1/2}\right)} \qquad \text{SI.(8)}$$

$$D_{prolate} = \frac{k_B T}{6\pi\eta \dfrac{\left(l^2 - R^2\right)^{1/2}}{\ln\left(\dfrac{l + \left(l^2 - R^2\right)^{1/2}}{R}\right)}} \Rightarrow R_{h,Prolate} = \frac{\left(l^2 - R^2\right)^{1/2}}{\ln\left(\dfrac{l + \left(l^2 - R^2\right)^{1/2}}{R}\right)} \qquad \text{SI.(9)}$$

$$D_{Cylinder} = \frac{k_B T}{6\pi\eta \dfrac{l}{\ln\left(\dfrac{l}{R}\right) + 0.312 + 1.13\dfrac{R}{2l} + 0.1\dfrac{R^2}{l^2}}} \Rightarrow R_{h,Cylinder} = \frac{l}{\ln\left(\dfrac{l}{R}\right) + 0.312 + 1.13\dfrac{R}{2l} + 0.1\dfrac{R^2}{l^2}}$$

SI.(10)

Where *l* and R are the major and minor semi axes of the ellipsoid. When R equals *l* these equations reduce to equations SI.(1) and SI.(2).

II.SI.9. References

1. Echalier, C., Jebors, S., Laconde, G., Brunel, L., Verdié, P., Causse, L., Bethry, A., Legrand, B., Van Den Berghe, H., Garric, X., Noël, D., Martinez, J., Mehdi, A. & Subra, G. Sol–gel synthesis of collagen-inspired peptide hydrogel. *Mater. Today* **20,** 59–66 (2017).

2. Cottet, H., Biron, J. P. & Martin, M. On the optimization of operating conditions for Taylor dispersion analysis of mixtures. *Analyst* **139,** 3552–3562 (2013).

3. Taylor, G. Conditions under which dispersion of a solute in a stream of solvent can be used to measure molecular diffusion. *Proc. R. Soc. London. Ser. A. Math. Phys. Sci.* **225,** 473–477 (1954).

4. Chamieh, J., Biron, J. P., Cipelletti, L. & Cottet, H. Monitoring Biopolymer Degradation by Taylor Dispersion Analysis. *Biomacromolecules* **16,** 3945–3951 (2015).

5. Cipelletti, L., Biron, J. P., Martin, M. & Cottet, H. Measuring Arbitrary Diffusion Coefficient Distributions of Nano-Objects by Taylor Dispersion Analysis. *Anal. Chem.* **87,** 8489–8496 (2015).

6. Cipelletti, L., Biron, J. P., Martin, M. & Cottet, H. Polydispersity analysis of Taylor dispersion data: The cumulant method. *Anal. Chem.* **86,** 6471–6478 (2014).

7. Hortschansky, P., Schroeckh, V., Christopeit, T., Zandomeneghi, G. & Fändrich, M. The aggregation kinetics of Alzheimer's beta-amyloid peptide is controlled by stochastic nucleation. *Protein Sci.* **14,** 1753–9 (2005).

8. Colvin, M. T., Silvers, R., Ni, Q. Z., Can, T. V., Sergeyev, I., Rosay, M., Donovan, K. J., Michael, B., Wall, J., Linse, S. & Griffin, R. G. Atomic Resolution Structure of Monomorphic Aβ42 Amyloid Fibrils. *J. Am. Chem. Soc.* **138,** 9663–9674 (2016).

9. Goddard, T. D., Huang, C. C., Meng, E. C., Pettersen, E. F., Couch, G. S., Morris, J. H. & Ferrin, T. E. UCSF ChimeraX: Meeting modern challenges in visualization and analysis. *Protein Sci.* **27,** 14–25 (2018).

10. Ortega, A., Amorós, D. & García De La Torre, J. Prediction of hydrodynamic and other solution properties of rigid proteins from atomic- and residue-level models. *Biophys. J.* **101,** 892–898 (2011).

11. Perrin, F. Mouvement Brownien d'un ellipsoide (II). Rotation libre et dépolarisation des fluorescences. Translation et diffusion de molécules ellipsoidales. *J. Phys. le Radium* **7,** 1–11 (1936).

12. IUPAC-IUB Joint Commission on Biochemical Nomenclature (JCBN). Nomenclature and symbolism for amino acids and peptides. Recommendations 1983. *Biochem. J.* **219,** 345–373 (1984).

Chapter II. Complement to Article 1. Application of Taylor Dispersion Analysis to the study of the inhibition of the aggregation of Aβ(1-42) in the presence of a β-sheet breaker

II.C.1. Introduction

Alzheimer disease (AD) is one of the common types of dementia leading to the slow degeneration of neurons and eventually death[1]. It starts in the hippocampus and for this reason it is frequently associated with discernment of time and place, lack of judgment, and memory loss[1,2]. One of the main hallmarks behind the development of AD is the formation of beta-amyloid (Aβ) aggregates that consequently lead to the formation of amyloid plaques in the brain[2]. Aβ monomers are produced during the amyloidogenic processing of the amyloid precursor protein (APP)[3]. The peptides further undergo a chain of supramolecular nucleation-condensation reactions that leads to a wide range of oligomeric and fibrillar species enriched in β-sheet content[4]. The most common isoforms are Aβ(1-40) and Aβ(1-42), the latter being considered the core of the aggregation process as it was found to generate more toxic species[4,5]. Nowadays, oligomers are considered the main therapeutic targets when developing compounds able to inhibit the aggregation process, whereas fibrils represent mainly a consequence of the amyloid chain of reactions as they are the end products of the aggregation and are believed to be less toxic[6,7]. In our previous study, we have demonstrated that Taylor dispersion analysis (TDA) allows the monitoring in real time of both the evolution and the hydrodynamic radius (R_h) of the main intermediates formed during the aggregation process, such as monomers, oligomers and protofibrils[8]. One important class of drugs capable to inhibit the formation of fibrils are β-sheet breakers[9]. One type of such inhibitor is iAβ5p (Ac-LPFFD-NH_2) and was initially reported by Soto *et.al*[10]. The authors showed that this inhibitor can bind the Aβ peptides to destabilize the β-sheet enriched structures and consequently prevent the formation of fibrils[9,10]. Hence, in this work we employ a TDA-UV method to check whether iAβ5p can also have an inhibitory effect upon the early stages of Aβ(1-42). Furthermore, we compared the results of the ThT assay obtained in this work with those obtained by De Bona *et al.*[11] which were acquired under similar experimental conditions.

II.C.2. Experimental part

II.C.2.1. Peptide pretreatment and sample preparation

Aβ(1-42) was pretreated using the protocol previously described[8,12]. Briefly, peptides were first dissolved in a 0.16% NH_4OH (2 g/L) solution and then incubated for 10 minutes at room temperature before being aliquoted. The stock aliquots used for TDA experiments contained 10 nmol of peptide, while the stock aliquots used for ThT fluorescence assay contained 30 nmol of peptide with or without the iAβ5p inhibitor. A stock solution containing the inhibitor was prepared by using the same concentration of 0.16% NH_4OH (2 g/L) and appropriate volumes were used in order to prepare the Aβ(1-42)/iAβ5p containing aliquots with the following ratios: 1/0; 1/1; 1/10; 1/25. Finally, both aliquots and the remaining inhibitor stock solutions were freeze-dried and stored at -20°C until use.

II.C.2.2. Aβ(1-42) inhibition study by Taylor dispersion analysis

TDA was performed using an Agilent 7100 (Waldbronn, Germany) capillary electrophoresis system with bare fused silica capillaries (Polymicro technologies, USA), having 60 cm × 50 µm i.d. dimensions and a UV detection window at 51.5 cm. The capillaries were conditioned with the following flushes: 1 M NaOH (30 min) followed by ultrapure water (30 min). Between each analysis, capillaries were rinsed for 2 min with a 20 mM phosphate buffer at pH 7.4 with or without the iAβ5p inhibitor by using a concentration of 0, 100, 1000 or 2500 µM respectively. Samples were injected hydrodynamically on the inlet end of the capillary (46 mbar, 6 s, injected volume of about 10.2 nL corresponding to 1.01% of the capillary volume with respect to the UV detection window). Experiments were performed at a mobilization pressure of 100 mbar. The temperature of the capillary cartridge was set at 37°C and the vial carrousel was thermostated using an external circulating water bath 600F from Julabo (Germany). The solutes were monitored by UV at 200 nm. The mobile phase was a 20 mM phosphate buffer (pH 7.4; viscosity at 37°C: 0.7×10^{-4} Pa.s)[12] with or without the inhibitor having a concentration of 0, 100, 1000 or 2500 µM, depending on the studied Aβ(1-42):iAβ5p ratios of 1:0, 1:1, 1:10 and 1:25 respectively. The concentration of the inhibitor was chosen to be the same as for the sample to avoid buffer mismatch during the TDA

analysis[13]. The mismatch can come from the UV absorption of the inhibitor which can alter the taylorgram profile, making it difficult to process[14]. The peptide aliquots were dissolved in 100 µL of 20 mM phosphate buffer, pH 7.4, containing the appropriate amount of inhibitor to reach a final concentration of 100 µM Aβ(1-42). The final solutions were then immediately transferred to a vial and incubated at 37°C in the capillary electrophoresis instrument's carrousel. The aggregation was conducted by injecting the sample every 11 min. The total TDA average recorded runs for each experiment was ~ 100, which corresponds to the total sample volume consumption of ~1000 nL (1 µL). Finally, to avoid the sample evaporation, the vial cap was changed three times a day. All taylorgrams were recorded with Agilent Chemstation software and then exported to Microsoft Excel for subsequent data processing.

II.C.2.3. ThT fluorescence assay

ThT fluorescence assay was realized to monitor the formation of fibrils under similar experimental conditions to those used for TDA. Fluorescence was monitored at room temperature for 24 h using a Berthold TriStar LB 941 instrument (Germany) (excitation wavelength 430 nm and emission wavelength 485 nm) equipped with a Costar® 96-well black polystyrene plate. A solution of 37.8 µM of ThT in 20 mM phosphate buffer, pH 7.4, was prepared by dilution from a 1 mM ThT stock solution. Each of the 30 nmol Aβ stock aliquots were dissolved in 300 µL of the ThT containing solution. Three wells were prepared for each aliquot containing 100 µL of 100 µM Aβ(1-42) with or without the inhibitor and 37.8 µM ThT in 20 mM phosphate buffer at pH 7.4. Three wells containing 100 µL of 37.8 µM of ThT in 20 mM phosphate buffer, pH 7.4, were used as control.

II.C.3. Results and Discussion

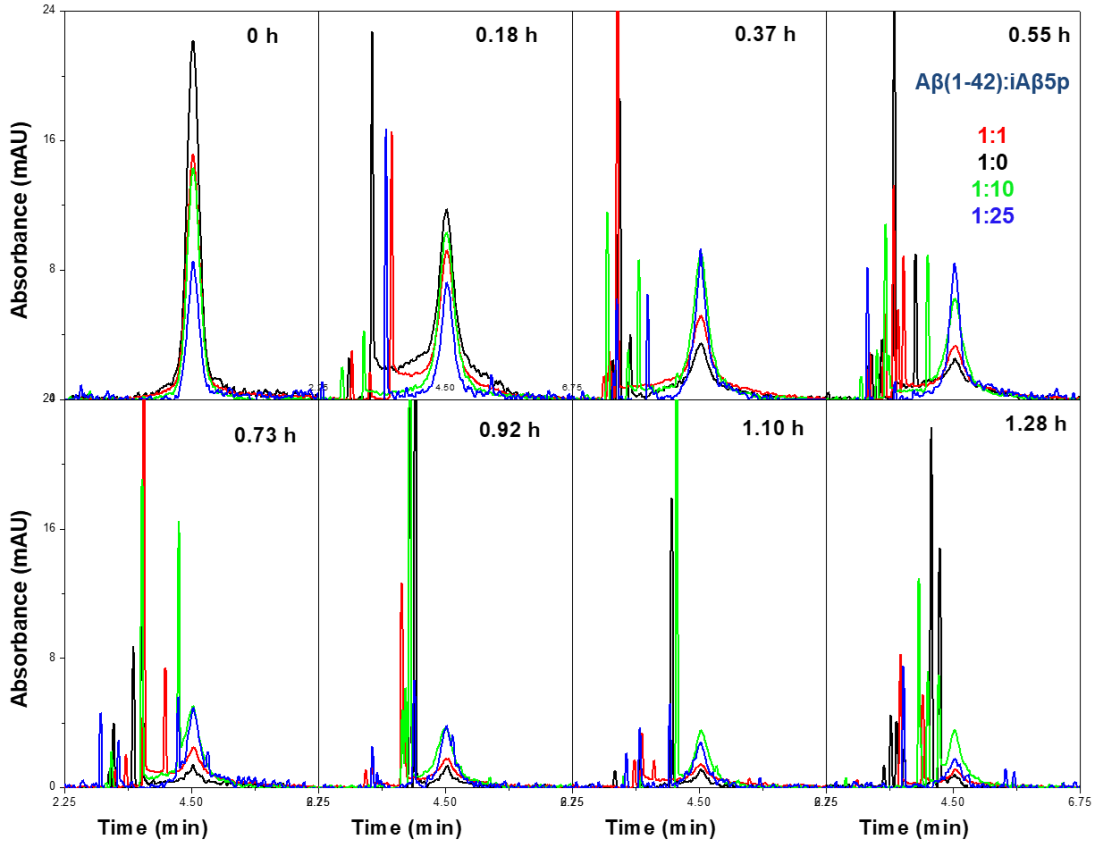

Figure 1. Comparison of experimental taylorgrams obtained for all the studied Aβ(1-42):iAβ5p ratios during the first hour of aggregation: 1:0 (black); 1:1 (red); 1:10 (green); 1:25 (blue). Experimental conditions: Sample: 100 µM with or without inhibitor; 20 mM phosphate buffer, pH 7.4. Incubation: quiescent conditions at 37 °C. Fused silica capillaries: 50 µm i.d. × 60 cm × 51.5 cm. Mobile phase: 20 mM phosphate buffer, pH 7.4. Mobilization pressure: 100 mbar. Injection: 46 mbar for 6 s, $V_i \approx 10$ nL (V_i / Vd ≈ 1 %). Analyses were performed at 37 °C. UV detection at 200 nm.

Figure 1 shows the experimental taylorgrams for the studied ratios (Aβ(1-42):iAβ5p 1:0, 1:1, 1:10, 1:25) and obtained during the first 1.28 h of incubation. As can be seen from the figure, a rapid decrease in peak intensity accompanied by a peak widening was observed within less than 1 h of aggregation in all cases. However, the decrease in peak area for the 1:25 ratio was observed at a lower rate than the other samples. After ~1.5 h of aggregation, the experimental peak decreased significantly in intensity and reached the baseline, suggesting that all soluble species were

consumed very rapidly and a fibril plateau was reached. These initial observations suggested that the aggregation occurred very quickly for all the studied ratios. It also appears that the abundance of spikes, representing nondiffusing insoluble fibrils able to enter the capillary[8], decreased in the order of increasing ratio of the inhibitor which further suggest a possible inhibition of the fibrils by iAβ5p as presented in Figure 3.

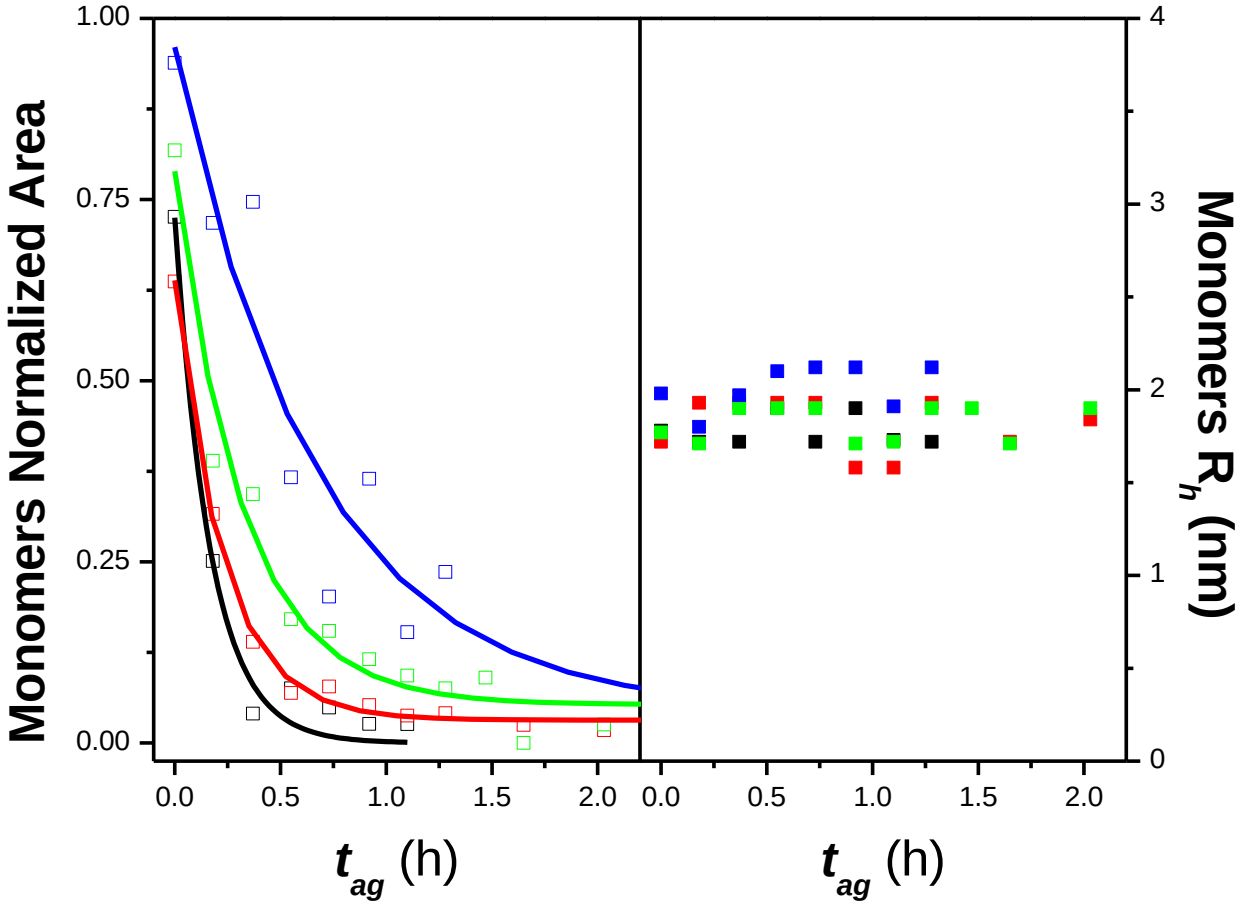

Figure 2. Monomer peak area (left layer) and hydrodynamic radius (right layer) evolution obtained during the first hour of aggregation for all the studied Aβ(1-42):iAβ5p ratios: 1:0 (black); 1:1 (red); 1:10 (green); 1:25 (blue). Open symbols represent the peak area and closed symbols correspond to the hydrodynamic radius. The straight lines are guides for the eyes. Peak area was independently normalized for each ratio by dividing each value to the total theoretical peak area obtained for the first run. Experimental conditions as in Figure 1.

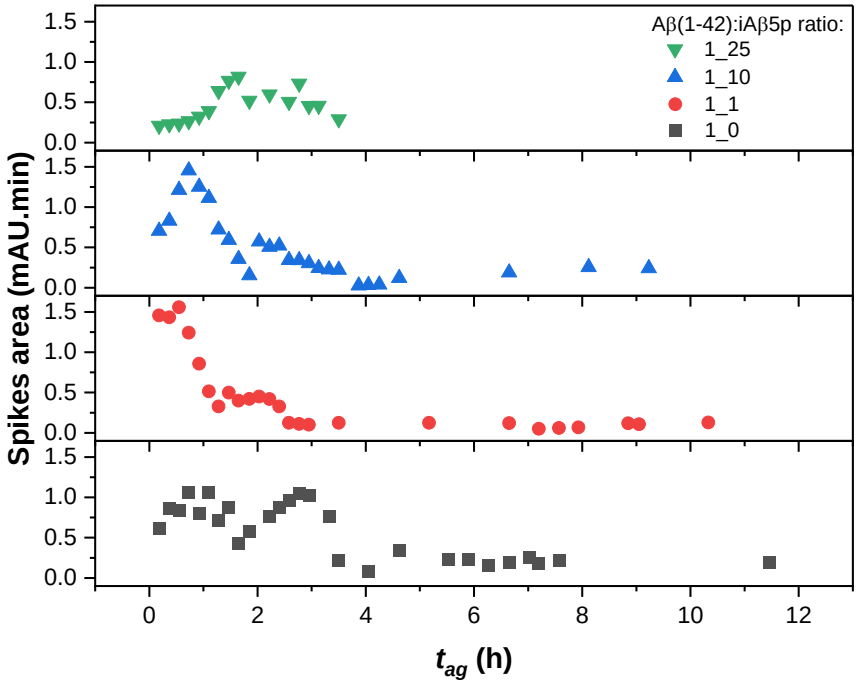

Figure 3. Representation of the area evolution of the nondiffusing species (detected suspended fibrils) for all the studied Aβ(1-42):iAβ5p ratios during 12 h of incubation. Spike values were smoothed to get a better visual insight of the evolution during each ratio. Experimental conditions as in Figure 1.

One inconvenience of using UV as a detection mode in this study, is that the inhibitor, present in the mobile phase, contributes to the total absorbance which lowers the sensitivity and increases the noise, leading to lower peak areas with increasing inhibitor ratio (see Figure 1 t_{ag} = 0 h for all ratios). In order to better compare the effect of the inhibitor on the peptide aggregation, especially the monomer consumption, a normalization of the peak areas was applied at all times by dividing the corresponding monomer population peak with the peak area of the monomer population obtained at t_{ag} = 0 h (Figure 2). Indeed, as demonstrated in our previous study, TDA analysis allows the monitoring of the aggregation kinetics in terms of monomer consumption[8]. As can be seen in Figure 2 (left layer) Aβ(1-42) (1:0) presented the fastest kinetics reaching the lower plateau after only 30 min. When the inhibitor was added to the sample, the kinetics were slightly delayed. The delay effect was slightly improved each time the inhibitor concentration increased (1:0>1:1>1:10>1:25) (Figure 2, left layer), while the size of the monomer (Figure 2, right layer) was constant with a R_h of ~1.9 nm during the whole aggregation process. These results suggest that Aβ(1-42) fibrils are inhibited by iAβ5p.

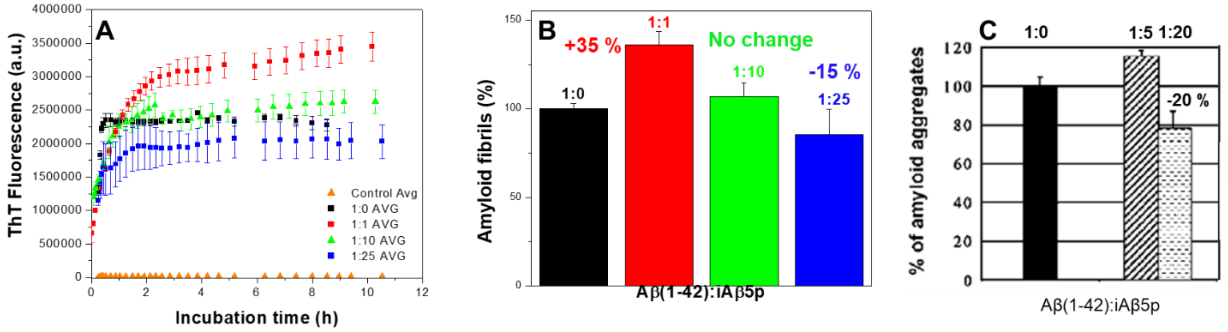

Figure 4. Comparison between the ThT fluorescence assays performed for all the studied Aβ(1-42):iAβ5p ratios: 1:0 (black); 1:1 (red); 1:10 (green); 1:25 (blue) obtained in this work (A and B) and the results employed by De Bona *et al.* (C, adapted from[11]). Experimental conditions for (A) and (B): 100 µM Aβ(1-42) (with or without inhibitor) + 38 µM ThT; 20 mM phosphate buffer, pH 7.4. Incubation: quiescent conditions at 37 °C. Fluorescence detection: λ_{Em}= 485 nm; λ_{Ex}= 430 nm. Error bars stand for standard deviation of three replicas. Experimental conditions for (C): 100 µM Aβ(1-42) (with or without inhibitor) + 10 µM ThT; 20 mM phosphate buffer, pH 7.4. Incubation: quiescent conditions at 37 °C. Fluorescence detection: λ_{Em}= 480 nm; λ_{Ex}=440 nm.

To confirm the results obtained by TDA, the inhibition effect of iAβ5p was verified by ThT fluorescence assay. For all studied Aβ(1-42):iAβ5p ratios, no lag phase was observed by ThT fluorescence assay (Figure 4 A), but rather a rapid increase in fluorescence intensity leading rapidly to a fibril plateau. In the case of the Aβ(1-42) independent experiment, a very high fluorescence intensity (black filled symbols) was observed immediately after the dissolution and the slope was only partially recorded, suggesting the presence of aggregates in the sample at t_{ag} = 0 h. When the inhibitor was added to the sample, no lag phase was observed however the final fluorescence intensity was slightly slower suggesting somehow a small inhibition effect. Further, it is noteworthy to mention that for all studied excess ratios, the fluorescence intensity could not recorded for t= 0 h due to the longer solubilization time of the Aβ(1-42):iAβ5p aliquots (reduced solubility), and the dead time was 10 min in the case of the 10-fold excess experiment and 15 min for the 25-fold ratio, respectively. These observations, are in agreement with the data published by De Bona *et al.*[11], under similar experimental conditions. The authors designed new trehalose-conjugated peptides derived from iAβ5p and used the latter as a control. In their study (Figure 4 C**)** a 20 % reduction in the fluorescence plateau was observed for the 20-fold ratio compared with the Aβ(1-42) independent experiment, whereas a ~15% reduction was recorded in the current study for the 25-fold ratio (Figure 4 B).

In conclusion, the results obtained by TDA were comparable to those obtained by ThT and are in accordance with the findings in the literature. No significant inhibition effect was observed for

the iAβ5p β-sheet breaker, which had only a small retarding effect on the kinetics of the aggregation. Nevertheless, TDA was shown to be a powerful method for screening potential drugs that could be used as aggregation inhibitors. Unfortunately, the presence of the inhibitor increased the signal's noise reducing the reliability of the results obtained on the intermediate species which are more influenced by the baseline during the data treatment, reason for which the oligomers and protofibrils populations are not discussed in this chapter.

In perspective, the use of non UV absorbing drugs or the combination of TDA with fluorescence detection (by tagging the Aβ peptides) could allow to reduce the effect of the baseline and to follow the Aβ aggregation inhibition by other drugs such as some recently designed ATC foldamers which can inhibit the self-assembly process from the beginning of the aggregation[16].

II.C.4. References

1. *2019 Alzheimer's disease facts and figures*. *Alzheimer's Dement.* **15,** (2019).
2. Folch, J., Ettcheto, M., Petrov, D., Abad, S., Pedrós, I., Marin, M., Olloquequi, J. & Camins, A. Review of the advances in treatment for Alzheimer disease: strategies for combating β-amyloid protein. *Neurol. (English Ed.* **33,** 47–58 (2018).
3. Chen, G. F., Xu, T. H., Yan, Y., Zhou, Y. R., Jiang, Y., Melcher, K. & Xu, H. E. Amyloid beta: Structure, biology and structure-based therapeutic development. *Acta Pharmacol. Sin.* **38,** 1205–1235 (2017).
4. Nasica-Labouze, J., Nguyen, P. H., Sterpone, F., Berthoumieu, O., Buchete, N. V., Coté, S., De Simone, A., Doig, A. J., Faller, P., Garcia, A., Laio, A., Li, M. S., Melchionna, S., Mousseau, N., Mu, Y., Paravastu, A., Pasquali, S., Rosenman, D. J., Strodel, B., Tarus, B., Viles, J. H., Zhang, T., Wang, C. & Derreumaux, P. Amyloid β Protein and Alzheimer's Disease: When Computer Simulations Complement Experimental Studies. *Chem. Rev.* **115,** 3518–3563 (2015).
5. Lesné, S. E. Breaking the code of amyloid-β oligomers. *Int. J. Cell Biol.* (2013). doi:10.1155/2013/950783
6. Cummings, J., Lee, G., Ritter, A., Sabbagh, M. & Zhong, K. Alzheimer's disease drug development pipeline: 2019. *Alzheimer's Dement. Transl. Res. Clin. Interv.* **5,** 272–293 (2019).
7. Iadanza, M. G., Jackson, M. P., Hewitt, E. W., Ranson, N. A. & Radford, S. E. A new era for understanding amyloid structures and disease. *Nat. Rev. Mol. Cell Biol.* **19,** 755–773 (2018).
8. Deleanu, M., Hernandez, J.-F., Cipelletti, L., Biron, J.-P., Rossi, E., Taverna, M., Cottet, H. & Chamieh, J. Unraveling the Speciation of β-Amyloid Peptides during the Aggregation Process by Taylor Dispersion Analysis. *Anal. Chem.* (2021).

9. Adessi, C. & Soto, C. Beta-sheet breaker strategy for the treatment of Alzheimer's disease. *Drug Dev. Res.* **56,** 184–193 (2002).

10. Soto, C., Kindy, M. S., Baumann, M. & Frangione, B. Inhibition of Alzheimer's amyloidosis by peptides that prevent β-sheet conformation. *Biochem. Biophys. Res. Commun.* **226,** 672–680 (1996).

11. De Bona, P., Giuffrida, M. L., Caraci, F., Copani, A., Pignataro, B., Attanasio, F., Cataldo, S., Pappalardo, G. & Rizzarelli, E. Design and synthesis of new trehalose-conjugated pentapeptides as inhibitors of Aβ(1-42) fibrillogenesis and toxicity. *J. Pept. Sci.* **15,** 220–228 (2009).

12. Brinet, D., Kaffy, J., Oukacine, F., Glumm, S., Ongeri, S. & Taverna, M. An improved capillary electrophoresis method for in vitro monitoring of the challenging early steps of Aβ(1-42) peptide oligomerization: Application to anti-Alzheimer's drug discovery. *Electrophoresis* **35,** 3302–3309 (2014).

13. Latunde-Dada, S., Bott, R., Hampton, K., Patel, J. & Leszczyszyn, O. I. Methodologies for the Taylor dispersion analysis for mixtures, aggregates and the mitigation of buffer mismatch effects. *Anal. Methods* **7,** 10312–10321 (2015).

14. Schmid, F.-X. Biological Macromolecules: UV-visible Spectrophotometry. *Encycl. Life Sci.* (2001). doi:10.1038/npg.els.0003142

15. Kaffy, J., Berardet, C., Mathieu, L., Legrand, B., Taverna, M., Halgand, F., Van Der Rest, G., Maillard, L. T. & Ongeri, S. Helical γ-Peptide Foldamers as Dual Inhibitors of Amyloid-β Peptide and Islet Amyloid Polypeptide Oligomerization and Fibrillization. *Chem. - A Eur. J.* **26,** 14612–14622 (2020).

Chapter III

Research Article 2

Taylor Dispersion Analysis and Atomic Force Microscopy Provide a Quantitative Insight into the Aggregation Kinetics of Aβ (1−40)/Aβ (1−42) Amyloid Peptide Mixtures

Chapter III. Article 2. Taylor dispersion analysis and atomic force microscopy provide a quantitative insight into the aggregation kinetics of Aβ (1−40)/Aβ (1−42) amyloid peptide mixtures

This chapter was published in *ACS Chem. Neurosci.*, 2022, 13, 786−795
https://doi.org/10.1021/acschemneuro.1c00784

Mihai Deleanu[1], Olivier Deschaume[2], Luca Cipelletti[3,4], Jean-François Hernandez[1], Carmen Bartic[2], Hervé Cottet*[1], Joseph Chamieh*[1]

[1] IBMM, Univ Montpellier, CNRS, ENSCM, 34095 Montpellier, France
[2] Department of Physics and Astronomy, Soft-Matter Physics and Biophysics Section, KU Leuven, Celestijnenlaan 200D, Box 2416, 3001 Heverlee, Belgium
[3] L2C, Université Montpellier, 34095 Montpellier, France
[4] Institut Universitaire de France (IUF), Paris, France

[*] CORRESPONDING AUTHORS
Tel: +33 4 6714 3920, Fax: +33 4 6763 1046. E-mail: joseph.chamieh@umontpellier.fr
Tel: +33 4 6714 3427, Fax: +33 4 6763 1046. E-mail: herve.cottet@umontpellier.fr

III. Abstract

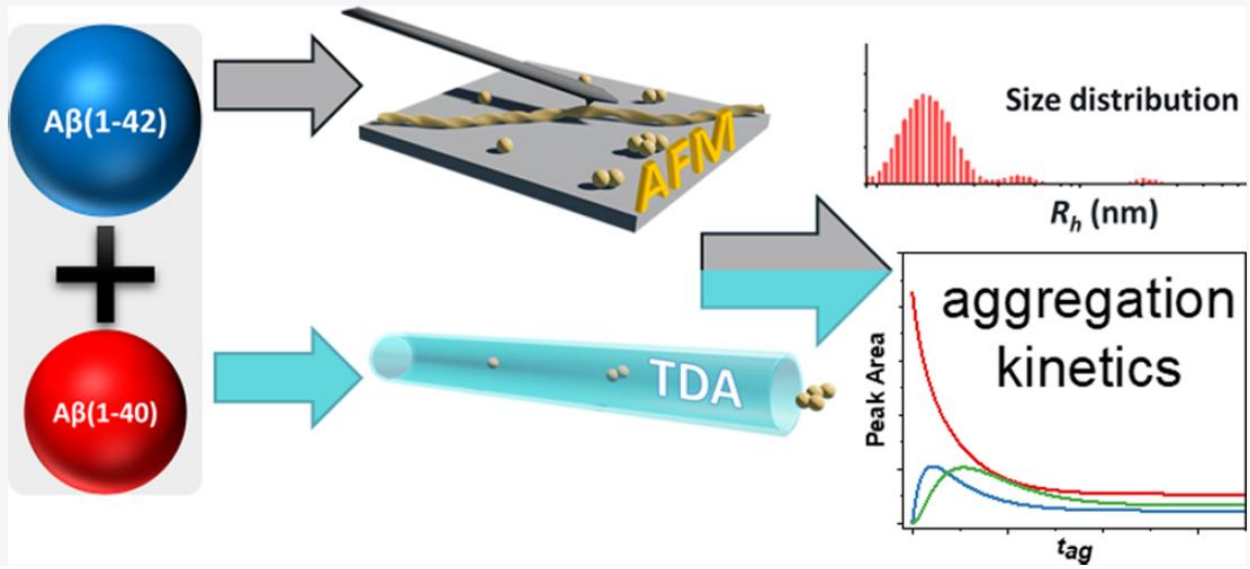

Aggregation of amyloid β peptides is known to be one of the main processes responsible for Alzheimer's disease. The resulting dementia is believed to be due in part to the formation of potentially toxic oligomers. However, the study of such intermediates and the understanding of how they form are very challenging because they are heterogeneous and transient in nature. Unfortunately, few techniques can quantify, in real time, the proportion and the size of the different soluble species during the aggregation process. In a previous work (Deleanu et al. Anal. Chem. 2021, 93, 6523−6533), we showed the potential of Taylor dispersion analysis (TDA) in amyloid speciation during the aggregation process of Aβ (1−40) and Aβ (1−42). The current work aims at exploring in detail the aggregation of amyloid Aβ (1−40): Aβ (1−42) peptide mixtures with different proportions of each peptide (1:0, 3:1, 1:1, 1:3, and 0:1) using TDA and atomic force microscopy (AFM). TDA allowed for monitoring the kinetics of the amyloid assembly and quantifying the transient intermediates. Complementarily, AFM allowed the formation of insoluble fibrils to be visualized. Together, the two techniques enabled us to study the influence of the peptide ratios on the kinetics and the formation of potentially toxic oligomeric species.

KEYWORDS. Taylor dispersion analysis; AFM; peptide aggregation; oligomers; amyloid beta peptides; diffusion coefficient; hydrodynamic radius.

III.1. Introduction

Alzheimer's disease (AD) is the most common primary dementia. It usually presents a progressive course and characteristically affects different cognitive and behavioral functions. Perhaps the cardinal, most frequently observed symptom of disease onset is memory loss[1], which results from initial lesions in the hippocampus (which lies in the medial temporal lobes of the brain and is responsible for long-term memory), further extending to the rest of the brain. At later stages, the degeneration of other cognitive and behavioral areas is observed, which will clearly indicate the type of dementia.

The brains of Alzheimer's patients present a series of characteristic hallmarks. First, neurofibrillary tangles composed of hyperphosphorylated tau protein are observed in neurons. Then, extracellular fibrillary structures called neuritic (or senile) plaques, which are due to the deposition of amyloid β peptides (Aβ), are observed[2]. In the 1990s, it was believed that the senile plaques were the most pathogenic forms of the Aβ[3,4], which resulted from the self-assembly of the two major amyloid peptides Aβ (1−40) and Aβ (1−42). During this self-assembly, species are formed with evolving morphology and size from oligomers to protofibrils and finally to fibrils and plaques through a highly complicated process.

More recent studies suggested that the main factor of AD pathogenesis was the formation of soluble oligomers of Aβ, which are believed to be more toxic than plaques because they are able to spread across neuronal tissue and bind to membrane receptors, including the prion protein, promoting neurotoxicity and synaptic loss[5–7]. However, in contrast to fibrils, which are highly stable and can be observed by microscopy, the soluble oligomers are more difficult to detect and to study in real time[8] because they are metastable, transient[8], and highly polydisperse in size. Studies have shown that Aβ (1−40) does not quantitatively form small oligomers during the aggregation process but rather goes from monomers to fibrils following a direct pathway[9,10]. On the other hand, Aβ (1−42) goes through the formation of intermediate species with diverse sizes and shapes[11,12]. Although these two amyloid peptides coexist in vivo[13,14], most of the in vitro studies on Aβ were focused on pure peptide solutions and only a small proportion of the vast AD literature was dedicated to mixtures of these peptides[15–18]. Many of the studies dealing with the mixtures were directed toward the kinetics of the aggregation process and more particularly the study of the amyloid fibers[15–17,19–21] and very few toward the oligomeric structures[18]. The

aggregation process in such mixtures was already studied by Thioflavin T fluorescence[17,21], sedimentation[15], atomic force microscopy (AFM)[16,19], nuclear magnetic resonance[22,23], or electron paramagnetic resonance[18] to name a few methods. The results from these studies indicated that both Aβ (1−40) and Aβ (1−42) interact during the aggregation process, with cross seeding between peptides. However, some authors claimed that the fibrils are homomolecular[17], while others stated that heteromolecular[18] fibrils are obtained. In all cases, it was observed that the presence of Aβ (1−42) accelerated the aggregation of Aβ (1−40) and vice versa. To our knowledge, an in-depth study on the species present during the early stages of the aggregation of amyloid peptide mixtures does not exist to date. For that reason, and to help develop drug candidates targeting the toxic oligomers, new analytical methodologies are required to monitor and size the different species in real time.

In this context, Taylor dispersion analysis[24–26] (TDA) appears as a very promising alternative analytical method. In our previous report[27], we showed the ability of TDA to follow the aggregation process of amyloid peptides using an extensive data treatment that revealed a complete picture of the aggregation process and allowed us to size the transient structures. As described elsewhere, TDA allows us to determine the molecular diffusion coefficient, *D*, and hydrodynamic radius, R_h, of a solute, including for mixtures, without any bias in size as compared to other sizing methods[28], because the small and the large solutes contribute proportionally to their mass abundance in the mixture[29]. The use of TDA in the field of protein aggregation presents several advantages[30–33]. It offers low sample consumption (less than 1 µL for the whole aggregation process), short analysis time allowing for a high number of sampling points and real time monitoring of the aggregation, a wide range of sizing (from angstrom to sub-micron) allowing us to size the monomers, oligomers, and higher size soluble prefibrillar structures, and a direct analysis without any sample pretreatment or filtration[34–36].

In this work, we used TDA to study peptide mixtures of Aβ (1−40) and Aβ (1−42) with the aim of revealing the size of the transient structures formed during the aggregation process. The results for the selected time points were compared with those obtained by AFM to correlate the observations from these two independent techniques. AFM also allowed us to study nonsoluble fibrils, which cannot be sized or directly observed by TDA.

III.2. Materials and methods

III.2.1. Materials

Synthesized Amyloid beta (1-40) (denoted Aβ (1-40) in this work) was prepared by fast conventional solid phase peptide synthesis (SPPS) using a *Fmoc* orthogonal strategy as described elsewhere[27]. Amyloid beta (1-42) [(Aβ (1-42), batch number 100002591, >95%)] was purchased from Bachem (Bubendorf, Switzerland). Sodium dihydrogen phosphate, tris(hydroxymethyl)aminomethane, hydrochloric acid fuming 37%, sodium chloride and sodium hydroxide were purchased from Sigma Aldrich (France). The ultrapure water used for all buffers was prepared with a MilliQ system from Millipore (France).

III.2.2. Peptide pretreatment

Both Aβ (1-40) and Aβ (1-42) were first pretreated independently as described elsewhere[54,55]. Briefly, Aβ (1-40) and Aβ (1-42) were dissolved in a 0.10 % (m/v) and 0.16 % (m/v) NH_4OH aqueous solution respectively to reach a final peptide concentration of 2 mg/mL. The peptide solutions were then incubated at room temperature for 10 min, separated into several aliquots and freeze-dried. The aliquot volume was calculated in order to obtain 10 nmol of peptide in each Eppendorf tube. The lyophilized peptide aliquots were stored at -20 °C until use.

III.2.3. Peptide aggregation study by Taylor dispersion analysis

Briefly, and as described thoroughly elsewhere[24,25,29,30], Taylor dispersion analysis allows for the determination of the molecular diffusion coefficient of a solute which can be obtained from the band broadening resulting from the combination of the Poiseuille parabolic flow and the molecular diffusion by quantifying the temporal variance (σ^2) of the elution profile. For that, a Gaussian function is used to fit the experimental elution peak allowing to obtain the peak variance σ^2 and thus calculate the molecular diffusion coefficient, D, and consequently the hydrodynamic radius, R_h. When more than one size populations are present, a sum of Gaussian functions can be used to fit the experimental trace, or Constrained Regularized Linear Inversion (CRLI)[40] can be used to

get the size distribution. For more details, the reader may refer to the supporting information for the theoretical aspects, equations and more details on the data processing.

TDA was performed on an Agilent 7100 (Waldbronn, Germany) capillary electrophoresis system using bare fused silica capillaries (Polymicro technologies, USA) having 40 cm × 50 µm i.d. dimensions and a detection window at 31.5 cm. New capillaries were conditioned with the following flushes: 1 M NaOH for 30 min; ultrapure water for 30 min. Between each analysis, capillaries were rinsed with 20 mM phosphate buffer, pH 7.4 (2 min). Samples were injected hydrodynamically on the inlet end of the capillary (44 mbar, 3 s, injected volume was about 7 nL corresponding to 1% of the capillary volume to the detection point). Experiments were performed using a mobilization pressure of 100 mbar. The temperature of the capillary cartridge was set at 37 °C. The vial carrousel was thermostated using an external circulating water bath 600F from Julabo (Germany). The solutes were monitored by UV absorbance at 191 nm. The mobile phase was a 20 mM, pH 7.4 phosphate buffer (viscosity at 37 °C is 0.7×10^{-4} Pa.s). To prepare the mixtures, freeze-dried mixed peptide aliquots were prepared so that the final sample would contain 13 nmol of total peptide except for the pure samples where the amount of peptide was of 10 nmol. First, each of the required stock aliquots (see previous section) were dissolved in 100 µL of 0.16% (m/v) NH_4OH to avoid aggregation during this step, and appropriate volumes were used to obtain the desired mixtures. The final aliquots were immediately subjected to freeze-drying and then stored at -20°C until further use. The resulting peptide powders were dissolved in 20 mM phosphate buffer at pH 7.4 to reach a final total peptide concentration of 133 µM : *i*) 100 % Aβ(1-40) contained 10 nmol of Aβ(1-40) dissolved in 75 µL of buffer; *ii*) 75 % Aβ(1-40) and 25 % Aβ(1-42) mixture contained 10 nmol of Aβ(1-40) and 3.33 nmol of Aβ(1-42) dissolved in 100 µL of buffer; *iii*) 50 % Aβ(1-40) and 50 % Aβ(1-42) mixture contained 6.67 nmol of each peptide and was dissolved in 100 µL of buffer; *iv*) 25 % Aβ(1-40) and 75 % Aβ(1-42) mixture contained 3.33 nmol of Aβ(1-40) and 10 nmol of Aβ(1-42) dissolved in 100 µL of buffer and finally *v*) 0 % Aβ(1-40) contained 10 nmol of Aβ(1-42) dissolved in 75 µL of buffer. After dissolution, the mixtures were immediately transferred to a capillary electrophoresis vial and incubated at 37°C in the capillary electrophoresis instrument carrousel. Aggregation was monitored by injecting the sample ($V_{inj} \approx 7$ nL) every 7 min in the case of pure Aβ(1-42) and the Aβ(1-40): Aβ(1-42) 1:3 mixture (25 % Aβ(1-40)), while it was injected every 20 min for the Aβ(1-40): Aβ(1-42) 1:1 mixture (50 % Aβ(1-40)) and every 30 min in the case of pure Aβ(1-40) and the Aβ(1-40): Aβ(1-42) 3:1 mixture

(75 % Aβ(1-40)). During the monitoring of the aggregation process, each sample was injected for 100 to 125 TDA runs, corresponding to a total injected sample volume between 700 nL and 875 nL. To avoid sample evaporation, the vial cap was changed three times a day. The taylorgrams were recorded with the Agilent Chemstation software, then exported to Microsoft Excel for subsequent data processing. In general, the obtained elution profiles were not Gaussian, meaning that the sample was polydisperse in size. All taylorgrams were fitted on the basis of the right-side elution profile (*i.e.* $t > t_0$, with t_0 the peak time) to get rid of the spikes that are present on the left side as described elsewhere[27].

III.2.4. Atomic force microscopy (AFM)

For atomic force microscopy characterisation, 5 µL aliquots of the peptide solutions collected at different aggregation times were dried on silicon substrates freshly cleaned with piranha solution, before gently rinsing with ultrapure water and drying in a flow of nitrogen gas. An Agilent 5500 AFM system with MSNL-F cantilevers (f = 110=120 kHz, k = 0.6 N/m, average tip radius of 2-12 nm) was used for topographical imaging in intermittent contact mode. The AFM topography images were levelled, line-corrected and analysed using Gwyddion[56], a free and open-source SPM (scanning probe microscopy) data visualization and analysis program. Maxima analysis was performed using ImageJ[57].

III.3. Results and discussion

III.3.1. TDA and data processing

TDA and Data Processing. One main objective of this work is to show the influence of the relative proportion of Aβ (1−40) with respect to Aβ (1−42) on the aggregation process. The aggregation of the peptides in the different mixtures was followed at 37 °C. Figure 1 shows the taylorgrams recorded at selected incubation times for Aβ (1−40), Aβ (1−40):Aβ (1−42) mixtures [with a molar ratio of Aβ (1−40) in the mixture of 25, 50, and 75% corresponding to 3:1, 1:1, and 1:3 mixtures], and Aβ (1−42). The total peptide concentration in each solution was set at 133.3 µM. All experimental taylorgrams, for all incubations times t_{ag}, are shown in Figures S1−S5. Figure 1 allows for a visual comparison of the aggregation kinetics between the different amyloid

peptide ratios. The absorbance decrease of the elution profile with t_{ag}, which is due to the decrease in concentration of the soluble species, was faster when increasing the Aβ (1−42) content in the mixture, as previously observed for pure peptide solutions[27].

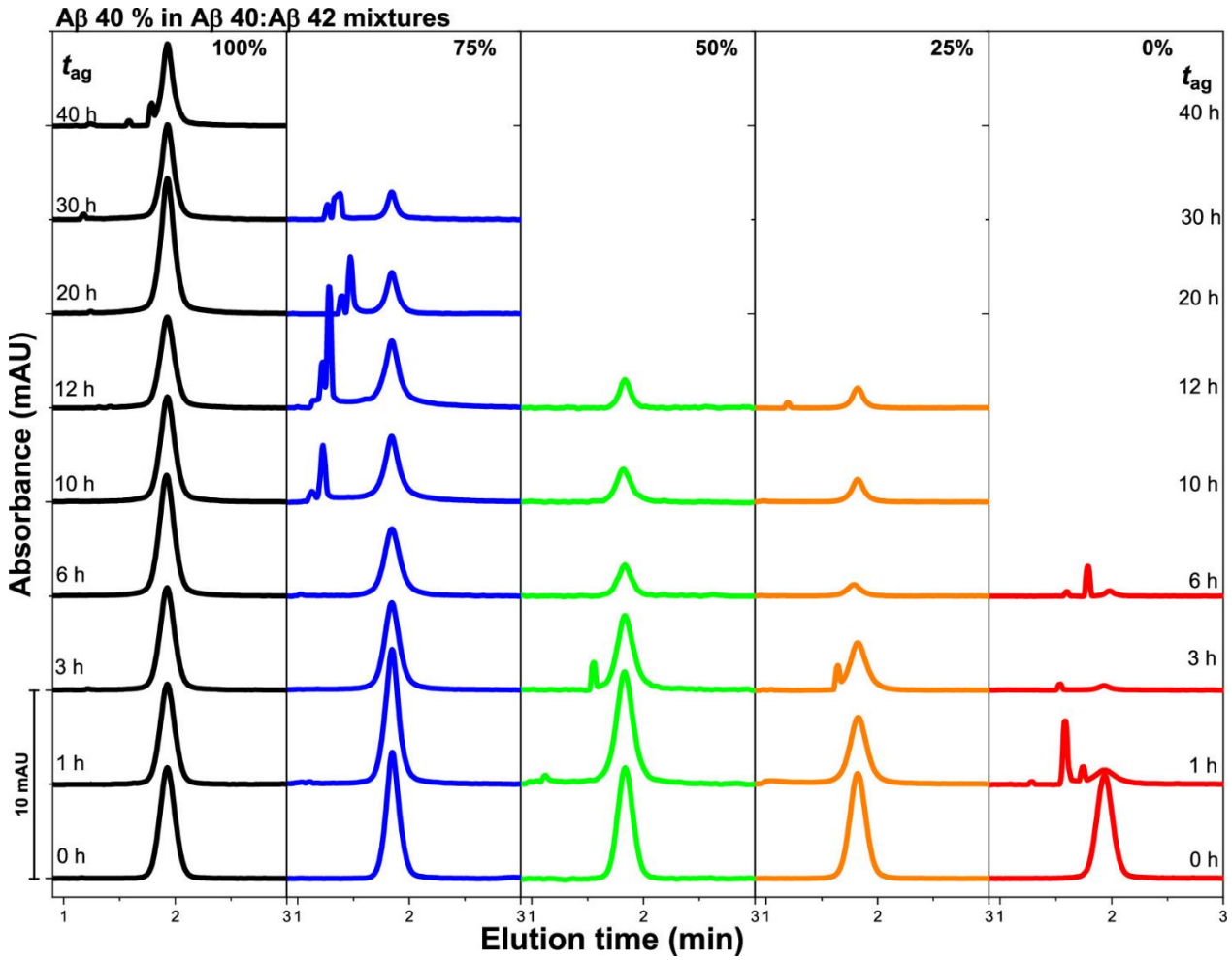

Figure 1. Overview of selected obtained taylorgrams during the aggregation process of Aβ (1-40):Aβ (1-42) mixtures [(Aβ(1-40) % of 100 %; 75%; 50%; 25% and 0%)] at different common incubation times. Experimental conditions: Sample: 133 µM of total peptide; 20 mM phosphate buffer, pH 7.4. Incubation: quiescent conditions at 37 °C. Fused silica capillaries: 50 µm i.d. × 40 cm × 31.5 cm. Mobile phase: 20 mM phosphate buffer, pH 7.4. Mobilization pressure: 100 mbar. Injection: 44 mbar for 3 s, Vi ≈ 7 nL (Vi / Vd ≈ 1 %). Analyses were performed at 37 °C. UV detection at 191 nm.

In order to elucidate the aggregation process in these solutions, an extensive data treatment was realized on all the obtained taylorgrams. As already observed in our previous report[27], sharp peaks or spikes sometimes appear on the left side of the elution peak because of the presence of large fibrils in suspension, which are out of the Taylor regime[37,38] and/or due to specific hydrodynamic behavior for suspended large aggregates[39]. The presence of these spikes imposes a data treatment on the right side of the elution profile. Two different approaches were used to treat

the experimental elution profiles. First, the fitting with a finite number of Gaussian functions (n =4 in this work) leads to the classification of the obtained size populations into four categories: (i) small unidentified molecules (R_h < 0.9 nm), (ii) monomers and small oligomers (0.9 nm < R_h < 5 nm), (iii) higher mass oligomers (5 nm < R_h < 50 nm), and finally (iv) soluble protofibrils (50 nm < R_h < 300 nm). The second approach is based on the Constrained Regularized Linear Inversion (CRLI), which aims at finding the probability density function $P_D(D)$ that fits the taylorgram without any hypothesis on the number of populations[40].

III.3.2. Aggregation process of pure and mixed solutions of Aβ peptides

In the case of Aβ (1−40) alone, the first sign of spikes (fibrils) appears at t_{ag} ∼12 h (Figure S1). However, the spike intensity remained relatively low and did not increase drastically over the whole aggregation process (see gray data points in Figure 2). In parallel, the monomer peak intensity remained constant until t_{ag} ∼ 20 h ("lag phase)" and then decreased rapidly to reach a lower plateau after t_{ag} ∼ 48 h (red squares in Figure 2). This suggests an initial slow aggregation step followed by a rapid fibrillization catalyzed by the formation of large aggregates (seeds) that do not enter the capillary upon injection[41], in accordance with our previous report where another concentration (100 μM) of Aβ (1−40) was used[27].

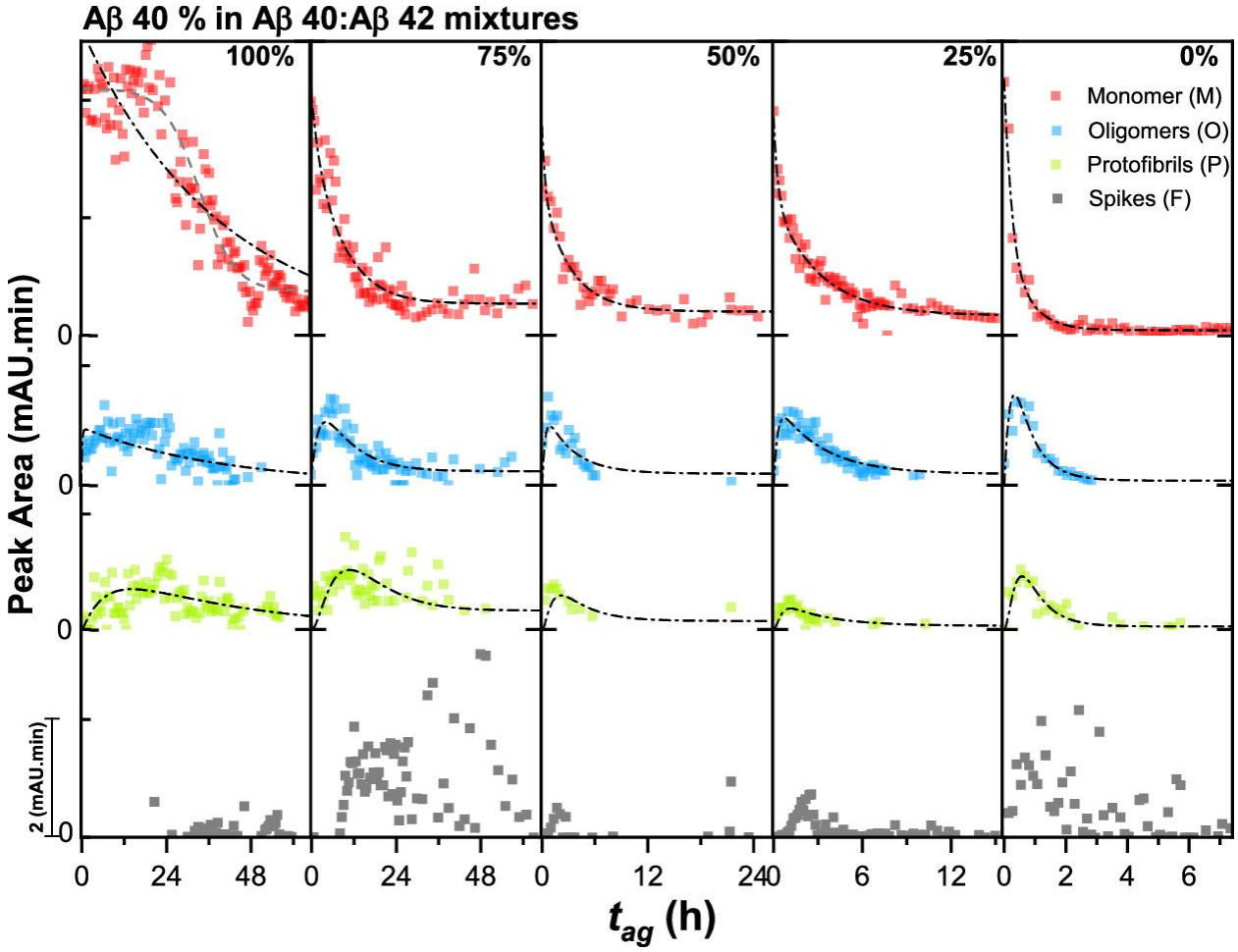

Figure 2. Peak area evolution of the different populations observed during the aggregation process of Aβ(1-40):Aβ(1-42) mixtures and obtained using a fit with finite number of Gaussian functions. Three size populations are represented: monomer and low molar mass oligomers (■), higher molar mass oligomers (■), soluble protofibrils (■) and non-diffusing species ("spikes") (■). Experimental conditions as in Figure 1. Dashed lines are guide for the eyes.

On the contrary, Aβ (1-42) alone did not show any lag phase and a fast decrease of this population was observed with a complete disappearance after less than 2 h. Meanwhile, when mixed together, Aβ (1-42) seemed to increase the kinetics of aggregation, with the monomer population decreasing after 15 h, 8 h and 6 h for the 75%, 50% and 25% Aβ (1-40) mixtures respectively, without any visible lag phase.

Table 1. Average hydrodynamic radius of the monomer, oligomers and protofibrils size populations obtained by the deconvolution of the taylorgrams with a finite number of Gaussian functions and as a function of the ratio of the proportion in Aβ(1-40) in the Aβ(1-40):Aβ(1-42) mixtures[a].

	Populations' size						**Kinetic parameters**							
% Aβ(1-40) in Aβ(1-40):Aβ(1-42) mixtures	**Monomer and small oligomers**		**Higher mass oligomers**		**Protofibrils**		**Forward reactions**			**Backward reactions**				
	$\langle R_h \rangle$ (nm)	**± SD**	**$\langle R_h \rangle$ (nm)**	**± SD**	**$\langle R_h \rangle$ (nm)**	**± SD**	**k_{MO} (h^{-1})**	**k_{OP} (h^{-1})**	**k_{PF} (h^{-1})**	**k_{OM} (h^{-1})**	**k_{PM} (h^{-1})**	**k_{FM} (h^{-1})**	**$t_{Oligomers}$, max (h)**	**M(t=0) (mAU.min)**
100	2.0	0.1	13.0	8.5	101.2	57.8	N.A.	N.A.	N.A.	N.A.	N.A.	N.A.	N.A.	N.A.
75	2.4	0.2	9.3	1.8	140.2	43.7	1.106	0.817	0.943	1.497	0.123	0.050	4.171	3.551
50	2.0	0.2	13.1	10.2	89.5	39.4	0.182	0.240	0.171	0.179	0	0.018	0.884	4.268
25	2.0	0.2	17.9	10.4	135.6	56.9	1.457	1.226	2.190	1.386	1.332	0.045	0.722	3.709
0	1.8	0.1	19.1	9.8	99.5	40.7	2.991	3.409	3.704	0	0.998	0.048	0.309	4.346

[a]Populations' size: Average hydrodynamic radii of the monomer, oligomer, and protofibril size populations obtained by the deconvolution of the taylorgrams with a finite number of Gaussian functions. Kinetics parameters: values of the rate constants k obtained by fitting the peak areas corresponding to the various populations with eqs 123. The last two columns show the time at which the oligomer population reaches its maximum, $t_{\text{oligomers,max}}$, and the initial concentration of the monomer population, M(t = 0).

Table 2. Average hydrodynamic radius in nm obtained by TDA over the whole aggregation process of each mixture[a].

% Aβ (1−40) in Aβ (1−40):Aβ (1−42) mixtures	TDA	AFM			
		small spherical objects		fibril	
	average R_h (nm) (n = number of points)	radii ± SD (nm)	t_{ag} (h)	half-width ± SD (nm)	t_{ag} (h)
0	1.96 ± 0.10 (n = 121)	2.15 ± 0.40	1.47	2.89 ± 0.70	0.80
25	2.42 ± 0.20 (n = 77)	2.22 ± 0.44	8.02	2.78 ± 0.72	27.83
50	2.00 ± 0.25 (n = 42)	N.A.	N.A.	N.A.	N.A.
75	1.98 ± 0.24 (n = 77)	2.32 ± 0.44	12.23	3.02 ± 1.17	27.97
100	1.81 ± 0.11 (n = 53)	2.43 ± 0.60	28.10	3.53 ± 0.93	28.10

[a]Average heights in nm obtained by AFM on the small spherical objects and on the fibrils for the different Aβ mixtures and at different aggregation times.

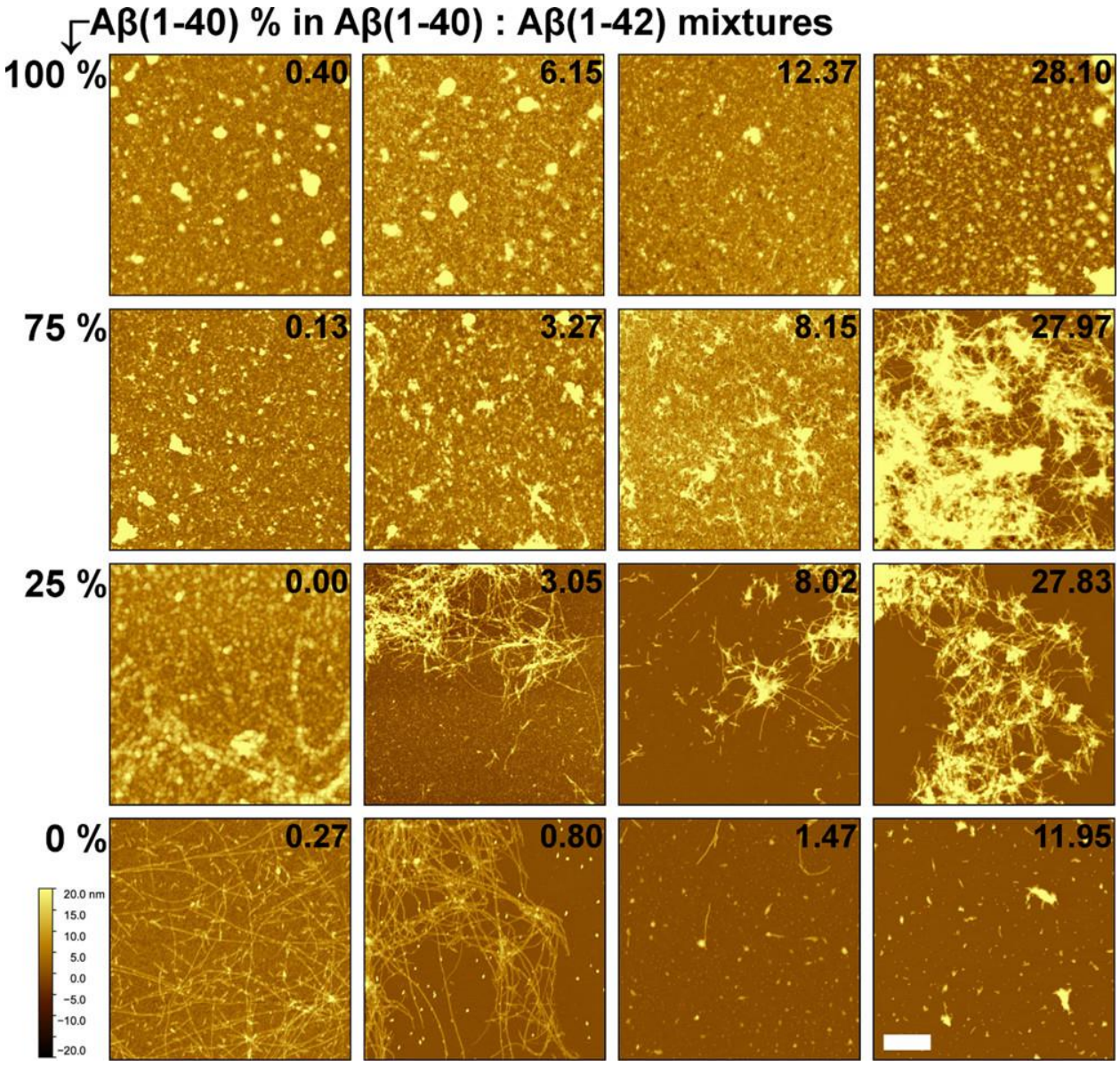

Figure 3: AFM images taken in alternated contact mode under dry conditions, for different key times of the aggregation process in the presence of different peptide proportions. The Aβ(1-40):Aβ(1-42) ratio is given on the left side of the panel, aggregation times in hours are overlayed on the images. The scale bar on the bottom right corner is valid for all images and equals 1 μm.

With the aim of verifying hypotheses formulated from TDA, we also performed AFM imaging for key times of the fibrillization process. The findings by TDA correlated well with AFM observations for Aβ (1-40) alone (Figure 3), which showed the number of fibrils rise only at t_{ag} = 28.10 h. In AFM images, the substrate remained covered with spherical objects in the 10 nm diameter range (including eventual tip convolution effects) that can be attributed to monomers and

oligomers. The coverage by these species only decreased significantly, exposing portions of the bare substrate, for t_{ag} = 28.10 h, which demonstrates the consumption of these objects by the fibrillization process.

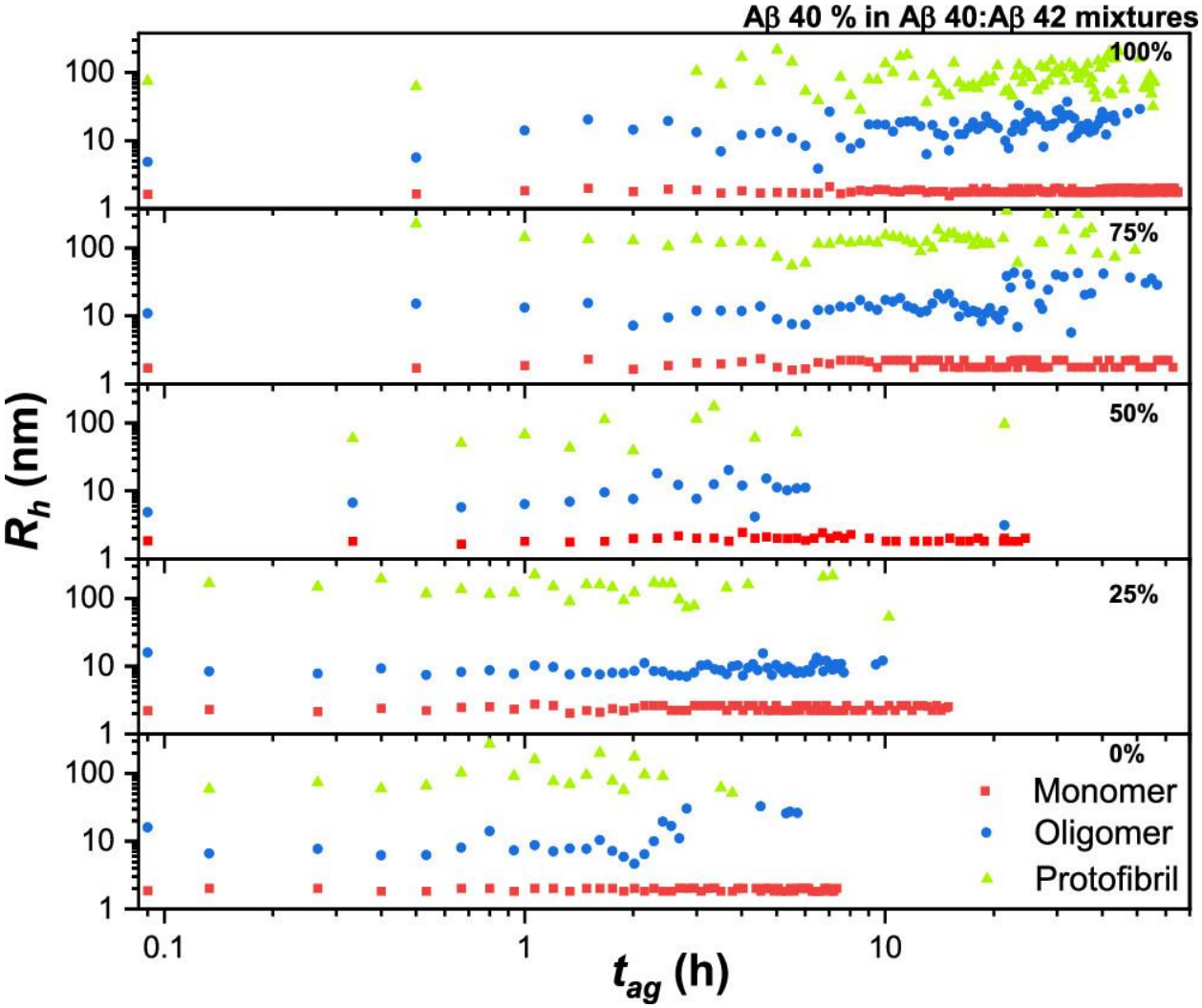

Figure 4. Hydrodynamic radius evolution of the different populations observed during the aggregation process of Aβ(1-40):Aβ(1-42) mixtures and obtained using a fit with finite number of Gaussian functions. Three size populations are represented: monomer and low molar mass oligomers 0.9 < R_h < 5 nm (■), higher molar mass oligomers 5 < R_h < 50 nm (●), and soluble protofibrils 50 < R_h < 300 nm (▲). Experimental conditions as in Figure 1.

In the case of Aβ (1-42) alone, the kinetics of aggregation were much faster than that of Aβ (1-40), as demonstrated by the taylorgrams (Figure 1) and the monomer consumption (Figure 2). The first spikes were observed only after t_{ag} ~ 10 min, in agreement with AFM showing fibrils for the shortest incubation times, and a complete disappearance of the soluble peptide species was observed after t_{ag} ~7 h (Figure 3). Similarly, only few monomeric/oligomeric species remained visible after 48 min in AFM images, which showed from this time onward mainly the substrate

and fibrils. The decrease in the number of fibrils observed by microscopy for the longest incubation times is likely due to the tangling of fibrils and compaction of these aggregates, that have less affinity for the substrate and are more easily removed during the rinsing and drying steps, as observed for other amyloid systems[42].

When mixed together, aggregation/fibrillization observed by both TDA and AFM accelerated with the proportion of Aβ(1-42). In the case of the 75% Aβ(1-40) mixture, the first spikes in TDA appeared after t_{ag}~6.5 h, while they were observed after only ~1.5 h and ~1 h for the 50 % and 25 % Aβ(1-40) mixtures respectively. In the case of the mixture with the highest amount of Aβ(1-40), the spikes intensity increased with time and remained visible even after 60 h of aggregation suggesting that the formed fibrillary structures are smaller in size than those formed with Aβ(1-40) alone, and can enter more easily in the capillary during the injection step. These observations were also conveyed in the AFM images, with fibers appearing increasingly early during the aggregation process, and the spherical objects attributed to monomers and oligomers being consumed faster upon raising the proportion of Aβ(1-42). Indeed, these small species remain predominant on the substrates up to 28.10, 8.15, 3.05 and 0.27 h respectively for 0, 25, 75 and 100% Aβ(1-42).

As mentioned earlier, the Taylorgrams were treated by fitting a sum of Gaussian functions to extract the abundance of size populations present under each elution peak during the aggregation process. Figure 4 shows the hydrodynamic radii of the populations in the studied mixtures as a function of incubation time, while Table 1 shows the average hydrodynamic radii values for the size populations and the different peptide mixtures.

As can be seen in Figure 4, the size of each population was relatively constant during the aggregation process. The population called ‘monomer’ corresponds to the monomers and small oligomers with an average size of about 2 nm in all mixtures. However, the statistical analysis showed that the monomer populations in Aβ(1-40) and in the 25 % Aβ(1-40) mixture were significantly smaller at a 95% confidence level than for the other three mixtures. Further, Aβ(1-40) alone showed the lowest ‘monomer’ population size average value of 1.81±0.11 nm, while the 25 % Aβ(1-40) mixture showed the highest average value of 2.42 ± 0.20 nm. The other three mixtures, 75 % Aβ(1-40) mixture, 50% Aβ(1-40) mixture and Aβ(1-42) alone were not statistically different and had average R_h values of 1.98 ± 0.24 nm, 2.00 ± 0.25 nm and 1.96 ± 0.10 nm, respectively. These results suggest that when the mixture contained an excess of Aβ(1-42) as

compared to Aβ(1-40), the formed oligomers were larger in size than those obtained for Aβ(1-42) alone and for the mixtures with a higher amount of Aβ(1-40). To explain this observation, the following hypothesis is proposed. First, it was already shown that Aβ(1-40) mainly forms fibrils directly from the monomeric state without passing through intermediate species[9,10]. The presence of the first fibrils of Aβ(1-40) catalyzed by the presence of Aβ(1-42) may play the role of seeds for the Aβ(1-42) peptide[21], and thus, oligomers with a higher molar mass are formed. When the amount of Aβ(1-42) decreases, the aggregation process tends to follow the pathway characteristic of Aβ(1-40) (direct formation of fibrils), and thus, the smallest oligomeric species tend to remain monomeric with a lower average size. For AFM, in the presence of biomolecules, the lateral dimensions are often affected by tip convolution, leading to unpredictable broadening of surface features[43,44]. We therefore measured the average heights of the various objects, which gave a good estimation of radii. The results obtained on the different mixtures of the radii (at times enabling to measure isolated objects) for small spherical objects attributed to monomers/oligomers and the derived half-widths for the fibers are shown in Table 2. The radii of monomers/ oligomers are in good agreement between TDA and AFM, although values measured for monomers, oligomers, and fibers with AFM are not significantly different between ratios.

As for the higher mass oligomer population, the size remained relatively constant throughout the aggregation process within a given mixture. However, it was observed that with an increase in the Aβ (1−40) proportion, the average size for the oligomer population was higher than in the case of an excess of Aβ (1−42) (∼18 nm as compared to ∼9 nm) (Figure S6). Moreover, a sudden increase of the oligomer Rh from about 10 nm to ∼30 nm can be observed when the “monomer” population decreased in area (Figure 2 for the size and Figure 4 for the area) after ∼2 h for Aβ (1−42), 24 h for the 75% Aβ (1−40) mixture, and 32 h for Aβ (1−40). This effect was not observed for the 50 and 25% Aβ (1−40) mixtures. Further, Figure 2 shows that this oligomeric population reaches a maximum in concentration at around 30 min for the Aβ (1−42) sample, while this maximum is shifted to higher times with the decrease in Aβ (1−42) proportion [1.3, 1.6, 5.5, and 16 h for 25, 50, 75, and 100% Aβ (1−40) mixtures, respectively]. Recent studies suggested that amyloid peptides can undergo liquid−liquid phase separation before the formation of amyloid fibrils[45−47]. The “high mass oligomers” population with R_h ranging from 5 to 50 nmfound in this work might correspond to high-density protein condensates. The size increase of the species over time can be explained by Ostwald ripening.

Regarding the protofibril population, the R_h values varied between 80 and 140 nm for all the mixtures independent of the peptide proportions (Figure 4).

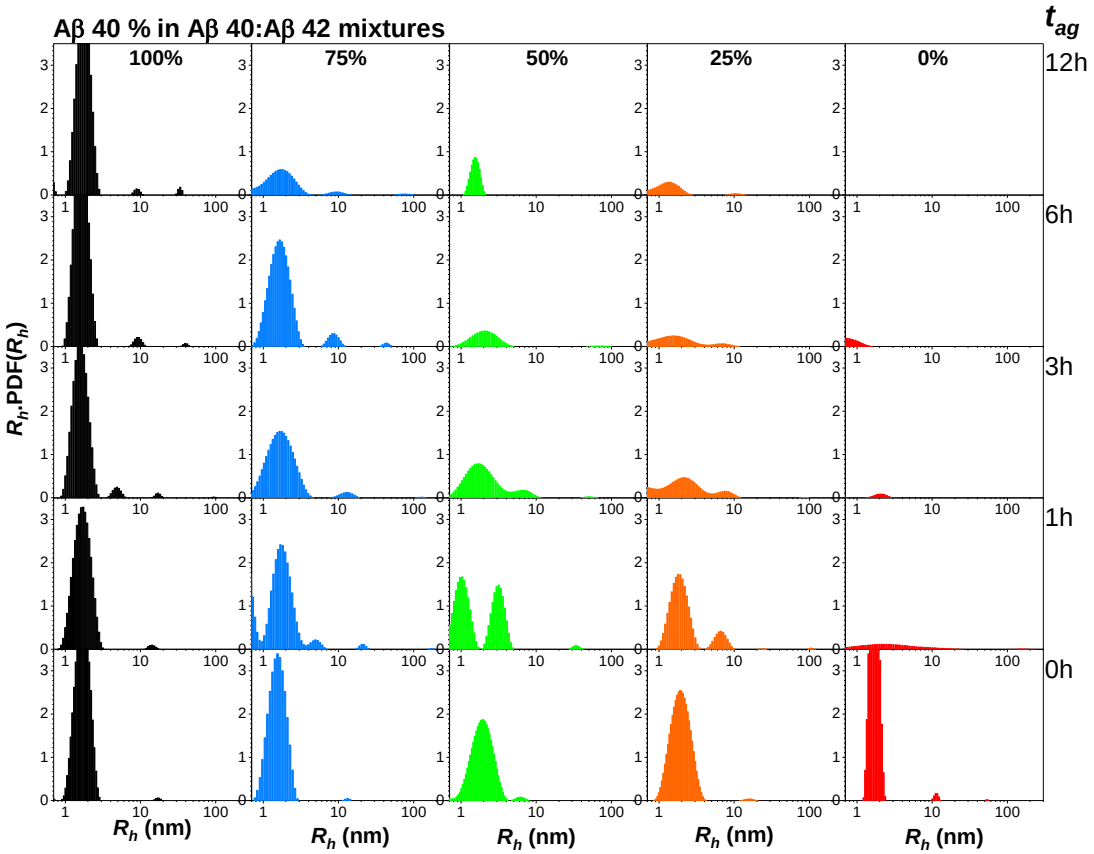

Figure 5. Size distributions of Aβ(1-40):Aβ(1-42) mixtures obtained by CRLI analysis at selected incubation times t_{ag} = 0 to 12 h. Experimental taylorgrams corresponding to these distributions are shown in Figure 1, the experimental conditions are as in Figure 1.

To get a deeper insight into the evolution of the species during the aggregation process, CRLI analysis[27,40] was applied on the right part of the taylorgrams (i.e., for $t > t_0$). Figure 5 shows the hydrodynamic radii distributions obtained by CRLI on TDA runs for selected aggregation times for all studied samples, while Figures S7−S11 show the distributions over the whole aggregation process for the studied samples. From these distributions, one can note that for Aβ (1−40) alone, only the monomer and small oligomer populations were observed throughout the aggregation process without the notable appearance of intermediate species. On the contrary, Aβ (1−42) aggregation led to intermediate oligomers having an average size around 10 nm accompanied with a broadening and disappearance of the monomeric population in accordance with our previous report[27]. When mixed together, the presence of intermediate species became more noticeable with the increase in the Aβ (1−42) proportion. These results provide an explanation to the increase in

Aβ mixtures toxicity with an increase in the Aβ (1−42)/Aβ (1−40) ratio[19,23,48], supporting the notion that this toxicity correlates with the amount of intermediate oligomeric species.

One of the major advantages of using TDA combined with advanced data treatment is the possibility to determine the size distributions of the different populations with high throughput during the whole aggregation process. These distributions provide an insight on the aggregation mechanism by modeling the data based on the chain of association and dissociation reactions shown in Figure 6[49].

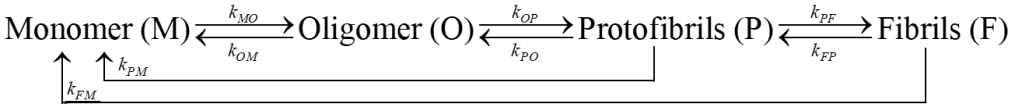

Figure 6. Scheme of the association and dissociation reactions of amyloid species used to model the aggregation process (adapted from[49]). The rate constant for each reaction is indicated close to the respective reaction arrow.

The forward and backward reactions going from the monomer (M) population to the oligomers (O), the protofibrils (P), and finally the fibrils (F), as shown in Figure 6, are modelled by the following set of equations:

$$\frac{dM(t)}{dt} = -k_{MO}M(t) + k_{OM}O(t) + k_{PM}P(t) + k_{FM}F(t) \quad (1)$$

$$\frac{dO(t)}{dt} = -\left(k_{OP} + k_{OM}\right)O(t) + k_{MO}M(t) \quad (2)$$

$$\frac{dP(t)}{dt} = -\left(k_{PF} + k_{OM}\right)P(t) + k_{OP}O(t) \quad (3)$$

$$\frac{dF(t)}{dt} = k_{PF}P(t) - k_{FM}F(t) \quad (4)$$

where, M(t), O(t), P(t) and F(t) are the concentrations of the monomers, oligomers, protofibrils and fibrils respectively. k_{MO} is the rate for the reaction transforming monomers into oligomers; similar notations are used for the other rate constants.

Note that TDA does not allow the fibrils population to be directly measured, so only eqs 123 were used. We fit eqs 123 to the temporal evolution of the population distributions obtained by

TDA by assuming that the (integrated) absorbance signal for each species is proportional to its concentration, and that the same proportionality constant applies to all species. Eq 4 was not used because TDA does not allow for the direct quantification of the fibril concentrations. The fit is performed using custom software based on the Scipy package[50], performing a least square minimization of the set of rate constants and solving numerically eqs 123 at each iteration. The resulting fitting curves are shown as dot-dashed lines in Figure 2 (see also Figures S12−S16), while the fitting parameters are reported in Table 1. Note that for most samples, the monomer population asymptotically tends for large *t* to a non-zero concentration value, due to the dissociation of the higher-order species. The 100% Aβ (1−40) could not be fitted entirely because of the presence of a lag phase at early times. However, data for this sample could be fitted by excluding the monomer population data points for $t < \sim 20$ h. For all other sample mixtures, the fit allowed us to extract the kinetics rate constants reported in Table 1. From these values, it can be deduced that the reaction rates tend to decrease with increasing amounts of Aβ (1−40) in the mixture. For the 0% Aβ (1−40) sample, the forward reactions were dominant as compared to the backward ones, suggesting that the aggregation is close to an irreversible reaction rather than to an equilibrium one. When a small amount of Aβ (1−40) is added (25%), the reaction rates of forward and backward reactions become similar. These results can explain the higher toxicity of this Aβ ratio observed in the literature[19]. Indeed, the backward reactions correspond to the dissociation of higher-order species into monomers or low molar mass oligomers, which are known to be toxic. To our knowledge, this is the first time that kinetic rates of the aggregation mechanism of Aβ peptides could be determined by measuring directly the monomer and oligomer distributions. When combined with models proposed in the literature, mainly based on measurements of the time-dependent aggregate mass[49,51,52] (e.g., by ThT fluorescence assay), or numerical simulations[53], TDA data such as those presented here will help in reaching a comprehensive understanding of the aggregation process of these amyloid species, potentially contributing to assess the effectiveness of drugs targeting the toxic oligomeric species.

III.4. Conclusion

This work demonstrated the potential of TDA in assisting the study of complex amyloid peptide mixtures and shed more light on the aggregation process in these systems. The comparison

of the results obtained in parallel by TDA and AFM showed the complementarity of the two techniques, where TDA is able to quantify and size small objects, while AFM can size the fibrillary structures not accessible by TDA. In addition, the results confirmed that the kinetics of aggregation strongly depend on the nature of amyloid-forming peptides and their environment. Under our working conditions, the more amyloid-prone Aβ (1−42) aggregates more rapidly (minutes scale) compared to Aβ (1−40), which aggregates in about 24 h, in agreement with previously published works[27,58]. When mixing together the two species, the aggregation rate was highly influenced by the ratio of Aβ (1−40):Aβ (1−42). Indeed, Aβ (1−42) was found to accelerate the aggregation rate of Aβ (1−40), probably by a cross-seeding mechanism. For example, the disappearance of the monomeric species decreased from 48 h in the case of 100% Aβ (1−40) to 12 h when 25% of Aβ (1−42) were present in the sample. In addition to the clear observation on the interplay between both Aβ peptides during the aggregation process of mixtures and the influence of the Aβ ratio on the aggregation rate, this work shows that this ratio modulates the formation of potentially toxic oligomers. In fact, when the peptides were mixed together, intermediate oligomeric species were observed and tended to increase in proportion upon increasing the Aβ (1−42) content. Modifying the Aβ ratio changed the onset of the oligomeric species appearance and monomeric species disappearance (monomers and small oligomers R_h lower than 5 nm), as well as the aggregation mechanism (direct formation of fibrils or formation of intermediate species). These results support the importance of understanding the mechanism of the aggregation process in the case of Aβ mixtures (in better accordance with the in vivo conditions), to better direct research toward an AD therapy able to inhibit the formation of intermediate species depending on the Aβ ratio. In this respect, TDA was shown to be a straightforward method able to give with unprecedented detail a new insight on the size and distribution of the species formed during the aggregation process. Finally, the combination of TDA with extensive data processing and highly resolved efficient methods such as AFM paves the way for building a comprehensive picture of the speciation and growth processes, as illustrated here for amyloid peptides, with potential applications to a wide range of biological, organic, and inorganic polymer systems.

III.5. References

1. *2019 Alzheimer's disease facts and figures*. *Alzheimer's Dement.* **15,** (2019).
2. Ando, K., Laborde, Q., Lazar, A., Godefroy, D., Youssef, I., Amar, M., Pooler, A., Potier, M. C., Delatour, B. & Duyckaerts, C. Inside Alzheimer brain with CLARITY: Senile plaques, neurofibrillary tangles and axons in 3-D. *Acta Neuropathol.* **128,** 457–459 (2014).
3. Hardy, J. A. & Higgins, G. A. Alzheimer's disease: The amyloid cascade hypothesis. *Science (80-.).* **256,** 184–185 (1992).
4. Liu, P. P., Xie, Y., Meng, X. Y. & Kang, J. S. History and progress of hypotheses and clinical trials for alzheimer's disease. *Signal Transduct. Target. Ther.* **4,** (2019).
5. Salazar, S. V. & Strittmatter, S. M. Cellular prion protein as a receptor for amyloid-β oligomers in Alzheimer's disease. *Biochem. Biophys. Res. Commun.* **483,** 1143–1147 (2017).
6. König, A. S., Rösener, N. S., Gremer, L., Tusche, M., Flender, D., Reinartz, E., Hoyer, W., Neudecker, P., Willbold, D. & Heise, H. Structural details of amyloid β oligomers in complex with human prion protein as revealed by solid-state MAS NMR spectroscopy. *J. Biol. Chem.* **296,** (2021).
7. Madhu, P., Das, D. & Mukhopadhyay, S. Conformation-specific perturbation of membrane dynamics by structurally distinct oligomers of Alzheimer's amyloid-β peptide. *Phys. Chem. Chem. Phys.* **23,** 9686–9694 (2021).
8. Guerrero-Muñoz, M. J., Castillo-Carranza, D. L., Sengupta, U., White, M. A. & Kayed, R. Design of metastable β-sheet oligomers from natively unstructured peptide. *ACS Chem. Neurosci.* **4,** 1520–1523 (2013).
9. Arosio, P., Knowles, T. P. J. & Linse, S. On the lag phase in amyloid fibril formation. *Phys. Chem. Chem. Phys.* **17,** 7606–7618 (2015).
10. Chen, Y.-R. & Glabe, C. G. Distinct Early Folding and Aggregation Properties of Alzheimer Amyloid-β Peptides Aβ40 and Aβ42. *J. Biol. Chem.* **281,** 24414–24422 (2006).
11. Novo, M., Freire, S. & Al-Soufi, W. Critical aggregation concentration for the formation of early Amyloid-β (1-42) oligomers. *Sci. Rep.* **8,** (2018).
12. Sengupta, U., Nilson, A. N. & Kayed, R. The Role of Amyloid-β Oligomers in Toxicity, Propagation, and Immunotherapy. *EBioMedicine* **6,** 42–49 (2016).
13. Wiltfang, J., Esselmann, H., Bibl, M., Hüll, M., Hampel, H., Kessler, H., Frölich, L., Schröder, J., Peters, O., Jessen, F., Luckhaus, C., Perneczky, R., Jahn, H., Fiszer, M., Maler, J. M., Zimmermann, R., Bruckmoser, R., Kornhuber, J. & Lewczuk, P. Amyloid β peptide ratio 42/40 but not Aβ42 correlates with phospho-Tau in patients with low- and high-CSF Aβ40 load. *J. Neurochem.* **101,** 1053–1059 (2007).
14. Hardy, J. Amyloid, the presenilins and Alzheimer's disease. *Trends Neurosci.* **20,** 154–

159 (1997).

15. Snyder, S. W., Ladror, U. S., Matayoshi, E. D., Krafft, G. A., Holzman, T. F., Barrett, L. W., Huffaker, H. J., Wang, G. T. & Wade, W. S. Amyloid-beta aggregation: selective inhibition of aggregation in mixtures of amyloid with different chain lengths. *Biophys. J.* **67,** 1216–1228 (1994).

16. Frost, D., Gorman, P. M., Yip, C. M. & Chakrabartty, A. Co-incorporation of Aβ40 and Aβ42 to form mixed pre-fibrillar aggregates. *Eur. J. Biochem.* **270,** 654–663 (2003).

17. Cukalevski, R., Yang, X., Meisl, G., Weininger, U., Bernfur, K., Frohm, B., Knowles, T. P. J. & Linse, S. The Aβ40 and Aβ42 peptides self-assemble into separate homomolecular fibrils in binary mixtures but cross-react during primary nucleation. *Chem. Sci.* **6,** 4215–4233 (2015).

18. Gu, L. & Guo, Z. Alzheimer's Aβ42 and Aβ40 form mixed oligomers with direct molecular interactions. *Biochem. Biophys. Res. Commun.* **534,** 292–296 (2021).

19. Kuperstein, I., Broersen, K., Benilova, I., Rozenski, J., Jonckheere, W., Debulpaep, M., Vandersteen, A., Segers-Nolten, I., Van Der Werf, K., Subramaniam, V., Braeken, D., Callewaert, G., Bartic, C., D'Hooge, R., Martins, I. C., Rousseau, F., Schymkowitz, J. & De Strooper, B. Neurotoxicity of Alzheimer's disease Aβ peptides is induced by small changes in the Aβ42 to Aβ40 ratio. *EMBO J.* **29,** 3408–3420 (2010).

20. Cerofolini, L., Ravera, E., Bologna, S., Wiglenda, T., Böddrich, A., Purfürst, B., Benilova, I., Korsak, M., Gallo, G., Rizzo, D., Gonnelli, L., Fragai, M., De Strooper, B., Wanker, E. E. & Luchinat, C. Mixing Aβ(1-40) and Aβ(1-42) peptides generates unique amyloid fibrils. *Chem. Commun.* **56,** 8830–8833 (2020).

21. Hasegawa, K., Yamaguchi, I., Omata, S., Gejyo, F. & Naiki, H. Interaction between Aβ(1-42) and Aβ(1-40) in alzheimer's β-amyloid fibril formation in vitro. *Biochemistry* **38,** 15514–15521 (1999).

22. Yan, Y. & Wang, C. Aβ40 Protects Non-toxic Aβ42 Monomer from Aggregation. *J. Mol. Biol.* **369,** 909–916 (2007).

23. Pauwels, K., Williams, T. L., Morris, K. L., Jonckheere, W., Vandersteen, A., Kelly, G., Schymkowitz, J., Rousseau, F., Pastore, A., Serpell, L. C. & Broersen, K. Structural basis for increased toxicity of pathological Aβ42:Aβ40 ratios in alzheimer disease. *J. Biol. Chem.* **287,** 5650–5660 (2012).

24. Chamieh, J. & Cottet, H. in *Colloid Interface Sci. Pharm. Res. Dev.* 173–192 (2014). doi:10.1016/B978-0-444-62614-1.00009-0

25. Taylor, G. Conditions under which dispersion of a solute in a stream of solvent can be used to measure molecular diffusion. *Proc. R. Soc. London. Ser. A. Math. Phys. Sci.* **225,** 473–477 (1954).

26. Taylor, G. I. Dispersion of soluble matter in solvent flowing slowly through a tube. *Proc. R. Soc. London. Ser. A. Math. Phys. Sci.* **219,** 186–203 (1953).

27. Deleanu, M., Hernandez, J.-F., Cipelletti, L., Biron, J.-P., Rossi, E., Taverna, M., Cottet,

H. & Chamieh, J. Unraveling the Speciation of β-Amyloid Peptides during the Aggregation Process by Taylor Dispersion Analysis. *Anal. Chem.* (2021). doi:10.1021/acs.analchem.1c00527

28. Hawe, A., Hulse, W. L., Jiskoot, W. & Forbes, R. T. Taylor dispersion analysis compared to dynamic light scattering for the size analysis of therapeutic peptides and proteins and their aggregates. *Pharm. Res.* **28,** 2302–2310 (2011).

29. Cottet, H., Biron, J. P. & Martin, M. Taylor dispersion analysis of mixtures. *Anal. Chem.* **79,** 9066–9073 (2007).

30. Bello, M. S., Rezzonico, R. & Righetti, P. G. Use of Taylor-Aris dispersion for measurement of a solute diffusion coefficient in thin capillaries. *Science (80-.).* **266,** 773–776 (1994).

31. Sharma, U., Gleason, N. J. & Carbeck, J. D. Diffusivity of solutes measured in glass capillaries using Taylor's analysis of dispersion and a commercial CE instrument. *Anal. Chem.* **77,** 806–813 (2005).

32. Cottet, H., Martin, M., Papillaud, A., Souaïd, E., Collet, H. & Commeyras, A. Determination of dendrigraft poly-L-lysine diffusion coefficients by Taylor dispersion analysis. *Biomacromolecules* **8,** 3235–3243 (2007).

33. d'Orlyé, F., Varenne, A. & Gareil, P. Determination of nanoparticle diffusion coefficients by Taylor dispersion analysis using a capillary electrophoresis instrument. *J. Chromatogr. A* **1204,** 226–232 (2008).

34. Chamieh, J., Merdassi, H., Rossi, J. C., Jannin, V., Demarne, F. & Cottet, H. Size characterization of lipid-based self-emulsifying pharmaceutical excipients during lipolysis using Taylor dispersion analysis with fluorescence detection. *Int. J. Pharm.* **537,** 94–101 (2018).

35. Urban, D. A., Milosevic, A. M., Bossert, D., Crippa, F., Moore, T. L., Geers, C., Balog, S., Rothen-Rutishauser, B. & Petri-Fink, A. Taylor Dispersion of Inorganic Nanoparticles and Comparison to Dynamic Light Scattering and Transmission Electron Microscopy. *Colloids Interface Sci. Commun.* **22,** 29–33 (2018).

36. Pedersen, M. E., Østergaard, J. & Jensen, H. Flow-induced dispersion analysis (FIDA) for protein quantification and characterization. *Methods Mol. Biol.* **1972,** 109–123 (2019).

37. Chamieh, J., Leclercq, L., Martin, M., Slaoui, S., Jensen, H., Østergaard, J. & Cottet, H. Limits in Size of Taylor Dispersion Analysis: Representation of the Different Hydrodynamic Regimes and Application to the Size-Characterization of Cubosomes. *Anal. Chem.* **89,** 13487–13493 (2017).

38. Cottet, H., Biron, J. P. & Martin, M. On the optimization of operating conditions for Taylor dispersion analysis of mixtures. *Analyst* **139,** 3552–3562 (2013).

39. Vedula, P. & Yeung, P. K. Similarity scaling of acceleration and pressure statistics in numerical simulations of isotropic turbulence. *Phys. Fluids* **11,** 1208–1220 (1999).

40. Cipelletti, L., Biron, J. P., Martin, M. & Cottet, H. Measuring Arbitrary Diffusion

Coefficient Distributions of Nano-Objects by Taylor Dispersion Analysis. *Anal. Chem.* **87,** 8489–8496 (2015).

41. Meisl, G., Yang, X., Hellstrand, E., Frohm, B., Kirkegaard, J. B., Cohen, S. I. A., Dobson, C. M., Linse, S. & Knowles, T. P. J. Differences in nucleation behavior underlie the contrasting aggregation kinetics of the Aβ40 and Aβ42 peptides. *Proc. Natl. Acad. Sci. U. S. A.* **111,** 9384–9389 (2014).

42. Deschaume, O., De Roo, B., Van Bael, M. J., Locquet, J. P., Van Haesendonck, C. & Bartic, C. Synthesis and properties of gold nanoparticle arrays self-organized on surface-deposited lysozyme amyloid scaffolds. *Chem. Mater.* **26,** 5383–5393 (2014).

43. Winzer, A. T., Kraft, C., Bhushan, S., Stepanenko, V. & Tessmer, I. Correcting for AFM tip induced topography convolutions in protein-DNA samples. *Ultramicroscopy* **121,** 8–15 (2012).

44. Godon, C., Teulon, J. M., Odorico, M., Basset, C., Meillan, M., Vellutini, L., Chen, S. wen W. & Pellequer, J. L. Conditions to minimize soft single biomolecule deformation when imaging with atomic force microscopy. *J. Struct. Biol.* **197,** 322–329 (2017).

45. Xing, Y., Nandakumar, A., Kakinen, A., Sun, Y., Davis, T. P., Ke, P. C. & Ding, F. Amyloid Aggregation under the Lens of Liquid-Liquid Phase Separation. *J. Phys. Chem. Lett.* **12,** 368–378 (2021).

46. Nakasone, Y. & Terazima, M. A Time-Resolved Diffusion Technique for Detection of the Conformational Changes and Molecular Assembly/Disassembly Processes of Biomolecules. *Front. Genet.* **12,** (2021).

47. Brocca, S., Grandori, R., Longhi, S. & Uversky, V. Liquid–liquid phase separation by intrinsically disordered protein regions of viruses: Roles in viral life cycle and control of virus–host interactions. *Int. J. Mol. Sci.* **21,** 1–31 (2020).

48. Kwak, S. S., Washicosky, K. J., Brand, E., von Maydell, D., Aronson, J., Kim, S., Capen, D. E., Cetinbas, M., Sadreyev, R., Ning, S., Bylykbashi, E., Xia, W., Wagner, S. L., Choi, S. H., Tanzi, R. E. & Kim, D. Y. Amyloid-β42/40 ratio drives tau pathology in 3D human neural cell culture models of Alzheimer's disease. *Nat. Commun.* **11,** (2020).

49. Dear, A. J., Michaels, T. C. T., Meisl, G., Klenerman, D., Wu, S., Perrett, S., Linse, S., Dobson, C. M. & Knowles, T. P. J. Kinetic diversity of amyloid oligomers. *Proc. Natl. Acad. Sci. U. S. A.* **117,** (2020).

50. Virtanen, P., Gommers, R., Oliphant, T. E., Haberland, M., Reddy, T., Cournapeau, D., Burovski, E., Peterson, P., Weckesser, W., Bright, J., van der Walt, S. J., Brett, M., Wilson, J., Millman, K. J., Mayorov, N., Nelson, A. R. J., Jones, E., Kern, R., Larson, E., Carey, C. J., Polat, İ., Feng, Y., Moore, E. W., VanderPlas, J., Laxalde, D., Perktold, J., Cimrman, R., Henriksen, I., Quintero, E. A., Harris, C. R., Archibald, A. M., Ribeiro, A. H., Pedregosa, F., van Mulbregt, P., Vijaykumar, A., Bardelli, A. Pietro, Rothberg, A., Hilboll, A., Kloeckner, A., Scopatz, A., Lee, A., Rokem, A., Woods, C. N., Fulton, C., Masson, C., Häggström, C., Fitzgerald, C., Nicholson, D. A., Hagen, D. R., Pasechnik, D. V., Olivetti, E., Martin, E., Wieser, E., Silva, F., Lenders, F., Wilhelm, F., Young, G., Price, G. A., Ingold, G. L., Allen, G. E., Lee, G. R., Audren, H., Probst, I., Dietrich, J. P.,

Silterra, J., Webber, J. T., Slavič, J., Nothman, J., Buchner, J., Kulick, J., Schönberger, J. L., de Miranda Cardoso, J. V., Reimer, J., Harrington, J., Rodríguez, J. L. C., Nunez-Iglesias, J., Kuczynski, J., Tritz, K., Thoma, M., Newville, M., Kümmerer, M., Bolingbroke, M., Tartre, M., Pak, M., Smith, N. J., Nowaczyk, N., Shebanov, N., Pavlyk, O., Brodtkorb, P. A., Lee, P., McGibbon, R. T., Feldbauer, R., Lewis, S., Tygier, S., Sievert, S., Vigna, S., Peterson, S., More, S., Pudlik, T., Oshima, T., Pingel, T. J., Robitaille, T. P., Spura, T., Jones, T. R., Cera, T., Leslie, T., Zito, T., Krauss, T., Upadhyay, U., Halchenko, Y. O. & Vázquez-Baeza, Y. SciPy 1.0: fundamental algorithms for scientific computing in Python. *Nat. Methods* **17,** 261–272 (2020).

51. Meisl, G., Kirkegaard, J. B., Arosio, P., Michaels, T. C. T., Vendruscolo, M., Dobson, C. M., Linse, S. & Knowles, T. P. J. Molecular mechanisms of protein aggregation from global fitting of kinetic models. *Nat. Protoc.* **11,** (2016).

52. Cohen, S. I. A., Linse, S., Luheshi, L. M., Hellstrand, E., White, D. A., Rajah, L., Otzen, D. E., Vendruscolo, M., Dobson, C. M. & Knowles, T. P. J. Proliferation of amyloid- 42 aggregates occurs through a secondary nucleation mechanism. *Proc. Natl. Acad. Sci.* **110,** 9758–9763 (2013).

53. Dear, A. J., Meisl, G., Šarić, A., Michaels, T. C. T., Kjaergaard, M., Linse, S. & Knowles, T. P. J. Identification of on- And off-pathway oligomers in amyloid fibril formation. *Chem. Sci.* **11,** 6236–6247 (2020).

54. Verpillot, R., Otto, M., Klafki, H. & Taverna, M. Simultaneous analysis by capillary electrophoresis of five amyloid peptides as potential biomarkers of Alzheimer's disease. *J. Chromatogr. A* **1214,** 157–164 (2008).

55. Brinet, D., Kaffy, J., Oukacine, F., Glumm, S., Ongeri, S. & Taverna, M. An improved capillary electrophoresis method for in vitro monitoring of the challenging early steps of Aβ(1-42) peptide oligomerization: Application to anti-Alzheimer's drug discovery. *Electrophoresis* **35,** 3302–3309 (2014).

56. Nečas, D. & Klapetek, P. Gwyddion: An open-source software for SPM data analysis. *Cent. Eur. J. Phys.* **10,** 181–188 (2012).

57. Schneider, C. A., Rasband, W. S. & Eliceiri, K. W. NIH Image to ImageJ: 25 years of image analysis. *Nat. Methods* **9,** 671–675 (2012).

58. Teplow, D. B., Bitan, G., Lomakin, A., Benedek, G. B., Kirkitadze, M. D. & Vollers, S. S. Amyloid -protein (A) assembly: A 40 and A 42 oligomerize through distinct pathways. *Proc. Natl. Acad. Sci.* **100,** 330–335 (2003).

Chapter III. Supporting information of Article 2

This part was published as SI in *ACS Chem. Neurosci.*, 2022, 13, 786−795

https://doi.org/10.1021/acschemneuro.1c00784

Mihai Deleanu[1], Olivier Deschaume[2], Luca Cipelletti[3,4], Jean-François Hernandez[1], Carmen Bartic[2], Hervé Cottet*[1], Joseph Chamieh*[1]

[1] IBMM, Univ Montpellier, CNRS, ENSCM, 34095 Montpellier, France
[2] Department of Physics and Astronomy, Soft-Matter Physics and Biophysics Section, KU Leuven, Celestijnenlaan 200D, Box 2416, 3001 Heverlee, Belgium
[3] L2C, Université Montpellier, 34095 Montpellier, France
[4] Institut Universitaire de France (IUF), Paris, France

* CORRESPONDING AUTHORS
Tel: +33 4 6714 3920, Fax: +33 4 6763 1046. E-mail: joseph.chamieh@umontpellier.fr
Tel: +33 4 6714 3427, Fax: +33 4 6763 1046. E-mail: herve.cottet@umontpellier.fr

III.SI.1. TDA: Theory and data processing

Conditions for TDA validity. The band broadening resulting from Taylor dispersion is easily quantified via the temporal variance of the elution profile. The diffusion coefficient D (m^2 s^{-1}) and the hydrodynamic radius R_h (m) are determined using Eq. (1) and Eq. (2), respectively:

$$D = \frac{R_c^2 t_0}{24\sigma^2} \quad \text{SI.(1)}$$

$$R_h = \frac{k_b T}{6\pi\eta D} \quad \text{SI.(2)}$$

where R_c is the capillary radius (m), t_0 is the average elution time (s), σ^2 is the temporal variance of the peak (s^2), k_B is the Boltzmann constant, T the temperature (K) and η the viscosity of the carrier liquid (Pa.s). It is noteworthy that Eq. (1) is valid when the peak appearance time t_0 is higher than the characteristic diffusion time of the solute over a distance equal to the capillary radius as verified by Eq. (3)[1,2]:

$$\tau = \frac{D t_0}{R_c^2} \geq 1.25 \quad \text{SI.(3)}$$

where τ is an adimensional characteristic time. Axial diffusion should also be negligible compared to convection as verified by Eq. (4)[1,2]:

$$P_e = \frac{uR_c}{D} \geq 40 \qquad \text{SI.(4)}$$

where P_e is the Péclet number and u is the linear mobile phase velocity (m/s).

Data processing of the taylorgrams. The taylorgram $S(t)$ of a sample mixture containing n different components of individual diffusion coefficient D_i can be expressed as a sum of n individual Gaussian contributions $S_i(t)$, all centered at the same elution time t_0:

$$S(t) = \sum_{i=1}^{n} S_i(t) = \sum_{i=1}^{n} \frac{A_i}{\sigma_i \sqrt{2\pi}} e^{-\frac{1}{2}\frac{(t-t_0)^2}{\sigma_i^2}} \qquad \text{SI.(5)}$$

where A_i is a coefficient that is proportional to the concentration in species i and depends on the response coefficient of the species i, at the specific detection wavelength. The diffusion coefficient of the species i is directly related to the standard deviation σ_i according to

$$D_i = \frac{R_c^2 t_0}{24\sigma_i^2} \qquad \text{SI.(6)}$$

Different approaches can be used to obtain information about the size distribution of the species in the mixture from the taylorgram $S(t)$.[3-5]

A first approach is based on a direct curve fitting with the sum of n Gaussian curves according to Eq. (5), when the total number of species, n, is limited ($n \leq 4$). The curve fitting was conducted using the Least Significant Difference method using the "GRG nonlinear" algorithm in Microsoft Excel.

A second approach is based on Constrained Regularized Linear Inversion (CRLI)[4] which aims at finding the probability density function $P_D(D)$ that fits the taylorgram according to the following equation:

$$s(t) = c\int_0^{\infty} P_D(D)\sqrt{D}\exp\left[-\frac{(t-t_0)^2 12D}{R_c^2 t_0}\right]dD \qquad \text{SI.(7)}$$

with $c = \left[\int_0^{\infty} P_D(D)\sqrt{D}dD\right]^{-1} = \left[\overline{D^{1/2}}\right]^{-1}$ a normalization factor and $P_D(D)$ the mass-weighted probability distribution function (PDF) of the diffusion coefficient. The main advantage of this approach, as compared to the first one, is that there is no need to hypothesize on the number of populations under the experimental distribution. For more details on that approach, the reader may refer to original publications [3,4].

III.SI.2. Experimental Taylorgrams

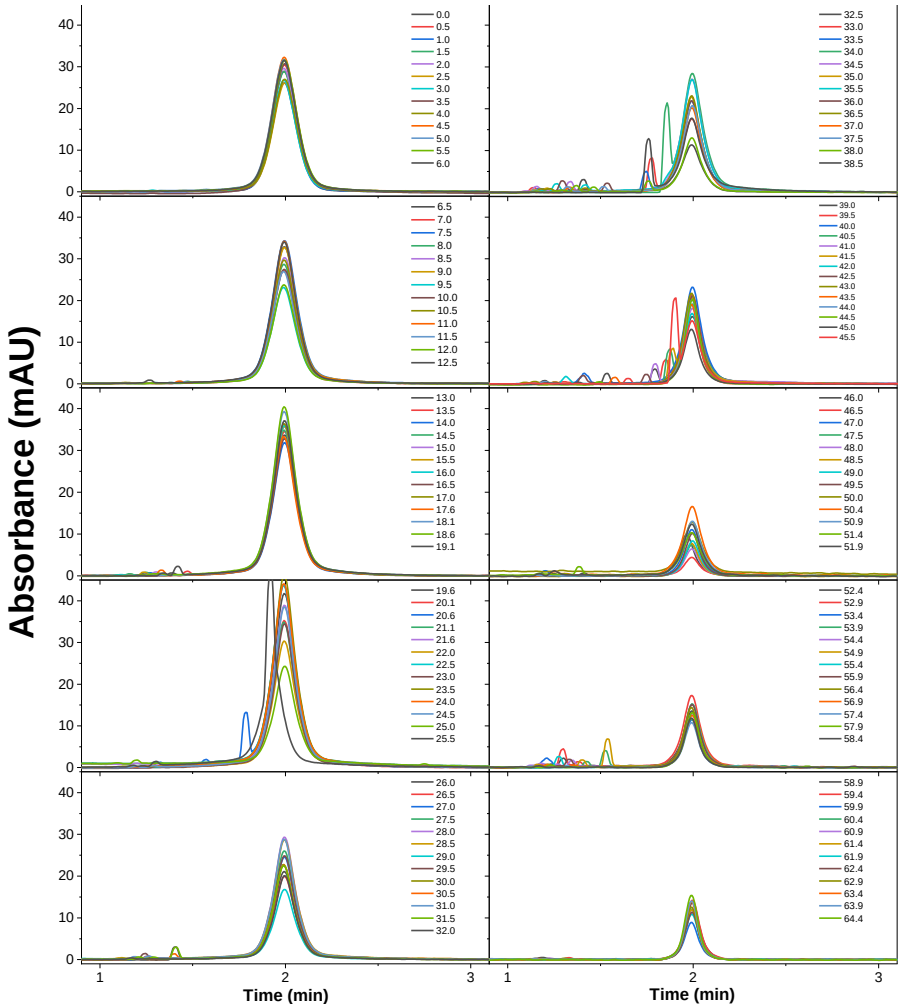

Figure SI.1. Experimental taylorgrams obtained for Aβ(1-40) aggregation monitoring over an incubation period of 65 h. The experimental traces are distributed into several graphs for better clarity. Curves are labelled by the incubation time, in h. Experimental conditions: Sample: 133 µM Aβ(1-40) in 20 mM phosphate buffer pH 7.4. Incubation: quiescent conditions at 37 °C. Fused silica capillary: 50 µm i.d. × 40 cm × 31.5 cm. Eluent: 20 mM phosphate buffer, pH 7.4. Mobilization pressure: 100 mbar. Injection: 44 mbar for 3 s (V_{inj} = 7 nL, corresponding to 1% of capillary volume to injection point). Analyses were performed at 37 °C. UV detection at 191 nm.

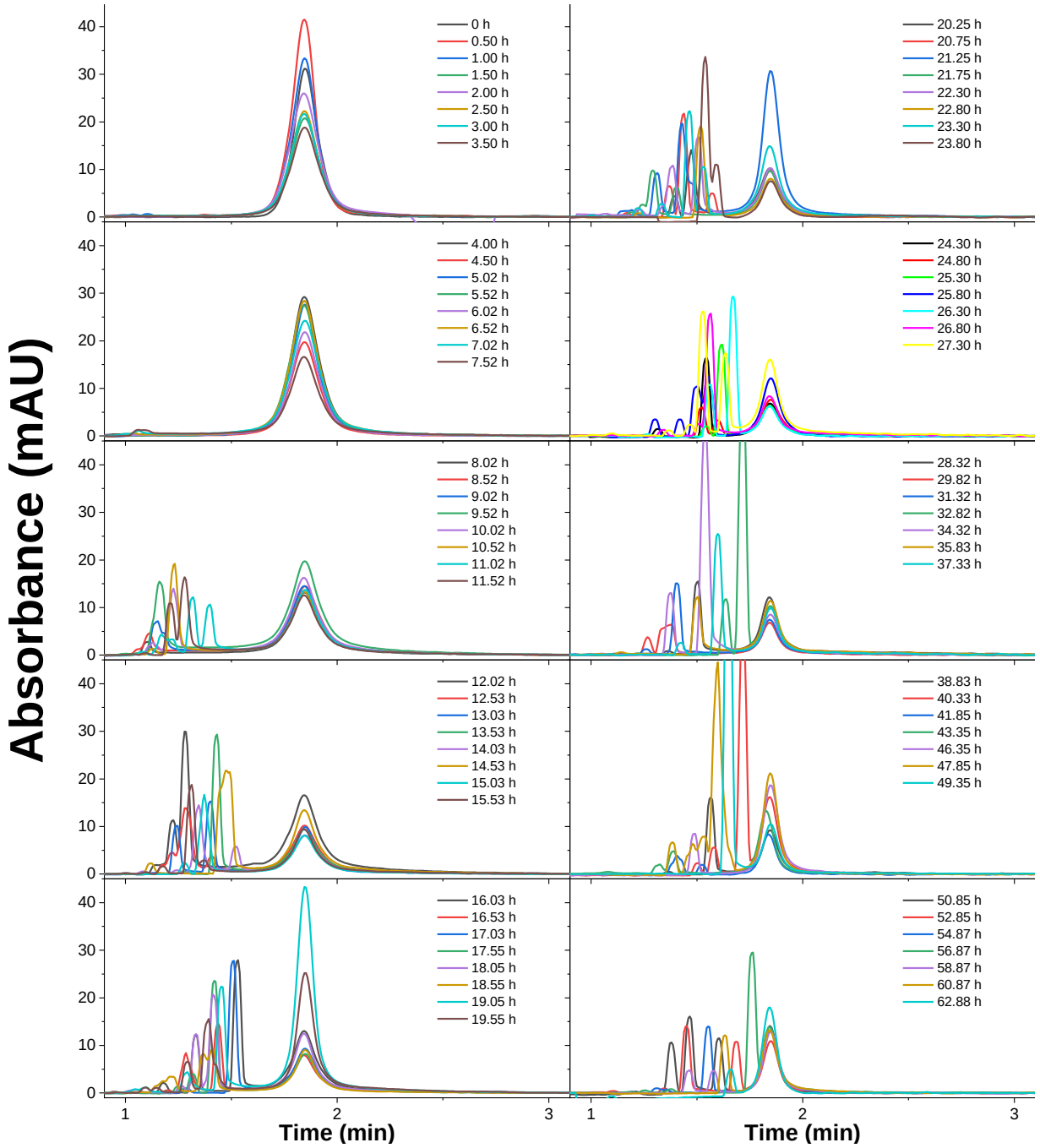

Figure SI.2. Experimental taylorgrams obtained for Aβ(1-40):Aβ(1-42) 3:1 mixture aggregation monitoring over an incubation period of 65 h. The experimental traces are distributed into several graphs for better clarity. Curves are labelled by the incubation time, in h. Experimental conditions: Sample: 100 µM of Aβ(1-40) and 33 µM Aβ(1-42) of in 20 mM phosphate buffer pH 7.4. Incubation: quiescent conditions at 37 °C. Fused silica capillary: 50 µm i.d. × 40 cm × 31.5 cm. Eluent: 20 mM phosphate buffer, pH 7.4. Mobilization pressure: 100 mbar. Injection: 44 mbar for 3 s (V_{inj} = 7 nL, corresponding to 1% of capillary volume to injection point). Analyses were performed at 37 °C. UV detection at 191 nm.

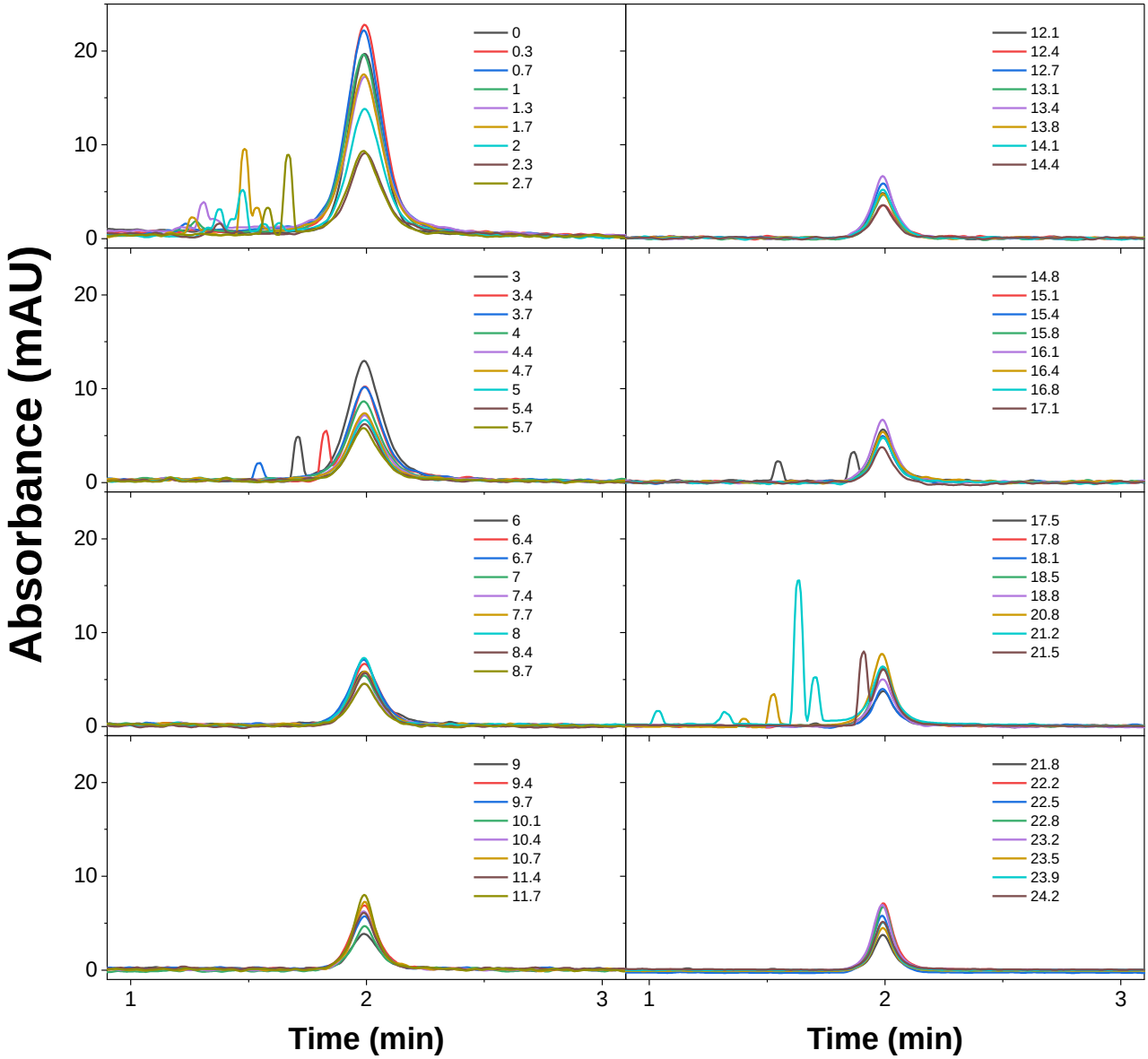

Figure SI.3. Experimental taylorgrams obtained for Aβ(1-40):Aβ(1-42) 1:1 mixture aggregation monitoring over an incubation period of 25 h. The experimental traces are distributed into several graphs for better clarity. Curves are labelled by the incubation time, in h. Experimental conditions: Sample: 66.7 µM of Aβ(1-40) and 66.7 µM Aβ(1-42) of in 20 mM phosphate buffer pH 7.4. Incubation: quiescent conditions at 37 °C. Fused silica capillary: 50 µm i.d. × 40 cm × 31.5 cm. Eluent: 20 mM phosphate buffer, pH 7.4. Mobilization pressure: 100 mbar. Injection: 44 mbar for 3 s (V_{inj} = 7 nL, corresponding to 1% of capillary volume to injection point). Analyses were performed at 37 °C. UV detection at 191 nm.

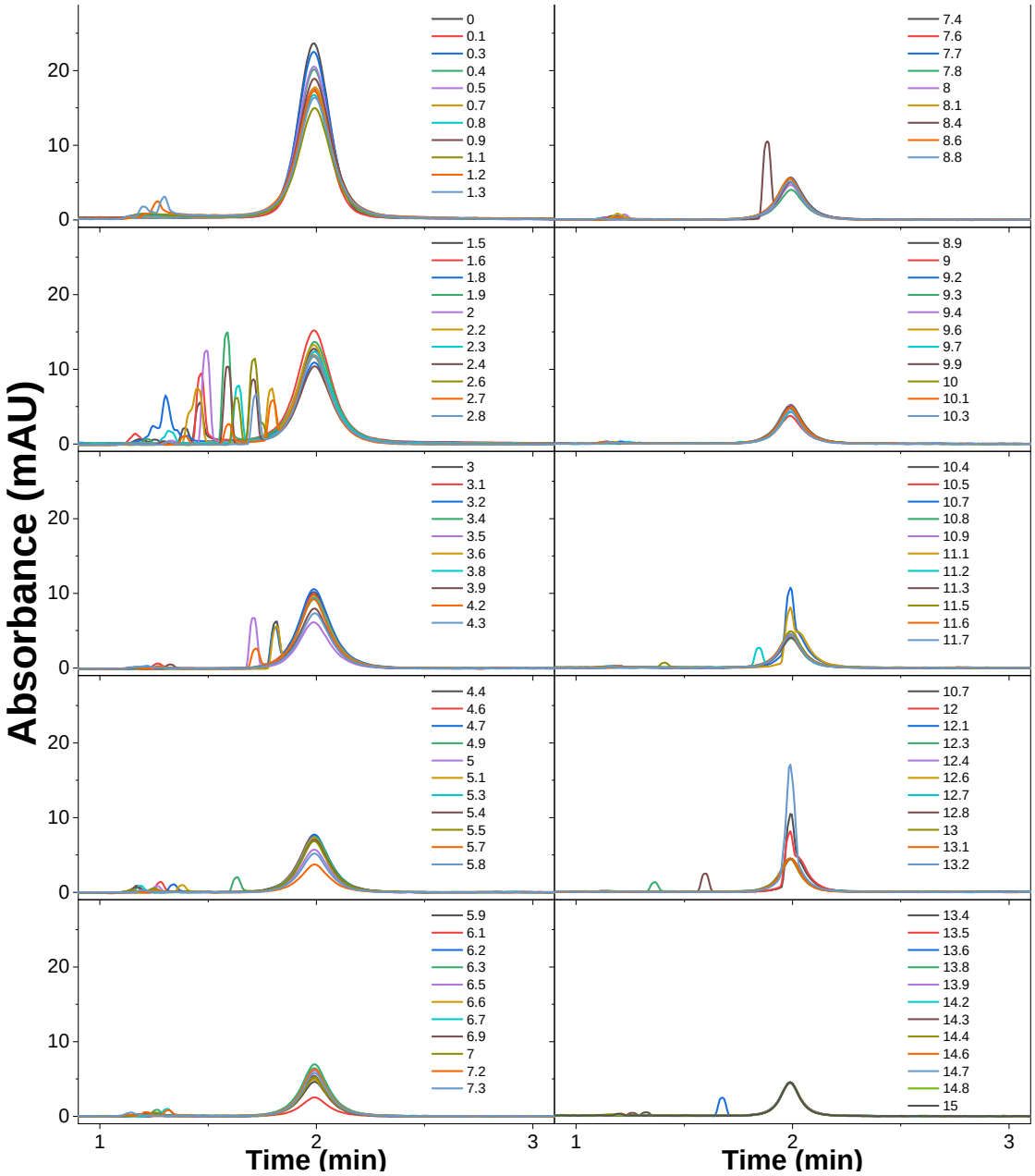

Figure SI.4. Experimental taylorgrams obtained for Aβ(1-40):Aβ(1-42) 1:3 mixture aggregation monitoring over an incubation period of 15 h. The experimental traces are distributed into several graphs for better clarity. Curves are labelled by the incubation time, in h. Experimental conditions: Sample: 33 µM of Aβ(1-40) and 100 µM Aβ(1-42) of in 20 mM phosphate buffer pH 7.4. Incubation: quiescent conditions at 37 °C. Fused silica capillary: 50 µm i.d. × 40 cm × 31.5 cm. Eluent: 20 mM phosphate buffer, pH 7.4. Mobilization pressure: 100 mbar. Injection: 44 mbar for 3 s (V_{inj} = 7 nL, corresponding to 1% of capillary volume to injection point). Analyses were performed at 37 °C. UV detection at 191 nm.

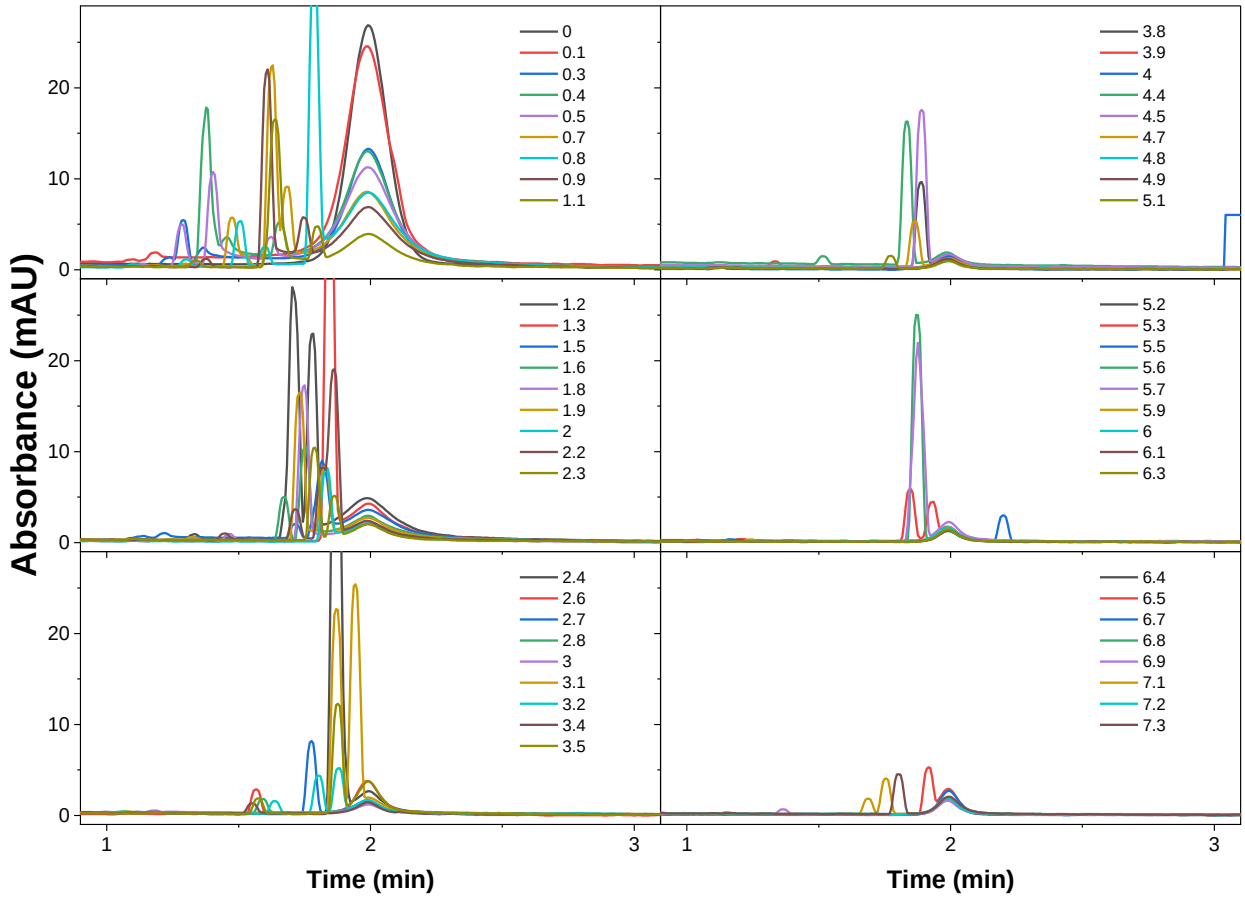

Figure SI.5. Experimental taylorgrams obtained for Aβ(1-42) aggregation monitoring over an incubation period of 8 h. The experimental traces are distributed into several graphs for better clarity. Curves are labelled by the incubation time, in h. Experimental conditions: Sample: 133 µM Aβ(1-42) in 20 mM phosphate buffer pH 7.4. Incubation: quiescent conditions at 37 °C. Fused silica capillary: 50 µm i.d. × 40 cm × 31.5 cm. Eluent: 20 mM phosphate buffer, pH 7.4. Mobilization pressure: 100 mbar. Injection: 44 mbar for 3 s (V_{inj} = 7 nL, corresponding to 1% of capillary volume to injection point). Analyses were performed at 37 °C. UV detection at 191 nm.

III.SI.3 Data treatment by Taylor dispersion analysis

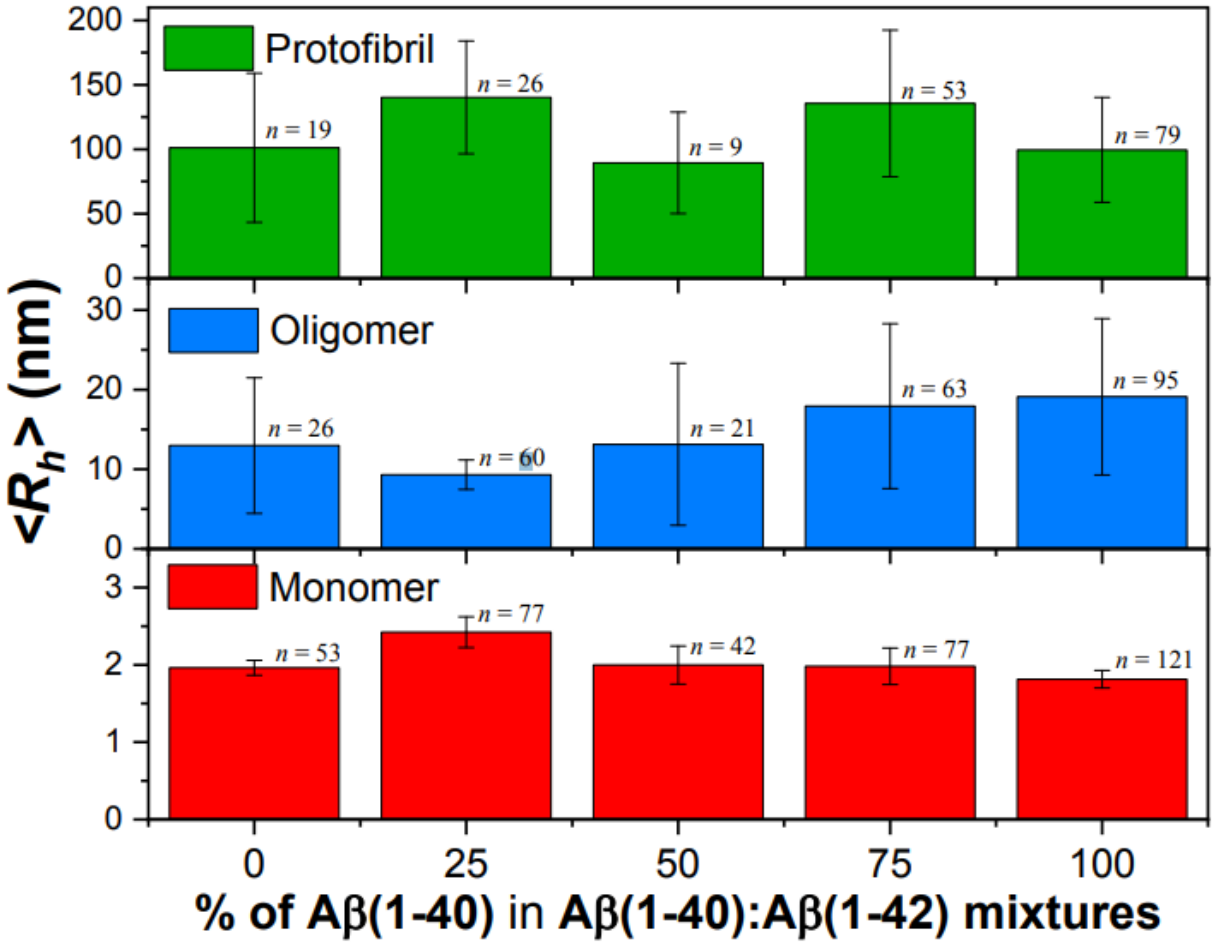

Figure SI.6. Average hydrodynamic radius of the monomer, oligomers and protofibrils size populations obtained by the deconvolution of the taylorgrams with a finite number of Gaussian functions and as a function of the ratio of Aβ(1-40):Aβ(1-42). The error bars are standard deviations calculated on n repetitions as indicated in the figure

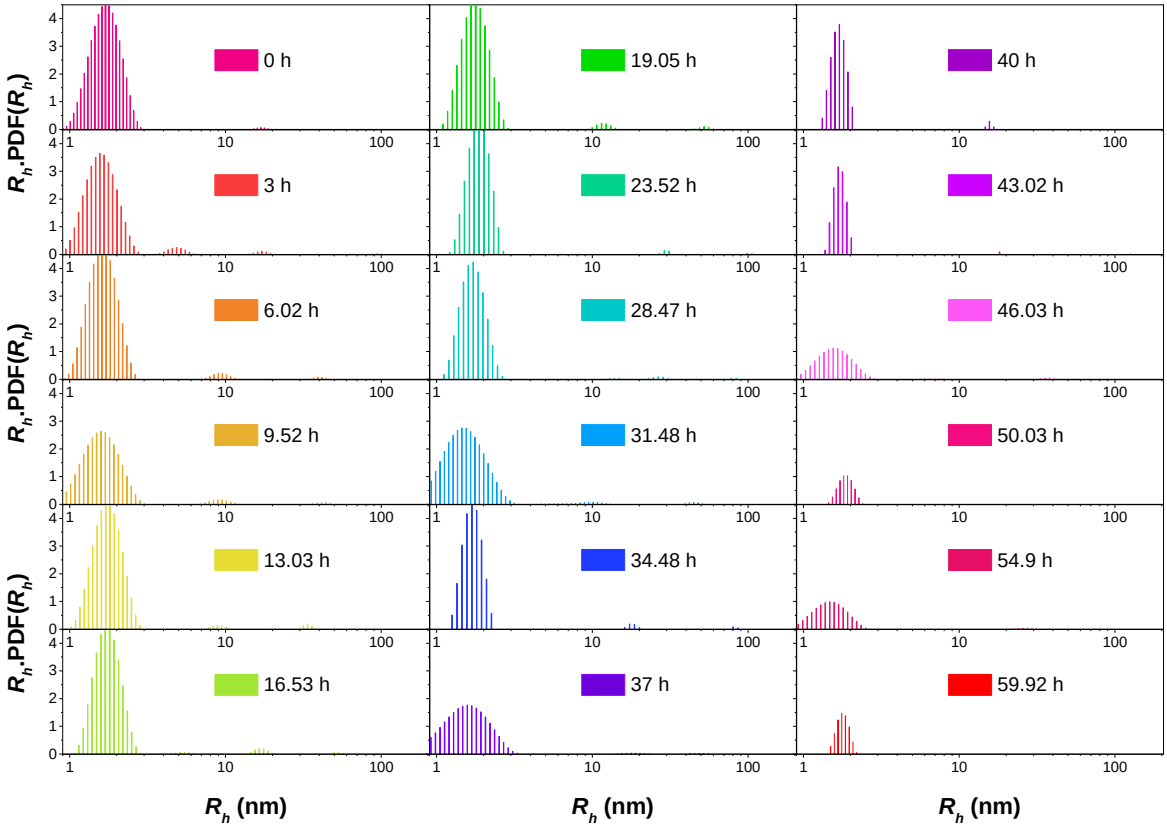

Figure SI.7. Size distributions of Aβ(1-40) (133.3 µM) obtained by CRLI analysis of the experimental taylorgrams as a function of incubation time t_{ag} = 0 to ~60 h. Experimental taylorgrams are shown in figure SI.1.

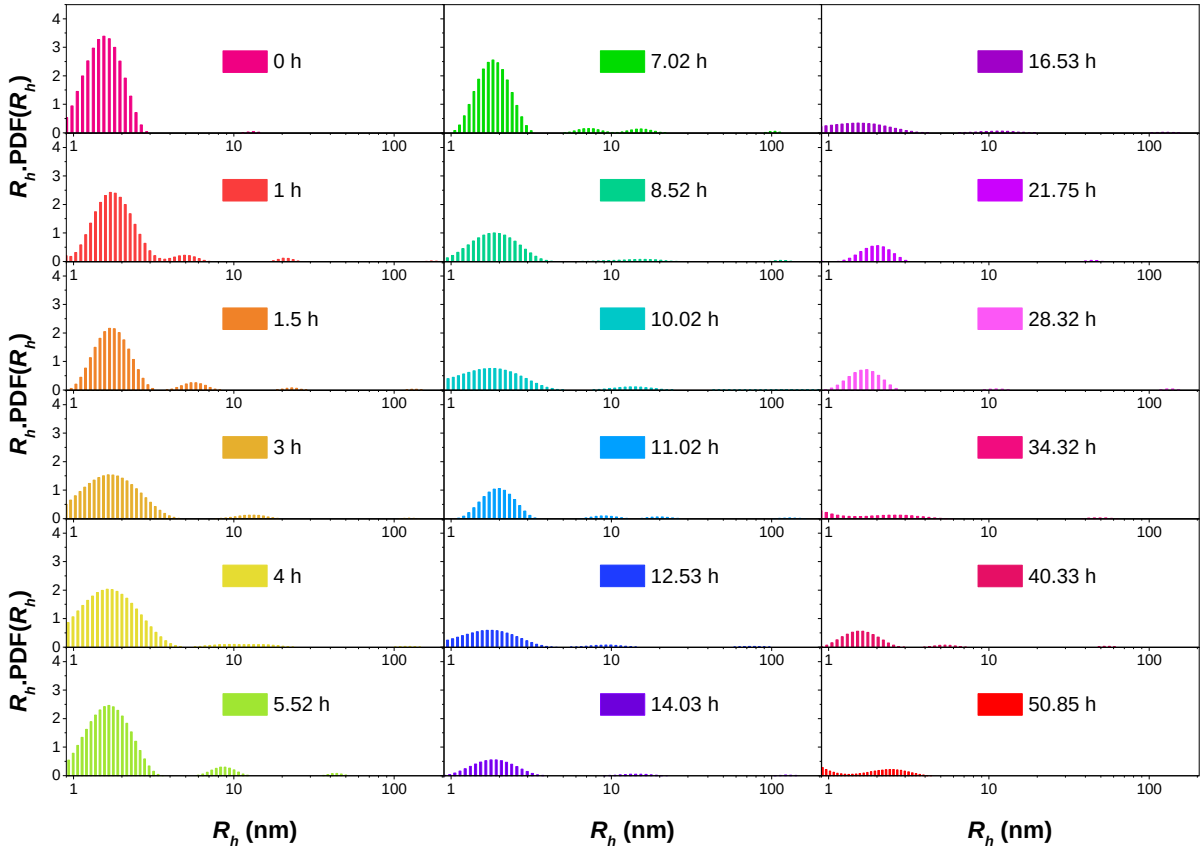

Figure SI.8. Size distributions of Aβ(1-40):Aβ(1-42) 3:1 mixture (100 µM and 33.3 µM respectively) obtained by CRLI analysis of the experimental taylorgrams as a function of incubation time t_{ag} = 0 to ~50 h. Experimental taylorgrams are shown in figure SI.2.

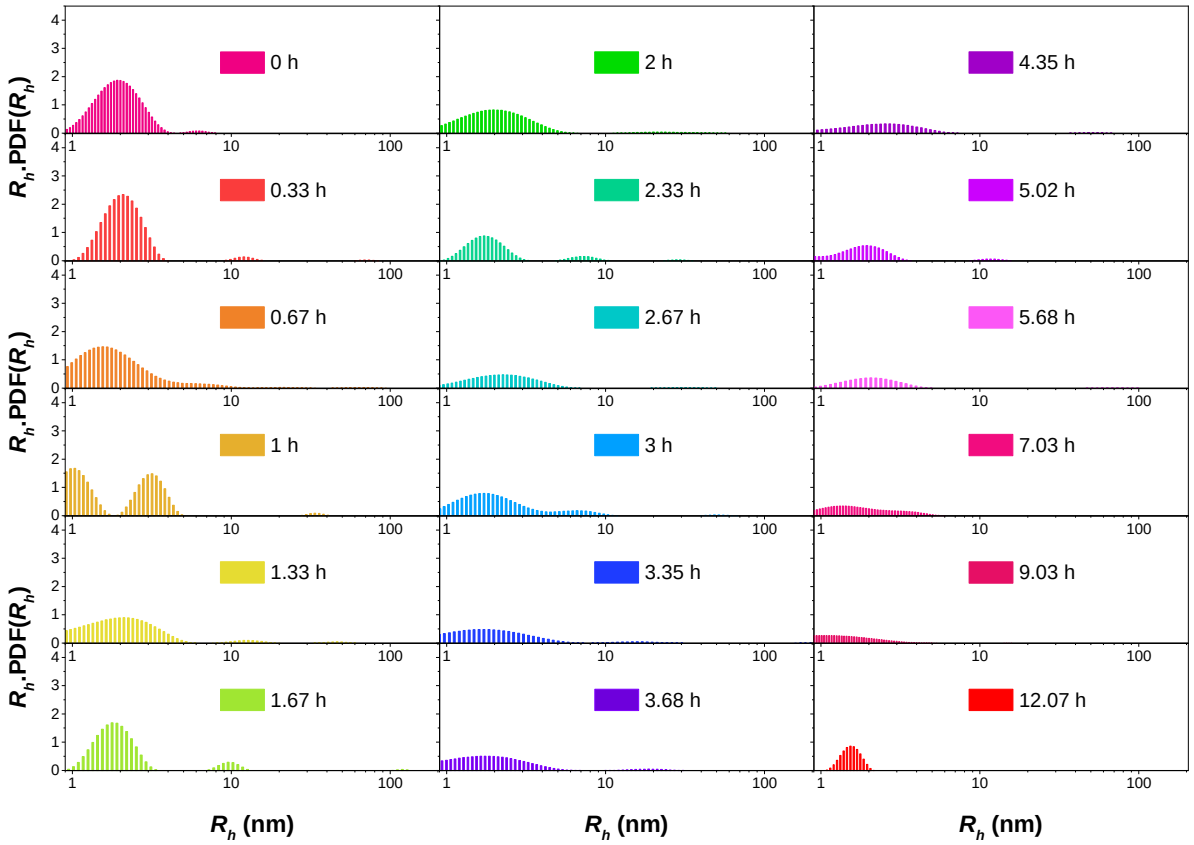

Figure SI.9. Size distributions of Aβ(1-40):Aβ(1-42) 1:1 mixture (66.7 µM and 66.7 µM respectively) obtained by CRLI analysis of the experimental taylorgrams as a function of incubation time t_{ag} = 0 to ~12 h. Experimental taylorgrams are shown in figure SI.3.

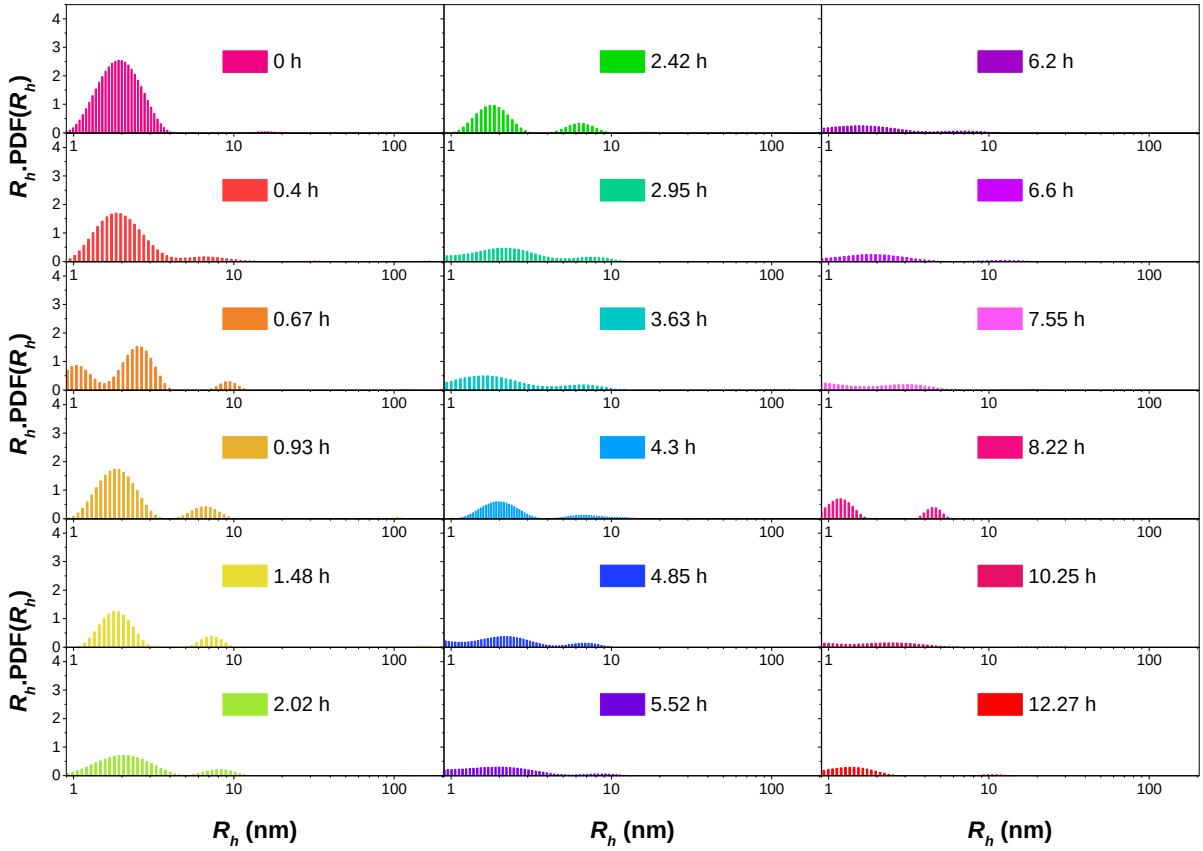

Figure SI.10. Size distributions of Aβ(1-40):Aβ(1-42) 1:3 mixture (33.3 µM and 100 µM respectively) obtained by CRLI analysis of the experimental taylorgrams as a function of incubation time t_{ag} = 0 to ~12 h. Experimental taylorgrams are shown in figure SI.4.

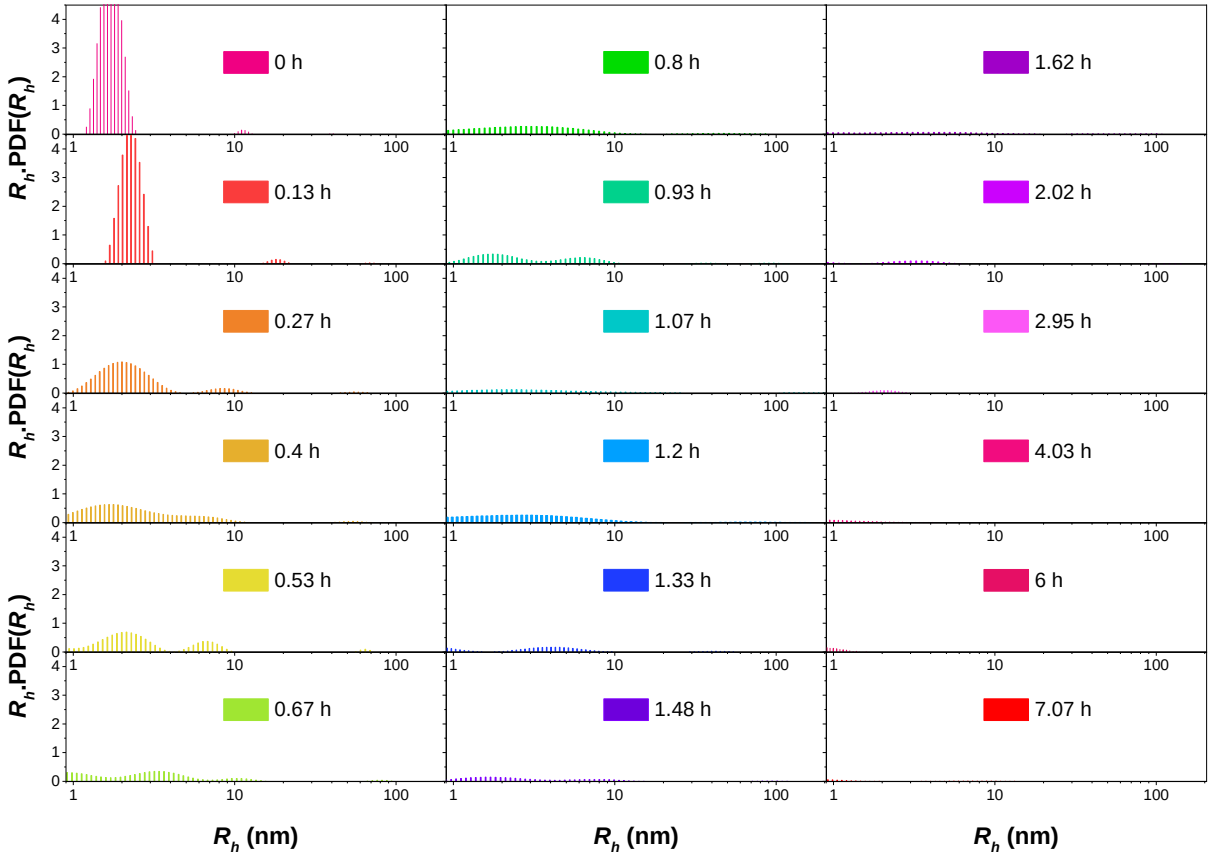

Figure SI.11. Size distributions of Aβ(1-42) (133.3 µM) obtained by CRLI analysis of the experimental taylorgrams as a function of incubation time t_{ag} = 0 to ~7 h. Experimental taylorgrams are shown in figure SI.5.

III.SI.4 Kinetics of the aggregation process

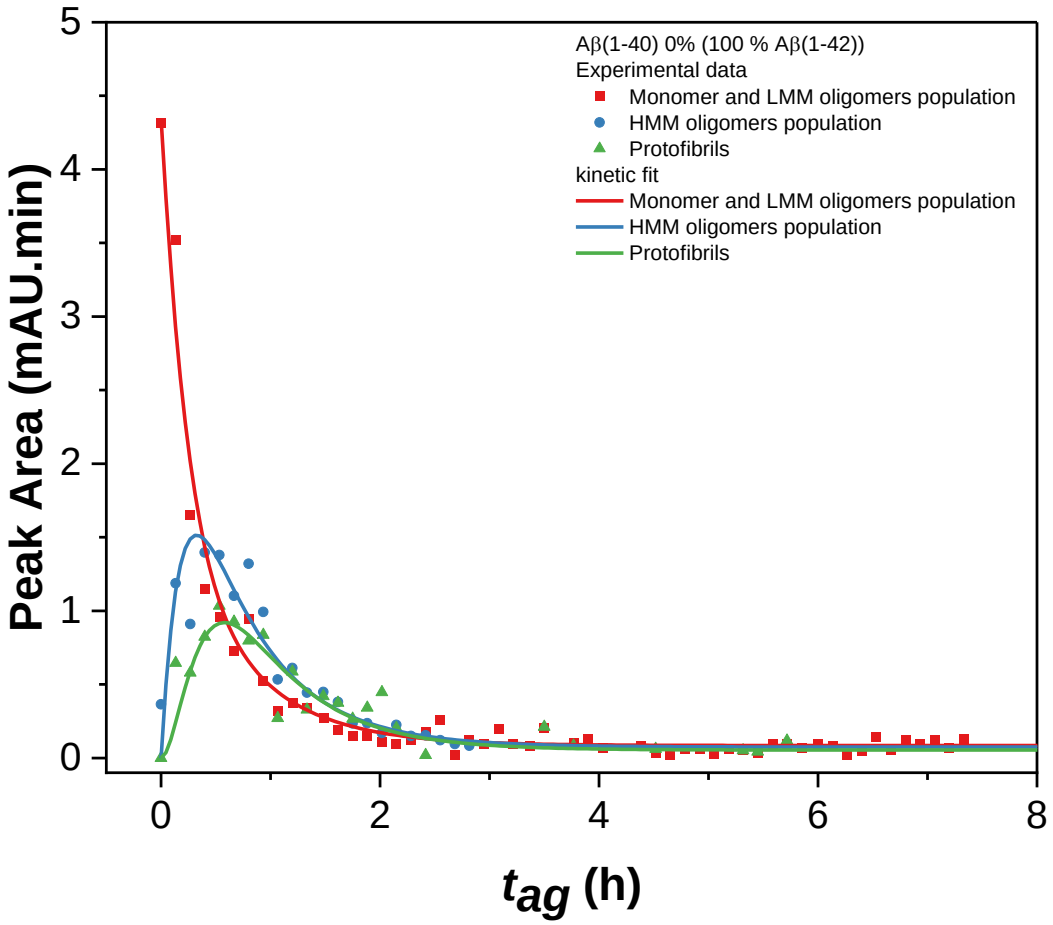

Figure SI.12. Symbols: time evolution of the peak area corresponding to the various populations obtained by deconvolution of the TDA signal for the Aβ(1-40) 0% sample. Lines: fits of the reaction kinetics, considering forward and backward reactions, Eqs. (5-7) in the main manuscript.

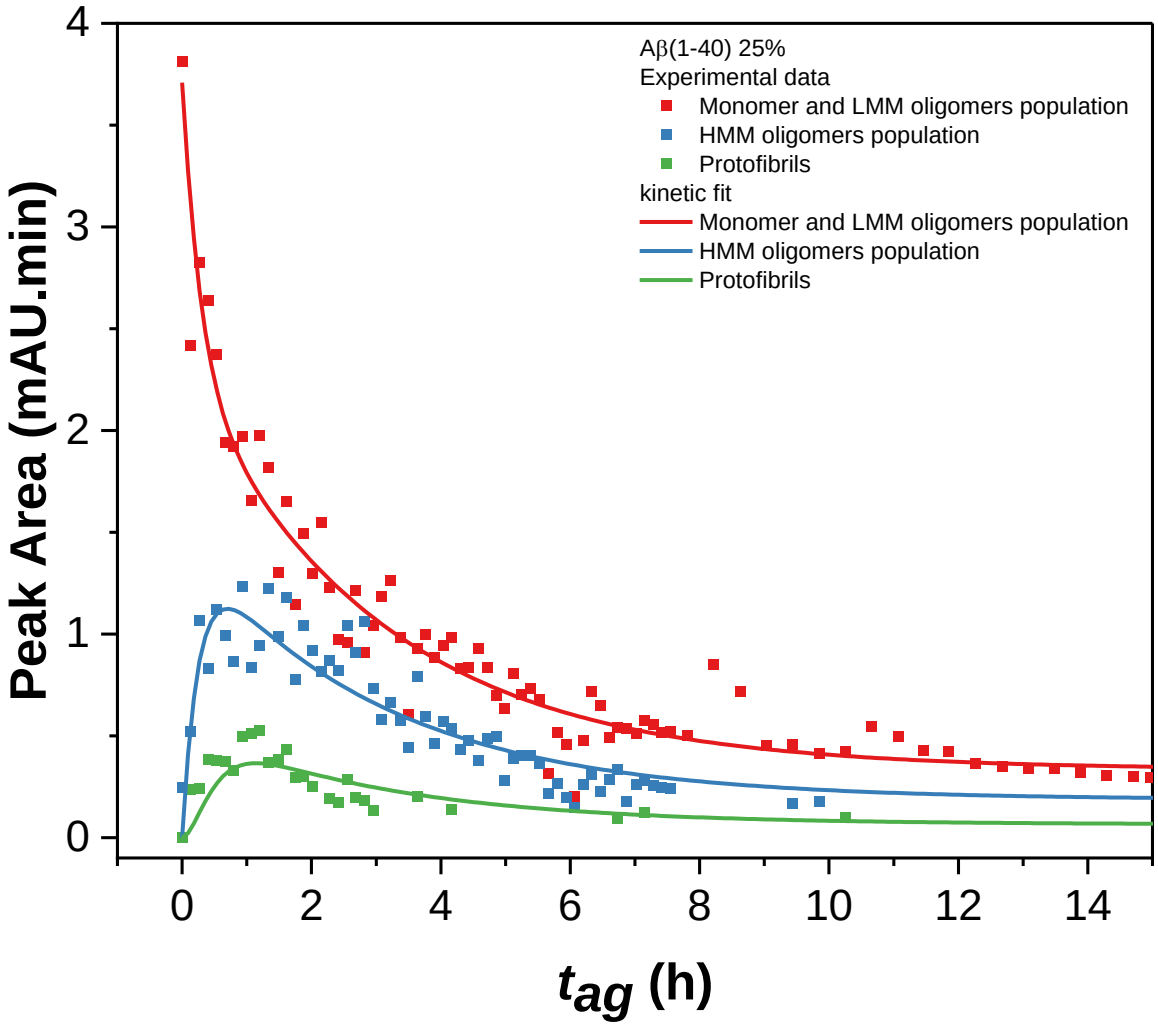

Figure SI.13. Symbols: time evolution of the peak area corresponding to the various populations obtained by deconvolution of the TDA signal for the Aβ(1-40) 25% sample. Lines: fits of the reaction kinetics, considering forward and backward reactions, Eqs. (5-7) in the main manuscript.

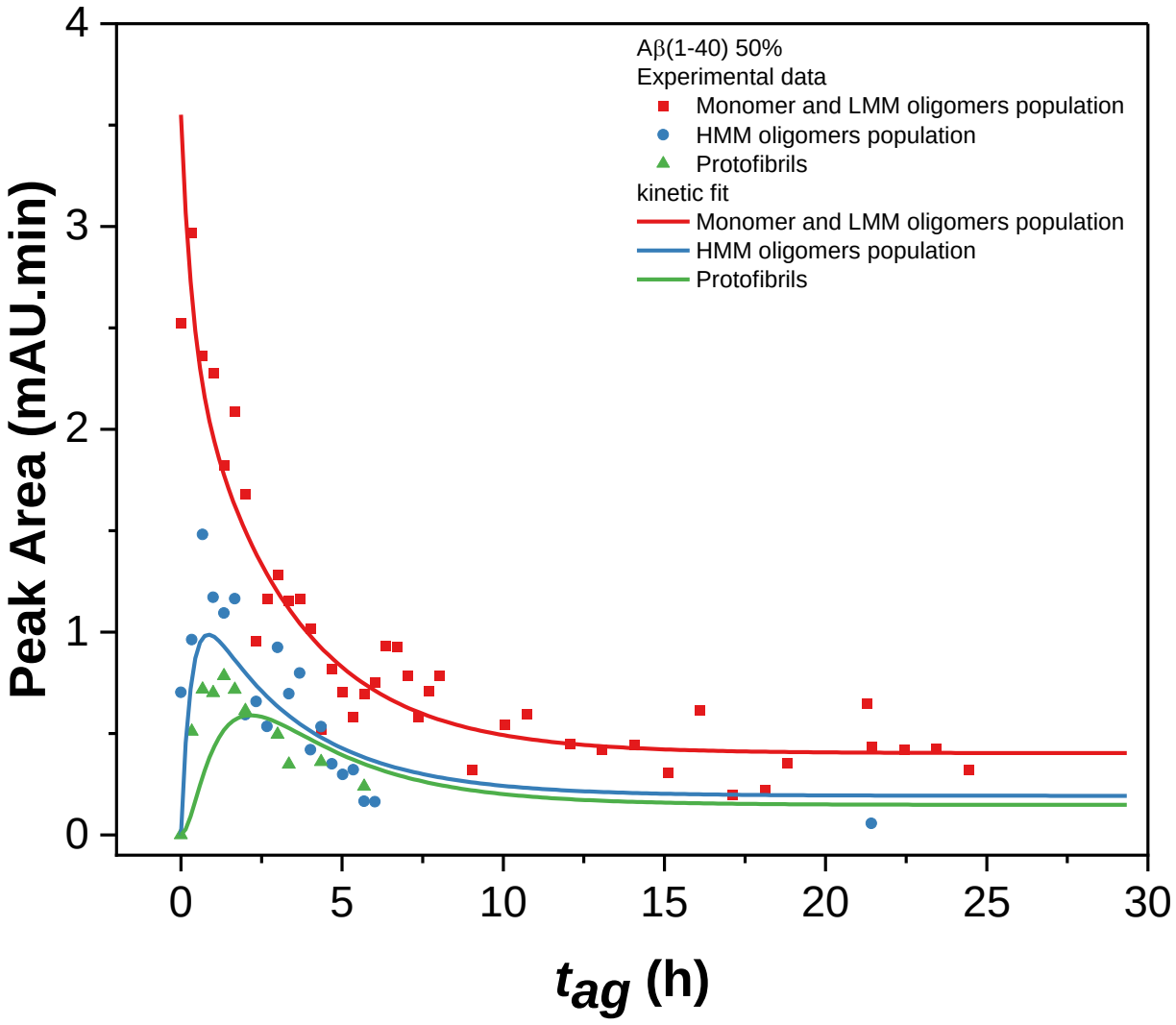

Figure SI.14. Symbols: time evolution of the peak area corresponding to the various populations obtained by deconvolution of the TDA signal for the Aβ(1-40) 50% sample. Lines: fits of the reaction kinetics, considering forward and backward reactions, Eqs. (5-7) in the main manuscript.

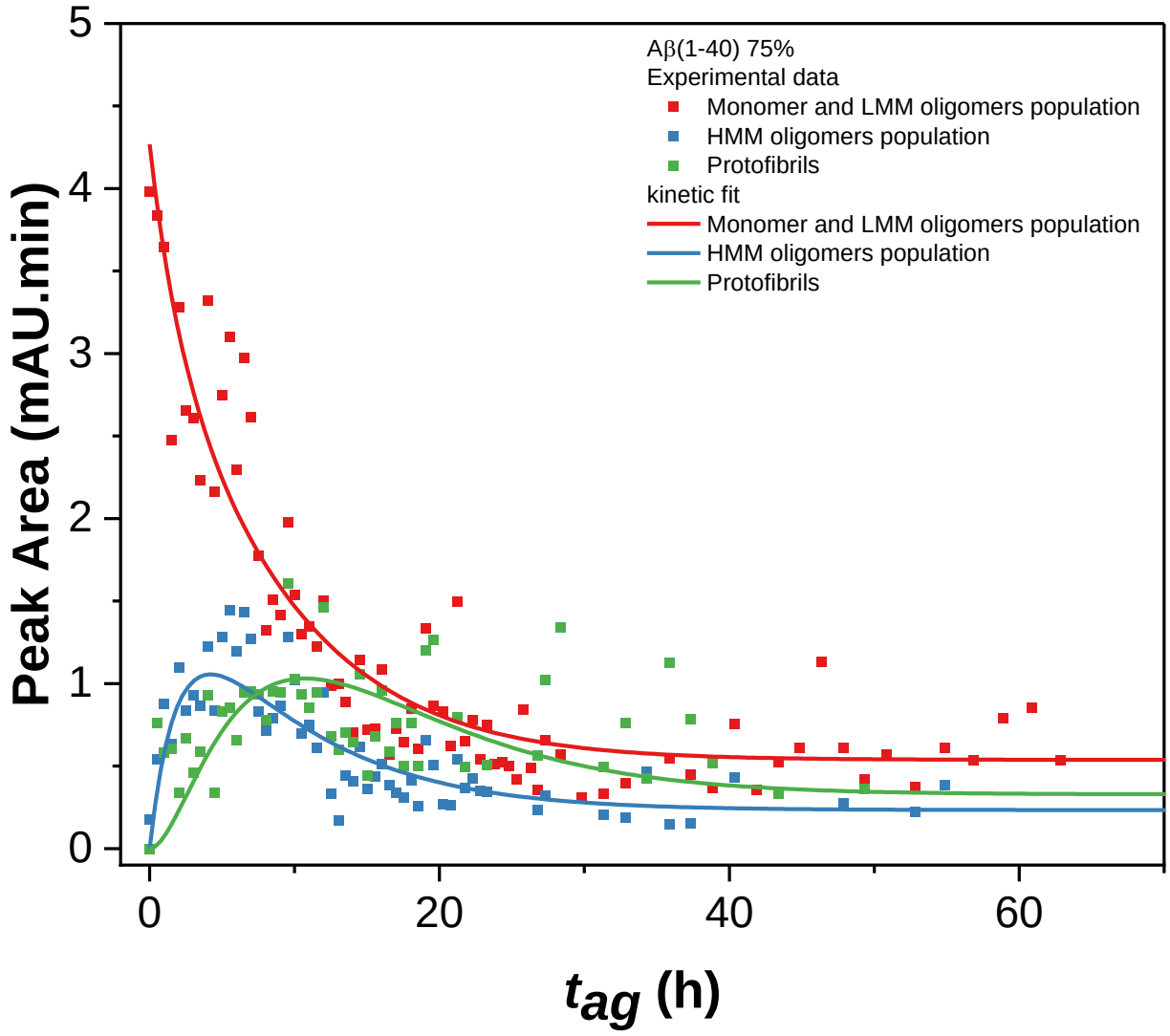

Figure SI.15. Symbols: time evolution of the peak area corresponding to the various populations obtained by deconvolution of the TDA signal for the Aβ(1-40) 75% sample. Lines: fits of the reaction kinetics, considering forward and backward reactions, Eqs. (5-7) in the main manuscript.

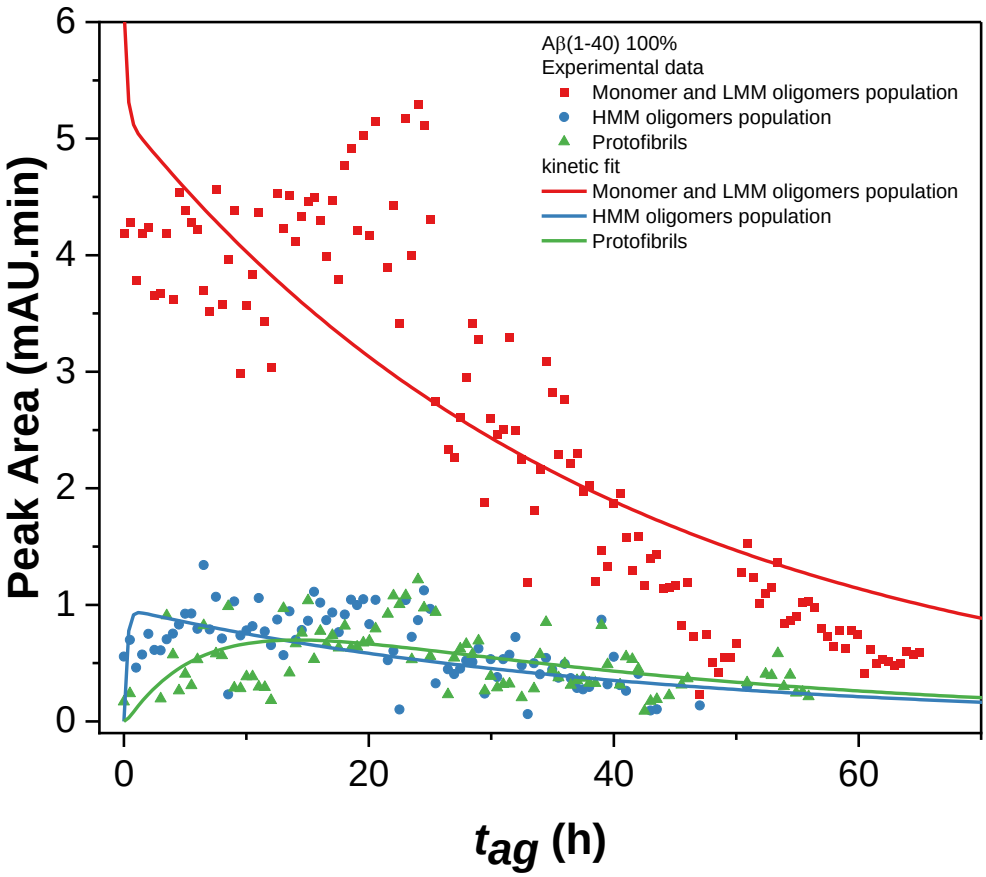

Figure SI.16. Symbols: time evolution of the peak area corresponding to the various populations obtained by deconvolution of the TDA signal for the Aβ(1-40) 100% sample. Lines: fits of the reaction kinetics, considering forward and backward reactions, Eqs. (5-7) in the main manuscript.

III.SI.5. References

1. Cottet, H., Biron, J. P. & Martin, M. On the optimization of operating conditions for Taylor dispersion analysis of mixtures. *Analyst* **139**, 3552–3562 (2013).

2. Taylor, G. Conditions under which dispersion of a solute in a stream of solvent can be used to measure molecular diffusion. *Proc. R. Soc. London. Ser. A. Math. Phys. Sci.* **225**, 473–477 (1954).

3. Chamieh, J., Biron, J. P., Cipelletti, L. & Cottet, H. Monitoring Biopolymer Degradation by Taylor Dispersion Analysis. *Biomacromolecules* **16**, 3945–3951 (2015).

4. Cipelletti, L., Biron, J. P., Martin, M. & Cottet, H. Measuring Arbitrary Diffusion Coefficient Distributions of Nano-Objects by Taylor Dispersion Analysis. *Anal. Chem.* **87**, 8489–8496 (2015).

5. Cipelletti, L., Biron, J. P., Martin, M. & Cottet, H. Polydispersity analysis of Taylor dispersion data: The cumulant method. *Anal. Chem.* **86**, 6471–6478 (2014).

Chapter IV

Monitoring the aggregation of FITC labelled Aß peptides by Taylor dispersion analysis using a simultaneous UV-LEDIF detection

Chapter IV. Monitoring the aggregation of FITC labelled Aβ peptides by Taylor dispersion analysis using a simultaneous UV-LEDIF detection

*Mihai Deleanu[1], Jean-François Hernandez[1], Hervé Cottet[*1], Joseph Chamieh[*1]*

[1]IBMM, Université Montpellier, CNRS, ENSCM, 34095 Montpellier, France

IV. Abstract

The amyloid cascade hypothesis has been considered a central event in Alzheimer disease for more than 30 years. In this work, four aggregation systems, consisting of native and FITC tagged Aβ(1-40) and Aβ(1-42), were explored using Taylor dispersion analysis coupled with a simultaneous UV-LEDIF detection. Results demonstrate that FITC had a strong inhibition effect upon the aggregation behavior of Aβ(1-42), where the lifetime of potentially toxic oligomers was prolonged, accompanied by a reduction in the abundance of the protofibril population. For the tagged Aβ(1-40) containing systems, only a retardation in kinetics was observed as compared to the native isoform. Interestingly, during the co-aggregation process of the mixed native (nAβ) and tagged (tAβ) peptides, the 100% nAβ peptide was found to be the dominant isoform of the aggregation pathway.

IV.1. Introduction

Beta-amyloid (Aβ) aggregation is one of the main causes that leads to Alzheimer disease (AD) and has been thoroughly investigated in the last 30 years[1,2]. The aggregation is favored in the neuronal synapses after amyloid precursor protein (APP) is processed in the amyloidogenic pathway by α- and β-secretase[2,3]. This leads to the generation of a wide range of Aβ isoforms and variants that further undergo a multistep chain of reactions leading to several toxic intermediates and fibrils that further accumulate in the extracellular space to form the amyloid deposits that consequently cause neuronal and cell death[4–6]. Both the aggregation mechanism and the species evolution are found to be governed by several intrinsic and extrinsic factors (*e.g.*, nature of the peptide[7], concentration[8], pH[9], ionic strength[10], and temperature[11]). The most common isoforms are Aβ(1-40) and Aβ(1-42), which differ only by two extra amino acids at the C-terminus that the latter isoform possess, making it more hydrophobic[4]. The co-aggregation mechanism of these two isoforms was intensively studied over the last decade[12–14]. Cukalevski *et al.* recently proposed that co-nuclei *i.e.* low molar mass oligomers, can form during the early stages. However, they did not observe heteromolecular fibrils[14]. While other reports suggested that mixed fibrils could be formed[15], and that cross-seeding can occur up to a certain extent[16]. Several studies used labelled peptides to gain more insights related to the aggregation mechanism, where the tags (fluorescent molecules) were attached at different amino acid residues (mainly at the N-terminus). This approach is very appealing because it allows to lower the limits of detection by using sensitive techniques such as fluorescence spectroscopy, and to study these amyloidogenic systems at physiological concentrations[17,18]. On the other hand, it was found that direct labeling of the peptides can alter the aggregation course in different ways[19–22]. In this work we show the use of Taylor dispersion analysis (TDA) coupled with simultaneous UV and LEDIF detections to check the influence of the fluorescent tag on the aggregation mechanism and to unravel if heteromolecular species are formed along the aggregation course. Four systems composed of a mixture of native and small amounts of FITC tagged Aβ(1-40) and Aβ(1-42) peptides were investigated by UV-LEDIF TDA.

IV.2. Experimental procedures

IV.2.1. Materials

Aβ(1–40) was prepared by fast conventional SPPS using a *Fmoc* orthogonal strategy, as described elsewhere[23]. Aβ(1-42) (batch number 100002591, >95% purity), FITC-β-Ala-Aβ(1-40) (batch number 1000019500, >90% purity) and FITC-εAhx-Aβ(1-42) (batch number 1000029066, >95% purity) were purchased from Bachem (Bubendorf, Switzerland). Sodium dihydrogeno phosphate and sodium hydroxide were purchased from Sigma Aldrich (France). All buffers were prepared using ultrapure water obtained from a MilliQ system (Millipore, France).

IV.2.2. Peptide pretreatment and sample preparation

Both native (nAβ) and tagged (tAβ) peptides were pretreated independently using the protocol previously described[23,24]. Briefly, the peptides were first dissolved at a concentration of 2 g/L in an ammonium hydroxide solution (NH_4OH) which concentration differed between the two studied peptides, for Aβ(1-40) it was of 0.10 % (m/v) while for Aβ(1-42) solutions it was of 0.16 % (m/v). The peptide solutions were then incubated for 10 minutes at room temperature, then aliquoted and freeze-dried. The stock aliquots contained 10 nmol of peptide, and lyophilized peptide aliquots were stored at -20 °C until use. The mixed aliquots containing both native and tagged Aβ were prepared in such a way so that the final sample would contain 7% of tAβ(1-40) or 10% of tAβ(1-42). Each of the required stock aliquots were dissolved in 100 µL of 0.16% (m/v) NH_4OH to avoid aggregation during this step, and appropriate volumes were used to obtain the desired systems having a total Aβ content of 10 nmol: i) 93% nAβ(1-40) + 7% tAβ(1-40) (9.3 nmol nAβ(1-40) + 0.7 nmol of tAβ(1-40)); ii) 3:1 Aβ(1-40):Aβ(1-42) – 93% nAβ(1-40) + 7% tAβ(1-40) + 100% nAβ(1-42) (6.8 nmols nAβ(1-40) + 0.7 nmol tAβ(1-40) + 2.5 nmol nAβ(1-42)); iii) 3:1 Aβ(1-40):Aβ(1-42) – 100% nAβ(1-40) + 90% nAβ(1-42) + 10% tAβ(1-42) (7.5 nmols nAβ(1-40) + 1.5 nmol nAβ(1-42) + 1 nmol tAβ(1-42)); iv) 90% nAβ(1-42) + 10% tAβ(1-42) (9 nmol nAβ(1-42) + 1 nmol of tAβ(1-42)). Figure 2 shows the proportion of the native and tagged peptides in the samples. The final aliquots were immediately subjected to freeze-drying and then stored at -20°C before being dissolved in 20 mM phosphate buffer at pH 7.4 to perform the aggregation study.

IV.2.3. Aβ aggregation study by Taylor dispersion analysis using a simultaneous UV-LEDIF detection

TDA was performed using an Agilent 7100 (Waldbronn, Germany) capillary electrophoresis system with bare fused silica capillary (Polymicro technologies, USA), having 60 cm × 50 µm i.d. dimensions and a UV detection window at 51.5 cm. The system was coupled with a Zetalif light-emitting diode induced fluorescence (LEDIF) detector (Picometrics, Toulouse, France) with a window at 33 cm. The capillary was conditioned with the following flushes: 1 M NaOH (30 min) followed by a flush with ultrapure water (30 min). Between each analysis, the capillary was rinsed with a 20 mM phosphate buffer at pH 7.4 for 2 min. Samples were injected hydrodynamically on the inlet end of the capillary (44 mbar, 4 s) and the injected volume was about 6.5 nL, corresponding to 1% of the capillary volume to the LEDIF detection point and 0.64% with respect to the UV detection window. Experiments were performed at a mobilization pressure of 100 mbar. The temperature of the capillary cartridge was set at 37°C and the vial carrousel was thermostated using an external circulating water bath 600F from Julabo (Germany). The solutes were simultaneously monitored by UV with an absorbance measured at 191 nm and by fluorescence with an excitation at 480 nm. Emission light was collected through a ball lens and a high-pass filter in the wavelength range from 515–760 nm. The proportion of tagged peptide in the mixtures was chosen so that the obtained LEDIF signal was at its highest without saturating the detector. The higher fluorescence intensity observed for tAβ(1-40) presumably stems from some trace amounts of unreacted FITC during synthesis and are thoroughly discussed in the data processing of the obtained taylorgrams section. The mobile phase was a 20 mM phosphate buffer (pH 7.4; viscosity at 37°C: 0.7×10^{-4} Pa.s)[24]. Peptide aliquots were first dissolved in 100 µL of a 20 mM phosphate buffer solution (pH 7.4) to reach a final concentration of 100 µM and then immediately transferred to a vial to be incubated at 37°C in the capillary electrophoresis instrument's carrousel. The aggregation was conducted by injecting the sample ($V_{inj} \approx 7$ nL) every 11 min for Aβ(1-42) independent experiments, and each 30 min for all the experiments containing Aβ(1-40). The total average TDA injections was between 124 and 185 TDA runs, corresponding to a total sample volume consumption between 870 to 1300 nL (0.87 and 1.3 µL). Finally, to prevent sample evaporation, the vial cap was changed three times a day. All taylorgrams were recorded using Agilent Chemstation software and then exported to Microsoft Excel for subsequent data

processing. The data obtained from the UV signal were treated mainly on the right side to avoid the spikes while those obtained by LEDIF were treated on the left side because of a peak deformation attributed to adsorption on the capillary surface possibly due to the fluorescent tag.

IV.3. Results and discussion

IV.3.1. Partially FITC labelled Aβ(1-40):Aβ(1-42) peptide mixtures

The main advantage of performing TDA with LEDIF detection using labelled peptides is that it can allow to study the aggregation process at physiological concentrations and can provide a better drug screening investigation compared to UV detection since inhibitors are generally UV absorbing. The fluorophore used in this study was fluorescein isothiocyanate (FITC). However, because no aggregation was observed for the FITC labelled peptides within a reasonable incubation timeframe at low Aβ concentrations (~ 10-100 nM), mixtures of native and tagged Aβ peptides were used instead at a total concentration of 100 µM. In order to obtain suitable conditions for performing a simultaneous LEDIF-UV analysis, the proportion of tagged peptide in the mixtures was chosen to be 7% and 10% for Aβ(1-40) and Aβ(1-42), so that the obtained LEDIF signal was at its highest without saturating the detector.

In this work, we have studied four different native (nAβ) and tagged (tAβ) systems as presented in the pie charts of Figure 1 by using a total content of FITC dye of 7% and 10% for Aβ(1-40) and Aβ(1-42), respectively. First, we investigated the influence of the tag for the independent Aβ systems (upper pie charts). Then, 3:1 Aβ(1-40):Aβ(1-42) mixtures were studied by changing the nature of the tagged peptide (bottom pie charts), with the aim to unravel whether heteromolecular Aβ(1-40)-Aβ(1-42) species can form during the co-aggregation process of the Aβ isoforms. To better understand the extent to which the tAβ peptide influenced the aggregation process, 100% nAβ systems were also investigated and analyzed only by UV.

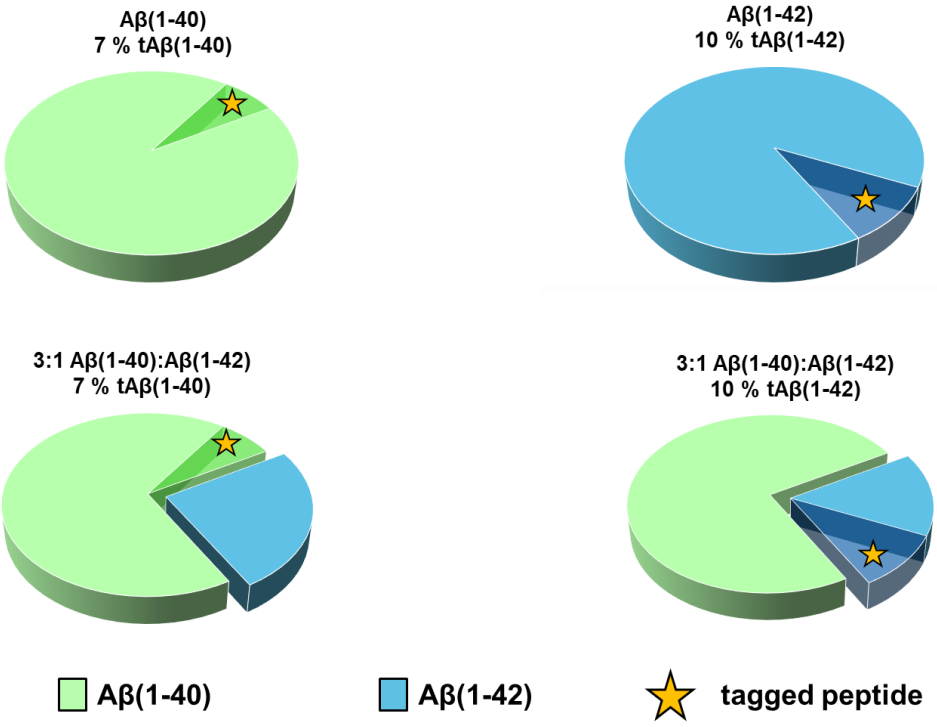

Figure 1. Pie charts outlining the proportion of the nAβ and tAβ content in the sample for all the studied tAβ containing systems. Legend: nAβ(1-40) – solid green pie/slice; nAβ(1-42) – solid blue pie/slice; transparency/orange star – tAβ.

As presented in our previous publication, a polydisperse mixture comprised of small molecules, monomers, oligomers, protofibrils and fibrils was obtained, and the species were distinguished based on their size. Small molecules (R_h < 1 nm), which could represent some impurities from the synthesis, counterions or unreacted FITC from the commercial samples were present during the whole aggregation process. Monomers and low molar mass oligomers (R_h= 1.6 – 4 nm), high molar mass oligomers (R_h= 5 – 50 nm), protofibrils (R_h= 50 – 250 nm) and some insoluble aggregates which most likely represent fibrils. Fibrils represent the end products of the aggregation; thus, they are very large species having a cross-sectional diameter of 2 – 20 nm and can reach lengths of more than 10 μm[19,27,28]. Due to their large size, these non-diffusing species could not be sized nor quantified by TDA[23]. Therefore, their evolution was mainly qualitatively assessed as only some of them managed to enter the capillary during the injection and appear in the shape of spikes on the left side of the elution profile[23].

IV.3.2. Data processing of the obtained taylorgrams

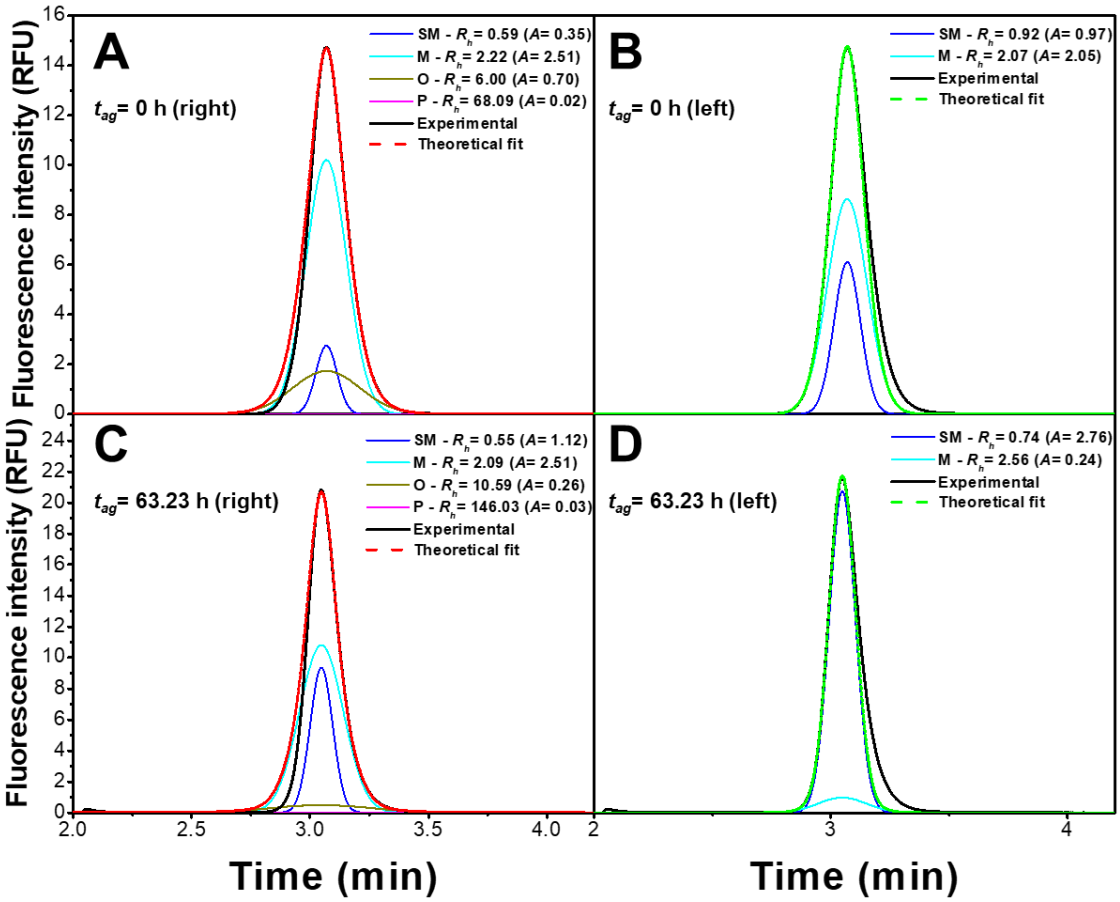

Figure 2. LEDIF-generated taylorgrams with data treatment processed on the right (A and C) or the left side of the experimental taylorgrams for 93% nAβ(1-40) + 7% tAβ(1-40) system at t_{ag} = 0 h (A and B) or at t_{ag} = 63.23 h (C and D). The experimental trace (black solid line) fitted with the sum of the required Gaussian peaks when data processing is performed either from the right side (dashed red) or the left side (dashed green) of the elution profile. The populations (Gaussians) are individually represented on the graph: SM (Small Molecules – blue solid line), M (Monomers – light blue solid line), O (Oligomers – dark yellow solid line) and P (Protofibrils – pink solid line). Experimental conditions: Sample: 100 µM Aβ (93 µM nAβ(1-40) + 7 µM tAβ(1-40)); 20 mM phosphate buffer, pH 7.4. Incubation: quiescent conditions at 37 °C. Fused silica capillaries: 50 µm i.d. × 60 cm × 33 cm. Mobile phase: 20 mM phosphate buffer, pH 7.4. Mobilization pressure: 100 mbar. Hydrodynamic injection: 44 mbar for 4 s, $V_{inj} \approx 7$ nL. Analyses were performed at 37 °C. Fluorescence excitation at 480 nm, emission light wavelength range from 515–760 nm. Baseline treatment was performed in Microcal Origin. The experimental fitting of the taylorgrams was performed by using Equation SI1 in Microsoft Excel.

Two examples of data processing are presented in Figure 2 for the system containing 7% tAβ(1-40) obtained immediately after the dissolution (t_{ag}= 0 h) and at a later aggregation time (t_{ag} = 63.23 h) respectively. The taylorgrams were analyzed on both left and right sides of the elution

profile since no significant spikes were detected. When the data treatment was performed from the right-side of the elution profile (Figure 2 A and C), the model required four Gaussians for solving the fitting (dashed red lines). However, the fittings were not optimal as the left side of peak was not properly integrated. This suggested that a non-desired adsorption of the FITC tagged peptide on the capillary walls occurs. This effect was observed in all the taylorgrams generated during the LEDIF analysis with no exception. On the other hand, when the experimental taylorgrams (black solid lines) were processed from the left-side of the elution profile (Figure 2 B and D), the theoretical fits (dashed green lines) required only two Gaussians, representative of monomer and small molecule populations, in accordance with the results obtained by UV detection. It can also be observed that the peak tailing on the right-side of the peak was avoided suggesting that the data processing approach was optimal. Consequently, in the case of LEDIF detection, the data processing was realized on the left-side of the elution peak. In our previous study[23] we have shown that because of the appearance of spikes, representing non-diffusing species in the sample, between $t_0/2$ and t_0 in the recorded taylorgram, a deformation occurs on the left-side of the elution profile, making the data processing difficult on this side, which is usually used to treat taylorgrams in TDA[25]. In the current study, a reduced appearance of both the number and the intensity of the spikes was observed on the left side of the LEDIF experimental elution profile.

To verify if it is possible to operate on both sides of the peak, the deconvolutions of the UV-generated taylorgrams were performed on both sides of the peak for some selected runs obtained for the 3:1 Aβ(1-40):Aβ(1-42) – 100% nAβ(1-40) + 90% nAβ(1-42) + 10% tAβ(1-42) system for which the broadening of the peak was high enough to detect all species. In Figure SI1, two examples of data processing on each side of the eluted peak are shown for the recorded UV run of the above-mentioned system at t_{ag}= 39.78 h. The obtained results were very similar on both sides (Figure SI2), validating the left-side treatment for fitting the LEDIF-generated experimental peaks. For obtaining reliable data from the LEDIF-generated taylorgrams by using this approach, different strategies were employed and are presented in the data treatment section in the SI (Figures SI3 and SI4). In the case of UV detection mode, no peak tailing was observed suggesting that mainly the fluorescent tag is responsible for the adsorption and that its contribution to the UV signal is negligible at the experimental wavelength. For that, all the peak fittings were successfully performed from the right-side of the elution profile in UV detection mode allowing a reliable processing and interpretation of the data, in the same manner described in our previous study[23].

An example of a full scale data processing performed from the right side which led to misleading results is presented in Figure SI18, for the system containing 10% tAβ(1-42) as compared the ones obtained from the left side of the experimental peak (Figure SI14) that, in contrast, yielded similar results to the ones determined during the UV analysis.

The second challenge that was encountered during the LEDIF analysis was the presence of a population of small molecules (R_h 0.7 – 0.9 nm) attributed to unreacted FITC that was found to be highly abundant (Figure SI17 C and D) throughout the whole aggregation process. In the case the UV detection mode, this population presented a R_h within the range of 0.3 – 0.5 nm (Figure SI17 A) and the contribution of the peak area was significantly smaller during the aggregation process compared to LEDIF (Figure SI17 B).

By using the data processing strategies described above, we were able to obtain the R_h and the peak areas of the relevant populations formed during the aggregation process. A better comparison of the results obtained by LEDIF and UV are presented in Figures SI13-16 where the R_h values of the species are very similar, while the area values of the populations presented the same evolution trend in both detection modes, further endorsing that the data processing strategies employed in this study were reliable.

IV.3.3. Monitoring the aggregation process of Aβ peptides by TDA-UV

Figure 3 shows the R_h evolution of the main soluble populations corresponding to monomers, low molar mass oligomers, high molar mass oligomers, and protofibrils, while Figure 4 presents the area of all the detected populations involved in the aggregation process by UV absorbance. The monomers and low molar mass oligomers presented an R_h of 1.60 – 2.25 nm which was relatively constant during the whole aggregation process (Figure 3, monomers). According to our previous study, these values suggest that this population is mainly comprised of monomers and dimers[23]. For all the studied systems, the R_h of protofibrils ranged from 50 to 250 nm and just a few events were observed in the case of the native Aβ(1-40) and 3:1 Aβ(1-40):Aβ(1-42) experiments, where protofibrils presented an R_h between 250 – 350 nm (Figure 3, protofibrils).

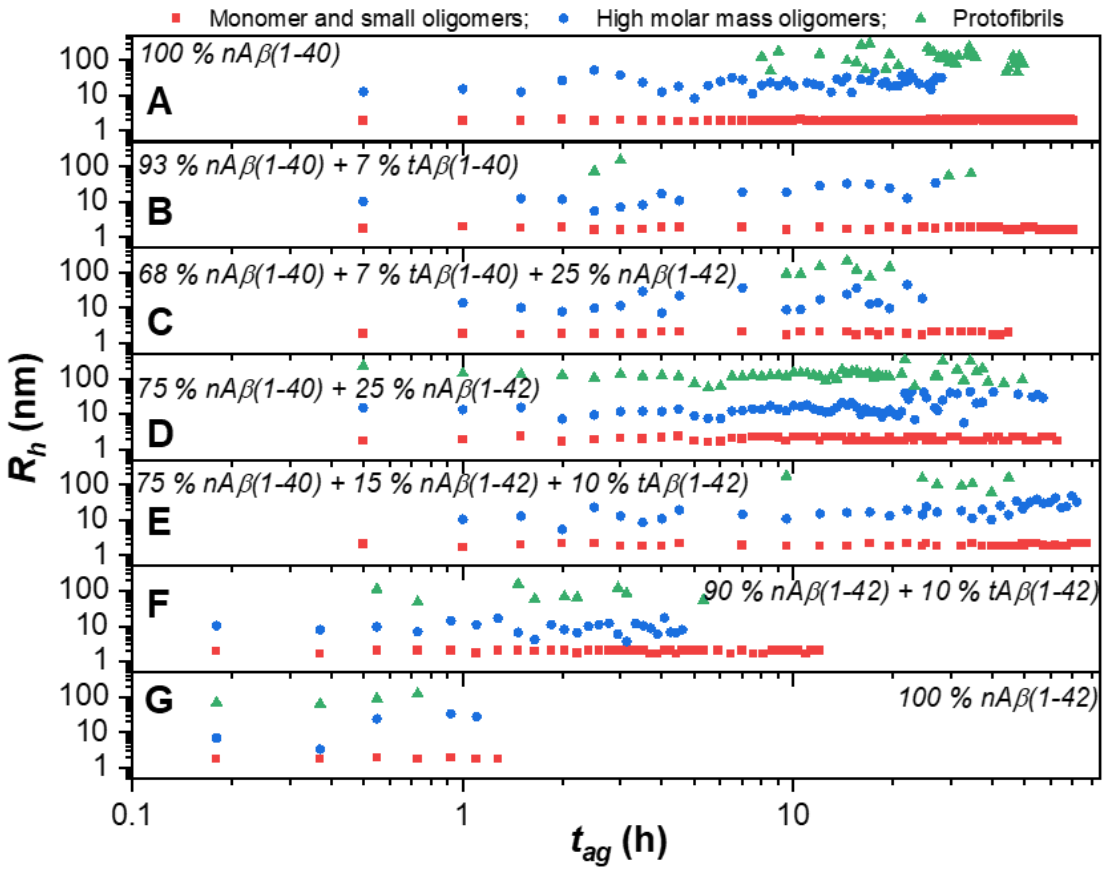

Figure 3. Hydrodynamic radius evolution of the species obtained for both nAβ + tAβ systems and 100 % nAβ experiments during the UV analysis: (A) 100% nAβ(1-40), (B) 93% nAβ(1-40) + 7% tAβ(1-40), (C) 3:1 Aβ(1-40):Aβ(1-42) - 68% nAβ(1-40) + 7% tAβ(1-40) + 25 % nAβ(1-42), (D) 3:1 Aβ(1-40):Aβ(1-42) - 75% nAβ(1-40) + 25% nAβ(1-42), (E) 3:1 Aβ(1-40):Aβ(1-42) - 75% nAβ(1-40) + 15% nAβ(1-42) + 10% nAβ(1-42), (F) 90% nAβ(1-42) + 10% tAβ(1-42), (G) 100% nAβ(1-42). The species are represented as follows: monomer and low molar mass oligomers (■), higher molar mass oligomers (●) and protofibrils (▲). Experimental conditions: Sample: 100 µM total Aβ; 20 mM phosphate buffer, pH 7.4. Incubation: quiescent conditions at 37 °C. Fused silica capillaries: 50 µm i.d. × 60 cm × 51.5 cm. Mobile phase: 20 mM phosphate buffer, pH 7.4. Mobilization pressure: 100 mbar. Injection: 44 mbar for 4 s, Vi ≈ 7 nL (Vi / Vd ≈ 0.6 %). Analyses were performed at 37 °C. UV detection at 191 nm.

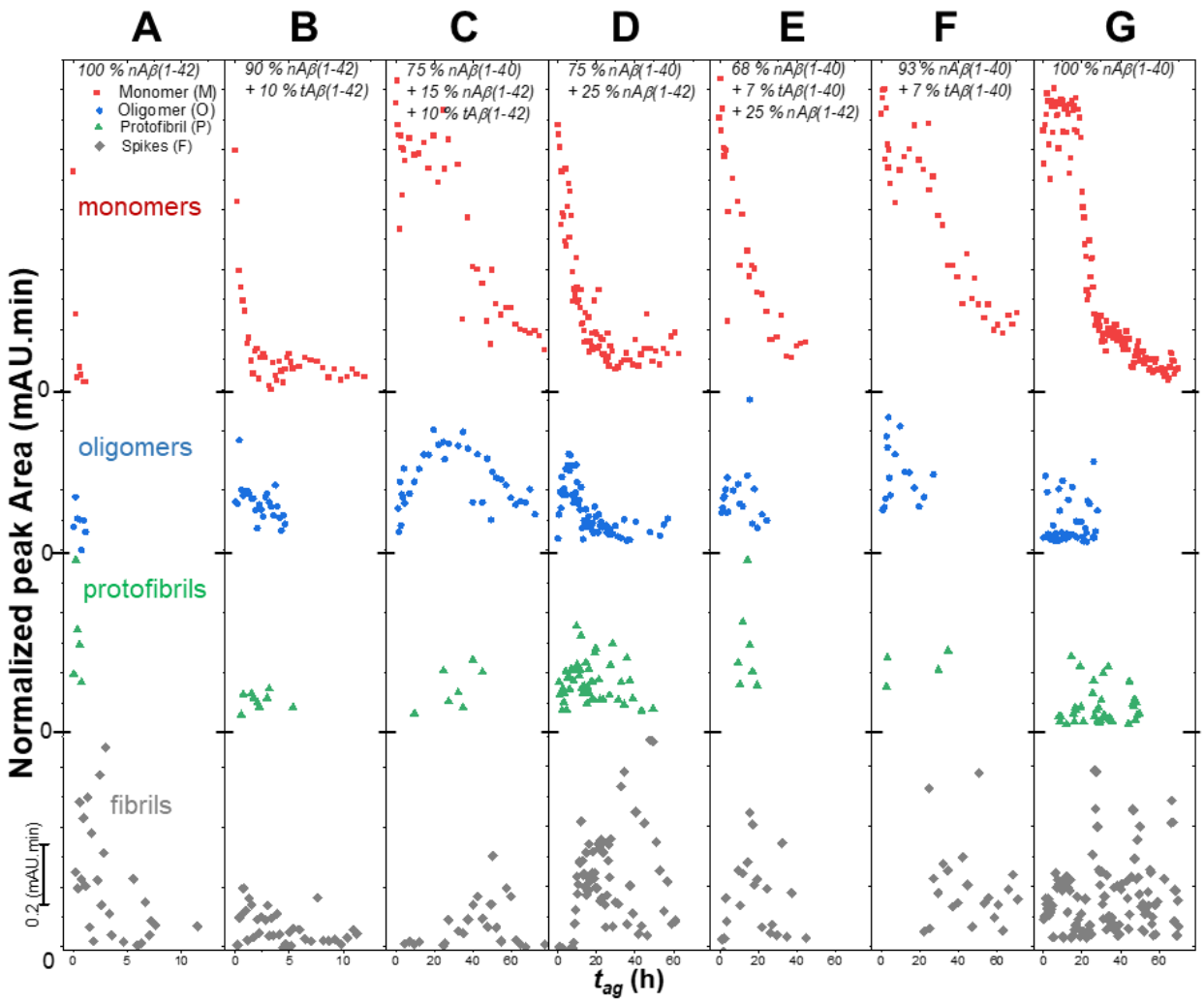

Figure 4. Peak area evolution of the species obtained for both nAβ + tAβ systems and 100 % nAβ experiments during the UV analysis: (A) 100% nAβ(1-42), (B) 90% nAβ(1-42) + 10% tAβ(1-42), (C) 3:1 Aβ(1-40):Aβ(1-42) - 75% nAβ(1-40) + 15% nAβ(1-42) + 10% nAβ(1-42), (D) 3:1 Aβ(1-40):Aβ(1-42) - 75% nAβ(1-40) + 25% nAβ(1-42), (E) 3:1 Aβ(1-40):Aβ(1-42) - 68% nAβ(1-40) + 7% nAβ(1-40) + 25% nAβ(1-42), (F) 93% nAβ(1-40) + 7% tAβ(1-40), (G) 100% nAβ(1-40). The populations of the species are represented as follows: monomer and low molar mass oligomers (■), higher molar mass oligomers (●), protofibrils (▲), and fibrils (non-diffusing species) (♦). Experimental conditions as in Figure 3. Peak area was normalized by dividing the area of each data point to the total peak area obtained for the first run at t= 0 h to obtain a better comparison of the species evolution.

The nAβ(1-42) peptide aggregated fast, as the area of the population corresponding to monomers and the low molar mass oligomers reached a minimum after less than 1 hour (Figure 4 A, monomers), while the area of the other soluble intermediates evolved and disappeared within the same time (Figure 4 A, oligomers and protofibrils). Meanwhile, the fibrils formed from the beginning of the aggregation reaching a maximum after the consumption of all the soluble species (Figure 4 A, fibrils). These observations are consistent with ones described in our previous

publication[23], where Aβ(1-42) first passes through an intermediate state, enriched in high molar mass oligomers and protofibrils before reaching mature fibrils. By looking next at the system containing 10% tAβ(1-42), the monomeric population was consumed after more than 2 h (Figure 4 B, monomers), while the evolution of the high molar mass oligomers was extended to about 5 h (Figure 4 B, oligomers), without observing a major difference in their size (R_h= 4 – 16 nm for the 10% tAβ(1-42) system (Figure 3 F, oligomers); R_h= 4 – 12 nm for the 100 % nAβ(1-42) experiment (Figure 3 F, oligomers). These results suggests that a delay in the aggregation rate occurred with 10% tagged Aβ(1-42) accompanied by an increase in life time of potentially toxic oligomers, with no impact upon their size as compared to the nAβ(1-42). Next, we observed a significant reduction in the abundance of both the protofibrils population (Figure 4 B, protofibrils) and the fibrils (Figure 4 B, fibrils) as compared to the ones generated by the native peptide (Figure 4 A, protofibrils and fibrils). These results suggest that not only the oligomerization and aggregation rate is retarded, but also the elongation phase of the process is affected. In a study performed by Zheng *et al.*, the effect of several fluorescent dyes upon the aggregation process of Aβ(1-42) was investigated using fluorescence correlation spectroscopy[21]. Among these dyes, the effect of FITC was also evaluated and the authors concluded that this dye decreased the propensity of oligomers to aggregate as the initial R_h value of their studied system was 1.3 nm and remained constant during the whole aggregation course[21]. By taking into account both the net charge and the hydrophilic character of the dye the authors suggested that the inhibition of the aggregation process occurred due to a decrease of electrostatic attractions and of the hydrophobic character of Aβ(1-42), but the authors did not provide a direct comparison with the nAβ(1-42). In this work, the main advantage of using the UV detection was that it allowed to monitor the extent to which the amount of tAβ peptides affected the aggregation process, by comparing those systems with the 100% nAβ experiments.

A similar effect was observed in 3:1 Aβ(1-40):Aβ(1-42) containing 10% tAβ(1-42) as compared to the Aβ(1-42) system containing 10% tAβ(1-42). First, a significant reduction in the aggregation rate as a lag phase of about 20 h was observed before the area of the monomers and the low molar mass oligomers population started to decrease reaching a minimum after ~50 h of incubation (Figure 4 C, monomers), in contrast to the 100% native 3:1 Aβ(1-40):Aβ(1-42) mixture where no lag phase was observed, and this population reached a minimum plateau after only 25 hours (Figure 4 D, monomers). The evolution of the higher molar mass oligomer population presented a bell-shaped profile with a maximum centered around 6 h, and reached a minimum after

~30 h during native 3:1 Aβ(1-40):Aβ(1-42) mixture (Figure 4 D, oligomers), and presented a R_h value in the range of 6 – 43 nm (Figure 3 D, oligomers), while in the case of mixture containing 10% tAβ(1-42), this profile was detected after more than 70 h (Figure 4 C, oligomers) with no difference observed in their size (R_h= 6 – 48 nm) (Figure 3 E, oligomers), further suggesting that lifetime of potentially toxic oligomers was significantly extended.

Further on, we investigated the influence of tAβ(1-40) on the aggregation process. As presented in our previous work, the aggregation of Aβ(1-40) is slower compared to Aβ(1-42) where a lag phase of about 20 h (Figure 4 G, monomers) was observed, and that followed a pathway where monomers are converted into fibrils (Figure 4 G, fibrils) without passing through a significant oligomerization (Figure 4 G, oligomers) and protofibrillar (Figure 4 G, protofibrils) state. In the case of the system containing 7% tAβ(1-40), a sigmoidal decrease of the area of the monomeric population started after 20 h (Figure 4 F, monomers), corresponding to the same incubation time for which the decrease started in the case of the 100% nAβ(1-40) experiment (Figure 4 G, monomers), but the slope presented a moderate decrease reaching a minimum after 60 h, in contrast to the one corresponding to 100% nAβ(1-40) where the decrease was faster reaching a plateau after 30 h (Figure 4 G, monomers). No significant change was observed during the evolution of the high molar mass oligomers (Figure 4 F, oligomers) and protofibrils (Figure 4 F, protofibrils), further suggesting that the aggregation process of Aβ(1-40) is only slightly affected by the presence of FITC. The evolution of the monomeric population (Figure 4 F, monomers), was also very similar to that of the one presented for the 3:1 Aβ(1-40):Aβ(1-42) mixture containing 10% tAβ(1-42) (Figure 4 C, monomers). This further suggests that the native Aβ(1-40) was the dominant isoform during this experiment. While, when looking at the results obtained for the 3:1 Aβ mixture containing 7% tAβ(1-40) (Figure 4 E) the aggregation pathway very similar with the 100% native mixture (Figure 4 D). It seems that Aβ(1-42) preserved its native electrostatic and hydrophobic character and was the dominant species during this experiment. These results suggest that Aβ(1-42) controls the aggregation kinetics and mechanism of the mixture. If the aggregation of Aβ(1-42) is controlled or influenced (i.e. with the FITC tag) then the aggregation of the mixture containing 10% of tAβ(1-42) will follow the aggregation rate of Aβ(1-40) meaning that fibrilization phase is retarded and the lifetime of the intermediate species is extended. These results also endorse the possibility that a co-oligomerization occurs, and the two isoforms influence each other's pathway. This does not exclude the fact that if the FITC content is increased, the overall

effect of this specific dye upon the system will become more significant. For further investigating this aspect, different FITC:nAβ ratios should be studied.

Finally, by comparing the fibrils evolution, it can be observed that in the case of both systems containing 10% tAβ(1-42), their abundance was lower (Figure 4 B and C, fibrils) compared to the ones formed during the 100% native experiments (Figure 4 A and D, fibrils). It is possible that either the fibril formation was inhibited or some of them became large enough not to enter the capillary. In the case of the systems containing 7% t(Aβ1-40), the fibrils started to appear after 20 h of incubation (Figure 4 F, fibrils) with no difference in the abundance as compared to the ones generated during the nAβ(1-40) experiment (Figure 4 G, fibrils). For the 3:1 Aβ mixture containing 7% tAβ(1-40), fibrils started to appear from the beginning of the process (Figure 4 E, fibrils) and presented a very similar evolution compared to the native 3:1 Aβ mixture (Figure 4 D, fibrils). These results further endorse the possibility that the native Aβ(1-42) represented the aggregation core of the complex system because it preserved its electrostatic and hydrophobic character. However, because TDA is not able to size and quantify these species, other methods such as Thioflavin T (ThT) assay, electron microscopy (EM) and atomic force microscopy (AFM) techniques should be employed for further exploring the effect of the fluorescent dye on the elongation phase, the final fibril yield, their size and morphology.

IV.3.4. Monitoring the aggregation process of Aβ peptides by TDA-LEDIF

Figure 5 shows the R_h evolution of the main soluble populations corresponding to monomers, low molar mass oligomers, high molar mass oligomers, and protofibrils, while Figure 6 presents the area of all the detected species involved in the aggregation process and detected during the LEDIF analysis. The monomers and low molar mass oligomers presented an R_h of 1.60 – 2.5 nm, which was relatively constant during the whole aggregation process (Figure 5, monomers). For all the studied systems, the R_h of protofibrils ranged from 50 to 250 nm with no significant differences between all four tAβ containing systems (Figure 5, protofibrils). These results are very similar with the ones obtained during the UV analysis.

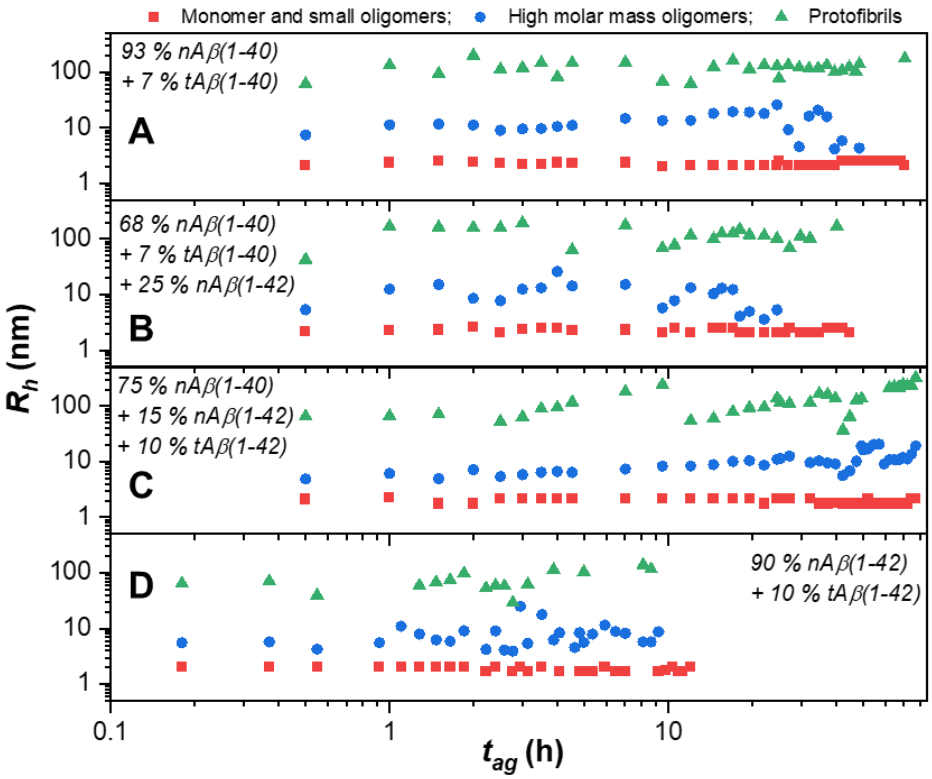

Figure 5. Hydrodynamic radius evolution of the species obtained for the nAβ + tAβ systems during the LEDIF analysis: (A) 93% nAβ(1-40) + 7% tAβ(1-40), (B) 3:1 Aβ(1-40):Aβ(1-42) - 68% nAβ(1-40) + 7% tAβ(1-40) + 25 % nAβ(1-42), (C) 3:1 Aβ(1-40):Aβ(1-42) - 75% nAβ(1-40) + 15% nAβ(1-42) + 10% nAβ(1-42), (D) 90% nAβ(1-42) + 10% tAβ(1-42). The species are represented as follows: monomer and low molar mass oligomers (■), higher molar mass oligomers (●) and protofibrils (▲). Experimental conditions: Sample: 100 µM total Aβ; 20 mM phosphate buffer, pH 7.4. Incubation: quiescent conditions at 37 °C. LEDIF: Fused silica capillaries: 50 µm i.d. × 60 cm × 33 cm. Mobile phase: 20 mM phosphate buffer, pH 7.4. Mobilization pressure: 100 mbar. Injection: 44 mbar for 4 s, Vi ≈ 7 nL (Vi / Vd ≈ 1 %). Analyses were performed at 37 °C. Fluorescence excitation at 480 nm, emission light wavelength range from 515–760 nm.

As described in more details in the data processing of the obtained taylorgrams section, the LEDIF analysis was affected both by an adsorption of FITC on the capillary walls and by the presence of unreacted FITC molecules. For this, different fitting strategies were employed to overpass these challenges. However, despite the adequate data processing approach, some results were still affected by the unreacted FITC. By looking first at the monomer and low molar mass oligomers area evolution, a significant drop in the area of this population was observed (Figure 6, monomers), but presented a similar trend compared to the one observed during the UV analysis (Figure 4, monomers). These effects were most likely caused by the presence of the unreacted FITC traces that masked the evolution of the monomeric population and consequently couldn't fit the overall evolution observed during the UV analyses. For all the other populations, both the

evolution and abundance were affected in the case of all the studied systems most likely due to the same reason. Therefore, a proper comparison between the results obtained by UV and LEDIF could not be performed. However, in contrast to what was obtained during the UV analysis (Figure 4 oligomers, protofibrils, fibrils), by LEDIF it was possible to observe more events of the intermediates (Figure 6 oligomers, protofibrils) and fibrils (Figure 6 fibrils). This can be attributed to the better sensitivity and lack of background noise that the LEDIF detection mode offers. The only exception for which an evolution trend of the high-ordered species could be observed was for the protofibrils population obtained during the 3:1 Aβ(1-40):Aβ(1-42) mixture containing 7% tAβ(1-40), where a bell-shaped profile presenting a maximum after ~15 h of incubation during both LEDIF (Figure 6, protofibrils) and UV (Figure 4 E, protofibrils) analyses but was better observed during the fluorescence detection mode. This result was most likely achieved due the fact that the abundance was high enough not to be masked neither by the FITC traces nor by the peak tailing occurring on the right side of the experimental peak. This result confirms the observations made during the UV analysis, where the aggregation process of this system was very similar to one presented for the 100% native 3:1 Aβ(1-40):Aβ(1-42) mixture, most likely because Aβ(1-42) preserved its native character. This result also outlines the accuracy of the data processing strategies employed for the data treatment of the obtained taylorgrams during the LEDIF analysis that led to the obtention of reliable results.

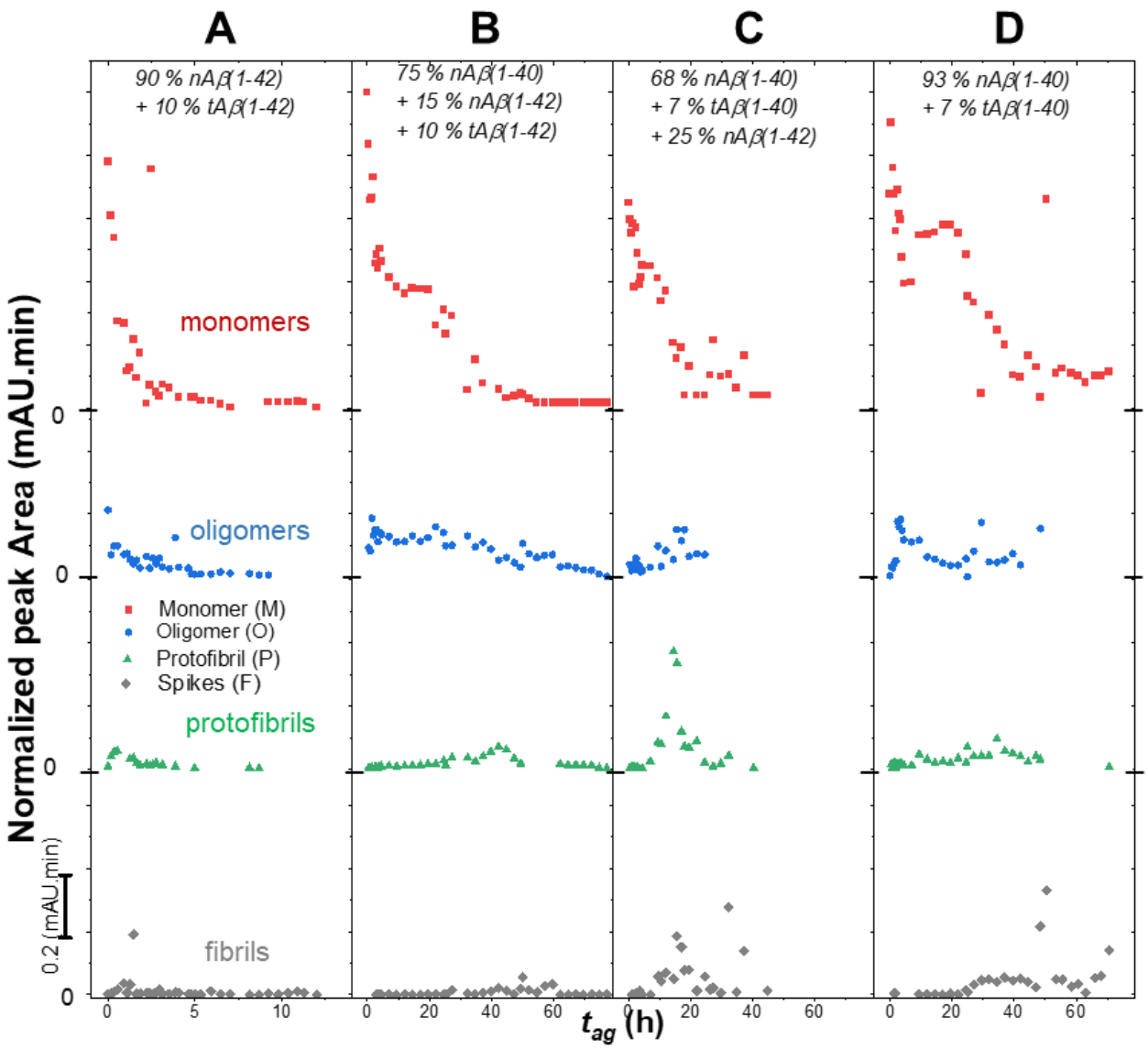

Figure 6. Peak area evolution of the species obtained for the nAβ + tAβ systems during the LEDIF analysis: (A) 90% nAβ(1-42) + 10% tAβ(1-42), (B) 3:1 Aβ(1-40):Aβ(1-42) - 75% nAβ(1-40) + 15% nAβ(1-42) + 10% nAβ(1-42), (C) 3:1 Aβ(1-40):Aβ(1-42) - 68% nAβ(1-40) + 7% nAβ(1-40) + 25% nAβ(1-42), (D) 93% nAβ(1-40) + 7% tAβ(1-40). The populations of the species are represented as follows: monomer and low molar mass oligomers (■), higher molar mass oligomers (●), protofibrils (▲), and fibrils (non-diffusing species) (♦). Experimental conditions as in Figure 5. Peak area was normalized by dividing the area of each data point to the total peak area obtained for the first run at t= 0 h to obtain a better comparison of the species evolution.

However, even though the aggregation process was affected by FITC and the LEDIF analysis was primarily affected by traces of unreacted FITC, the observed species evolution trends, especially the evolution of the monomer and low molar mass population, lead to the hypothesis that heterospecies form during the co-aggregation process. To properly answer this question,

suitable dyes that can preserve the aggregation behavior of the native peptide could be used, such as Atto488 which was found to be suitable for monitoring the aggregation of both Aβ isoforms[22]. Also, since the main advantages of LEDIF over absorption spectroscopy is that it does not provide excess noise and gives a great sensitivity of the analysis[29], TDA-LEDIF could prove to be a powerful tool to thoroughly investigate the aggregation process compared to TDA-UV and can allow to study the aggregation mechanism at physiological relevant concentrations.

IV.4. Conclusion

Herein we reported the extent to which the aggregation of Aβ(1-40) and Aβ(1-42) was affected by a small proportion of FITC dye. In contrast to what was described in the literature, it was observed that FITC had an impact on the aggregation rate of the native Aβ(1-42) isoform, with a substantial increase of the lifetime of potentially toxic oligomers. In the case of Aβ(1-40), only the aggregation kinetics were affected by the presence of tagged peptide without a significant impact upon the evolution of the oligomers and protofibrils, outlining a smaller inhibition effect of FITC upon this isoform. Moreover, our results suggest that during the co-aggregation process, the conjugated electrostatic and hydrophilic effect of FITC recognizes and consequently changes the aggregation behavior of native isoform to which it is attached, allowing the 100% native peptide to dominate the aggregation process of the complex system. These changes in the aggregation mechanism can be attributed to the conjugated electrostatic and hydrophilic effect that FITC provides as previously described in the literature[21]. The LEDIF analysis presented two limitations in this study. First, the right-side of the experimental peak was affected by an adsorption of the FITC dye on the capillary surface during the LEDIF analysis, but by using adequate data processing strategies, reliable data was obtained. Second, the obtained results from the LEDIF analysis were affected by some traces of unreacted FITC. To avoid this, very high purity samples should be used. Interestingly, during LEDIF analysis, more intermediates and fibrils were observed compared to the UV analysis, most likely due to the better sensitivity and lack of background noise that LEDIF presents over the UV mode. Therefore, if those two limitations are overpassed, TDA-LEDIF could prove to be a very powerful tool to thoroughly investigate the aggregation process as it can allow to study the aggregation process at physiological concentrations.

IV.5. References

1. Folch, J., Ettcheto, M., Petrov, D., Abad, S., Pedrós, I., Marin, M., Olloquequi, J. & Camins, A. Review of the advances in treatment for Alzheimer disease: strategies for combating β-amyloid protein. *Neurol. (English Ed.* **33,** 47–58 (2018).
2. Chen, G. F., Xu, T. H., Yan, Y., Zhou, Y. R., Jiang, Y., Melcher, K. & Xu, H. E. Amyloid beta: Structure, biology and structure-based therapeutic development. *Acta Pharmacol. Sin.* **38,** 1205–1235 (2017).
3. Faller, P., Hureau, C. & Berthoumieu, O. Role of metal ions in the self-assembly of the Alzheimer's amyloid-β peptide. *Inorg. Chem.* **52,** 12193–12206 (2013).
4. Nasica-Labouze, J., Nguyen, P. H., Sterpone, F., Berthoumieu, O., Buchete, N. V., Coté, S., De Simone, A., Doig, A. J., Faller, P., Garcia, A., Laio, A., Li, M. S., Melchionna, S., Mousseau, N., Mu, Y., Paravastu, A., Pasquali, S., Rosenman, D. J., Strodel, B., Tarus, B., Viles, J. H., Zhang, T., Wang, C. & Derreumaux, P. Amyloid β Protein and Alzheimer's Disease: When Computer Simulations Complement Experimental Studies. *Chem. Rev.* **115,** 3518–3563 (2015).
5. Törnquist, M., Michaels, T. C. T., Sanagavarapu, K., Yang, X., Meisl, G., Cohen, S. I. A., Knowles, T. P. J. & Linse, S. Secondary nucleation in amyloid formation. *Chem. Commun.* **54,** 8667–8684 (2018).
6. Lesné, S. E. Breaking the code of amyloid-β oligomers. *Int. J. Cell Biol.* (2013). doi:10.1155/2013/950783
7. Teplow, D. B., Bitan, G., Lomakin, A., Benedek, G. B., Kirkitadze, M. D. & Vollers, S. S. Amyloid -protein (A) assembly: A 40 and A 42 oligomerize through distinct pathways. *Proc. Natl. Acad. Sci.* **100,** 330–335 (2003).
8. Meisl, G., Yang, X., Frohm, B., Knowles, T. P. J. & Linse, S. Quantitative analysis of intrinsic and extrinsic factors in the aggregation mechanism of Alzheimer-associated Aβ-peptide. *Sci. Rep.* **6,** (2016).
9. Kobayashi, S., Tanaka, Y., Kiyono, M., Chino, M., Chikuma, T., Hoshi, K. & Ikeshima, H. Dependence pH and proposed mechanism for aggregation of Alzheimer's disease-related amyloid-β(1-42) protein. *J. Mol. Struct.* **1094,** 109–117 (2015).
10. Abelein, A., Jarvet, J., Barth, A., Gräslund, A. & Danielsson, J. Ionic Strength Modulation of the Free Energy Landscape of Aβ40 Peptide Fibril Formation. *J. Am. Chem. Soc.* **138,** 6893–6902 (2016).
11. Ghavami, M., Rezaei, M., Ejtehadi, R., Lotfi, M., Shokrgozar, M. A., Abd Emamy, B., Raush, J. & Mahmoudi, M. Physiological temperature has a crucial role in amyloid beta in the absence and presence of hydrophobic and hydrophilic nanoparticles. *ACS Chem. Neurosci.* **4,** 375–378 (2013).
12. Chang, Y. J. & Chen, Y. R. The coexistence of an equal amount of Alzheimer's amyloid-β 40 and 42 forms structurally stable and toxic oligomers through a distinct pathway. *FEBS J.* **281,** 2674–2687 (2014).

13. Kuperstein, I., Broersen, K., Benilova, I., Rozenski, J., Jonckheere, W., Debulpaep, M., Vandersteen, A., Segers-Nolten, I., Van Der Werf, K., Subramaniam, V., Braeken, D., Callewaert, G., Bartic, C., D'Hooge, R., Martins, I. C., Rousseau, F., Schymkowitz, J. & De Strooper, B. Neurotoxicity of Alzheimer's disease Aβ peptides is induced by small changes in the Aβ42 to Aβ40 ratio. *EMBO J.* **29,** 3408–3420 (2010).

14. Cukalevski, R., Yang, X., Meisl, G., Weininger, U., Bernfur, K., Frohm, B., Knowles, T. P. J. & Linse, S. The Aβ40 and Aβ42 peptides self-assemble into separate homomolecular fibrils in binary mixtures but cross-react during primary nucleation. *Chem. Sci.* **6,** 4215–4233 (2015).

15. Cerofolini, L., Ravera, E., Bologna, S., Wiglenda, T., Böddrich, A., Purfürst, B., Benilova, I., Korsak, M., Gallo, G., Rizzo, D., Gonnelli, L., Fragai, M., De Strooper, B., Wanker, E. E. & Luchinat, C. Mixing Aβ(1-40) and Aβ(1-42) peptides generates unique amyloid fibrils. *Chem. Commun.* **56,** 8830–8833 (2020).

16. Jan, A., Gokce, O., Luthi-Carter, R. & Lashuel, H. A. The ratio of monomeric to aggregated forms of Aβ40 and Aβ42 is an important determinant of amyloid-β aggregation, fibrillogenesis, and toxicity. *J. Biol. Chem.* **283,** 28176–28189 (2008).

17. Iljina, M., Garcia, G. A., Dear, A. J., Flint, J., Narayan, P., Michaels, T. C. T., Dobson, C. M., Frenkel, D., Knowles, T. P. J. & Klenerman, D. Quantitative analysis of co-oligomer formation by amyloid-beta peptide isoforms. *Sci. Rep.* **6,** (2016).

18. Nag, S., Sarkar, B., Bandyopadhyay, A., Sahoo, B., Sreenivasan, V. K. A., Kombrabail, M., Muralidharan, C. & Maiti, S. Nature of the amyloid-β monomer and the monomer-oligomer equilibrium. *J. Biol. Chem.* **286,** 13827–13833 (2011).

19. Nichols, M. R., Moss, M. A., Reed, D. K., Lin, W. L., Mukhopadhyay, R., Hoh, J. H. & Rosenberry, T. L. Growth of β-amyloid(1-40) protofibrils by monomer elongation and lateral association. Characterization of distinct products by light scattering and atomic force microscopy. *Biochemistry* **41,** 6115–6127 (2002).

20. Jungbauer, L. M., Yu, C., Laxton, K. J. & LaDu, M. J. Preparation of fluorescently-labeled amyloid-beta peptide assemblies: The effect of fluorophore conjugation on structure and function. in *J. Mol. Recognit.* **22,** 403–413 (2009).

21. Zheng, Y., Xu, L., Yang, J., Peng, X., Wang, H., Yu, N., Hua, Y., Zhao, J., He, J. & Hong, T. The effects of fluorescent labels on Aβ 42 aggregation detected by fluorescence correlation spectroscopy. *Biopolymers* **109,** (2018).

22. Wägele, J., De Sio, S., Voigt, B., Balbach, J. & Ott, M. How Fluorescent Tags Modify Oligomer Size Distributions of the Alzheimer Peptide. *Biophys. J.* **116,** 227–238 (2019).

23. Deleanu, M., Hernandez, J.-F., Cipelletti, L., Biron, J.-P., Rossi, E., Taverna, M., Cottet, H. & Chamieh, J. Unraveling the Speciation of β-Amyloid Peptides during the Aggregation Process by Taylor Dispersion Analysis. *Anal. Chem.* (2021). doi:10.1021/acs.analchem.1c00527

24. Brinet, D., Kaffy, J., Oukacine, F., Glumm, S., Ongeri, S. & Taverna, M. An improved capillary electrophoresis method for in vitro monitoring of the challenging early steps of Aβ(1-42) peptide oligomerization: Application to anti-Alzheimer's drug discovery. *Electrophoresis* **35,** 3302–3309 (2014).

25. Jan, A., Hartley, D. M. & Lashuel, H. A. Preparation and characterization of toxic aβ aggregates for structural and functional studies in alzheimer's disease research. *Nat. Protoc.* **5,** 1186–1209 (2010).

26. Michaels, T. C. T., Šarić, A., Habchi, J., Chia, S., Meisl, G., Vendruscolo, M., Dobson, C. M. & Knowles, T. P. J. Chemical Kinetics for Bridging Molecular Mechanisms and Macroscopic Measurements of Amyloid Fibril Formation. *Annu. Rev. Phys. Chem.* **69,** 273–298 (2018).

27. Chamieh, J. & Cottet, H. Comparison of single and double detection points Taylor Dispersion Analysis for monodisperse and polydisperse samples. *J. Chromatogr. A* **1241,** 123–127 (2012).

28. Picó, Y. Chemical Analysis of Food: Techniques and Applications. *Chem. Anal. Food Tech. Appl.* (2012). doi:10.1016/C2010-0-64808-5

Chapter IV. Supporting information

IV.SI.1. TDA theoretical aspects and data processing of the experimental taylorgrams.

Briefly, TDA is a modern dispersion-based separation method that allows the determination of the molecular diffusion coefficient (D), and of the hydrodynamic radius (R_h), of an injected solute under Poiseuille laminar flow conditions[25]. The experimental Gaussian peaks are obtained from the combination of parabolic velocity profile of the Poiseuille laminar flow that occurs when pressure is applied in a capillary and the molecular diffusion of the solutes, also known as Taylor dispersion[1]. The experimental peaks can be assessed by performing adequate fittings which allow the determination of the temporal peak variance (σ^2) using different data processing approaches[2,3].

In this work, a direct curve fitting was applied using the Least Significant Difference approach with the "GRG nonlinear" algorithm in Microsoft Excel according to Eq. (1), when the total number of species, n, is limited ($n \leq 4$).

$$S(t) = \sum_{i=1}^{n} S_i(t) = \sum_{i=1}^{n} \frac{A_i}{\sigma_i \sqrt{2\pi}} e^{-\frac{1}{2}\frac{(t-t_0)^2}{\sigma_i^2}} \qquad \text{SI. (1)}$$

where $S(t)$ represents the taylorgram, t_0 is the average elution time of the solute (s), σ_i is the temporal variance corresponding to a species i, A_i is the area coefficient that is proportional to the concentration of the species i that depends on the response factor of each species at a specific detection wavelength.

This further allows the calculation of D ($m^2\ s^{-1}$) and the R_h (m) for each species from Eq. (2) and Eq. (3), respectively:

$$D = \frac{R_c^2 t_0}{24\sigma^2} \qquad \text{SI. (2)}$$

$$R_h = \frac{k_b T}{6\pi\eta D} \qquad \text{SI. (3)}$$

where R_c is the capillary radius (m), σ^2 is the temporal peak variance (s^2), k_b is the Boltzmann constant (Pa $m^3\ K^{-1}$), T is the analysis temperature (K), and η is the viscosity of the sample (Pa s).

Eq. (1) is valid only when the characteristics analysis time t_0 is higher than the characteristic diffusion time of a species over a distance equal to R_c, and if the contribution of longitudinal diffusion is also found to be insignificant compared to convection. These aspects can be verified by Eq. (4) and Eq. (5) respectivelly[4,5]:

$$\tau = \frac{Dt_0}{R_c^2} \geq 1.25 \qquad \text{SI. (4)}$$

$$P_e = \frac{uR_c}{D} \geq 40 \qquad \text{SI. (5)}$$

where τ is an adimensional characteristic time, P_e is the Péclet number and u is the linear mobile phase velocity (m/s)

IV.SI.2. Data Treatment

In the case of UV-detection mode, the chosen operating conditions allowed to obtain taylorgrams that could be treated on both sides (left or right) as shown in Figure SI 1 for the selected runs obtained for the 3:1 Aβ(1-40):Aβ(1-42) – 100% nAβ(1-40) + 90% nAβ(1-42) + 10% tAβ(1-42) at t_{ag} = 39.78 h. In both peak deconvolutions, the data treatment was performed on the same baseline adjustment. As described in our previous study[6], the data treatment on the right side allowed to obtain good fitting of the experimental elution peak. When the deconvolution was performed from the left side, small mainly non-significant differences in both the area and the size of the populations were noticed (Figures SI1 and SI2).

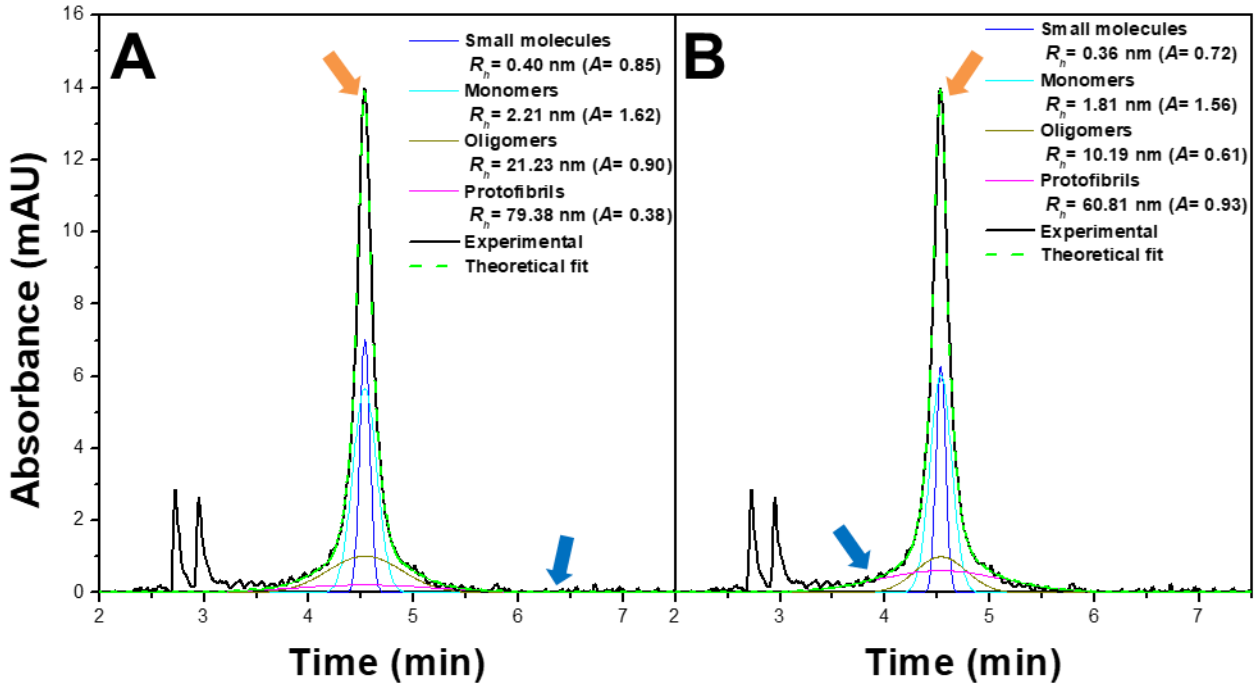

Figure SI1. Data processing examples of the experimental UV taylorgrams for 3:1 Aβ(1-40):Aβ(1-42) – 100% nAβ(1-40) + 90% nAβ(1-42) + 10% tAβ(1-42) system at t= 39.78 h from (A) right and (B) left side of the elution profile. The experimental data (black solid line) was fitted with the sum of the required Gaussian peaks (dashed green line). The populations (Gaussians) are individually represented on the graph: Small Molecules (blue solid line), Monomers (light blue solid line), (Oligomers – dark yellow solid line) and Protofibrils (pink solid line). The arrows are representing the starting (blue) and the ending (orange) integration points. Experimental conditions: Sample: 100 µM Aβ (75 µM nAβ(1-40) + 15 µM nAβ(1-42) + 10 µM tAβ(1-42)); 20 mM phosphate buffer, pH 7.4. Incubation: quiescent conditions at 37 °C. Fused silica capillaries: 50 µm i.d. × 60 cm × 51.5 cm. Mobile phase: 20 mM phosphate buffer, pH 7.4. Mobilization pressure: 100 mbar. Injection: 44 mbar for 4 s, Vi ≈ 7 nL (Vi / Vd ≈ 0.6 %). Analyses were performed at 37 °C. UV detection at 191 nm. Baseline treatment was performed in Microcal Origin. The experimental fitting of the taylorgrams was performed by using Equation 5 in Microsoft Excel.

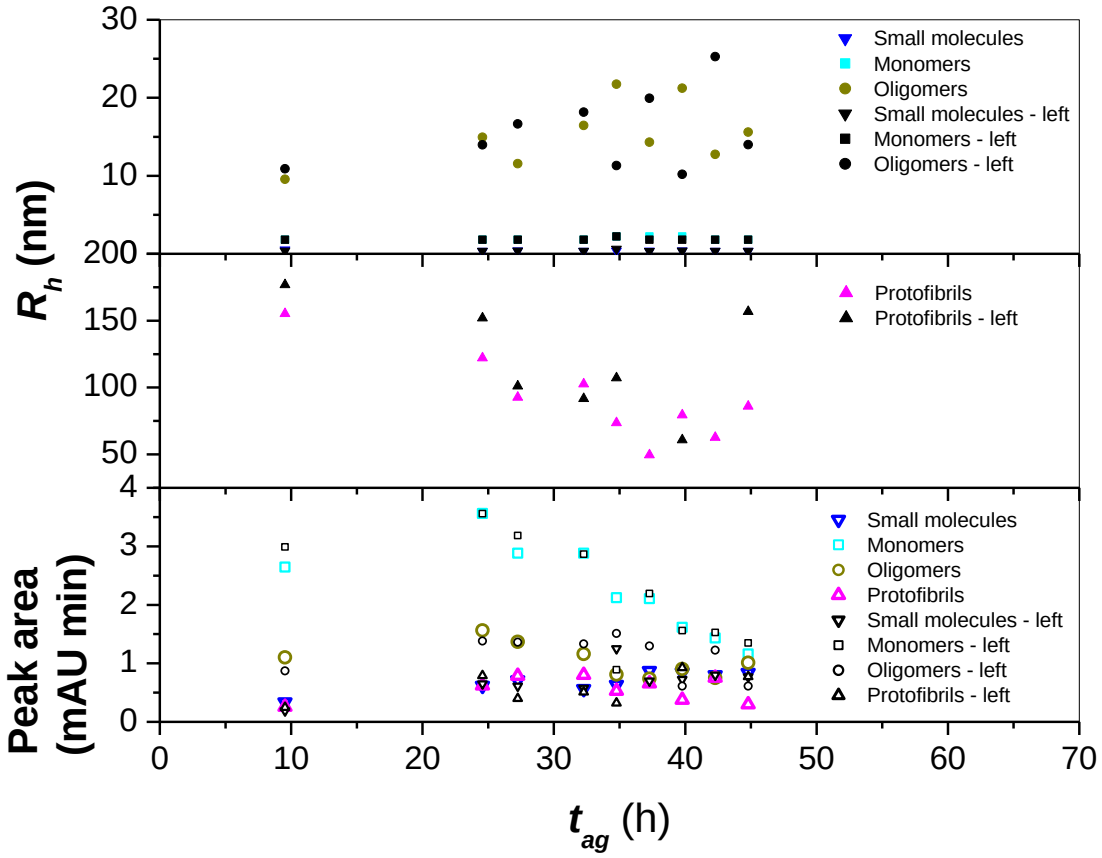

Figure SI2. Hydrodynamic radius (upper and middle layer) and peak area (bottom layer) values obtained during the deconvolutions performed from both sides of the elution profile for some selected runs of the 3:1 Aβ(1-40):Aβ(1-42) – 100% nAβ(1-40) + 90% nAβ(1-42) + 10% tAβ(1-42) system using a 4 Gaussians fitting of the taylorgrams. Closed symbols are for the hydrodynamic radius: small molecules (▼▼), monomer and low molar mass oligomers (■■), higher molar mass oligomers (●●), and soluble protofibrils (▲▲). Open symbols correspond to the peak area of each species: small molecules (▽▽), monomer and low molar mass oligomers (□□), higher molar mass oligomers (○○), soluble protofibrils (△△). Colored symbols stand for values obtained during the deconvolutions performed from the right-side of the elution profile while the black symbols stand for the values obtained from the left-side. UV experimental conditions as in Figure SI1.

In the case of fluorescence detection, the obtained taylorgrams were more difficult to treat as compared to UV, mainly due to the spikes on the left side (peak deformation) and the non-desired adsorption on the right side (peak tailing), for that different deconvolution strategies were employed to provide accurate and reliable information of the Aβ aggregation process, as presented in the following subsections.

IV.SI.2.1. Data processing from the left side of the eluted peak

When no spikes are observed or when their intensity was low, a left side data treatment was preferred as shown in Figure SI3.

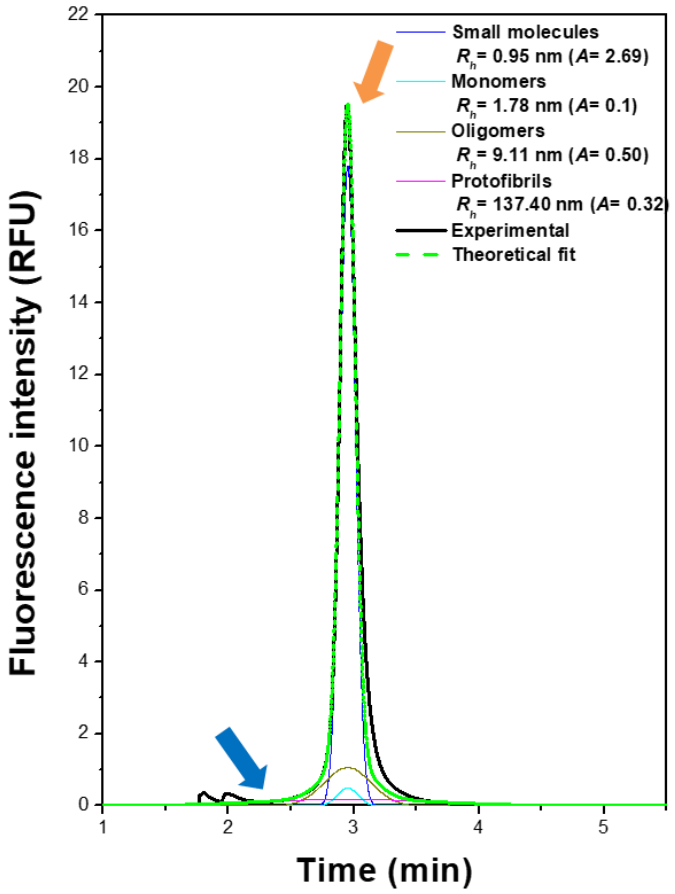

Figure SI3. Data processing example from the left-side of the experimental LIF taylorgram obtained for the 3:1 Aβ(1-40):Aβ(1-42) – 100% nAβ(1-40) + 90% nAβ(1-42) + 10% tAβ(1-42) system at t= 39.78 h. The experimental data (black solid line) was fitted with the sum of the required Gaussian peaks (dashed green line). The populations (Gaussians) are individually represented on the graph: Small Molecules (blue solid line), Monomers (light blue solid line), (Oligomers – dark yellow solid line) and Protofibrils (pink solid line). The arrows are representing the starting (blue) and the ending (orange) integration points. Baseline treatment was performed in Microcal Origin. The experimental fitting of the taylorgrams was performed by using Equation 5 in Microsoft Excel. Experimental conditions: Sample: 100 µM Aβ (7.5 nmols nAβ(1-40) + 1.5 nmol nAβ(1-42) + 1 nmol tAβ(1-42)); 20 mM phosphate buffer, pH 7.4. Incubation: quiescent conditions at 37 °C. LIF: Fused silica capillaries: 50 µm i.d. × 60 cm × 33 cm. Mobile phase: 20 mM phosphate buffer, pH 7.4. Mobilization pressure: 100 mbar. Injection: 44 mbar for 4 s, Vi ≈ 7 nL (Vi / Vd ≈ 1 %). Analyses were performed at 37 °C. Fluorescence excitation at 480 nm, emission light wavelength range from 515–760 nm; 20 mM phosphate buffer, pH 7.4

IV.SI.2.2. Combined data processing from both the right and the left side of the eluted peak

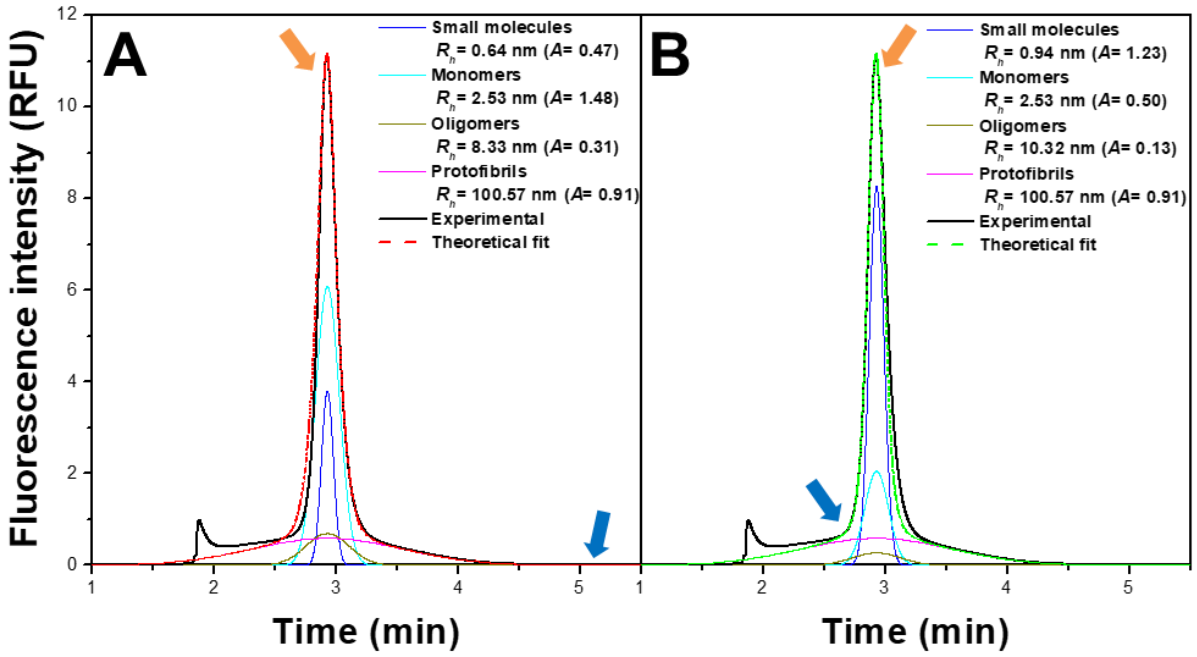

Figure SI4. Double data processing example performed from both right (A) and left (B) sides of the elution profiles obtained for the experimental LIF taylorgram of the 3:1 Aβ(1-40):Aβ(1-42) – 93% nAβ(1-40) + 7% tAβ(1-40) + 100% nAβ(1-42) system at t= 14.53 h. The experimental data (black solid line) was fitted with the sum of the required Gaussian peaks (dashed green line). The populations (Gaussians) are individually represented on the graph: Small Molecules (blue solid line), Monomers (light blue solid line), (Oligomers – dark yellow solid line) and Protofibrils (pink solid line). The arrows are representing the starting (blue) and the ending (orange) integration points. Experimental conditions: Sample: 100 µM Aβ (68 µM nAβ(1-40) + 7 µM tAβ(1-40) + 2.5 µM nAβ(1-42)); 20 mM phosphate buffer, pH 7.4. Incubation: quiescent conditions at 37 °C. LIF experimental conditions as in Figure SI3.

When the deconvolution on the left was not reliable by applying the first two approaches, the elution peak was treated by a double deconvolution, first on the right side (Figure SI4 A) to determine the number of possible populations and have an estimation of their size and proportions, then a left side deconvolution (Figure SI4 B) was applied by fixing the σ and the area obtained from the right side of the protofibril population in the fitting parameters. This choice showed a good estimation of the size and the areas of the different populations. However, one major drawback is that for it to work the protofibril population needed to be sufficiently abundant to

neglect the effect of the adsorption (the peak tailing) on the band broadening. This strategy was mainly used in the case of the 3:1 Aβ(1-40):Aβ(1-42) – 93% nAβ(1-40) + 7% tAβ(1-40) + 100% nAβ(1-42) system, where the protofibrils population was more abundant and the results were very similar to the ones obtained by UV (Figure SI16 C and F).

IV.SI.3. UV and LIF Experimental Taylorgrams

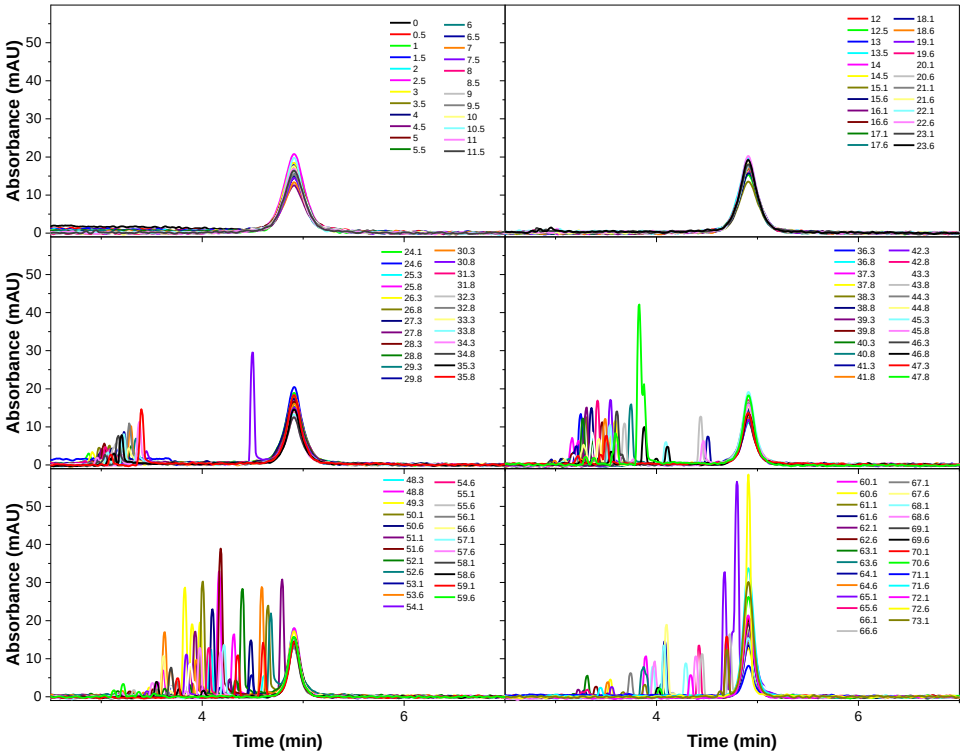

Figure SI5. Experimental taylorgrams obtained by UV detection for the 93% nAβ(1-40) + 7% tAβ(1-40) system for a total incubation time of 73 h. Experimental conditions: Sample: 100 µM Aβ (9.3 nmol nAβ(1-40) + 0.7 nmol of tAβ(1-40)); 20 mM phosphate buffer, pH 7.4. Incubation: quiescent conditions at 37 °C. UV experimental conditions as in Figure SI1.

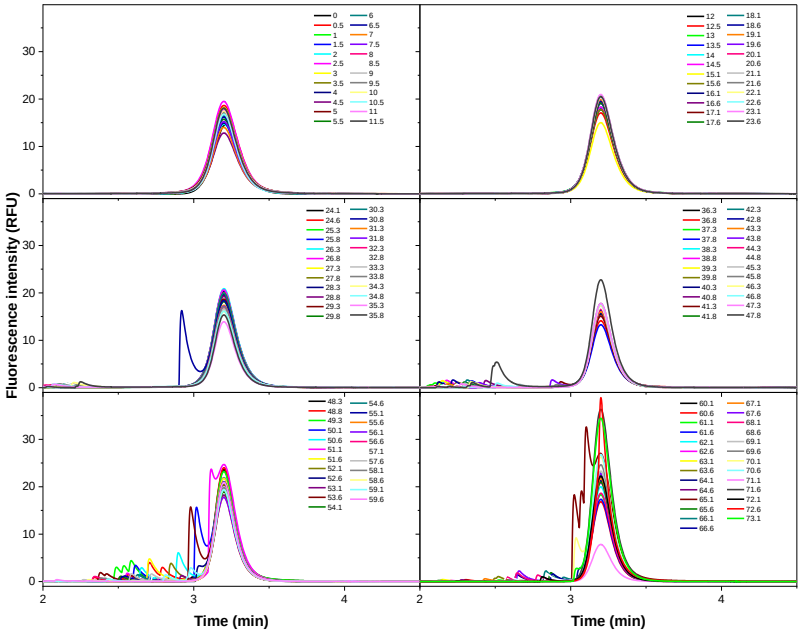

Figure SI6. Experimental taylorgrams obtained by LIF detection for the 93% nAβ(1-40) + 7% tAβ(1-40) system for a total incubation time of 73 h. Experimental conditions: Sample: 100 µM Aβ (9.3 nmol nAβ(1-40) + 0.7 nmol of tAβ(1-40)); 20 mM phosphate buffer, pH 7.4. Incubation: quiescent conditions at 37 °C. LIF experimental conditions as in Figure SI3.

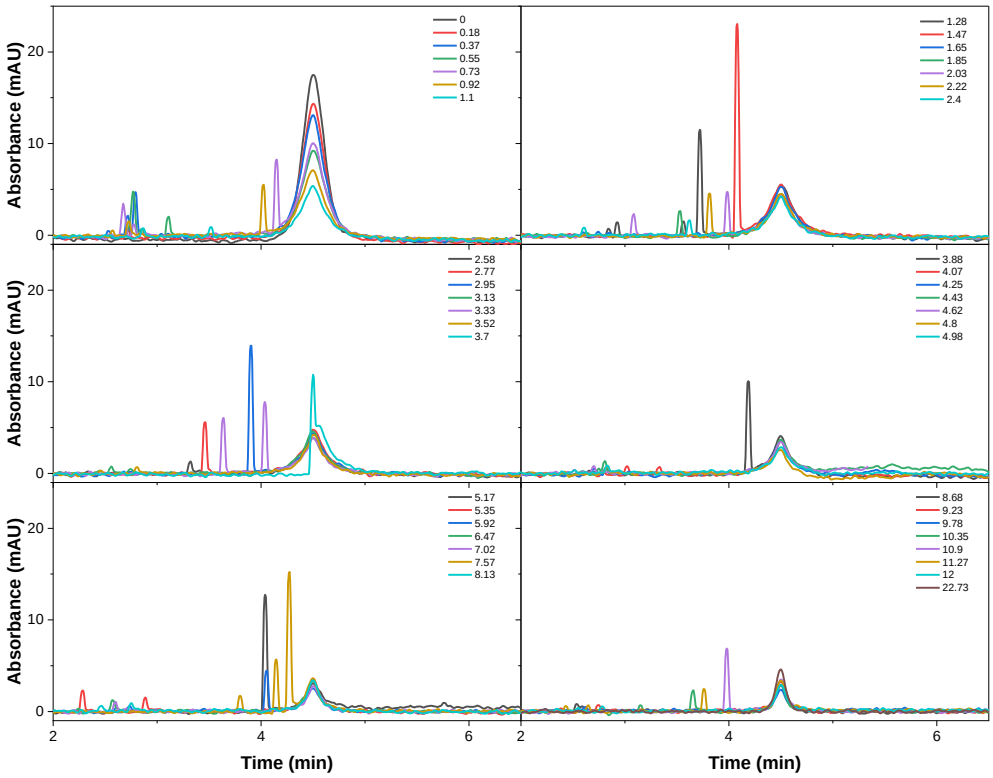

Figure SI7. Experimental taylorgrams obtained by UV detection for the 90% nAβ(1-42) + 10% tAβ(1-42) system for a total incubation time of 12 h. Experimental conditions: Sample: 100 µM Aβ (9 nmol nAβ(1-42) + 1 nmol of tAβ(1-42)); 20 mM phosphate buffer, pH 7.4. Incubation: quiescent conditions at 37 °C. UV experimental conditions as in Figure SI1.

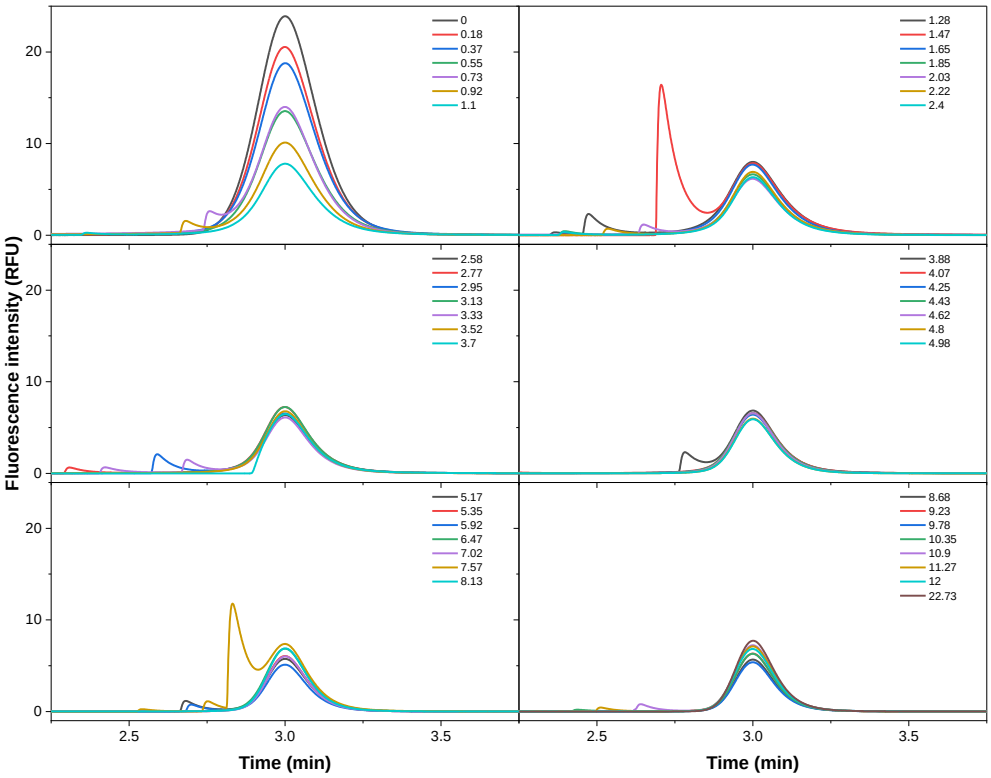

Figure SI8. Experimental taylorgrams obtained by LIF detection for the 90% nAβ(1-42) + 10% tAβ(1-42) system for a total incubation time of 12 h. Experimental conditions: Sample: 100 µM Aβ (9 nmol nAβ(1-42) + 1 nmol of tAβ(1-42)); 20 mM phosphate buffer, pH 7.4. Incubation: quiescent conditions at 37 °C. LIF experimental conditions as in Figure SI3.

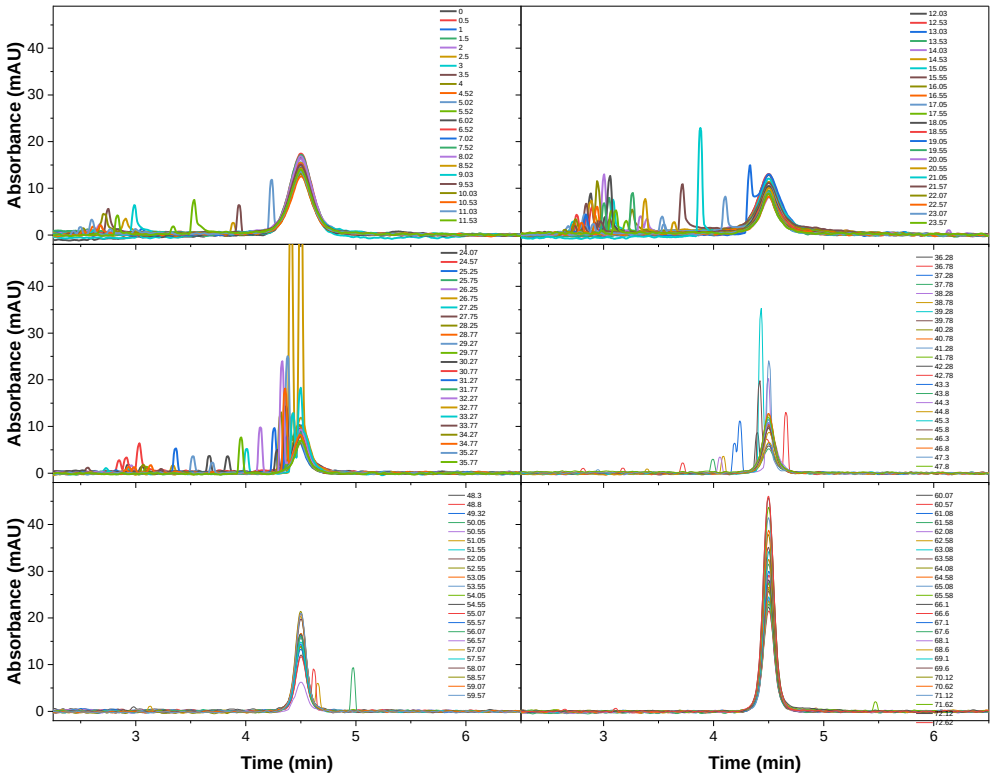

Figure SI9. Experimental taylorgrams obtained by UV detection for the 3:1 Aβ(1-40):Aβ(1-42) – 93% nAβ(1-40) + 7% tAβ(1-40) + 100% nAβ(1-42) system for a total incubation time of 73 h. Experimental conditions: Sample: 100 µM Aβ (6.8 nmols nAβ(1-40) + 0.7 nmol tAβ(1-40) + 2.5 nmol nAβ(1-42)); 20 mM phosphate buffer, pH 7.4. Incubation: quiescent conditions at 37 °C. UV experimental conditions as in Figure SI1.

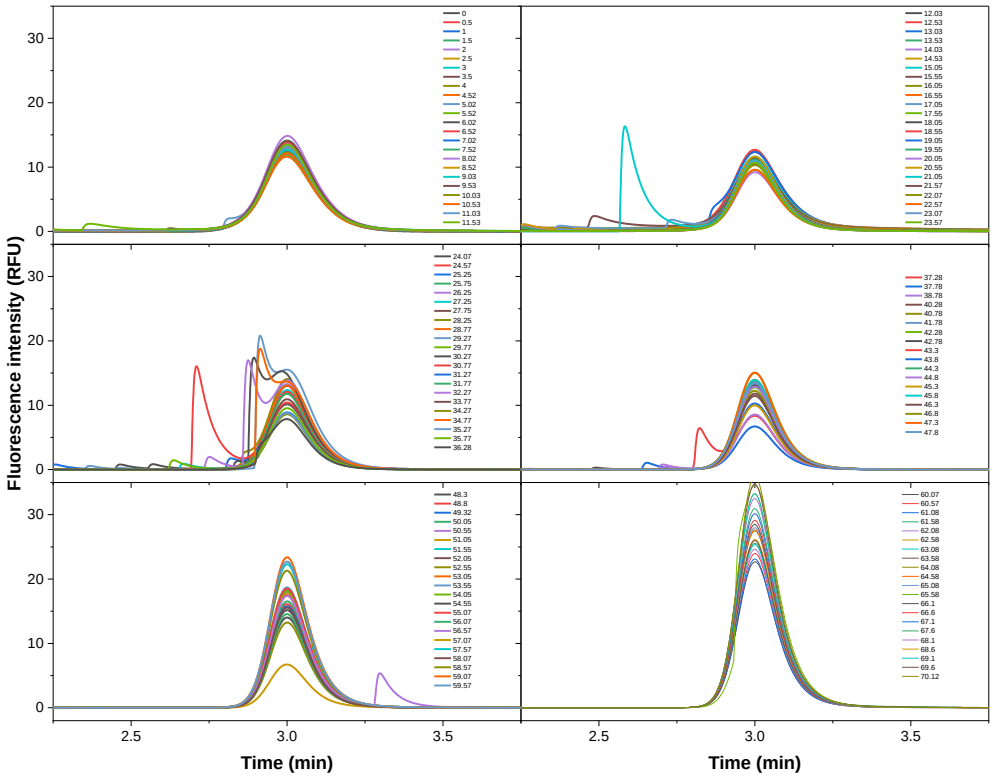

Figure SI10. Experimental taylorgrams obtained by LIF detection for the 3:1 Aβ(1-40):Aβ(1-42) – 93% nAβ(1-40) + 7% tAβ(1-40) + 100% nAβ(1-42) system for a total incubation time of 73 h. Experimental conditions: Sample: 100 µM Aβ (6.8 nmols nAβ(1-40) + 0.7 nmol tAβ(1-40) + 2.5 nmol nAβ(1-42)); 20 mM phosphate buffer, pH 7.4. Incubation: quiescent conditions at 37 °C. LIF experimental conditions as in Figure SI3.

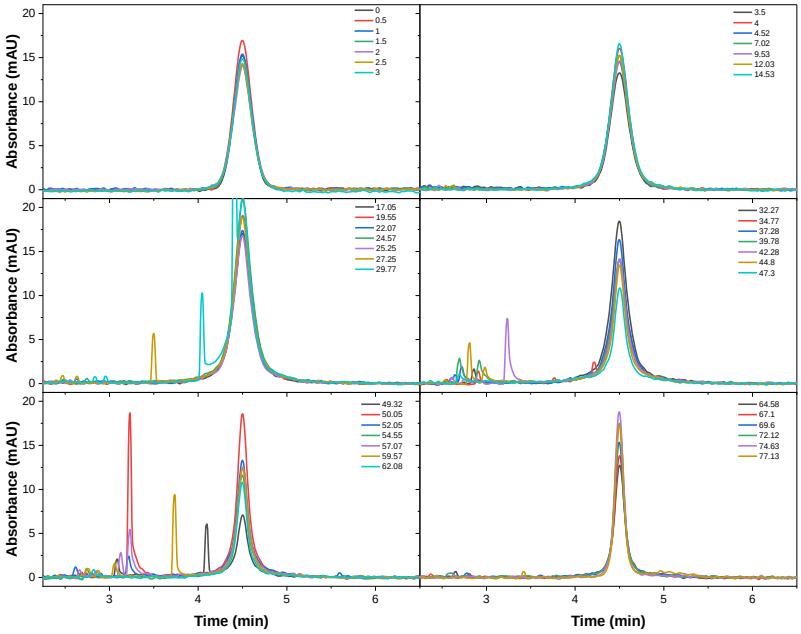

Figure SI11. Experimental taylorgrams obtained by UV detection for the 3:1 Aβ(1-40):Aβ(1-42) – 100% nAβ(1-40) + 90% nAβ(1-42) + 10% tAβ(1-42) system for a total incubation time of 73 h. Experimental conditions: Sample: 100 µM Aβ (7.5 nmols nAβ(1-40) + 1.5 nmol nAβ(1-42) + 1 nmol tAβ(1-42)); 20 mM phosphate buffer, pH 7.4. Incubation: quiescent conditions at 37 °C. UV experimental conditions as in Figure SI1.

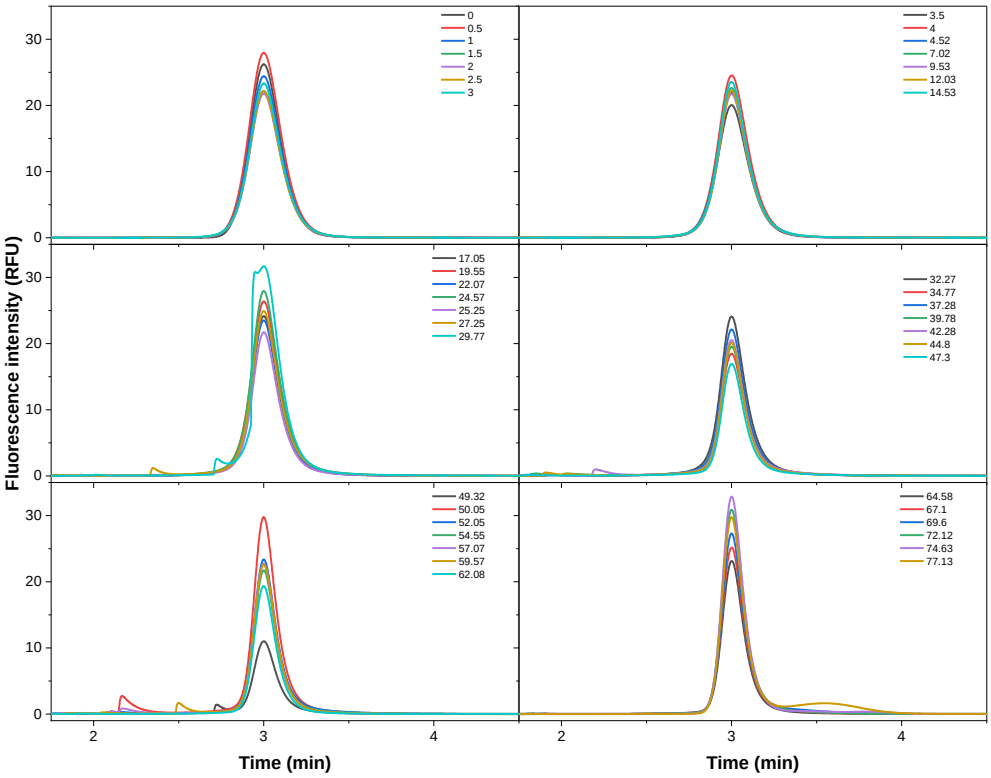

Figure SI12. Experimental taylorgrams obtained by LIF detection for the 3:1 Aβ(1-40):Aβ(1-42) – 100% nAβ(1-40) + 90% nAβ(1-42) + 10% tAβ(1-42) system for a total incubation time of 73 h. Experimental conditions: Sample: 100 µM Aβ (7.5 nmols nAβ(1-40) + 1.5 nmol nAβ(1-42) + 1 nmol tAβ(1-42)); 20 mM phosphate buffer, pH 7.4. Incubation: quiescent conditions at 37 °C. LIF experimental conditions as in Figure SI3.

IV.SI.4. UV vs LIF area and R_h comparison

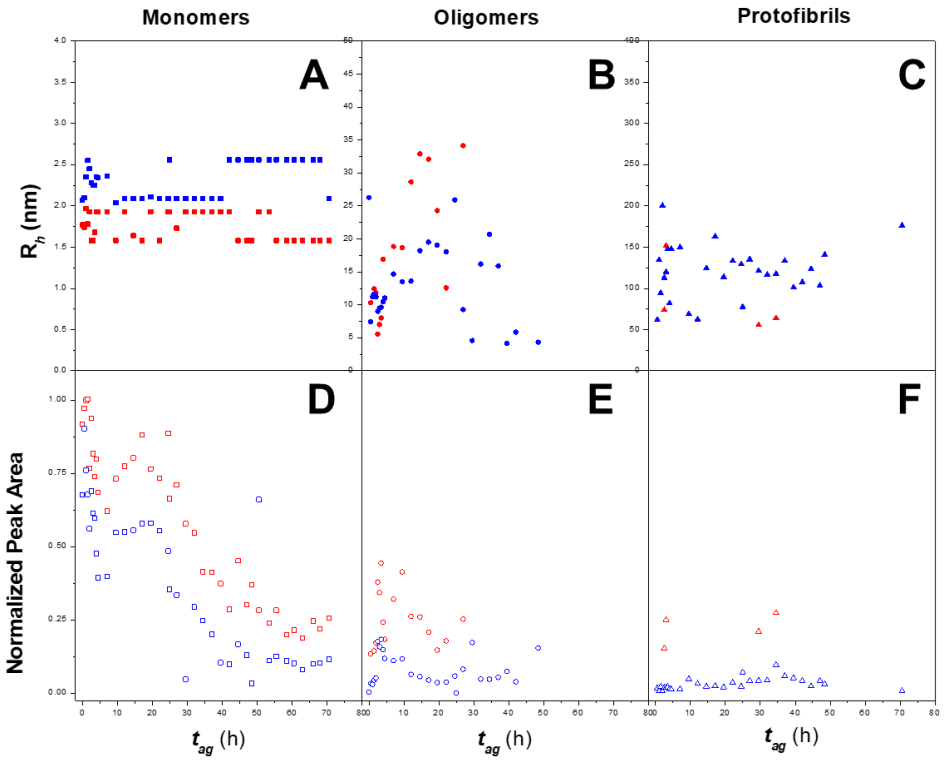

Figure SI13. Hydrodynamic radius (upper layers) and peak area evolution (bottom layers) of the (A) and (D) monomers, (B) and (E) oligomers, (C) and (F) protofibrils obtained for the 93% nAβ(1-40) + 7% tAβ(1-40) system. Red symbols represent the results obtained from UV and the blue symbols stand for the results obtained from LIF. Peak area was normalized by dividing the area of each data point to the total peak area obtained for the first run at t= 0 h to obtain a clear comparison between the two detection modes. Experimental conditions: Sample: 100 µM Aβ (9.3 nmol nAβ(1-40) + 0.7 nmol of tAβ(1-40)); 20 mM phosphate buffer, pH 7.4. Incubation: quiescent conditions at 37 °C. UV and LIF experimental conditions as in Figure SI1 and Figure SI3 respectively.

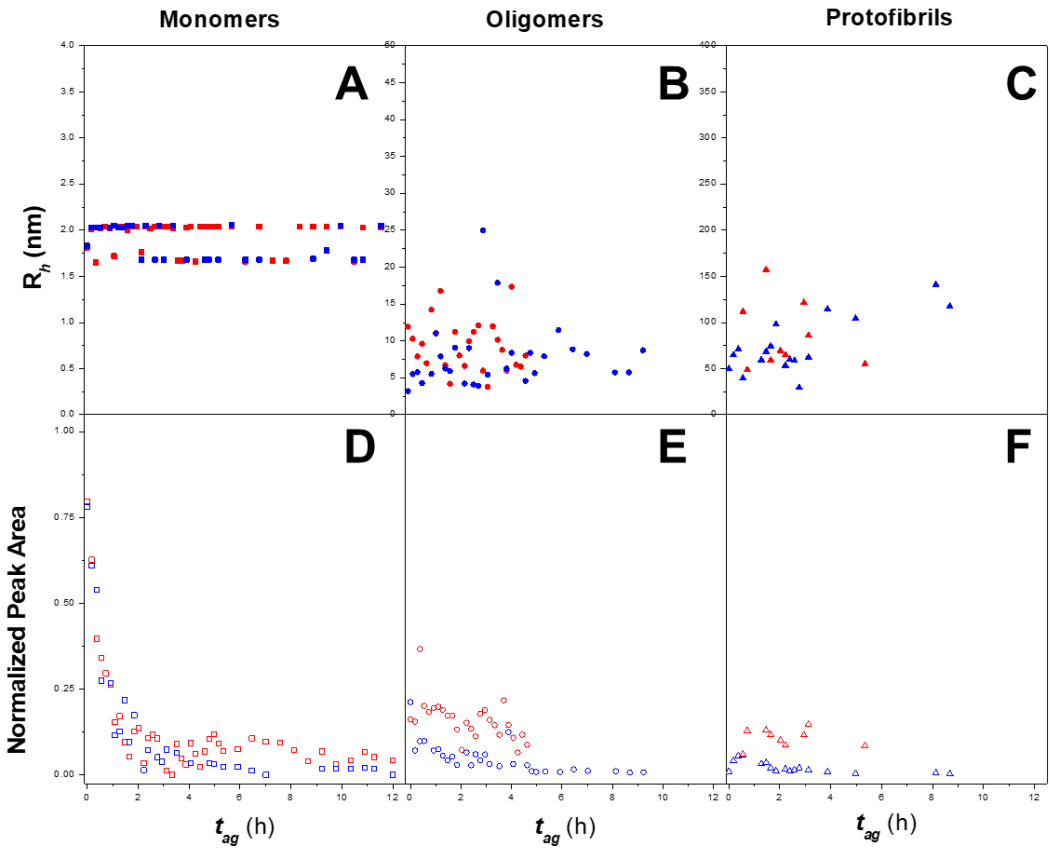

Figure SI14. Hydrodynamic radius (upper layers) and peak area evolution (bottom layers) of the (A) and (D) monomers, (B) and (E) oligomers, (C) and (F) protofibrils obtained for the 90% nAβ(1-42) + 10% tAβ(1-42) system. Red symbols represent the results obtained from UV and the blue symbols stand for the results obtained from LIF. Peak area was normalized by dividing the area of each data point to the total peak area obtained for the first run at t= 0 h to obtain a clear comparison between the two detection modes. Experimental conditions: Sample: 100 µM Aβ (9 nmol nAβ(1-42) + 1 nmol of tAβ(1-42)); 20 mM phosphate buffer, pH 7.4. Incubation: quiescent conditions at 37 °C. UV and LIF experimental conditions as in Figure SI1 and Figure SI3 respectively.

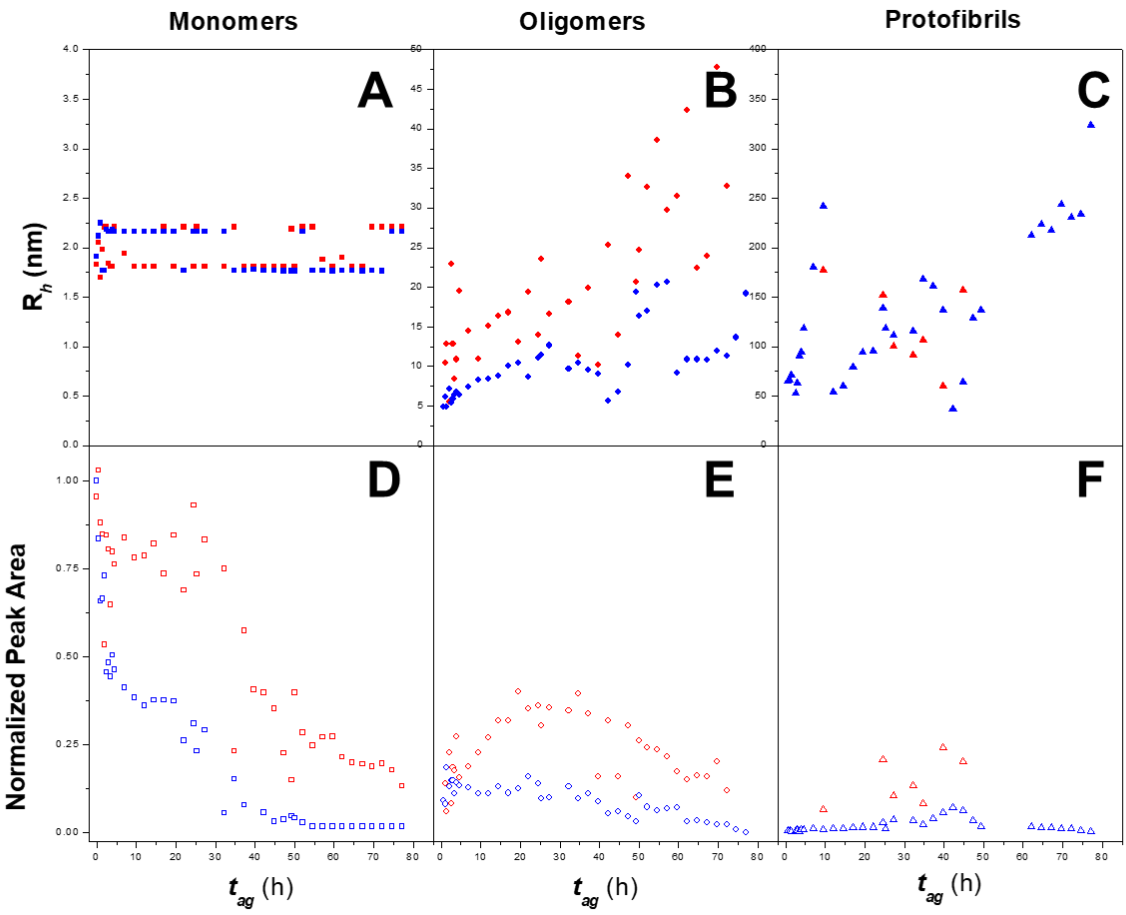

Figure SI15. Hydrodynamic radius (upper layers) and peak area evolution (bottom layers) of the (A) and (D) monomers, (B) and (E) oligomers, (C) and (F) protofibrils obtained for the 3:1 Aβ(1-40):Aβ(1-42) – 100% nAβ(1-40) + 90% nAβ(1-42) + 10% tAβ(1-42) system. Red symbols represent the results obtained from UV and the blue symbols stand for the results obtained from LIF. Peak area was normalized by dividing the area of each data point to the total peak area obtained for the first run at t= 0 h to obtain a clear comparison between the two detection modes. Experimental conditions: Sample: 100 µM Aβ (7.5 nmols nAβ(1-40) + 1.5 nmol nAβ(1-42) + 1 nmol tAβ(1-42)); 20 mM phosphate buffer, pH 7.4. Incubation: quiescent conditions at 37 °C. UV and LIF experimental conditions as in Figure SI1 and Figure SI3 respectively.

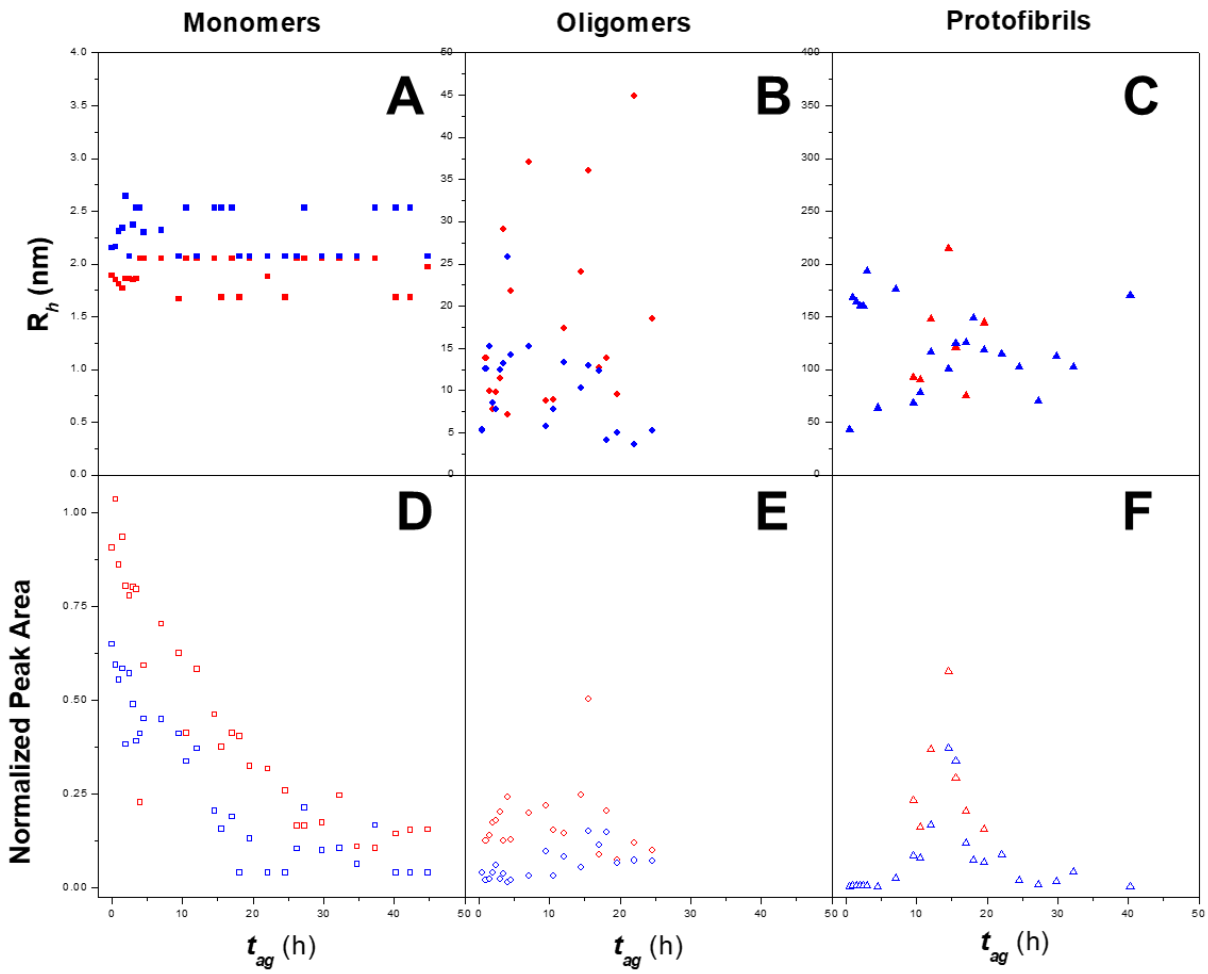

Figure SI16. Hydrodynamic radius (upper layers) and peak area evolution (bottom layers) of the (A) and (D) monomers, (B) and (E) oligomers, (C) and (F) protofibrils obtained for the 3:1 Aβ(1-40):Aβ(1-42) – 93% nAβ(1-40) + 7% tAβ(1-40) + 100% nAβ(1-42) system. Red symbols represent the results obtained from UV and the blue symbols stand for the results obtained from LIF. Peak area was normalized by dividing the area of each data point to the total peak area obtained for the first run at t= 0 h to obtain a clear comparison between the two detection modes. Experimental conditions: Sample: 100 µM Aβ (68 µM nAβ(1-40) + 7 µM tAβ(1-40) + 2.5 µM nAβ(1-42)); 20 mM phosphate buffer, pH 7.4. Incubation: quiescent conditions at 37 °C. UV and LIF experimental conditions as in Figure SI1 and Figure SI3 respectively.

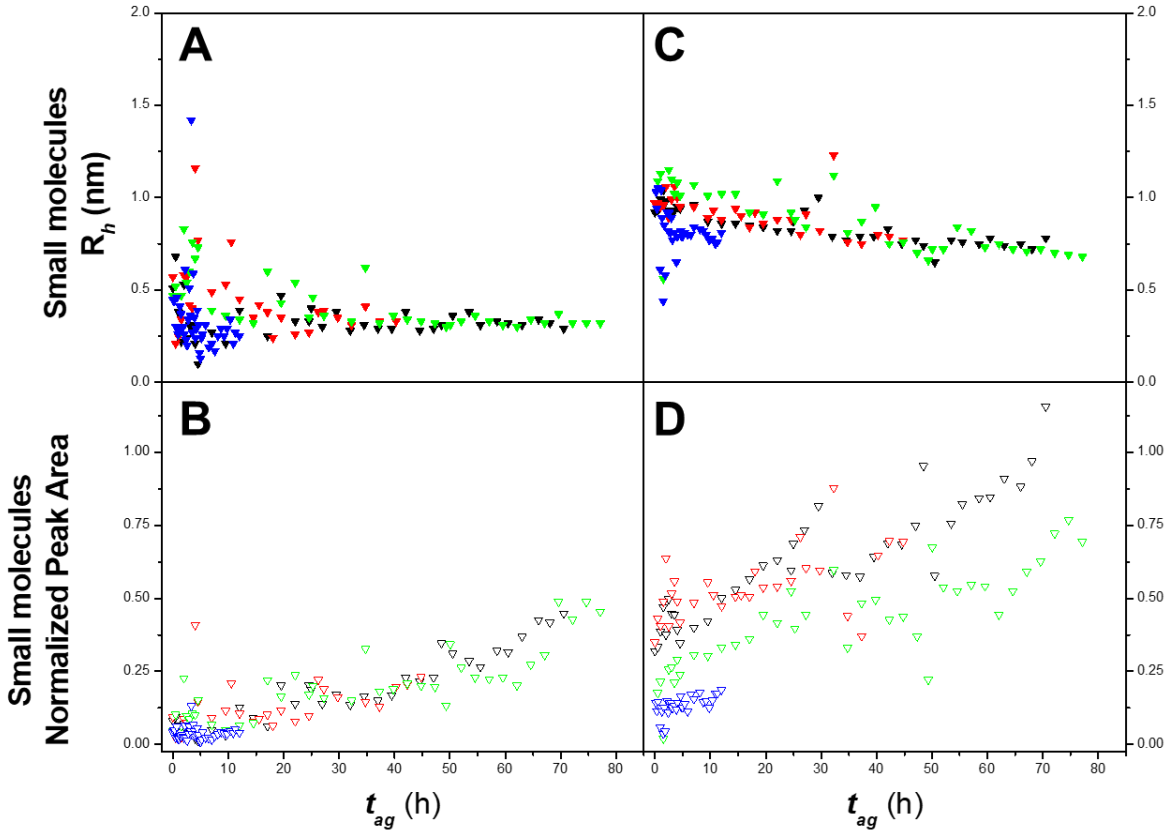

Figure SI17. Hydrodynamic radius (upper layers) and peak area evolution (bottom layers) of the small molecules population obtained by (A) and (B) UV and by (C) and (D) LIF for all the fours all the four nAβ + tAβ systems. Legend: 93% nAβ(1-40) + 7% tAβ(1-40) system (▼▽), 3:1 Aβ(1-40):Aβ(1-42) – 93% nAβ(1-40) + 7% tAβ(1-40) + 100% nAβ(1-42) system (▼▽), 3:1 Aβ(1-40):Aβ(1-42) – 100% nAβ(1-40) + 90% nAβ(1-42) + 10% tAβ(1-42) system (▼▽), 90% nAβ(1-40) + 10% tAβ(1-40) system (▼▽). Closed symbols represent the hydrodynamic radius and open symbols stand for the peak area. Peak area was normalized by dividing the area of each data point to the total peak area obtained for the first run at t= 0 h to obtain a clear comparison between the two detection modes. Sample and incubation experimental conditions as in Figures SI13, SI14, SI15 and SI16. UV and LIF experimental conditions as in Figure SI1 and Figure SI3 respectively.

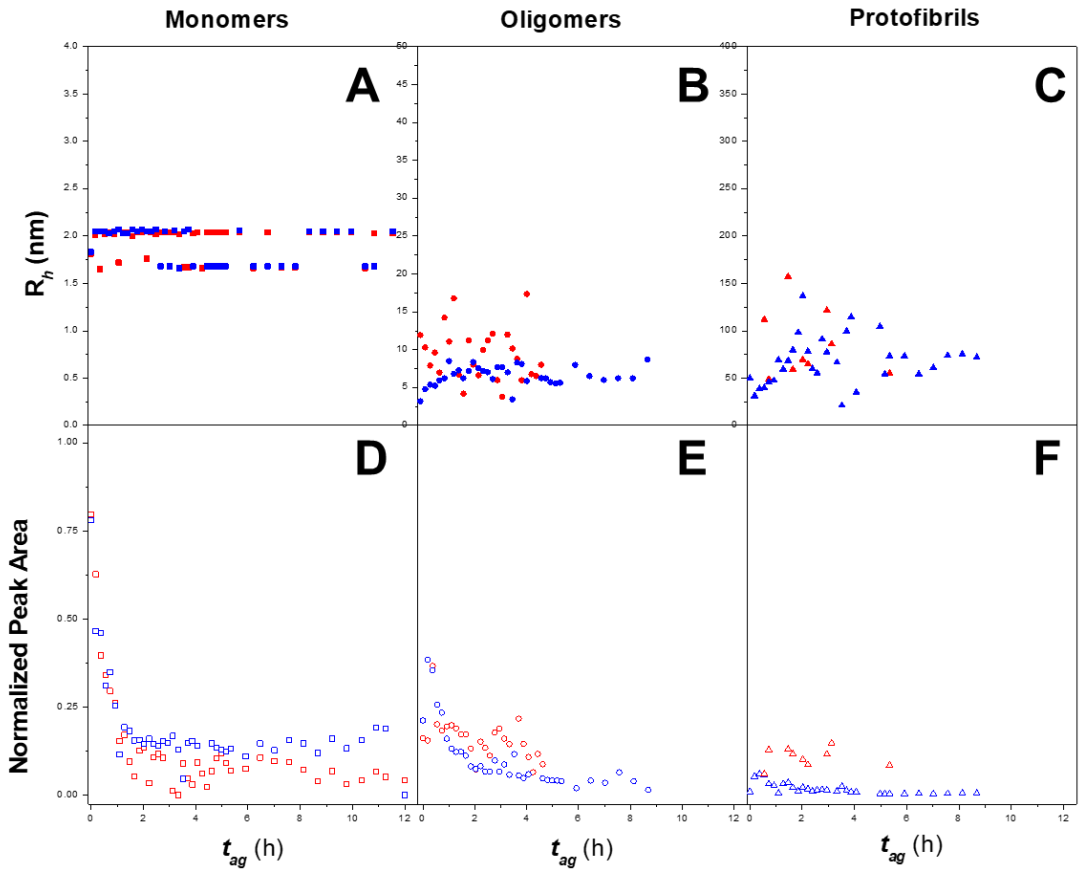

Figure SI18. Hydrodynamic radius (upper layers) and peak area evolution (bottom layers) of the (A) and (D) monomers, (B) and (E) oligomers, (C) and (F) protofibrils obtained for the 90% nAβ(1-42) + 10% tAβ(1-42) system by treating the experimental peak from the right side (misleading results). Red symbols represent the results obtained from UV and the blue symbols stand for the results obtained from LIF. Peak area was normalized by dividing the area of each data point to the total peak area obtained for the first run at t= 0 h to obtain a clear comparison between the two detection modes. Experimental conditions: Sample: 100 µM Aβ (9 nmol nAβ(1-42) + 1 nmol of tAβ(1-42)); 20 mM phosphate buffer, pH 7.4. Incubation: quiescent conditions at 37 °C. UV and LIF experimental conditions as in Figure SI1 and Figure SI3 respectively.

IV.SI.5. References

1. Chamieh, J. & Cottet, H. in *Colloid Interface Sci. Pharm. Res. Dev.* 173–192 (2014). doi:10.1016/B978-0-444-62614-1.00009-0
2. Chamieh, J., Biron, J. P., Cipelletti, L. & Cottet, H. Monitoring Biopolymer Degradation by Taylor Dispersion Analysis. *Biomacromolecules* **16,** 3945–3951 (2015).
3. Cipelletti, L., Biron, J. P., Martin, M. & Cottet, H. Measuring Arbitrary Diffusion Coefficient Distributions of Nano-Objects by Taylor Dispersion Analysis. *Anal. Chem.* **87,** 8489–8496 (2015).
4. Taylor, G. Conditions under which dispersion of a solute in a stream of solvent can be used to measure molecular diffusion. *Proc. R. Soc. London. Ser. A. Math. Phys. Sci.* **225,** 473–477 (1954).
5. Cottet, H., Biron, J. P. & Martin, M. On the optimization of operating conditions for Taylor dispersion analysis of mixtures. *Analyst* **139,** 3552–3562 (2013).
6. Deleanu, M., Hernandez, J.-F., Cipelletti, L., Biron, J.-P., Rossi, E., Taverna, M., Cottet, H. & Chamieh, J. Unraveling the Speciation of β-Amyloid Peptides during the Aggregation Process by Taylor Dispersion Analysis. *Anal. Chem.* (2021). doi:10.1021/acs.analchem.1c00527

General Conclusions

This thesis presented the first study in which TDA was employed for a real-time monitoring of the aggregation process of Aβ peptides. During the experimental studies, several important original features about TDA methodology have been made:

(*i*) TDA requires very low sample volumes (only nL are injected and only µL are required) due to the miniaturized capillary format, can be used as a label-free technique, and offers a relatively high throughput analysis (about 10 injections/h);

(*ii*) TDA allows to monitor the transient species (oligomers, protofibrils) during the aggregation process, leading to relevant information on the aggregation mechanism/pathways of Aβ peptides. TDA experiments confirmed that the aggregation pathway of Aβ(1-40) goes from the monomeric state directly to a fibrillary structure, in contrast to Aβ(1-42), which passes through different intermediate states (oligomers and protofibrils) before reaching the fibrils, in agreement with previous reports;

(*iii*) Quantitative data related to the proportion and the size of the different Aβ species have been obtained using adequate data processing of the taylorgrams such as Gaussian fitting and Constrained Regularized Linear Inversion method;

(*iv*) Molecular simulations performed on several monomer and LMM oligomer structures of Aβ(1-42) revealed that the experimental hydrodynamic radius of the monomers and LMM oligomers population obtained from TDA was mainly comprised of monomers and dimers.

(*v*) By checking the inhibition properties of a β-sheet breaker, iAβ5p, known to inhibit the formation of fibrils upon the aggregation process of Aβ(1-42). It was found that iAβ5p had an inhibition effect upon the formation of fibrils and only a little effect upon the aggregation rate was observed with no significant changes on the formation of the early-stage species. However, these results endorse that TDA can be used as a drug screening tool if suitable inhibitors able to have an effect on the early-stages of the process are used.

(*vi*) The information obtained by TDA was further correlated by using the alternative ThT fluorescence assays, DLS and AFM analyses. The results obtained in parallel by TDA and AFM showed the complementarities of the two techniques, where TDA can quantify and size small nanomolecular intermediates while AFM can characterize the fibrillar structures which are not accessible by TDA.

(*vii*) It was demonstrated that the kinetics of aggregation strongly depend on the nature of the amyloid peptide. Thus, under proposed working conditions, the amyloid-prone Aβ(1-42) aggregates more rapidly (minutes scale) than Aβ(1-40), which aggregates in about 24h in agreement with previously published works. During the co-aggregation, the kinetics were highly influenced by the Aβ(1-40):Aβ(1-42) ratio. The monomers and LMM oligomers population disappeared after an incubation period of 2 h for Aβ(1-42) independent experiment, after 12, 18 when 24 h corresponding to an amount of 75%, 50% and 25 % of Aβ(1-42) present in the co-aggregation systems and after 60 h in the case of the Aβ(1-40) independent experiment. In the same manner, a decrease in the HMM oligomer population was also observed with decreasing Aβ(1-42) proportion.

(*viii*) By applying a kinetic model taking into account association and dissociation of the species, an increase of the reaction rates of aggregation was observed by increasing the amount of Aβ(1-42) in the mixture. On the contrary, the dissociation of the high ordered species into monomers is more favored for the Aβ(1-42) containing mixtures, while for the Aβ(1-40) independent experiment the aggregation process seemed to be more irreversible.

(*ix*) By monitoring the aggregation and co-aggregation of Aβ peptides in the presence of an small amount of FITC tagged peptide (tAβ), it was revealed that this hydrophilic dye significantly reduced the aggregation behavior of Aβ(1-42) where both the kinetics and the formation of potentially toxic oligomers were prolonged. A significant inhibition of the protofibril population was also observed further suggesting that FITC could have an impact upon the elongation phase. In case of the Aβ(1-40) system, only a retardation in kinetics was depicted compared to the native (nAβ).

(*x*) During the co-aggregation process of the mixed nAβ and tAβ systems, the 100% native isoform was found to be the dominant isoform of the system as the conjugated electrostatic and hydrophilic effect of the attached dye to a specific isoform tends to reduce the aggregation behavior of the corresponding Aβ peptide.

(*xi*) TDA using LEDIF detection was affected both by some traces of unreacted FITC dye and by a tailing of the elution profile that was most likely caused by an adsorption of the FITC dye on the capillary surface. By using adequate data processing, the results obtained by LEDIF were correlated with the ones obtained by UV. During the LEDIF analysis more protofibril events where

observed compared to UV and this was most likely due the difference in the sensitivity between the two detection modes.

Taking altogether, TDA was proved to be a powerful technique which allowed not only to speciate different soluble Aβ intermediates, but also provided a more detailed picture of the early stages of the aggregation process and the extent to which early stages species are affected by the Aβ(1-40):Aβ(1-42) ratio. As a perspective, TDA-LEDIF could be a more powerful tool that can provide a more in-depth evaluation of the aggregation process at concentrations close to physiological conditions if suitable fluorophores that do not change the aggregation behavior of the native isoforms are used, if no traces of free labels are present in the sample, and if the adsorption of the dyes on the capillary surface is overpassed

Résume en Anglais

Alzheimer Disease (AD) is one of the major public health challenges of the 21st century and its development is centered around the amyloid hypothesis which states that extracellular formation of amyloid plaques and the intracellular accumulation of neurofibrillary Tau tangles (NFTs) are caused by the aggregation of β-amyloid (Aβ) peptides. Several biophysical techniques have been employed for studying the aggregation process of Aβ peptides such as thioflavin T (ThT) assay, dynamic light scattering (DLS), capillary electrophoresis (CE), electron microscopy (EM) and atomic force microscopy (AFM). Despite the useful information these methods provide, not all of them are suitable for monitoring the early stages of the process. The main objective of this thesis is to apply Taylor dispersion analysis (TDA) for the monitoring of the Aβ peptide aggregation mechanism. TDA is a modern technique that can size and quantify soluble species ranging from 0.1 nm to a few hundred nm. TDA has yet been employed for a real-time monitoring of the Aβ peptide aggregation. TDA revealed that the aggregation process of Aβ(1-40) and Aβ(1-42) isoforms occurs through distinct pathways. These results have been correlated with ThT assay and DLS. The co-aggregation of Aβ(1-40):Aβ(1-42) mixtures was further explored by TDA and AFM, highlighting the influence of the peptide ratios on the kinetics and the formation of potentially toxic oligomeric species. Finally, the aggregation process of Aβ peptides by TDA was conducted using a simultaneous UV-LIF detection in the presence of FITC-tagged Aβ peptides. This study demonstrated that the aggregation pathways of the native Aβ peptides are altered by the presence of the fluorophore. In conclusion, TDA provided a complete speciation of the different soluble species (monomer, oligomers, protofibrils) during Aβ aggregation, which brings valuable information on the mechanism of aggregation.

Keywords: Alzheimer disease; β-amyloid peptides; Taylor dispersion analysis; aggregation studies; atomic force microscopy; ThT assay; dynamic light scattering.

Résume en Français

La maladie d'Alzheimer (MA) est l'un des principaux défis de santé publique du 21ème siècle et son développement repose sur l'hypothèse amyloïde qui stipule que la formation extracellulaire de plaques amyloïdes et l'accumulation intracellulaire d'enchevêtrements neurofibrillaires Tau (NFTs) sont causées par l'agrégation de peptides β-amyloïdes (Aβ). Plusieurs techniques biophysiques ont été employées pour étudier le processus d'agrégation des peptides Aβ, comme le dosage de la thioflavine T (ThT), la diffusion dynamique de la lumière (DLS), l'électrophorèse capillaire (CE), la microscopie électronique (EM) et la microscopie à force atomique (AFM), mais malgré les informations utiles qu'elles fournissent, toutes ne sont pas adaptées au suivi des premières étapes du processus agrégatif. L'objectif principal de cette thèse et d'évaluer l'analyse de dispersion de Taylor (TDA) pour le suivi des mécanismes d'agrégation des peptides Aβ. Le TDA est une technique moderne qui permet de déterminer le rayon hydrodynamique et de quantifier des espèces en solution pour des objets moléculaires dont la tailles est comprise entre 0,1 nm et centaines de nm. Jusqu'à présent, la TDA n'a pas encore été employée pour un suivi en temps réel de l'agrégation des peptides Aβ. La TDA a révélé que le processus d'agrégation des isoformes Aβ(1-40) et Aβ(1-42) se produit selon des mécanismes distincts. Ces résultats ont été corrélés avec le test ThT et la DLS. La co-agrégation des mélanges Aβ(1-40):Aβ(1-42) a aussi été explorée conjointement par TDA et AFM, mettant en évidence l'influence de la composition du mélange sur la cinétique et la formation d'espèces oligomériques potentiellement toxiques. Enfin, le processus d'agrégation des peptides Aβ par TDA a été réalisé à l'aide d'une détection simultanée UV-LIF utilisant des peptides fluorescents marqués FITC. Cette étude a démontré que les voies d'agrégation des peptides Aβ natifs sont modifiées par la présence du fluorophore. En conclusion, la TDA permet une spéciation des espèces solubles (monomères, oligomères, protofibriles) lors de l'agrégation des peptides Aβ, ce qui apporte des informations très précises sur le mécanisme d'agrégation.

Mots-clés: Maladie d'Alzheimer ; peptides β-amyloïdes ; analyse de dispersion de Taylor ; études d'agrégation ; microscopie à force atomique ; ThT assay; diffusion dynamique de la lumière.

Intitulé et adresse de l'unité ou du laboratoire

IBMM, University of Montpellier, CNRS, ENSCM, Montpellier, France.